amt-2018-438

Interactive comment on "Aerosol Optical Depth comparison between GAW-PFR and AERONET-Cimel radiometers from long term (2005–2015) 1-minute synchronous measurements" by Emilio Cuevas et al.

Anonymous Referee #1 (amt-2018-438-RC1):

G.1. This is a very thorough and overall quite clearly written manuscript of great use to anyone relying on PFR or Aeronet derived AODs. It establishes how well the master instruments used in both networks compare over the long term and where and why minute differences arise. It does not address how well these calibrations are transferred across the networks and what the resulting uncertainties are for various stations. However, such questions have been addressed by many others as evidenced by citations in this manuscript. This reviewer only has a very small number of relatively minor comments

Authors:

We appreciate the positive comments of the Referee, and his/her specific corrections and comments that are addressed below.

The Referee must take into account that, according to the requirements and comments of the Referees # 3 and # 4, new relevant analysis have been incorporated in the paper what has required large additional workload, resulting in a significant improvement of the paper.

The most relevant new analyses have been:

1) Comparison of GAW-PFR with version V3 of AERONET and previous comparison between V2 and V3.

2) New study on modelling the impact of near-forward scattering on the AOD measured by the PFR and Cimel radiometers (with different FOVs).

3) Study of AOD variability in 1 minute to rule out possible differences in AOD due to a non-perfect synchronization of the PFR and Cimel sampling data.

4) Incorporation of case studies on the impact on AOD due to small inaccuracies in the calibrations or the clouds contamination.

Much more information about the above points has been included in a new Supplement material document of 24 pages.

S.1. Page 1, Line 4. Suggest to say "wavelength near" instead of "nearby wavelength"

Authors:

Rephrased.

S.2. Page 2, Line 15. Suggest mentioning some other sunphotometer networks, PHOTON, Japanese network etc.

Authors:

References to other networks have been requested by the four Referees. Although we referred to global networks with centralized data processing and databases, as well as standard calibration procedures in each of the networks, we fully agree to include a reference to other similar sunphotometer networks of global regional scope.

The new paragraphs introduced in the manuscript are as follows:

"…These are GAW-PFR (Global Atmosphere Watch - Precision Filter Radiometer; http://www.pmodwrc.ch/worcc/; last access: 05 September 2018) and AERONET-Cimel (AErosol RObotic NETwork - Cimel Electronique radiometer; http://aeronet.gsfc.nasa.gov; last access: 01 September 2018) networks. AERONET is, in fact, a federation of ground-based remote sensing aerosol networks established by NASA (National Aeronautics and Space Administration) and PHOTONS (PHOtométrie pour le Traitement Opérationnel de Normalisation Satellitaire; University of Lille- Service d'Observation de l'INSU, France; Goloub et al., 2007), being complemented by other sub-networks, such as, AEROCAN (Canadian sunphotometry network; Bokoye et al., 2001), AeroSibnet (Siberian system for Aerosol monitoring; Sakerin et al., 2005), AeroSpan (Aerosol characterisation via Sun photometry: Australia Network; Mitchell et al., 2017), CARSNET (China Aerosol Remote Sensing NETwork; Che et al., 2015), and RIMA (The Iberian network for aerosol measurements; Toledano et al., 2011).

There are other radiometer networks that in recent years have incorporated centralized protocols for data evaluation and databases, and performed regular intercomparisons with GAW-PFR and AERONET-Cimel. These include, for example, SKYNET (SKYradiometer NETwork), and its seven associated sub-networks, that uses the Prede-POM sky radiometer to investigate aerosol-cloud-solar radiation interactions (e.g. Campanelli et al., 2004; Nakajima et al., 2007; Takamura et al., 2004)."

The corresponding references have been added.

S.3. Page 2, Line 30. Suggest inserting "NASA" before "Goddard"

Authors: Done

S.4. Page 3, Line 6. Numerous is an understatement.

Authors: Replaced "numerous" by "many".

S.5. Page 4, Line 5. The use of "absolute" is misleading here. A Langley calibration alone is never absolute (i.e. the calibration value is just a signal in an engineering unit not W/m^2. The beauty is that an absolute calibration is not needed to derive AOD.

Authors: We agree. "Absolute" has been removed.

S.6. Page 5, Line 5. Suggest replacing "constant" with "signal" here and everywhere else in the manuscript. Or maybe just explain once that in sunphotometry the calibration "constant" is the signal the instrument would read outside the atmosphere (extraterrestrial) at a normalized earth-sun distance?

Authors: We have added:

"Note, that the extraterrestrial constant (calibration constant) is the signal the instrument would measure outside the atmosphere at a normalized earth-sun distance."

S.7. Page 6, Line 24. Font issue.

Authors: Corrected

S.8. Page 6, Line 6. Incorrect grammar: "were" not "was".

Authors: We have not found this mistake. The paper has now been corrected throughout for English.

S.9. Page 14: Line 14. This is misleading as the error in AOD due to error in the calibration "constant" is independent of AOD.

Authors:

We agree, but we guess the misleading statement was in Page 13, Line 14. So, the paragraph:

"A not sufficiently accurate determination of the calibration constant results in a fictitious AOD diurnal evolution presenting a concave or convex characteristic curve due to the calibration error dependence on solar air mass. The largest error occurs in the central part of the day (or lower air masses), mainly, in clean days with very low aerosol load (< 0.02 in 500 nm), as reported by Romero and Cuevas (2002) and Cachorro et al. (2004)."

has been replaced by the following one:

"A not sufficiently accurate determination of the calibration constant results in a fictitious AOD diurnal evolution presenting a concave or convex characteristic curve due to the calibration error dependence on solar air mass. The largest error occurs in the central part of the day (lower air masses), mainly, in clean days with very low aerosol load (< 0.02 in 500 nm) as reported by Romero and Cuevas (2002) and Cachorro et al. (2004), and as can be derived from Equation 2."

Aerosol Optical Depth comparison between GAW-PFR and AERONET-Cimel radiometers from long-term (2005-2015) 1-minute synchronous measurements

Emilio Cuevas[1], Pedro Miguel Romero-Campos[1], Natalia Kouremeti[2], Stelios Kazadzis[2], Petri Räisänen[3], Rosa Delia García[4,1], Africa Barreto[5,1,4], Carmen Guirado-Fuentes[4,1], Ramón Ramos[1], Carlos Toledano[4], Fernando Almansa[5,1,4], and, Julian Gröbner[2]

[1]Izaña Atmospheric Research Center (IARC), State Meteorological Agency (AEMET), Spain

[2]Physikalisch-Meteorologisches Observatorium Davos, World Radiation Center (PMOD/WRC), Davos, Switzerland

[3]Finnish Meteorological Institute, Helsinki, Finland

[4]Atmospheric Optics Group, Valladolid University, Valladolid, Spain

[5]Cimel Electronique, Paris, France

Correspondence: Emilio Cuevas
(ecuevasa@aemet.es)

Abstract

A comprehensive comparison of more than 70000 synchronous 1-minute aerosol optical depth (AOD) data from three Global Atmosphere Watch-Precision Filter Radiometers (GAW-PFR), traceable to the World AOD reference, and 15 Aerosol Robotic Network-Cimel (AERONET-Cimel, Versions V2 and V3) radiometers, calibrated individually with the Langley plot technique, was performed for four common or near wavelengths 380 nm, 440 nm, 500 nm and 870 nm in the period 2005-2015. The goal of this study is to assess whether, despite the marked technical differences between both networks (AERONET, GAW-PFR) and the number of instruments used, their long-term AOD data are comparable and consistent. The percentage of data meeting the WMO traceability requirements (95% of the AOD differences of an instrument compared to the WMO standards lie within specific limits) is > 92 % at 380 nm, > 95 % at 440 nm and 500 nm, and 98 % at 870 nm, with the results being quite similar for both AERONET V2 and V3. For the data outside these limits the contribution of calibration and differences in the calculation of the optical depth contribution due to Rayleigh scattering, and O_3 and NO_2 absorption have a negligible impact. For AOD > 0.1, a small but non-negligible percentage (~ 1.9 %) of the AOD data outside the WMO limits at 380 nm can be partly assigned to the impact of dust aerosol forward scattering on the AOD calculation due to the different field of view of the instruments. Due to this effect the GAW-PFR provides AOD values which are ~3% lower at 380 nm, and ~2% lower at 500 nm, compared with AERONET-Cimel. The comparison of the Angström exponent shows that under non-pristine conditions (AOD > 0.03 and AE < 1) the AE differences remain < 0.1. This long-term comparison shows an excellent traceability of AERONET-Cimel AOD with the World AOD reference at 440 nm, 500 nm and 870 nm channels and a fairly good agreement at 380 nm.

1. Introduction

In recent decades there has been a growing interest in the role played by atmospheric aerosols in the radiation budget and the Earth's hydrological cycle, mainly through their physical and optical properties (IPCC, 2013). The most comprehensive and important parameter that accounts for the optical activity of aerosols in the atmospheric column is the aerosol optical depth (AOD) (WMO, 2003, 2005). This is also a key parameter used in atmospheric column aerosol modelling (e.g. Basart et al.,2012; Benedetti et al., 2018; Cuevas et al., 2015; Huneeus et al., 2016) and in satellite observations (e.g. Sayer et al., 2012, 2013; Kahn

and Gaitley, 2015; Amiridis et al., 2015). The second aerosol optical parameter in importance is the Angström exponent (AE) (Angstrom, 1929) that accounts for the spectral dependency of the AOD. Since the AE is inversely related to the average size of the aerosol particles, it is a qualitative indicator of the atmospheric aerosol particle size and therefore a useful parameter to assess the aerosol type (WMO, 2003). At present, two global ground-based radiometer networks provide aerosol optical properties of the atmospheric column using centralized data processing procedures based on their respective standard criteria and also centralized protocols for calibration and quality control, linking all network instruments. These are GAW-PFR (Global Atmosphere Watch - Precision Filter Radiometer; http://www.pmodwrc.ch/worcc/; last access: 05 September 2018) and AERONET-Cimel (AErosol RObotic NETwork - Cimel Electronique radiometer; http://aeronet.gsfc.nasa.gov; last access: 01 September 2018) networks. AERONET is, in fact, a federation of ground-based remote sensing aerosol networks established by NASA (National Aeronautics and Space Administration) and PHOTONS (PHOtométrie pour le Traitement Opérationnel de Normalisation Satellitaire; University of Lille- Service d'Observation de l'INSU, France; Goloub et al., 2007), being complemented by other sub-networks, such as, AEROCAN (Canadian sunphotometry network; Bokoye et al., 2001), AeroSibnet (Siberian system for Aerosol monitoring; Sakerin et al., 2005), AeroSpan (Aerosol characterisation via Sun photometry: Australia Network; Mitchell et al., 2017), CARSNET (China Aerosol Remote Sensing NETwork; Che et al., 2015), and RIMA (The Iberian network for aerosol measurements; Toledano et al., 2011).

There are other radiometer networks that in recent years have incorporated centralized protocols for data evaluation and databases, and performed regular intercomparisons with GAW-PFR and AERONET-Cimel. These include, for example, SKYNET (SKYradiometer NETwork), and its seven associated sub-networks, that uses the Prede-POM sky radiometer to investigate aerosol-cloud-solar radiation interactions (e.g. Campanelli et al., 2004; Nakajima et al., 2007; Takamura et al., 2004).

The World Optical Depth Research Calibration Center (WORCC) was established in 1996 at the Physikalisch Meteorologisches Observatorium Davos / World Radiation Center (PMOD / WRC). The GAW-PFR network (Wehrli, 2005) was initiated within PMOD/WRC for global and long-term atmospheric aerosol monitoring and accurate detection of trends. Aerosol data series measured at 12 core sites away from local and regional pollution sources, representative of atmospheric background conditions in different climates and environments of the planet, in addition to another 20 associated stations are included in this global network (Kazadzis et al., 2018a). For this reason, GAW-PFR uses the PFR, an accurate and reliable instrument regarding its absolute response stability over time that was designed for long-term AOD measurements (Wehrli, 2008a). The GAW-PFR was specifically designed by WORCC for this goal following the technical specifications defined by WMO (2003; 2016). In 2006, the Commission for Instruments and Methods of Observation (CIMO) of WMO (WMO, 2007) recommended that the WORCC at the PMOD/WRC should be designated as the primary WMO Reference Centre for AOD measurements (WMO, 2005).

The AERONET-Cimel network (Holben et al., 1998) was, in principal, designed to validate satellite products and to characterize the spatial-temporal distribution of atmospheric aerosols based on their optical

properties. It is the largest surface-based global aerosol network with more than 84 sites with measurement series longer than 10 years and more than 242 sites having data sets > 5 years. Cimel radiometer data, part of AERONET, are processed centrally and freely delivered in near real time by the NASA Goddard Space Flight Center. Both networks, although designed to meet different objectives, are now global benchmarks for the study and characterization of aerosol optical properties worldwide, and for the evaluation of aerosol observations on board satellites and simulations with models. Multiple studies have proliferated in recent years to obtain aerosol climatology and to determine AOD trends in different parts of the world (e.g. Nyeki et al., 2012; Klingmüller et al., 2016; Chedin et al., 2018). However, these networks use radiometers with significant technical differences. Moreover, calibration methodologies, AOD calculation algorithms and data evaluation methods are also relatively different between the two networks. Consequently, the objective of this study is to assess whether, despite the marked differences between both networks, including the different day-to-day maintenance and operation procedures of the respective instruments during the study period, the long-term AOD provided by the two networks is comparable and consistent.

The WMO has defined the GAW-PFR Triad (three Master PFR instruments) as the world-wide reference for AOD measurements (WMO, 2005). Based on this concept, an instrument provides traceable measurements of AOD to this WMO reference, when this instrument can demonstrate an unbroken chain of calibrations between itself and the GAW-PFR Triad with AOD measurements within specified limits of the GAW-PFR reference. This can either be achieved by a direct comparison to the GAW-PFR Triad (Kazadzis et al., 2018a), or by using a portable transfer standard radiometer as presented in this study. Several comparisons between AERONET-Cimel, GAW-PFR and other radiometers have been carried out in different places (Barreto et al., 2016; Kazadzis et al., 2014, 2018b; Kim et al., 2008; McArthur et al., 2003; Mitchell and Forgan, 2003; Nyeki et al., 2015; Schmid et al., 1999; Toledano et al., 2012). However, these comparisons have been performed during field intercomparison campaigns or during relatively short periods of time, so they are not representative of a large variety of atmospheric conditions. In addition, the type of instrument maintenance and the number and qualifications of staff serving them during campaigns is generally of a higher quality compared to that of the instrument daily operation in unattended mode. This might cause an improvement of the instrument performance during intensive campaigns compared to the operational mode.

The growing interest in the analysis of long-term AOD and AE data series for climatological purposes requires an assessment of their quality assurance and long-term intercomparability. This is the first study to analyse the long-term traceability of AERONET-Cimel with respect to GAW-PFR, and therefore to assess the validity of the long AOD and AE AERONET-Cimel data series for climatological and climate change studies under specific quality control requirements.

GAW-PFR has a comprehensive calibration system (Kazadzis et al., 2018a; Schmid and Wehrli, 1995) that is transferred by a worldwide suite of reference instruments. AERONET-Cimel does not have a CIMO-WMO linked reference and, as described by Holben et al. (1998), Eck et al. (1999), and Toledano et al. (2018), is based on:

Maintaining Reference AERONET radiometers based on the Langley calibration technique at Izaña, Spain and Mauna Loa, USA. Calibration of all other instruments based on raw voltage ratios comparisons with Reference instruments at dedicated sites (Carpentras-France, Washington DC-USA, Valladolid-Spain). There are few places in the world where synchronous observations of these two networks are available for long time periods and variable AOD conditions. The Izaña Observatory (IZO; Tenerife, Canary Islands) is one of them. The GAW-PFR measurements started at Izaña Observatory in 2001 (Wehrli, 2005) while AERONET-Cimel started in 2003 (Goloub et al., 2007). Since 2005, synchronous measurements (1-minute values), that have been evaluated following the calibration procedures of each of the networks, are available.

In addition, the Izaña Observatory is one of the two places in the world (the other is Mauna Loa - Hawaii, USA) where sun-calibrations are performed using the Langley plot technique for both AERONET-Cimel and GAW-PFR reference instruments (Toledano et al., 2018) because of stable (and very low) AOD conditions during many days per year. Consequently, the instruments compared at the Izaña Observatory have been calibrated under the same environmental conditions, and therefore AOD differences can be directly linked with calibration principles, AOD post-processing and other instrumental differences. In this work, we analyse and evaluate the comparison of 11 years (2005-2015) of 1-minute synchronous observations of AOD with AERONET-Cimel and GAW-PFR in four common or near wavelengths, assessing the results and explaining the possible causes of these differences. Some preliminary technical details on the traceability between GAW-PFR and AERONET-Cimel were reported in a technical report by Romero-Campos et al. (2017).

In Section 2 the facility in which this long-term comparison has been carried out is described. The technical characteristics of the AERONET-Cimel and GAW-PFR instruments are shown in Section 3, with special emphasis on the technical and methodological differences of both networks. Section 4 describes the methodology followed in this intercomparison based on the concept of WMO-GAW traceability. Results are given in Section 5. A summary and conclusions are provided in Section 6.

2. Site Description

Izaña Observatory (28.3◦ N, 16.5◦ W; 2373 m a.s.l.) is located in Tenerife (Canary Islands, Spain) and is managed by the Izaña Atmospheric Research Center (IARC), which is part of the State Meteorological Agency of Spain (AEMET). It is a suitable place for long-term studies of aerosol optical properties under contrasting atmospheric and meteorological conditions. This is because IZO is located in the free troposphere (FT) above the temperature inversion caused by the trade wind regime in lower levels and general subsidence associated with the branch of the decay of Hadley's cell aloft (Carrillo et al., 2016). This meteorological feature favours, during most of the year, the presence of pristine skies and clean air representative of atmospheric background conditions (Cuevas et al., 2013; Rodríguez et al., 2009). On the other hand, its proximity to the African continent makes it a privileged site for observing and characterizing the Saharan Air Layer (SAL) that normally presents a high burden of desert mineral dust, especially during the summer months (Basart et al., 2009; Rodríguez et al., 2011; Cuevas et al., 2015). At this time of the

year, the SAL impacts the subtropical free troposphere over the North Atlantic with large interannual (Rodríguez et al., 2015) and sharp intraseasonal (Cuevas et al., 2017a) variability. The contrasting atmospheric conditions that occur at IZO allow the comparison of the two networks, which can be performed under a wide range of AOD values; mostly for pristine conditions (AOD ≤ 0.03) but also for relatively high turbidity (AOD > 0.6) linked with dust aerosol related intrusions. In addition, the location offers the possibility of observing rapid changes in AOD, going from pristine conditions to dusty skies, and vice versa, in a matter of a few hours, especially in the summer period. The periodical presence of a dust laden SAL allows us to evaluate the impact that the dust forward scattering into the field of view has on AOD retrieval. All this defines IZO as an excellent atmospheric aerosol natural laboratory to compare the performance of different radiometers measuring AOD. One of the first international AOD intercomparison campaigns was carried out at IZO in April 1984 (WMO, 1986) promoted and coordinated by PMOD / WRC.

The privileged conditions of pristine skies that characterize IZO during many days a year have allowed this observatory to become a calibration site for the GAW-PFR and AERONET-Cimel networks since 2001 and 2003, respectively, where the extraterrestrial constants are determined with direct sun observations using the Langley plot technique (Toledano et al., 2018). Note that the extraterrestrial constant (calibration constant) is the signal the instrument would read outside the atmosphere at a normalized earth-sun distance. In addition, since July 2014, IZO has also been designated by the WMO as a CIMO (WMO, 2014) testbed for aerosols and water vapour remote sensing instruments. IZO is a station of the Baseline Surface Radiation Network (BSRN) (Driemel et al., 2018; García et al., 2019). Details of IZO facilities, measurement programmes and main research activities can be found in Cuevas et al. (2017b).

3. GAW-PFR and AERONET-Cimel radiometers

The two types of radiometers intercompared in this study are Cimel CE318-N (Holben et al., 1998), hereinafter referred to as Cimel, the standard instrument of AERONET until the recent appearance of CE318-T (Barreto et al., 2016), and the PFR (Wehrli, 2005) standard instrument of the GAW-PFR network. The main features of these two radiometers are described in Table 1. The Cimel (Holben et al., 1994, 1998) is a radiometer equipped with a 2-axis robot that performs two types of basic radiation measurements: direct solar irradiance and sky (radiance) observations, thanks to an automatic pointing robot that executes the observation sequences that have been scheduled. The robot performs automatic pointing to the sun by stepping azimuth and zenith motors using ephemeris based on time, latitude and longitude. Additionally, a four-quadrant detector is used to improve the sun tracking before each scheduled measurement sequence. This sensor guides the robot to the point where the intensity of the signal channel is maximum. Diffuse-sky measurements are also performed by Cimel to infer aerosol optical and microphysical properties. Two different routines are executed: almucantar (varying the azimuth angle keeping constant the zenith angle) and principal plane (varying the zenith angle keeping constant the azimuth angle). The ability of Cimel to perform both direct and diffuse-sky measurements makes it necessary to use a specific robot rather than a simple sun tracker. The field of view angle (FOV) of the instrument is 1.29° (~1.3° from now on) (Torres

et al., 2013). The wavelengths in which the measurements are sequentially made by a single detector depend on the interference filters that each version of the radiometer has installed in the filter wheel, which is located inside the sensor head and which is moved by a stepper motor. The Cimel versions used in this study have at least eight interference filters centred at 340 nm, 380 nm, 440 nm, 500 nm, 675 nm, 870 nm, 940 nm, and 1020 nm and 10 nm full width at half maximum (FWHM) bandwidth, except for 340 nm and 380 nm which have 2 nm and 4 nm FWHM, respectively. Solar irradiance is measured with a Silicon detector in these channels. The possible deterioration of the interference filters is reduced since they are only sun-exposed during three consecutive 1-second direct-sun measurements per channel, this cycle being scheduled every ~15 minutes. The rest of the time the Cimel is taking sky radiance measurements, or at rest position, looking downwards.

The PFR (Wehrli, 2000, 2005, 2008a, b) is designed for continuous and automated operation under a broad range of weather conditions. It accurately measures direct solar radiation transmitted in four independent narrow wavelength channels centred at 368 nm, 412 nm, 500 nm and 862 nm, with 5 nm FWHM bandwidth. The FOV of the instrument is 2.5° and the slope angle is 0.7°. Dielectric interference filters manufactured by the ion-assisted-deposition technique are used to assure significantly larger stability in comparison to the one manufactured by classic soft-coatings. The PFR was designed for long-term stable measurements, therefore the instrument is hermetically sealed with an internal atmosphere slightly pressurized (2000 hPa) with dry nitrogen, and is stabilized in temperature with a Peltier-type thermostatic system maintaining the temperature of the detector head at 20° C ± 0.5° C. This system makes corrections of the sensitivity for temperature unnecessary, and also prevents accelerated ageing of filters, ensuring the high stability of the PFR. The PFR is mounted on a sun tracker, pointing always at the sun without any active optimization of the sun-pointing. The detectors are only exposed for short time periods, since an automated shutter opens every minute for 10s for sun measurements, minimizing degradation related to the filters exposure.

The expected uncertainty of AOD in the four channels of the PFR radiometer is from 0.004 (862 nm) up to 0.01 (368 nm) (Wehrli, 2000). For the Cimel radiometer, the expected uncertainty of level 2-AOD product is between 0.002 and 0.005, for reference instruments, larger for shorter wavelengths, and between 0.01 and 0.02 for field instruments, larger in the UV, under conditions of clear skies (Eck et al., 1999; Barreto et al., 2016). It should be taken into account that, in general, in the ultraviolet range the AOD uncertainty is higher and depends on the optical mass (Carlund et al., 2017).

In relation to the calibration of both networks, GAW and AERONET, they use measurements at high mountain stations with very stable and low AOD over a day in which consecutive measurements can be performed over a wide range of optical air mass (approximately between 2 and 5) in the shortest possible time, in order to calibrate Reference instruments using the Langley plot technique. In case of AERONET-Cimel these calibrations are subsequently transferred to the field instruments of the network in other sites through regular intercomparison campaigns. In case of the GAW-PFR, the calibration system is more complex in order to ensure traceability with the WORCC world reference. The maintenance of the AOD standard by the WORCC Calibration Central laboratory is described in Kazadzis et al. (2018). It consists

of a triad of instruments that measure continuously, and three additional portable transfer standard radiometers located at Mauna Loa (one instrument) and Izaña (two instruments) observatories. Every six months, one of the portable transfer standard radiometers visits the reference triad based at PMOD/WRC (Davos) and compares the calibration constants defined by the 6-month Langley calibrations in the two high mountain stations (Table 1 of Kazadzis et al. 2018) with the one defined by the triad. The comparison is based on the signals (voltages) and not on AOD values. The differences between the Izaña GAW-PFR radiometers and the reference triad have been always lower than 0.5%, being within the uncertainty of the Langley method plus the small possible instrument degradations that can be detected in a 6-12 month period. Such degradations are quite small and are accounted for in the calibration analysis since extraterrestrial constants are linearly interpolated between two triad visits or every 6-month periods. Additionally, the Izaña GAW-PFR "field" radiometers are calibrated on a routine basis using the Langley-plot technique for double checking quality assurance. Therefore, these radiometers cannot be considered as simple "field" instruments, but as regularly calibrated radiometers with assured traceability with the WORCC triad reference.

IZO is one of the two sites of Langley-plot calibration of both networks, which represents an advantage when comparing the two instruments, eliminating, to a large extent, errors caused by the calibration transfer. However, there are differences between the calibration methodologies used by both networks. AERONET obtains the calibration by means of the average of a few extraterrestrial constants (V_o), obtained from Langleys, performed in a relatively short time (the time needed to collect data from at least 10 morning Langley plots). However, PFR related Langleys are calculated by temporal lineal fit to a larger number of extra-terrestrial constants V_0 obtained from Langley plots performed during 6 months (Wehrli, 2000; Kazadzis et al., 2018a). Details on requirements for performing Langley calibrations of reference instruments by GAW-PFR and AERONET, and their uncertainties, are analysed in detail by Toledano et al. (2018).

4. Data and methodology used in this study

The AOD at each wavelength is obtained from the Beer-Bouguer-Lambert law (Thomason et al. 1982; WMO, 2003) for radiometers collecting spectral direct sun measurements.

$$I(\lambda) = I_0(\lambda)\exp(-\tau m) \quad (1)$$

where $I(\lambda)$ is the direct sun signal at ground level at wavelength λ, $I_0(\lambda)$ is the extraterrestrial signal of the instrument corrected by the Earth-Sun distance, and m is the optical air mass in the measurement path (Kasten and Young, 1989). A detailed description of how AOD is obtained and the determination of extraterrestrial constants by GAW-PFR and AERONET-Cimel are provided by Holben et al. (1994, 1998; 2001), Toledano et al. (2018), and Wehrli (2000; 2008b).

4.1. GAW-PFR and AERONET-Cimel data

GAW-PFR provides AOD values every 1 minute as an average of 10 sequential measurements of total duration less than 1 second (20 ms for each channel), then dark current is measured, going to the sleep

mode until the next minute. AERONET-Cimel takes a sequence of three separate measurements (1-second per filter) in one minute interval (each one every 30 seconds). This sequence of measurements is called "triplet" and it is performed every ~15 minutes for air masses lower than 2, and with higher frequency for lower solar elevations. Therefore, AERONET-Cimel provides AOD values for each triplet, at least, every ~15 minutes. Note that AERONET-Cimel performs AOD measurements interspersed with sky radiance measurements, whose duration varies throughout the day, and therefore the AOD measurements are not necessarily provided at full minutes. We consider the 1-minute data as synchronous when GAW-PFR and AERONET-Cimel AOD data were obtained with a difference of ~30 s.

GAW-PFR and AERONET-Cimel instruments use the same time reference. The synchronization between PC and GAW-PFR data-logger was performed every 12 hours since 2005, and improved to 6 hours after 2013 using NTP servers via Internet. From 2005 to 2012 the time of the AERONET-Cimel reference instruments was checked manually once per day using a handheld GPS. From 2012 onwards, the time was adjusted automatically three times per day using the ASTWIN Cimel software. In turn, the PC time is adjusted through the AEMET internal time server every 15 minutes. The AOD comparison has been performed using 1-minute synchronous data from the four closest channels of both instruments in the period 2005-2015 (more than 70000 data-pairs in each channel). Thus, in the case of GAW-PFR, the four available channels of 368 nm, 412 nm, 500 nm and 862 nm were analysed, while in the case of AERONET-Cimel, only the 380 nm, 440 nm, 500 nm and 870 nm channels were considered (Table 1). For the 500 nm channel, the nominal wavelengths of the two networks differ by a maximum of 1.8 nm. However, the nominal wavelengths in the rest of the compared channels present higher differences. Therefore, the AOD values of the original GAW-PFR 368 nm, 412 nm and 862 nm channels have been interpolated or extrapolated to the corresponding AERONET-Cimel channels (380 nm, 440 nm and 870 nm) using the Angström power law, and the GAW-PFR AE calculated from the four PFR AOD measurements.

Synchronous AE data provided by both instruments have also been compared (see section 5.5). GAW-PFR determines AE using all four PFR wavelengths (Nyeki et al., 2015), while AERONET-Cimel uses different wavelength ranges (340-440 nm, 380-500 nm, 440-675 nm, 440-870 nm, 500-870 nm) (Eck et al., 1999). As a consequence, we have calculated a new AE for the Cimel radiometer using the four channels equivalent to those of the PFR.

In this study we have used the two versions of the AERONET database. Version 2 (V2; https://aeronet.gsfc.nasa.gov/new_web/Documents/AERONETcriteria_final1.pdf; last access: 2 February 2019) has been used so far in many scientific publications in high impact journals, and Version 3 (V3) has been released just recently (Giles et al., 2019). In section 5.1., a comparison of V2 and V3 is presented. A total of three GAW-PFR and 15 AERONET-Cimel instruments have participated in this intercomparison study covering the period 2005-2015. Their corresponding reference numbers are shown in Table 2.

Table 1. Main features of the GAW-PFR (PFR (Wehrli, 2000, 2005, 2008a, b) and AERONET-Cimel (Holben et al., 1994, 1998; Torres et al., 2013) radiometers used in this study.

	GAW-PFR	AERONET-Cimel
Type of instrument	Standard version	Standard version Reference instrument
Type of observation	Automatic continuous direct sun irradiance	Automatic sun-sky tracking
Available standard channels	368, 412, 500, 862 nm	340, 380, 440, 500, 675, 870, 1020 nm
FWHM	5 nm	2 nm (340 nm), 4 nm (380 nm), 10 nm(VIS-NIR)
AOD uncertainty	± 0.01	± 0.005 (Reference instruments)
FOV (FWHM)	2.5° (1.2° plateau, 0.7° slope angle)	1.3° (slope angle unknown)
Sun tracker	Anysun tracker with a resolution of at least 0.08°	Robot specifically designed by Cimel and controlled in conjunction with the radiometer
Temperature control	Temperature controlled 20°C ± 0.5°C	Temperature correction is applied in V2. Corrections from filter-specific temperature characterization in V3 (Giles et al., 2019)
Power	Grid	Solar panels/grid
Data transmission	Local PC /FTP	Local PC / FTP Satellite transmission
Calibration	Comparison with reference triad. Additional in situ long-term Langleys	At least 10 good morning Langleys plots

4.2. Cloud filtering

The data matching in our comparison analysis was performed with synchronous 1-minute AOD values of both networks labelled with quality control (QC) flags that guarantee proven quality data not affected by the presence of clouds. In the case of the AERONET-Cimel network, the selected AOD data are Level 2 data from both V2 and V3 AERONET databases, which have been cloud filtered by the Smirnov algorithm (Smirnov et al., 2000), based on the triplet method, with a second-order temporal derivative constraint (McArthur et al., 2003), and visually screened in V2. The cloud screening in AERONET V3 has been completely automated, and notably improved, especially by refining the triplet variability and cirrus cloud detection and removal (Giles et al., 2019). GAW-PFR cloud screening algorithms also use the Smirnov triplet measurement, and the second-order derivative check, but add a test for optically thick clouds with $AOD_{500nm} > 2$ (Kazadzis et al., 2018b). In the case of the GAW-PFR network (Wehrli, 2008a) the flags take

the value 0 (cloudless conditions, no wavelength crossings and sun pointing within certain limits, more details in Kazadzis et al. (2018a)) for all those selected records.

Table 2. GAW-PFR and AERONET-Cimel instrument numbers used in this study in the period 2005-2015. Data from Reference Cimel #398 was not upgraded to Level 2 in V3 during the period 12 July 2008 - 15 September 2008.

Instruments used in this study	Period 2005-2009	Period 2010-2015
GAW-PFR	2 instruments: #6,#25	2 instruments: #6,#21
AERONET-Cimel	13 instruments: #25,#44,#45,#79,#117,#140 #244,#245,#380,#382,#383,#398,#421	5 instruments: #244, #347, #380 #421, #548

4.3. WMO traceability criteria

The criterion for traceability used in this study follows the recommendation of the WMO (WMO, 2005) which states that 95% of the AOD measurements fall within the specified acceptance limits, taking the PFR as a reference:

$$U_{95} = \pm(0.005 + 0.010/m) \quad (2)$$

where m is the optical air mass. Note that the U95 range is larger for smaller optical mass. The acceptance limits proposed by WMO take into account, on the one hand, the uncertainty inherent in the calculations of the AOD, and on the other hand, the uncertainty associated with the calibration of the instrument. The latter, for the case of instruments with finite field of view direct transmissions, such as the PFR and the Cimel, is dominated by the influence of the top-of-the-atmosphere signal determined by Langley plot measurements, divided by the optical air mass. The first term of Eq. 2 (0.005) represents the maximum tolerance for the uncertainty due to the atmospheric parameters used for the AOD calculation (additional atmospheric trace gas corrections, and Rayleigh scattering). The second term describes the calibration related relative uncertainties. The WMO recommends an upper limit for the calibration uncertainty of 1%.

4.4. Modelling the impact of near-forward scattering on the AOD measured by the PFR and Cimel radiometers

In order to study the impact of near-forward scattering on the irradiance measured by the PFR and Cimel instruments, a forward Monte Carlo model (Barker 1992, Barker 1996, Räisänen et al. 2003) was employed. For the present work, the model was updated to account for the finite width of the solar disk. The starting point of each photon was selected randomly within the solar disk, assuming a disk half-width of 0.267° and the impact of limb darkening on the intensity distribution was included following Böhm-Vitense (1989). Some diagnostics were also added to keep track of the distribution of downwelling photons at the surface with respect to the angular distance from the centre of the sun. Gaseous absorption was

accounted for following Freidenreich and Ramaswamy (1999), while the Rayleigh scattering optical depth was computed using Bodhaine et al. (1999).

5. Results

5.1. Comparison of long-term AERONET V2 and V3 datasets at Izaña site

Since V3 has been released recently (Giles et al., 2019), we present a comparison between V2 and V3 for the Cimel channels 380 nm, 440 nm, 500 nm and 870 nm for the period 2005-2015. The results indicate that for the Izaña site the agreement and consistency between the two AERONET versions is very high for the four channels (R^2>0.999) in full agreement with the results of the V2-V3 comparison reported by Giles et al. (2019). It follows that the results of the comparison between GAW-PFR and the two versions of AERONET are very similar as shown throughout this work. A detailed description of AERONET V3 and its improvements with respect to V2 is given in Giles et al. (2019). As such improvements depend on aerosol type, according to the changes introduced in V3, for the high mountain site such as Izaña characterized by low background AOD values or, alternatively, by the presence of dust (no pollution or biomass burning aerosols), the AOD differences between V2 and V3 are expected to be minimum as is confirmed in this study (Figure 1).

However, it should be noted that AERONET V3 does not restrict the calculation of AOD to optical masses less than 5.0 (Giles et al., 2019), as V2 does. This results in an increase in the number of solar measurements occurring in the early morning and the late evening. Consequently, the GAW-PFR comparisons with AERONET V3 consisted of ~ 5000 more data pairs than the GAW-PFR comparison with V2 (see Supplement S.1.1.).

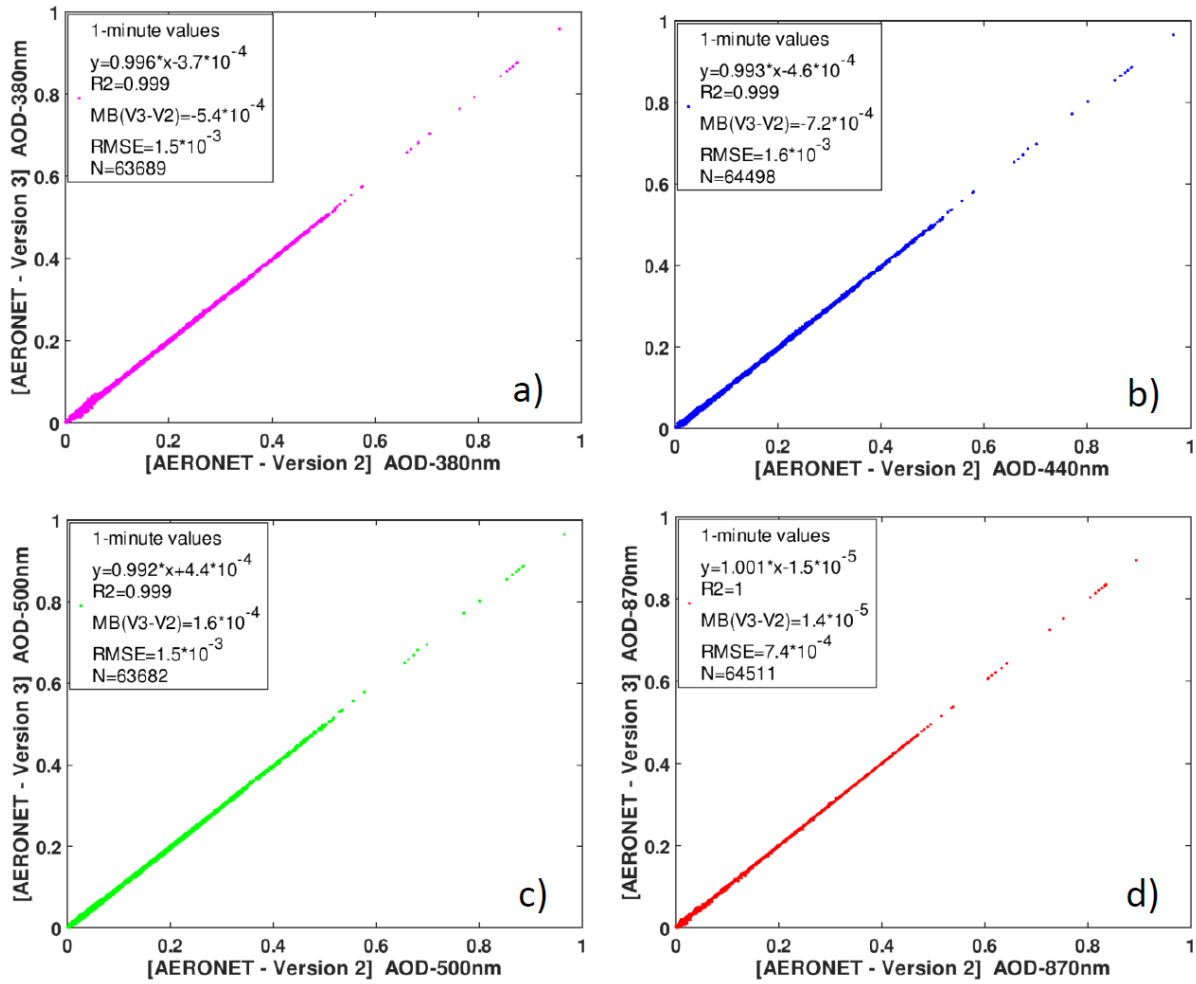

Figure 1. AERONET Version 3 (V3) vs Version 2 (V2) AOD 1-minute data scatterplot at Izaña Observatory for the period 2005-2015: a) 380 nm; b) 440 nm; c) 500 nm and d) 870 nm. The corresponding equations of the linear fits, the coefficients of determination (R2), Mean Bias (MB), Root Mean Square Error (RMSE) and the number of data pairs (N) used are included in each legend.

5.2. AERONET-Cimel AOD comparison with GAW-PFR data

The comparison with GAW-PFR AOD shows that the AOD from AERONET-Cimel radiometers meet the WMO traceability criteria ("traceable AOD data" from now on) at 440 nm, 500 nm and 870 nm channels. The lowest agreement is found in the UV channel (380 nm) with 92.7 % of the data, and the highest in the infrared channel (870 nm) with 98.0 % for V2 (Figure 2; Table 3). Almost identical results are obtained for V3 (Supplement S1 and S2). However, in the first half of the comparison period (2005-2009) there were some mechanical problems in the solar tracker where the GAW-PFR was mounted on, which caused sporadic problems of sun pointing. This finding was confirmed with data from the four–quadrant silicon detector (Wehrli, 2008a) that showed diurnal variation of the PFR sensors position up to 0.3°. From 2010 onwards, the PFR was mounted on an upgraded solar tracker of higher performance and precision. This reduced problems in sun pointing, that were the main cause of most of the AOD discrepancies between PFR and Cimel, and therefore not attributable to the instruments themselves.

In addition, since 2010, Cimel #244 has been in continuous operation for most of the time at the Izaña Observatory, greatly simplifying calibration procedures and the corresponding data evaluation, and

minimizing errors of calibration uncertainties introduced by the use of a high number of radiometers in the intercomparison. During the 2010-2015 period, the fraction of traceable AOD measurements of the total between the AERONET-Cimel radiometer and the GAW-PFR improves to 93.46 % in the 380 nm channel, and this percentage rises to 99.07 % for the 870 nm channel. Despite the technical differences between both radiometers, described above, and the different calibration protocols, cloud screening and data processing algorithms, the data series of both instruments, can be considered as equivalent, except for 380 nm, according to the WMO traceability criteria defined previously (Eq. 2). This explains the excellent agreement in the long-term AOD climatology shown for GAW-PFR and AERONET-Cimel in Toledano et al. (2018).

We have compared the percentages of AERONET-Cimel AOD V2 data meeting the WMO criteria for the four interpolated GAW-PFR channels with those of AERONET V3 (Table 3). A more detailed statistical evaluation for different scenarios of aerosol loading (three ranges of AOD) and aerosol size (three ranges of AE) for each compared channel has been performed (see Table 4). We observe that the poorest agreement is obtained at the shorter wavelength channels (440 nm, and especially 380 nm). Kazadzis et al. (2018b) also found a decrease in the percentage of AOD meeting the WMO criteria for 368 nm and 412 nm spectral bands during the Fourth WMO Filter Radiometer Comparison for aerosol optical depth measurements. As these authors pointed out, the shorter the wavelength, the poorer the agreement because of several reasons: AOD in the UV suffers from out-of-band or at least different blocking of the filters, small differences in central wavelength or FWHM have a larger impact, the Rayleigh correction is more critical, and NO_2 absorptions are treated differently. Regarding the effect of the aerosol load and particle size on the AOD differences, our results confirm the decrease of agreement between the two instruments for very large particles coincident with almost pure dust ($AE \leq 0.3$), and high turbidity conditions ($AOD > 0.1$). However, it should be noted that the percentage of data pairs in these situations is relatively low (e.g., 6% for $AOD > 0.1$, and 3.2% for $AE > 0.25$ at 380nm) with respect to the total data (Table 4). A similar result was reported by Kim et al. (2008), who attributed these discrepancies to the possible spatial and temporal variability of aerosols under larger optical depths in addition to the effect of the different FOV of both radiometers. In our case, and according to previous studies on AOD climatology at IZO (Barreto et al., 2014), the presence of high mineral dust burden when the station is within the SAL, does not necessarily imply lower atmospheric stability conditions resulting in daily AOD means with greater standard deviation. For these reasons, we assumed that the different FOV of these instruments is the main cause of part of the AOD 1-minute differences outside the U95 limits, under high AOD conditions. This issue is specifically addressed in Section 5.3.

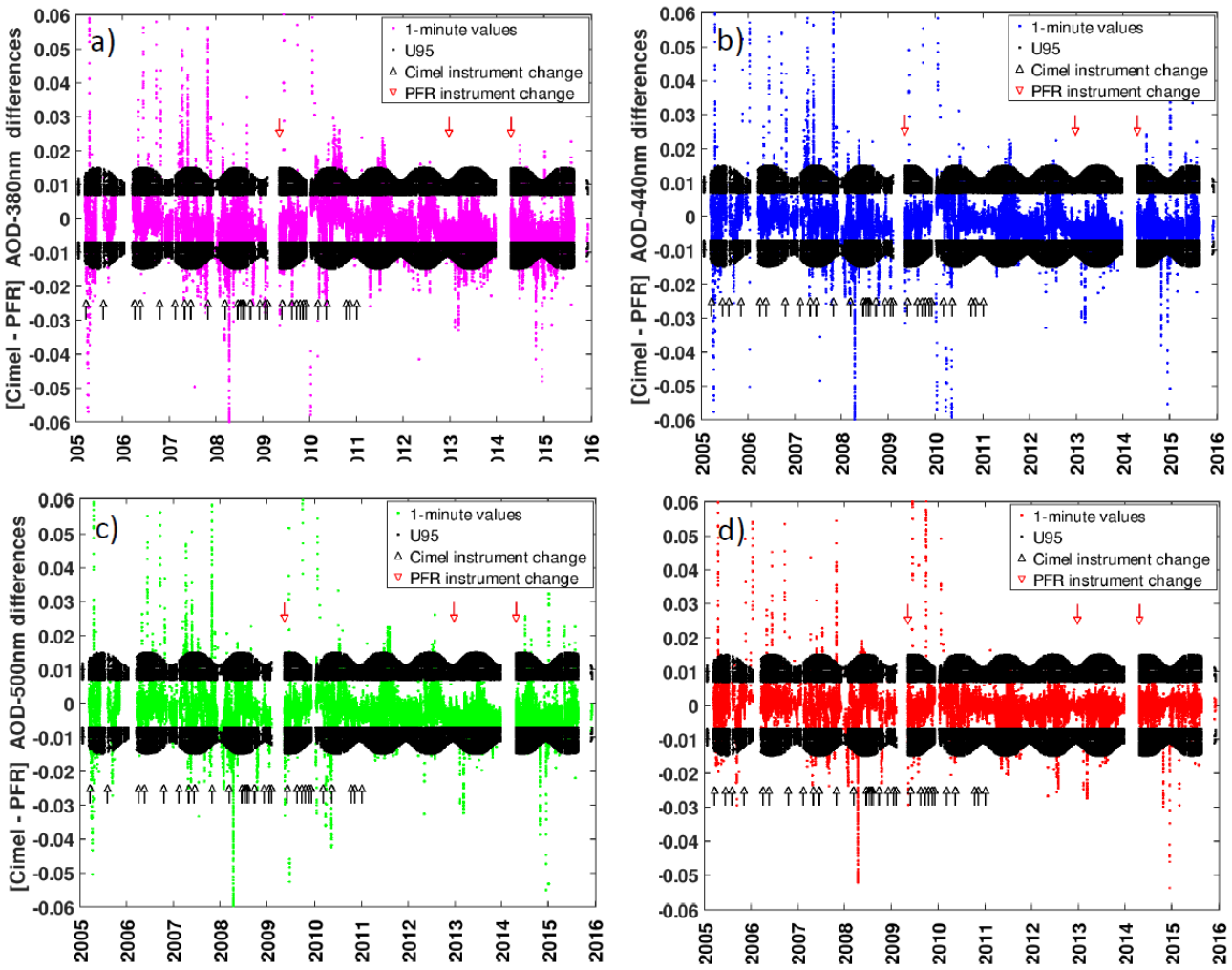

Figure 2. One-minute AOD data differences between AERONET-Cimel (V2) and GAW-PFR for (a) 380 nm (70838 data-pairs), (b) 440 nm (71645 data-pairs), (c) 500 nm (70833 data-pairs) and (d) 870 nm (71660 data-pairs) for the period 2005-2015. Black dots correspond to the U95 limits. A small number of outliers are out of the ±0.06 AOD differences range. Black arrows indicate a change of Reference AERONET-Cimel radiometer and red arrows indicate a change of the GAW-PFR instrument.

Table 3. Percentage of AERONET-Cimel (V2 and V3) 1-minute AOD data meeting the WMO criteria for the four interpolated GAW-PFR channels for the period 2005-2015.

Channel	V2 (%)	V3 (%)
380 nm	92.7	92.3
440 nm	95.7	95.2
500 nm	95.8	95.7
870 nm	98.0	97.8

Table 4. Percentage of AERONET-Cimel 1-minute AOD data (V2) meeting the WMO criteria for the four compared channels, and different AOD and AE scenarios for the period 2005-2015, number of data pairs are shown in brackets. The last row corresponds to the total percentages for the sub-period 2010-2015. AOD and AE traceability > 95% are marked in bold. Number of data pairs are in brackets.

% of data within WMO limits	380 nm	440 nm	500 nm	870 nm
AOD ≤ 0.05	94.4 (57008)	**96.8 (59130)**	**97.0 (58572)**	**98.5 (60191)**
0.05 < AOD ≤ 0.10	91.0 (4723)	93.1 (4850)	92.8 (4817)	94.2 (4908)
AOD > 0.10	75.0 (3938)	86.5 (4615)	85.1 (4466)	**95.9 (5118)**
AE ≤ 0.25	73.1 (2145)	82.3 (2417)	80.1 (2351)	**96.2 (2824)**
0.25 < AE ≤ 0.6	91.2 (5407)	**96.2 (5810)**	**96.0 (5691)**	**97.9 (5911)**
AE > 0.6	94.6 (55114)	**96.9 (57089)**	**97.0 (56504)**	**98.7 (58146)**
Total 2005-2015	92.7 (65669)	**95.7 (68595)**	**95.8 (67855)**	**98.0 (70217)**
Total 2010-2015	93.5 (41977)	**97.4 (43745)**	**97.2 (43627)**	**99.1 (44498)**

In general, the agreement obtained with the 1-minute AOD data is slightly lower than that obtained during short campaigns, such as those reported by Barreto et al. (2016) at IZO (5566 data-pairs), with agreements > 99 % for AOD_{870nm} and AOD_{500nm}. However, our results for AOD_{500nm} (> 95 % of 70833 data-pairs) are significantly better that that observed by Kazadzis et al. (2014) (~ 48 % of 468 data-pairs) covering a relatively narrow range of AOD. In addition, short-term campaigns usually cover a small range of AOD, and instruments are carefully and frequently supervised. On the contrary, during our intercomparison over a period of 11 years, the operation of the instruments can be considered as the normal operation of such a system. An additional interesting aspect of this study is that it is not a simple intercomparison exercise between two instruments but a comparison of a number of instruments that acted as reference instruments for the AERONET/Europe Network.

Table 5. Basic skill-scores from the AOD intercomparison between GAW-PFR and AERONET-Cimel V2 for the period 2005-2015. The skill scores definitions are found in Huijnen and Eskes (2012).

Period	2005-2015			
Wavelengths (nm)	380	440	500	870
Mean Bias (MB)	-0.0026	-0.0018	-0.0021	-0.0001
Modified Normalized Mean Bias (MNMB)	-0.1301	-0.1046	-0.1474	0.0129
Fractional Gross Error (FGE)	0.1727	0.1546	0.1918	0.1837
Root Mean Square Error (RMSE)	0.0081	0.0070	0.0064	0.0049

Pearson's correlation coefficient (r)	0.9910	0.9925	0.9939	0.9949
Number of data-pairs	70838	71645	70833	71660

In the first period (2005-2009), a total of 13 Cimel radiometers were used, while in the second period (2010-2015), five Cimel radiometers have participated, and for much of this period, the Cimel #244 was operating as the permanent AERONET reference instrument at IZO. Once the most important causes of non-traceability in the first period, which were associated with a poor pointing of GAW-PFR due to problems in the sun-tracker, were discounted, we can conclude that there are no significant differences in the percentages of traceable data between the two periods. This means that the continuous change of Reference Cimel instruments used in the 2005-2009 period did not have a significant impact on AOD data comparison differences. This provides proof of the consistency and homogeneity of the long AERONET-Cimel AOD data series, and their comparability with the GAW-PFR AOD data series, regardless of the number of instruments used to generate these data series. In our study, with a number of comparison data-pairs one or two orders of magnitude higher than those used in short campaigns, the results shown in Table 4 can be considered as fairly good.

In addition to the traceability scores, we have introduced some basic skill scores corresponding to the AOD intercomparison between GAW-PFR and AERONET-Cimel for the period 2005-2015 (Table 5) to be in line with previous studies that have performed short-term comparisons between these two instruments. The definitions of the used skill scores can be found in Huijnen and Eskes (2012). The Pearson's correlation coefficient (r) values of the PFR-Cimel 1-minute AOD data-pairs are higher than 0.99 in all channels. Concerning Mean Bias (MB) and Root Mean Square Error (RMSE) associated with AOD differences, our results show quite similar skill scores to those found at Mauna Loa, USA for AOD_{500nm} (Kim et al., 2008), although the number of data pairs used at IZO (~71000) is much higher, and the AOD range of our study is much larger than that of the comparison performed in Mauna Loa. Kim et al. (2008) summarize results of previous short-term intensive studies (McArthur et al., 2003; Mitchell and Forgan, 2003; Kim et al., 2005; Schmid et al., 1999) carried out in stations where the radiometers were calibrated by intercomparison with Reference instruments. These results show MB values to be within 0.01 bias, one order of magnitude lower than in Mauna Loa and Izaña Observatories, highlighting the importance of having well calibrated instruments to carry out these type of comparisons. For the period 2010-2015 (not shown here), as expected, the RMSE and the Pearson's correlation improve slightly compared with the whole period 2005-2015.

5.3. Non-traceability assessment

As presented in Table 3, data outside the WMO traceability criteria vary from 2% for 870 nm up to 7.3% for 380 nm. In this section, the different possible causes of non-traceability in AOD are evaluated and, if possible, quantitatively estimated. In order to assess the relevance and quantitative impact of these causes, and estimate errors derived from a non-perfect AOD data synchronization, we first made an analysis on the natural variability of AOD in a very short time period (1 minute) shown below.

5.3.1. Short-time AOD variability

In order to determine the variability of AOD within one minute, we have performed two independent analyses with AOD data from the PFR and Cimel for the 368/380 nm and 501/500nm channels during one year (2013). On the one hand, and taking into account that GAW-PFR provides AOD every minute, we have calculated all the AOD differences for each channel in the successive minutes. So we have the variation of AOD from one minute to the next one during a whole year. On the other hand, for AERONET-Cimel, we have taken advantage of the triplets, since each triplet consists of three successive measurements made in one minute . In this case, the strategy has been to calculate the standard deviation of the triplet AOD measurements during a whole year. We have verified that the AOD variability in 1 minute is independent of AOD (see Supplement S3).

Table 6. Percentage of AOD data with variability within 1 minute less than 0.01 and 0.005, respectively, using AOD data from GAW-PFR (at 368 and 501nm) and AERONET-Cimel (at 380 and 500 nm) for 2013. A total of ~32000 data-pairs per channel have been used from GAW-PFR, and 20117 triplets (60351 individual AOD measurements) from the Cimel#244 to calculate the AOD variability.

GAW- PFR Percentage of data with 1-minute AOD variability (%)		
	368 nm	501 nm
< 0.01	99.88	99.91
< 0.005	99.21	99.35
AERONET-Cimel Percentage of data with 1-minute AOD variability (%)		
	380 nm	500 nm
< 0.01	99.87	99.99
< 0.005	99.82	99.42

The results obtained on the AOD variability in 1-minute from PFR data are very similar and consistent to those obtained with Cimel. Less than ~ 0.8% of the AOD data show variability higher than 0.005 in all wavelength ranges. It should be noted that the possible instrumental noise is included in this variability, so that the actual natural AOD variability would be, in any case, lower than that expressed in Table 6. The percentage of data with 1-minute AOD variability for all four GAW-PFR channels are given in Supplement S3. These results indicate that the natural AOD variability is very low thus the non-ideal measurement synchronization cannot explain the percentages of non-traceable AOD cases shown in Tables 3 and 4.

5.3.2. Uncertainties of GAW-PFR channel interpolation to AERONET-Cimel channels

The interpolation of the CIMEL AODs to the PFR AOD wavelengths can be one of the sources of uncertainty in this comparison assessment. The greatest uncertainty arises in the extrapolation of the $AOD_{412\ nm}$ of the PFR to the Cimel wavelength 440 nm. Using the Angström formula we have calculated that for an uncertainty of ±0.5 in the AE the introduced uncertainty in the AOD extrapolation from 412 nm to 440 nm is ~5% (i.e., 0.005 for AOD_{412nm}=0.1). The introduced uncertainty in AOD extrapolation is reduced to ~2% for an uncertainty of ±0.3 in AE. For all other AOD interpolations the errors are smaller.

5.3.3 Calibration related errors

As described in Section 3, the calibration procedures of the AERONET-Cimel and GAW-PFR radiometers are different. While in the case of GAW-PFR, frequent calibrations are established throughout the year and the calibration value is linearly interpolated in time, in AERONET- Cimel a constant calibration value is assumed in the intermediate period between two consecutive calibrations carried out on an annual basis. The typical calibration uncertainty for a single Langley plot is 0.7-0.9 % (at the 95 % confidence level), and it is reduced to 0.4 % in the case of IZO when averaging at least 10 Langley-derived extraterrestrial constants (which is the normal procedure) (Toledano et al., 2018). Regarding the GAW-PFR radiometers operated at IZO, a direct yearly comparison of the Langley based V_o's with the reference triad at PMOD/WRC showed differences lower than 1 % for all channels for the 2005-2015 period.

A not sufficiently accurate determination of the calibration constant results in a fictitious AOD diurnal evolution presenting a concave or convex characteristic curve due to the calibration error dependence on solar air mass. The largest error occurs in the central part of the day (lower air masses), mainly, in clean days with very low aerosol load (< 0.02 in 500 nm) as reported by Romero and Cuevas (2002) and Cachorro et al. (2004), and as can be derived from Equation 2. According to Cachorro et al. (2004, 2008) fictitious differences of up to 0.06 between the minimum and the maximum AOD can be recorded in a day with constant AOD as a result of a non-accurate calibration or non-cleaned instruments. However, these fictitious differences in AOD depend on the related calibration magnitude errors.

We have represented the AOD differences between GAW-PFR and AERONET-Cimel versus optical air mass for the four channels for pristine conditions ($AOD_{500nm} \leq 0.03$) for both V2 and V3 (See Supplement S4). It should be noted that although the few outliers are evenly distributed throughout the whole airmass range, they are not equally distributed with respect to the zero of the AOD difference, but there is a bias with positive large outliers (higher Cimel AOD), already reported by Nyeki et al. (2013), and small negative outliers for optical air mass lower than 2.

The total percentage of AOD traceable data pairs under pristine conditions ($AOD_{500nm} \leq 0.03$) is very high for all wavelengths (> 97.7 %) falling within the *U*95 limits (Table 7), except for 380 nm. There is no dependence on 1-minute AOD differences with optical air mass for 440, 500 and 870 nm, and a slight dependence for 380 nm (Table 7) with higher percentage of AOD differences outside the U95 limits at

lower optical air masses. For the extended range of optical mass > 5 in V3, the AOD differences do not increase with optical mass (Supplement S5). The lower traceability at 380 nm for low air masses is especially clear in V3 with 92.9% of traceable data (See Supplement S5). This result is consistent with the fact that the highest uncertainty in the determination of the calibration constants is observed in the UV range, and the lowest uncertainty in the near-infrared channel (Eck et al., 1999; Jarosyawski et al. 2003; Toledano et al., 2018). This is attributable to an imperfect calibration, or to very small changes in the filters' transmittance, that can only be detectable in extreme conditions: UV range, very low optical air mass, and pristine conditions. According to Toledano et al. (2018), the greatest variance in the extraterrestrial constant in the UV channel could be due to a number of factors: 1) higher AOD variability at the shorter wavelengths; 2) filter blocking issues; and 3) temperature effects affecting AERONET-Cimel instruments that have not been accounted for in the UV range.

Table 7. Percentage of 1-minute AOD data (V2) meeting the WMO criteria for each wavelength for different optical air mass intervals under pristine conditions ($AOD_{500nm} \leq 0.03$) in the period 2005-2015. See Supplement S5 for equivalent results with V3.

Percentage of AOD differences within the U95 limits AOD500*nm*≤ 0.03	Total (%)	1 ≤ m < 2 (%)	2 ≤ m < 3 (%)	3 ≤ m < 4 (%)	4 ≤ m < 5 (%)
380 nm	95.8	94.5	96.0	97.4	97.2
440 nm	97.9	97.9	97.7	98.2	97.7
500 nm	98.3	98.4	98.1	98.6	98.4
870 nm	99.2	99.4	99.3	99.2	98.6

The correct cause attribution of each outlier would require manual inspection and additional specific information on instrumental checking and maintenance information that is not always available. We have investigated in more detail the origin of the outliers and whether one of the two instruments predominantly caused them. Thus, we have calculated for the non-traceable AOD data the diurnal range of AOD variation (maximum value minus minimum value of AOD in one day) at 380 nm for each instrument under pristine conditions (Figure 3) using Cimel AOD_{500nm} daily mean < 0.03 to select the pristine days. According to this approach, the instrument that shows the highest daytime AOD range is the one that is responsible for the outlier. As the wavelength increases both the number of outliers and the magnitude thereof decreases significantly (Supplement S6). Then, we identified those outliers with a diurnal AOD range higher than 25% of the mean daily AOD value and investigated their possible causes. A total of 51 cases for GAW-PFR and 81 cases for AERONET Cimel V3 were obtained and analysed in detail, using auxiliary information, such as 1-minute in-situ meteorological data, 5-minute all-sky images, 1-minute BSRN data, and satellite imagery (not shown here). We obtained the percentage of AOD outliers of GAW-PFR and AERONET Cimel (V3) for which a certain cause has been identified, such as calibration uncertainties, cloud screening algorithm failures, mixture of the two previous causes, poor sun pointing, or not well-

defined causes (electronic problems, humidity inside the lenses, filter dirtiness, obstruction of the lenses collimators, insects on the optics outside, etc.) (see Supplement S7).

From the analysis of these cases, under the conditions described above, it should be noted that ~ 44% of the cases with fictitious AOD diurnal cycles were due to small uncertainties in the calibration of AERONET-Cimel (V3), while for this same cause ~ 8% of cases were identified in GAW-PFR. Some examples of AOD non-traceability for both AERONET-Cimel and GAW-PFR in the ~380 nm channel are shown in Supplement S8. The fictitious diurnal AOD cycle is mainly visible in the UV channels as shown in the examples reported in Supplement S9. Note that the fictitious diurnal AOD can be more easily identified under very low AOD conditions.

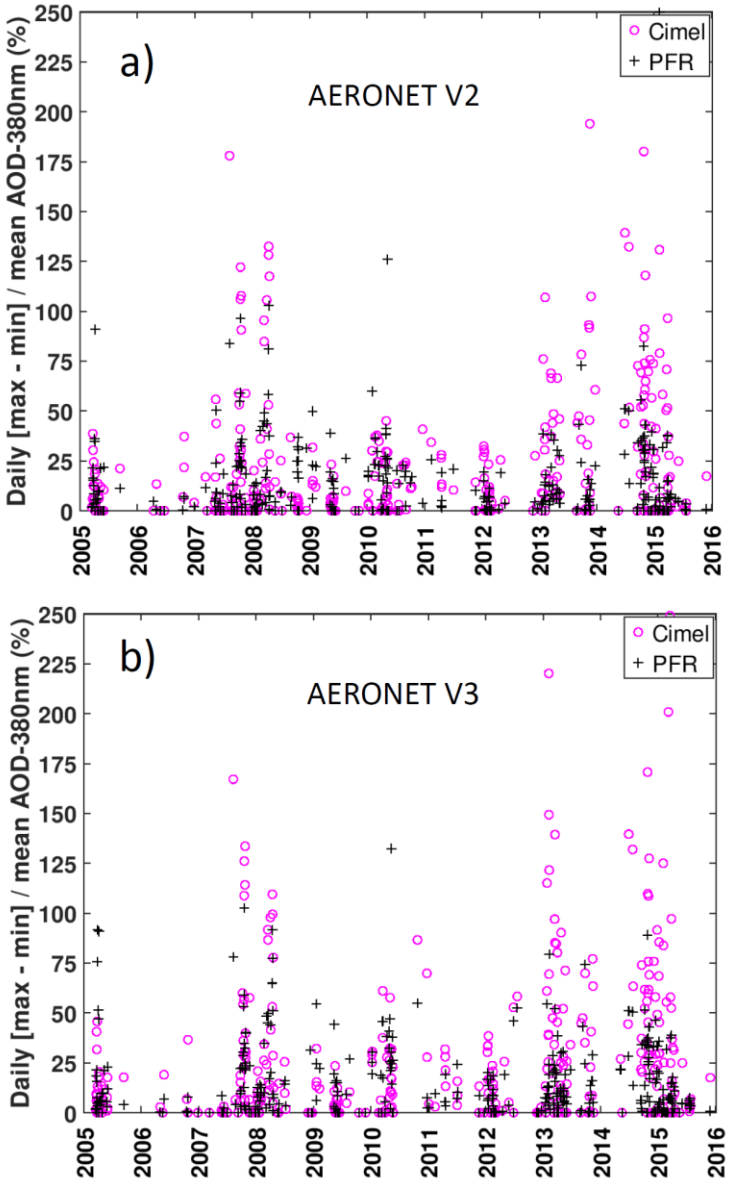

Figure 3. AOD diurnal range variation (maximum value minus minimum value of AOD in one day) at 380nm corresponding to AOD outliers (non-traceable AOD) under pristine conditions ($AOD_{Cimel\text{-}500nm} \leq 0.03$) in the period 2005-2015 for AERONET V2 (a) and V3 (b).

5.3.4. Differences in cloud-screening and sun tracking

We have examined the effect that the presence of clouds might have on AOD differences and the percentage of cases outside the U95 limits. The impact of clouds on AOD differences only occurs when both GAW-PFR and AERONET-Cimel cloud screening algorithms fail to identify clouds in the direct sun path. In order to assess the impact that cloud conditions might cause on AOD traceability, we have used the concept of daily fractions of clear sky (FCS) that has been applied before to solar radiation data at IZO (García et al., 2014). FCS represents the percentage of observed sunshine hours in a day with respect to the maximum possible sunshine hours in that day. The higher the daily FCS, the higher the clear sky percentage we have on that day. The percentages of traceable and non-traceable AOD data versus FCS values grouped into five intervals are shown in Table 8. It should be emphasized that the number of cases linked with FCS between 0% and 60% are less than 2% of the total cases. As the fraction of clear sky increases, the percentage of traceable AOD data significantly exceeds the number of non-traceable AOD data. The percentage of traceable data is especially large (> 90 %) when FCS > 80 % (almost clear skies).

This is the FCS range in which a significant percentage of days with cases presenting scattered clouds are recorded, which qualitatively confirms that V3 has introduced more efficient cloud screening than V2. However, the real impact of clouds on AOD traceability at IZO is very low due to its special characteristics of a high mountain station with very little cloudiness. Therefore, in practice, the possible impact of clouds on the non-traceability of AOD data-pairs is insignificant at IZO. GAW-PFR and AERONET-Cimel cloud screening algorithms provide successful identification on clear direct-sun conditions during cloudy skies (FCS < 40 %) for 99.75 % of the cases, excluding those with very thin clouds.

In the particular case of Izaña there are some very specific cloud scenarios in which cloud screening algorithms could fail resulting in non-AOD traceability: 1) Altostratus above the top of the SAL, at ~6 Km altitude (see Supplement S10); 2) Cirrus clouds (see Supplement S11); and 3) low clouds (stratocumulus) that sometimes exceed the observatory height level (see Supplement S11). As can be deduced from the analysis of these cloud cases, the impact of the different types of clouds on AOD retrieval is very complex and further specific investigations are required in order to understand the reasons behind failures in the GAW-PFR and AERONET-Cimel cloud screening algorithms.

Table 8. Percentage of AOD data within the U95 limits for each channel and 5 daily fractions of clear sky (FCS) intervals. In brackets, relative frequency of each FCS interval for AERONET V2 and V3, respectively. In bold, the percentages of V3 that are greater than those of V2.

	380 nm		440 nm		500 nm		870 nm	
	V2	V3	V2	V3	V2	V3	V2	V3
0%≤FCS<20% (0.03%) (0.04%)	47.6	44.4	43.5	44.4	47.6	44.4	87.0	**92.6**
20%≤FCS<40% (0.22%) (0.22%)	69.3	**76.6**	73.3	**82.2**	73.6	**80.8**	86.3	**94.1**
40%≤FCS<60% (1.08%) (1.09%)	79.1	77.5	87.8	84.8	88.8	87.2	91.9	**92.0**
60%≤FCS<80% (7.10%) (7.17%)	88.4	**89.6**	93.9	93.9	93.4	**94.4**	97.8	97.6
FCS≥80% (91.6%) (91.5%)	93.3	92.8	96.2	95.6	96.2	96.1	98.3	98.1

5.3.5. Rayleigh scattering, absorption by O_3 and NO_2 corrections

In this section, we evaluate the possible impact on the 1-minute AOD data outside the *U*95 limits due to the different processing of each network regarding the correction by Rayleigh scattering and by the light absorption of column O_3 and NO_2. Although GAW-PFR and AERONET-Cimel use spectral channels with weak absorption by atmospheric gases, AOD can only be determined if optical depth contributions from those gases are well estimated and subtracted from the total optical depth (τ). GAW-PFR and AERONET-Cimel separate the contributions of the molecules (Rayleigh scattering, τ_R), aerosols (τ_a; in this study referred to as AOD) and absorbing gases: total column ozone (τ_{O3}) and nitrogen dioxide (τ_{NO2}) due to their different optical air masses at low solar elevation:

$$I(\lambda) = I0(\lambda)\exp-(\tau_R m_R + AOD m_a + \tau_{O3} m_{O3} + \tau_{NO2} m_{NO2}) \quad (3)$$

So, AOD can be derived from:

$$AOD = \frac{1}{m_a}(ln\frac{I_0(\lambda)}{I(\lambda)} - \tau_R m_R - \tau_{O3} m_{O3} - \tau_{NO2} m_{NO2}) \quad (4)$$

5.3.5.1 Rayleigh scattering

The Rayleigh scattering contribution to total optical depth would be:

$$\tau_R = \delta_R \frac{m_R}{m_a} \quad (5)$$

where, m_R is calculated, according to Kasten and Young (1989):

$$m_R = \frac{1}{sin\theta + 0.50572(\theta + 6.07995)^{(-1.6364)}} \quad (6)$$

and m_a, according to Kasten (1966), has the following expression:

$$m_a = \frac{1}{sin\theta + 0.0548(\theta + 2.65)^{(-1.452)}} \quad (7)$$

where θ is the sun elevation, and δ_R can be expressed as (Bodhaine et al., 1999):

$$\delta_R(\lambda) = 0.00864\lambda^{-(3.916+0.074\lambda+\frac{0.050}{\lambda})}\frac{P}{P_o} \quad (8)$$

where P_o = 1013.25 hPa, λ is the wavelength in microns (μ) and P is the pressure in hPa at the measurement site. The depolarization factor recommended by (Young, 1980) is already included in Eq. 8. From Eq. 8, we can derive the differences in τ_R contribution ($4\tau_R$):

$$\triangle\tau_R = (0.00864\lambda^{-(3.916+0.074\lambda+\frac{0.050}{\lambda})}\frac{1}{1013.25}\frac{m_R}{m_a})(P_{PFR} - P_{Cimel}) \quad (9)$$

Accordingly, the main $\Delta\tau_R$ from GAW-PFR and AERONET-Cimel can arise from the different way the two instruments obtain the atmospheric pressure (P_{PFR} and P_{Cimel}, respectively). While AERONET-Cimel obtains the site station pressure from the National Centers for Environmental Prediction (NCEP) and the National Center for Atmospheric Research (NCAR) reanalysis at standard levels, GAW-PFR has a solid-state pressure transducer in the control box to read barometric pressure simultaneously with each PFR measurement. As Giles et al. (2018) have stated, the expected error in the station pressure P_{Cimel} is generally < 2 hPa provided the elevation of the station is well-known and the weather conditions are stable. In order to assess this possible difference, we have compared the 1-minute synchronous pressure data of both instruments, and the corresponding 1-minute $\Delta\tau_R$ from Eq. 9. Note that, in practice, this comparison is performed at 6-hour intervals since the NCEP/NCAR reanalysis data are available routinely with this temporal resolution (Kalnay et al., 1996). The results are depicted in Figure 4.

The results indicate that most of the 1-minute pressure differences are within ± 5 hPa (Figure 4a), resulting in 1-minute $\Delta\tau_R$ data within ± 0.001. However, when pressure differences are significantly higher, such as those registered at the end of 2014 (> 30 hPa) (Figure 4a), $\Delta\tau_R$ increases significantly (~ 0.01) (Figure 4b). However, it should be noted that only 99 AOD data pairs have been registered for which the pressure difference between PFR and Cimel is greater than 20 hPa at 870nm and 440nm, and one AOD data pair at 500nm and 380nm channels. Taking into account that the accuracy of the new barometers built into new radiometers is ~3 hPa only dramatic barometer malfunctioning could cause $\Delta\tau_R$ > 0.01. As stated by Kazadzis et al. (2018b), the use of erroneous pressure values can lead to wavelength-dependent AOD errors and to large errors in AE. However, these flagrant barometer malfunctions are quickly detected and easily corrected if there are other pressure measurements at the station, as is the case in Izaña.

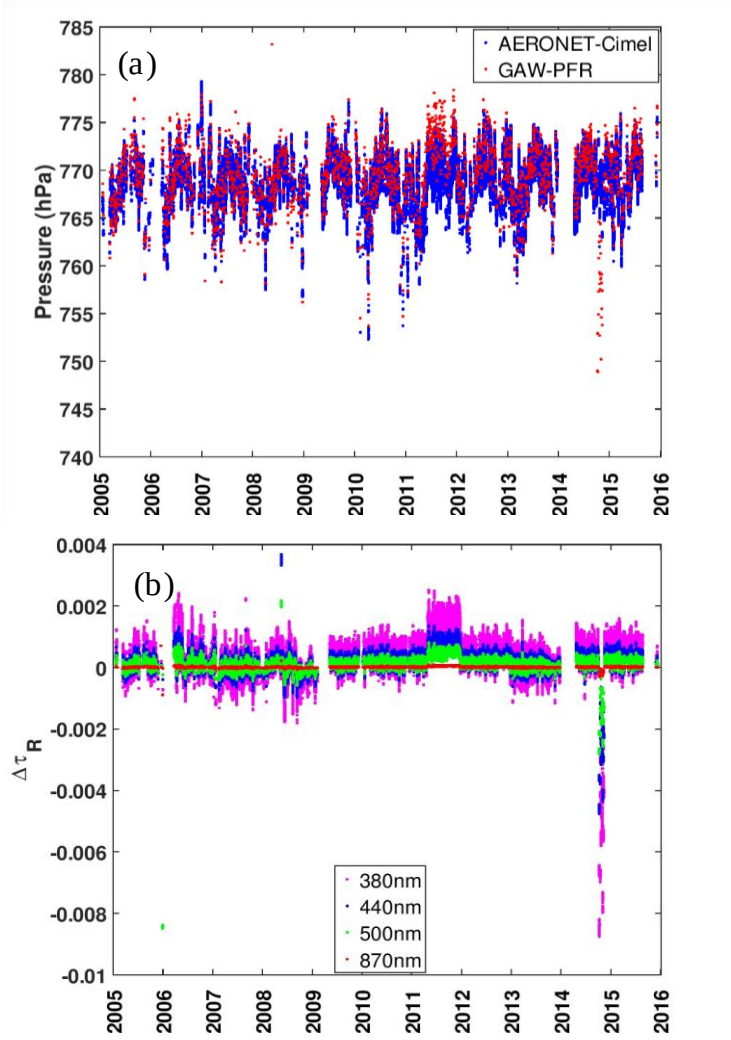

Figure 4. (a) 1-minute pressure data (hPa) from GAW-PFR and 6-hour pressure data at Izaña Observatory altitude from the National Centers for Environmental Prediction (NCEP) and the National Center for Atmospheric Research (NCAR) reanalysis for the case of AERONET-Cimel, and (b) corresponding 1-minute $\Delta\tau_R$ caused by pressure differences in the period 2005-2015.

5.3.5.2 Differences in O_3 absorption

The O_3 related optical depth is determined with the following expression:

$$\tau_{O3}(\lambda) = \sigma_{O3}(\lambda)\frac{O_3}{1000}\frac{m_{O3}}{m_a} \quad (10)$$

Where O_3 is expressed in Dobson units (DU), and the absorption coefficients ($\sigma_{O3}(\lambda)$) take the following values (Gueymard, 1995): 0.0026 cm^{-1} (440 nm), 0.03150 cm^{-1} (500 nm), and 0.00133 cm^{-1} (870 nm). The ozone absorption is maximum in the 500 nm channel and practically zero in the 380 nm channel. GAW-PFR uses the following expression for m_{O3} (Komhyr, 1980):

$$m_{O3} = \frac{R+h}{\sqrt{(R+h)^2-(R+r)^2(cos\theta)^2}} \quad (11)$$

where R = 6370 km is the mean radius of the Earth, r = 2.370 km is the altitude of the station, h = 22 km is the estimated height of the ozone layer, and θ is the solar elevation. However, AERONET-Cimel uses an updated expression (Komhyr et al., 1989) in which h is not fixed and takes a value as a function of the latitude, and the absorption coefficients are obtained for each particular filter using the spectral response provided by the manufacturer. For most of the period covered in this study, measured total ozone values from IZO (Brewer spectrometer) were used to calculate τ_{O3} (Wehrli, 2008a). If no Brewer data is available, data are retrieved from the Total Ozone Mapping Spectrometer (TOMS) or more recently from the Ozone Monitoring Instrument (OMI) (McPeters et al., 2015) for daily operations (Kazadzis et al., 2018b). In the case of Izaña, if the OMI overpass fails, GAW-PFR uses the Brewer O_3 climatology. Concerning AERONET-Cimel Version 2, a NASA TOMS 1° x 1.25° resolution O_3 climatology is used. From Eq. 10, the differences in O_3 optical depth $\Delta\tau_{O3}$ can be derived:

$$\triangle\tau_{O3} = \sigma_{O3}(\lambda)\frac{1}{1000}\frac{m_{O3}(O_{3PFR} - O_{3Cimel})}{m_a} \quad (12)$$

The largest influence of total ozone data uncertainty in τ_{O3} occurs at 500 nm (Figure 5). According to Wehrli (2008b) and Kazadzis et al. (2018b), total ozone needs to be determined to ± 30 DU or 10 % of typical values, to ensure an uncertainty of ± 0.001 in τ_{O3} at 500 nm. In the case of the GAW-PFR / AERONET-Cimel comparison, and due to the very different method in which both networks obtained O_3 values for their corresponding corrections, the ozone differences found on some days (1761 out of 71965 days; 2.4 %) are very large (> 40 DU), exceeding a difference in the ozone optical depth of 0.001. Even so, the potential contribution to AOD differences outside the $U95$ limits between the two networks is negligible. Total O_3 over IZO shows a relatively small amplitude throughout the year, but both surface ozone concentrations and column ozone amount could sharply increase under the influence of cut-off lows injecting air from the high-mid troposphere into the lower subtropical troposphere, which is not uncommon in spring and the first half of summer (Cuevas et al., 2015; Kentarchos et al., 2000). In addition through exchange processes in the Upper Troposphere Lower Stratosphere (UTLS) due to the presence of the subtropical jet (mainly from February to April) (Rodríguez-Franco and Cuevas, 2013). However, if we wanted to repeat this traceability study of 1-minute AOD data in mid or high latitude stations where sharp O_3 variations (several tens of DU) could be registered in a few hours, the correction of 1-minute AOD measurements by τ_{O3} might be a challenging issue.

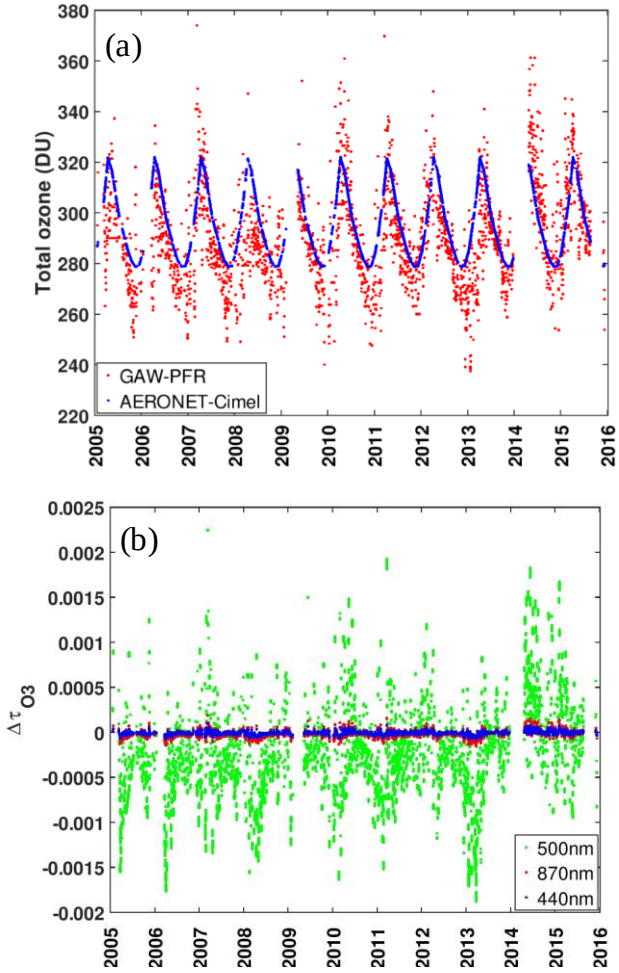

Figure 5. (a) Total O_3 used by GAW-PFR (measured Brewer O_3 values from IZO, OMI O_3 overpass or Brewer O_3 climatology) and AERONET-Cimel (TOMS O_3 climatology), and (b) $\Delta\tau_{O3}(\lambda)$ caused by differences in daily total O_3 between the two instruments in the period 2005-2015.

5.3.5.3 Differences in NO_2 absorption

AERONET-Cimel applies a correction by absorption of NO_2, but GAW-PFR does not include this correction. AERONET-Cimel obtains daily total NO_2 data from a 0.25° x 0.2° resolution NO_2 monthly climatology obtained from the ESA Scanning Imaging Absorption SpectroMeter for Atmospheric CHartographY (SCIAMACHY) (Eskes and Boersma, 2003). In order to assess the contribution to AERONET-Cimel 1-minute AOD data non-traceability by NO_2 absorption we have to estimate the NO_2 optical depth ($\tau_{NO2}(\lambda)$) of AERONET-Cimel since GAW-PFR does not perform this correction. Analogously to $\Delta\tau_{O3}$, the differences in nitrogen dioxide optical depth $\Delta\tau NO_2$ can be obtained from:

$$\triangle\tau_{NO2} = \sigma_{NO2}(\lambda)\frac{1}{1000}\frac{m_{NO2}}{m_a}(-NO_{2Cimel}) \quad (13)$$

Where m_a is given by Eq. 7, NO_{2Cimel} (DU) is the daily total NO_2 used by AERONET-Cimel, $\sigma_{NO2}(\lambda)$ is the NO_2 absorption (Gueymard, 1995) weighted by the specific filter response: 15.6 cm^{-1} (380 nm), 12.3 cm^{-1} (440 nm), and 4.62 cm^{-1} (500 nm). Finally m_{NO2} has the following expression (Gueymard, 1995):

$$m_{NO2} = \frac{1}{sin\theta + 602.30(90-\theta)^{0.5}(27.96+\theta)^{-3.4536}} \quad (14)$$

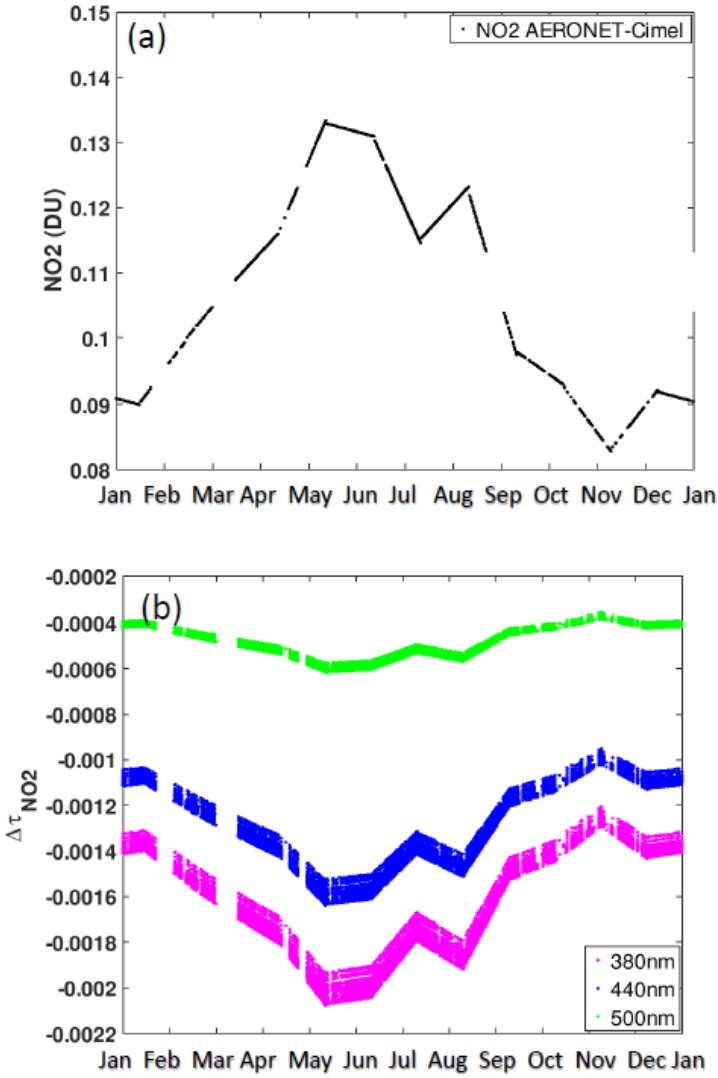

Figure 6. (a) NO_2 monthly climatology obtained from the ESA SCanning Imaging Absorption SpectroMeter for Atmospheric CHartographY (SCIAMACHY), used by AERONET-Cimel at IZO, and (b) $\Delta\tau_{NO2}(\lambda)$ caused by differences in daily total NO_2 between GAW-PFR and AERONET-Cimel in the period 2005-2015. Note that GAW-PFR does not take into account the correction for the NO_2 absorption.

Table 9. Percentage (%) of additional traceable AERONET-Cimel AOD 1-minute data (V2 and V3) after correcting by pressure, and total column O_3 and NO_2 for the period 2005-2015.

Channel	Increment (%) of traceable AOD data after P, O_3 and NO_2 corrections	
	V2	V3
380 nm	1.3	1.7
440 nm	0.2	0.3
500 nm	0.3	0.1
870	~0.0	~0.1

In Figure 6a the total NO_2 used by AERONET-Cimel to evaluate $\tau_{NO2}(\lambda)$ is depicted. Figure 6b shows the $\Delta\tau_{NO2}(\lambda)$ caused by differences in daily total NO_2 between GAW-PFR and AERONET-Cimel. $\Delta\tau_{NO2}$ is of the order of 10^{-3} for 380 and 440 nm channels, while, for 500 nm channel, it is of the order of 10^{-4}. However, it should be noted that an impact on AOD calculation is expected when replicating similar analysis in highly NO_2 polluted regions. Such cases include large industrial cities from East Asia and Central and Eastern Europe (e.g., Chubarova et al., 2016).

Taking into account the corrections for Rayleigh scattering and for the absorptions by O_3 and NO_2, we have calculated the additional traceable AOD data (Table 9). This percentage is maximum at 380 nm with 1.3% (V2) and 1.7% (V3) of the whole dataset. The 870 nm channel is only affected by the Rayleigh correction component and therefore the increment of traceable data after the mentioned corrections is minimal.

5.4. GAW PFR and AERONET-Cimel comparison under high AOD conditions: the impact of dust forward scattering for different FOVs

When we present the AOD differences between AERONET-Cimel and GAW-PFR versus AOD (GAW-PFR) for AOD > 0.1 (dusty conditions), we note that AERONET-Cimel shows slightly higher AOD values than GAW-PFR (Figure 7). In fact, the percentage of data outside the U95 limits increases as AOD increases (Table 10), so for dust-related aerosol conditions (AOD_{500nm} > 0.3) the percentage of AOD data outside the *U*95 limits is > 50 % for 380 nm and 440 nm (Table 10, percentages in brackets). Similar results are found when using AERONET V3 (see Supplement S13). Taking into account the number of data compared with the total cases, these results show a small but non-negligible percentage of AOD differences outside the *U*95 limits for AOD > 0.1, ranging from ~0.3 % at 870 nm to ~ 1.9 % at 380 nm (Table 10).

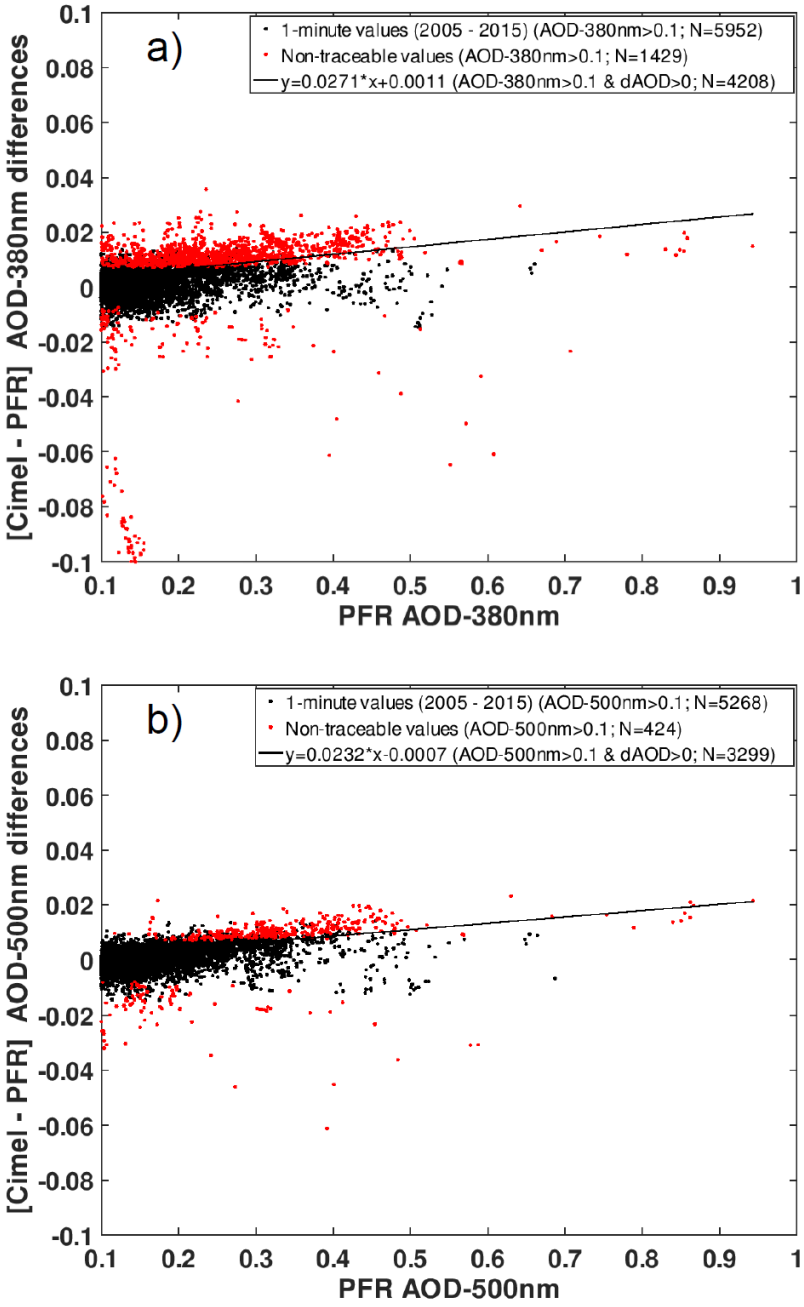

Figure 7. Actual AOD differences between AERONET-Cimel V2 and GAW-PFR vs AOD_{PFR} at (a) 380 nm (b) and 500 nm for the period 2005-2015. The fitting line has been calculated with those data points with AOD > 0.1 and Cimel-PFR AOD difference > 0. The number of data used in the plots are indicated in the legend. The percentage of non-traceable AOD data with these conditions is ~24% for 380 nm, and ~8% for 500 nm. Note that some traceable (black) points show larger AOD differences than non-traceable (red) points because of the air mass dependence of the WMO traceability criterion.

Table 10. Percentage of AERONET V2 AOD data outside the U95 limits at 380, 440, 500 and 870 nm channels and for three AOD_{500nm} thresholds respect to all data and respect to all data for each AOD interval (in brackets).

	Percentage of AOD data outside the *U*95 limits (%)		
	AOD_{500nm}>0.1	AOD_{500nm}>0.2	AOD_{500nm}>0.3
380 nm	1.9 (25.0)	1.2 (47.2)	0.5 (59.8)
440 nm	1.0 (13.5)	0.8 (32.0)	0.5 (57.6)
500 nm	0.6 (8.0)	0.5 (18.7	0.3 (39.3)
870 nm	0.3 (4.1)	0.2 (6.4)	0.1 (14.0)

Aerosol forward scattering within the FOV of various instruments and calculated AOD was investigated some decades ago by Grassl (1971) who determined that at AOD=1 the circumsolar radiation increases by >10% the incoming radiation. Russell et al (2004), using dust and marine aerosols data, quantified the effect of diffuse light for common sun photometer FOV. They reported that the correction to AOD is negligible (<1% of AOD) for sun photometers with narrow FOV (< 2°), which is greater than the Cimel FOV and slightly smaller than the PFR FOV (2.5°). Sinyuk et al. (2012) assessed the impact of the forward scattering aerosol on the uncertainty of the AERONET AOD, concluding that only dust aerosol with high AOD and low solar elevation could cause a significant bias in AOD (> 0.01).

GAW-PFR has double the FOV (2.5°; Wehrli (2000)) compared to the AERONET-Cimel (1.3° ± 4.8 %; Torres et al., 2013), so it is reasonable to expect that it is more affected by the circumsolar radiation than the AERONET-Cimel radiometer. Taking advantage of the fact that Saharan dust intrusions regularly affect IZO, we provide a detailed analysis on the impact that dust forward scattering causes on the AOD retrieval of the two radiometers with different FOV, explaining the AOD differences under moderate-to-high dust load (AOD > 0.1) conditions. For this purpose we have used a forward Monte Carlo model (see section 4.4) with which we perform simulations that include accurate dust aerosol near-forward scattering effects.

Dust aerosol single-scattering properties were computed using Mie theory, assuming a refractive index of 1.47+0.0025i at the wavelengths 380 nm, 440 nm and 500 nm and 1.46+0.012i at 870 nm, based on AERONET measurements at IZO. Seven values of aerosol effective radius (r_e) in the range 0.2 to 3.0 μm were considered, and a lognormal size distribution with a geometric standard deviation of 2 was assumed. A mid-latitude summer atmospheric profile starting from the Izaña altitude (2.4 km a.s.l.) was assumed, with the aerosol layer located at 5-6 km a.s.l. (typical of summertime). A spectrally uniform surface albedo of 0.11 was employed. Computations were performed for nine AOD values (AOD= 0, 0.1, 0.2, 0.3, 0.4, 0.5, 0.6, 0.8, and 1.0) and for five solar elevation angles (θ=80°, 60°, 45°, 30° and 20°). The Monte Carlo

model assumes a plane-parallel atmosphere, so the air mass factor is m=1/sinθ. Ten million photons were used for each case and wavelength.

Supplement S15 shows the ratio of scattered to direct radiation for cases with AOD up to 0.5. The ratio increases with increasing r_e, as the aerosol forward-scattering peak grows stronger. In the case of Saharan dust intrusions at IZO, the median r_e determined from both AERONET data inversion and the in-situ aerodynamic particle sizer (APS) analyzer is ~1.5 μm. This value agrees with the dust size distribution found during SAMUM-2 during long-range transport regime (Weinzierl et al., 2011). For this particle size, the ratio of scattered to direct radiation is ~3 times larger for FOV of 2.5° than FOV of 1.3°.

The error in the retrieved AOD due to scattered radiation within the instrument FOV was evaluated by comparing the apparent AODs, defined as:

$$AOD_{app,PFR} = -\frac{1}{m} ln \frac{F_{PFR}}{F_{PFR}(AOD=0)} \quad (15)$$

$$AOD_{app,Cimel} = -\frac{1}{m} ln \frac{F_{Cimel}}{F_{Cimel}(AOD=0)} \quad (16)$$

with the true AOD

$$AOD_{true} = -\frac{1}{m} ln \frac{F_{dir}}{F_{dir}(AOD=0)}. \quad (17)$$

Here, F_{dir} is the irradiance due to direct (i.e., non-scattered) radiation, and F_{PFR} (F_{Cimel}) is the total irradiance that would be measured by the PFR (Cimel) radiometer, considering the instrument FOV and the FOV angular function. The relative error in AOD depends strongly on the particle size but it is fairly constant for each r_e value considered (see Supplement S16). For r_e ~1.5 μm, the relative error in AOD at 380 nm (500 nm) is ~1.6% (1.0%) for Cimel, and ~5% (~3%) for PFR. These errors are in good agreement with those estimated by Russell at al. (2004), and slightly higher than the relative AOD error of 0.7% due to coarse dust aerosol forward scattering reported by Eck et al. (1999).

The Monte-Carlo-simulated relative differences in retrieved AOD (in %) that would result from the scattered radiation within the FOV of the PFR and Cimel instruments, and the difference in retrieved AOD between PFR and Cimel as a function of the AOD retrieved with PFR, for 380 nm and 500 nm, are shown in Figure 8. The main results of these simulations are: 1) the higher FOV of the PFR, compared to that of the Cimel, results in lower AOD values for the PFR; 2) the fractional AOD difference related to the different FOVs of PFR and Cimel is fairly constant for any aerosol effective radius, but increases with increasing the effective radius; and 3) this fact might explain at least some of the systematic differences seen in Fig. 7. Note that, as lower AOD values derived from the PFR are expected based on its larger FOV, the linear fits in Fig. 7 have been calculated for those data points with the Cimel-PFR AOD differences> 0. In this way, we discard those pairs of AOD data whose difference is not only due to the different FOV between both instruments, obtaining in this way a better approximation to quantify this effect.

The slopes of the fitting lines of the Cimel-PFR AOD differences vs. PFR AOD for AOD> 0.1 (dusty conditions) are 2.7% for 380 nm and 2.3% for 500 nm (Figure 7), which are quite consistent with the percentage differences of AOD between Cimel and PFR for an effective radius of 1.5 μm (Figures 8a and

8b). These percentages correspond to absolute AOD differences of 0.016 at 380 nm, and 0.011 at 500 nm for AOD=0.5 (Figures 8c and 8d), that are of sufficient magnitude to cause an appreciable number of 1-minute AOD data outside the U95 limits, as indicated in Table 10.

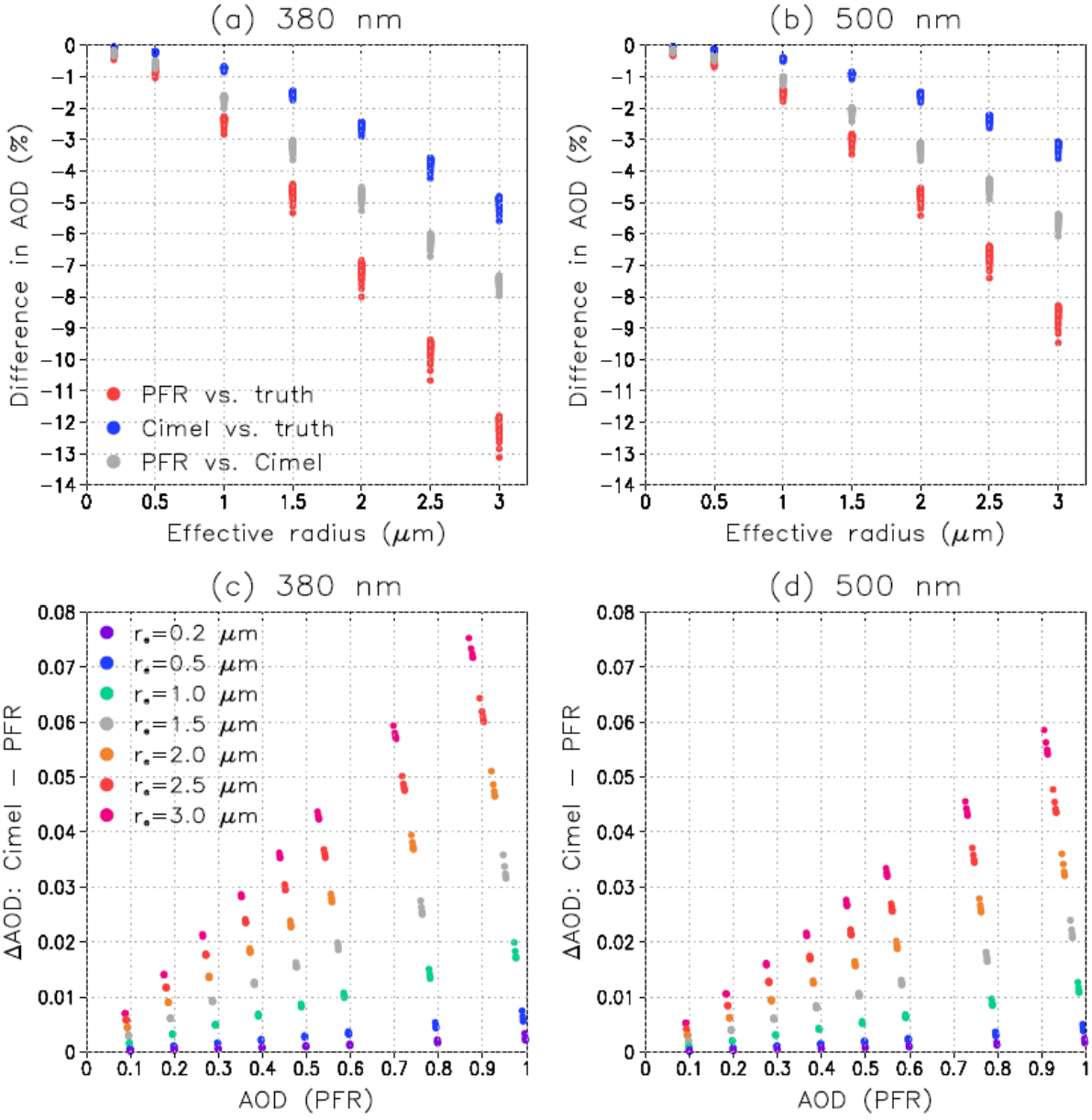

Figure 8. Panels a) and b): the simulated relative differences in retrieved AOD (in %) that would result from the scattered radiation within the FOV of the PFR and Cimel instruments. The red (blue) dots show the differences between the AOD that would be retrieved using PFR (Cimel) and the actual AOD, and the grey dots the difference between PFR and Cimel, at wavelengths (a) 380 nm and (b) 500 nm. Panels c) and d): the difference in retrieved AOD between PFR and Cimel, plotted as a function of the AOD retrieved with PFR, for seven values of aerosol effective radius between 0.2 and 3.0 μm, at (c) 380 nm and (d) 500 nm.

If we apply the corresponding corrections to the 1-minute AOD PFR data > 0.1 assuming an effective radius of 1.5μm, + 3.3% at 380nm and + 2.2.% at 500 nm, it turns out that the slopes of the fitting lines of the Cimel-PFR AOD differences vs. PFR AOD become practically zero (Figure 9). Moreover, the number

of AOD data outside the U95 limits is reduced by approximately 53% for 380 nm and by 13% for 500 nm. It must be taken into account that the percentage of AOD data for AOD> 0.1 outside the U95 limits, before the corrections, is only 8% at 500 nm, while at 380 nm it is a significant value (24%).

This AOD "correction" reduces the Cimel-PFR AOD differences substantially but does not eliminate them completely, mainly for two reasons. The first one is the inherent limitation of data correction using the percentage difference in AOD obtained by model simulation for a fixed effective radius.

We have assumed an effective radius of 1.5 μm but, in reality, the radius of dust particles varies. A reasonable range of dust particle radius is between 0.1 and 3 μm (Balkanski et al., 1996; Denjean et al., 2016; Mahowald et al., 2014). So, depending on the distance from the dust source to IZO and the size of the emitted dust, the effective radius could vary slightly between dust episodes. As can be seen in Figures 8a and 8b, the percentage differences in AOD between Cimel and PFR for a 1-2μm effective radius interval, the PFR-Cimel AOD relative difference at 380 nm (500 nm) might change between ~-1.8% (-1.1%) to -4.9% (3.3%). The second reason is a possible cloud contamination in AOD retrieval when altostratus are present above the SAL, as discussed in Section 5.3.4.

A similar analysis has been carried out for AERONET V3 (see Supplement S17), where we observe that the corrections obtained are not as good as those obtained for V2. This may be due to the very high AOD data retention in V3 which could include more cases in which altostratus clouds and dust are present. The effect of FOV on AOD retrieval should be taken into account for those radiometers with a relatively high FOV (>3°) measuring in regions with relatively high AOD (> 0.2) for most of the year, as is the case in many sites of Northern Africa, the Middle East and East Asia (Basart et al., 2009; Cuevas et al., 2015; Eck et al., 1999; Kim et al., 2007). This effect leads to AOD underestimation, and the variable number of high AOD episodes in each season of the year might affect the AOD long-term trends. AOD measurements under these conditions would be especially affected for optical air mass < 3.

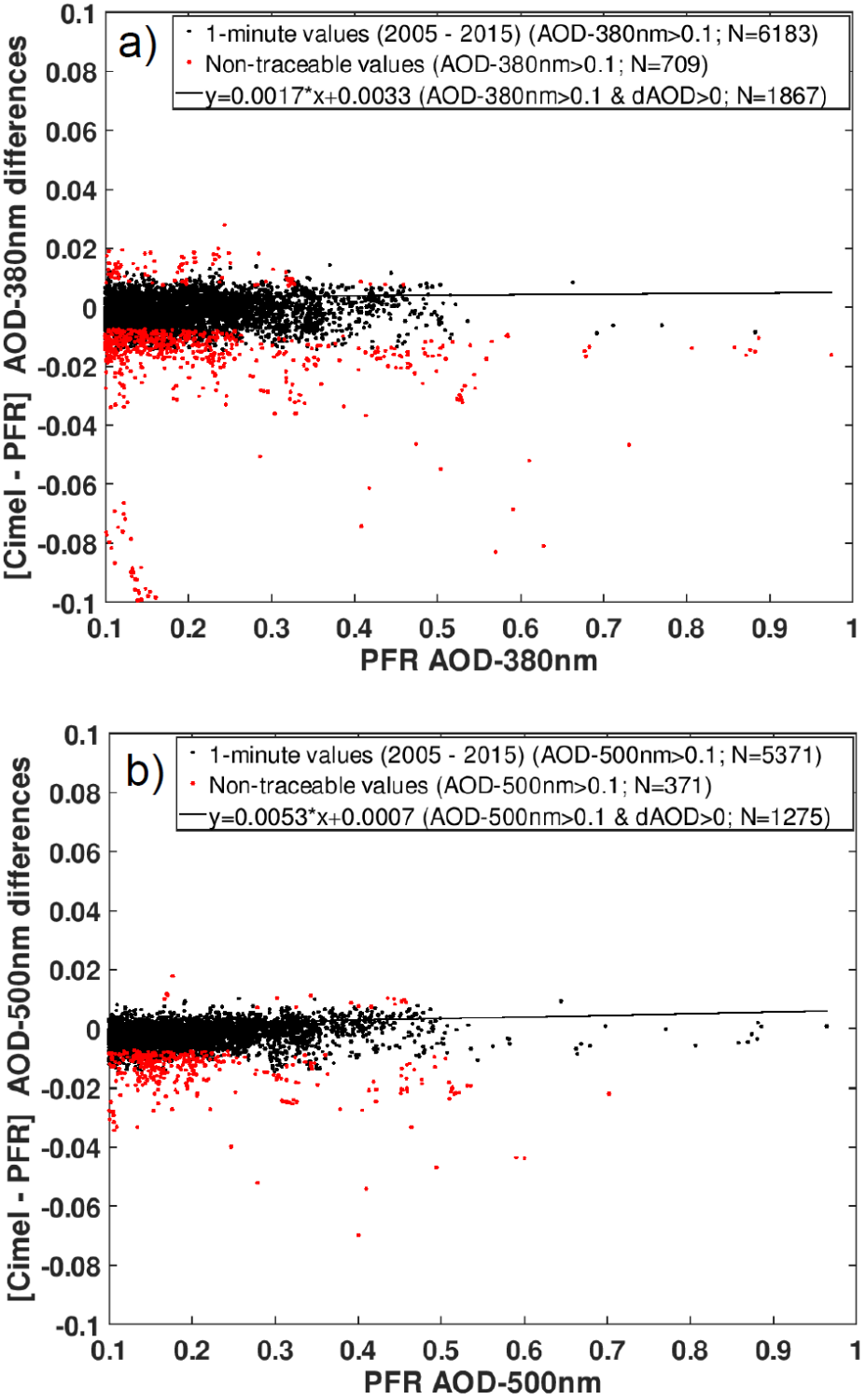

Figure 9. The same as Figure 7 after "correcting" the PFR AOD data by adding + 3.3% at 380nm and + 2.2.% at 500 nm to the 1-minute PFR AOD data > 0.1.

5.5. Angström exponent comparison

We have performed a comparison of the AE provided by GAW-PFR and AERONET-Cimel using in both cases the AOD data obtained from the four common channels (380 nm, 440 nm, 500 nm and 870 nm) with a total of 70716 data-pairs. The PFR-AOD values have been ordered from lowest to highest by

grouping them in intervals of 500 values for which the averages (and corresponding standard deviations) of the PFR-Cimel AE differences have been calculated (Figure 10a). In a similar way we proceeded with the PFR-AE values (Figure 10b).

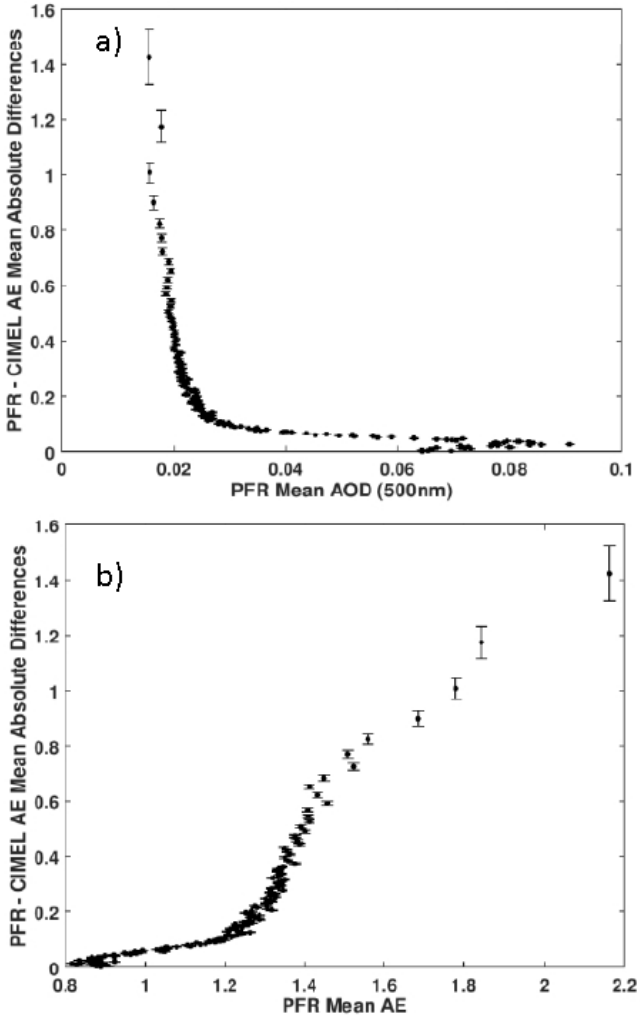

Figure 10. (a) PFR-Cimel AE mean absolute differences (and corresponding standard deviations) vs PFR mean AOD_{500nm} in 500 data intervals (b) and vs PFR mean AE in 500 data intervals. AE has been computed for both PFR and Cimel using the four common channels (380, 440, 500 and 870nm).

AE differences > 0.2 increase exponentially for AOD < 0.02, reaching AE differences of up to 1.6 under pristine conditions (Figure 10a). For very low AOD the provided instruments uncertainty is the source of the sharp increase in AE, and at the same time AE becomes very sensitive to slight AOD changes. However, for AOD < 0.02 the atmospheric aerosol load is practically zero and so, its characterization with AE have in practice relatively minor importance.

In addition, the AE differences remain < 0.1 when AE_{PFR} values are < 1 (Figure 10b), which shows that these differences are small in most of the possible atmospheric scenarios. For $1 < AE_{PFR} < 1.2$ the AE differences increase slightly to values < 0.2, and for $AE_{PFR} > 1.2$ (very fine particles or pristine conditions) the AE differences increase sharply to reach values of ~ 1.2. In our case, the non-pristine conditions, or those with a high content of mineral dust, have associated AOD > 0.03 and AE < 1, where the AE

differences remain < 0.1. In case of pristine conditions AOD ≤ 0.03 and AE ≥ 1 the AE differences can reach a maximum of 1.6. Wagner and Silva (2008) estimated the usual maximum AE error by error propagation using a pair of spectral channels in which AOD is measured. Their results show that for clean optical conditions (AOD_{440nm}= 0.06) the maximum AE error is 1.17, and for hazy conditions (AOD_{440nm}=0.17) the error is 0.17, assuming an underlying AE of 1.5. These values decrease to 0.73 and 0.11, respectively, if AE=0. The AE differences found between GAW-PFR and AERONET-Cimel lie within the estimated errors reported by Wagner and Silva (2008).

Table 11. Uncertainty in AE determination for three typical atmospheric situations.

	Uncertainty in AE
Normal pristine conditions AOD_{500nm}= 0.03 and AE = 1.4	≥ 1
Hazy conditions AOD_{500nm}= 0.14 and AE = 1.15	≥ 0.2
Strong dust intrusion AOD_{500nm}= 0.3 and AE = 0.3	~ 0

In any case, as in our study the AE has been determined from AOD measured in the four common channels of GAW-PFR and AERONET-Cimel, we estimated the uncertainty in the calculation of the AE for three typical aerosol scenarios at Izaña. Following the methodology shown by Wagner and Silva (2008), the AE uncertainty estimations have been calculated using AOD measurements at four wavelengths and AOD uncertainty error propagation (Table 11). The AE derived from more than 2 wavelengths is less affected by AOD uncertainties than AE calculated with pairs of wavelengths, since the latter are calculated from the ratio of AOD at two channels (Cachorro et al., 2008).

The AE differences of our study (Figure 10) are within the AE uncertainty estimated for each type of atmospheric condition (pristine, hazy and heavily dust loaded). However, although AE is a quantitative parameter, it is only used in a qualitative way to estimate the range of sizes (fine, medium, coarse) of the predominant aerosol in the inevitable mixture of aerosols that we observe. With this parameter, and together with the information that is available in the measurement site about the most frequent types of aerosols and their concentration, we can estimate the type of aerosols that are being measured. There are many publications with different thresholds of AE and AOD in order to classify different types of aerosols (e.g. Basart et al., 2009; Cuevas et al., 2015; Dubovik et al., 2002; Guirado et al., 2014; Holben et al., 2001; Kim et al., 2007; Todd et al., 2007; Toledano et al., 2007; Wang et al., 2004). However, there is no consensus on these thresholds since at each site there are different mixtures of aerosols, and each type of aerosol shows

specific frequencies of appearance and different concentrations. An alternative way of analyzing the degree of agreement in AE between GAW-PFR and AERONET-Cimel is to verify to what extent both networks provide the same information regarding the type of aerosol they observe in a certain site.

Considering the AE criteria established by Cuevas et al. (2015) and Berjón et al. (2019), we have identified the following four main categories according to the AE_{PFR} and AE_{Cimel} values:

1. AE_{PFR} & $AE_{Cimel} > 0.6$: Pristine conditions.
2. $0.25 < AE_{PFR}$ & $AE_{Cimel} \leq 0.6$: Hazy, mineral dust being the main aerosol component.
3. AE_{PFR} & $AE_{Cimel} \leq 0.25$: Pure dust.
4. AE_{PFR} and AE_{Cimel} do not fit any of the previous categories.

In 94.9 % of the cases, GAW-PFR and AERONET-Cimel V2 match the AE intervals of each aerosol scenario. Similar results (93.4%) were obtained when comparing with AERONET V3. Most of the agreement (>80 %) occurs in the predominant scenario of pristine conditions despite the AE uncertainty under pristine conditions being ≥ 1. See Supplement S18 for more details. Notice that given the special characteristics of the Izaña Observatory, and according to Cuevas et al. (2015) and Berjón et al. (2019), AE is a self-sufficient parameter to define different types of aerosol scenarios without the need to combine its information with AOD.

6. Summary and Conclusions

While GAW-PFR is the WMO-defined global AOD reference, being directly linked to WMO / CIMO, and was specifically designed to detect long-term AOD trends, AERONET-Cimel is the densest AOD measurement network globally, and the network most frequently used for aerosol characterization and for model and satellite observation evaluation.

An AERONET-Cimel 11-year AOD data series at IZO was obtained using a large number of radiometers. A total of 13 Reference instruments were used in the period 2005-2009 which means that every 4 and a half months, approximately, an instrument was replaced by another one to be calibrated. Their calibrations were performed during their respective measurement time periods at IZO. Therefore, these calibrations were not in any way linked with those of the instruments that preceded or replaced them, nor with GAW-PFR reference. These facts led us to investigate the homogeneity of the AERONET-Cimel AOD data series and their intercomparability with the much more homogeneous AOD data series from GAW-PFR (3 instruments in 11 years). The traceability concept for AOD suggested by WMO consists in determining whether the AOD difference of the AERONET CIMELs vs the GAW PFRs lie within the U95 limits. We have used uncertainty limits for AOD traceability established by WMO (2005) for these type of instruments with finite FOV. The acceptable traceability is when 95 % of the absolute AOD differences lie within these limits, in which case both data populations are considered equivalent. It should be clarified that “traceability” is not used in a strict metrological sense. This study has addressed the comparison of the GAW-PFR dataset with the two versions of AERONET (V2 and V3) in the period 2005-2015. An excellent agreement between V2 and V3 for the four analysed channels ($R^2 > 0.999$) has been obtained.

More than 70000 synchronous GAW-PFR (PFR) and AERONET-Cimel (Cimel) 1-minute data-pairs in each channel in the period 2005-2015 were analysed. An excellent traceability of AOD from the AERONET-Cimel (V2 and V3) is found for 440 nm, 500 nm and 870 nm, and fairly good results for 380 nm. The lowest percentage of traceable AOD data is registered in 380 nm with 92.7 % of the 1-minute data within the WMO limits, and the highest in 870 nm with 98.0 % of the data.

The different possible causes of non-traceability in AOD were investigated as follows:

- Absolute AOD measurements synchronization.

Analyzing 1-minute AOD variability we concluded that its impact on the AOD differences is negligible as only ~0.8% of the AOD data has a variability larger than 0.005 in all spectral ranges.

- Sun tracking misalignments.

Sun tracking misalignments constitute a serious problem and a major cause of non-traceability of AOD data-pairs as demonstrated by the AOD data outside the U95 limits from the period 2005-2009 as a consequence of episodic problems with the sun-tracker of the GAW-PFR radiometer. For the 2010-2015 period the percentage of traceable data-pairs improves to 93.5% (380 nm), 97.4% (440 nm), 97.2% (500 nm) and 99.1% (870 nm). However, most of these cases could be identified and excluded from the analysis.

- Cloud screening failure by both network algorithms.

According to our observations, the simultaneous failure of both cloud screening algorithms might occur only under the presence of large and stable cirrus, or altostratus (~ 6000 m a.s.l.) on the top of a heavily dust loaded Saharan air layer, hiding very wide and stable clouds. In these cases, the radiometers interpret these clouds as aerosol layers and might provide values very different from the real AOD. For the comparison at IZO, however, this effect is negligible since GAW-PFR and AERONET-Cimel cloud screening algorithms provide successful cloud identification on clear direct-sun conditions during cloudy skies (FCS < 40 %) for 99.75 % of the cases.

- Pressure measurements related errors.

Since the accuracy of the new barometers built into new radiometers is about 3 hPa, and only errors in atmospheric pressure > 30 hPa might produce an impact on Rayleigh scattering, the AOD non-traceability due to errors in Rayleigh scattering is negligible.

- Total column ozone input uncertainty.

The largest influence of total ozone data uncertainty on ozone absorption occurs mainly at 500 nm. Total ozone needs to be determined to ±30 DU or 10 % of typical values, to ensure an uncertainty of ±0.001 ozone absorption at 500 nm. In the case of the GAW-PFR / AERONET-Cimel comparison, despite the very different methods in which both networks obtained O_3 values for their corresponding corrections, large ozone differences were found (> 40 DU) only on 2.4 % of the days, resulting in a difference in the ozone optical depth slightly above ~0.001. The potential contribution to non-traceable AOD values between the two networks is negligible. However, in mid or high latitude stations where fast O_3 variations of several tens of DU might be registered, the correction of 1-minute AOD measurements by ozone absorption might be an issue to be considered.

- Total column NO_2 input uncertainty.

The differences in NO_2 absorption caused by differences in daily total NO_2 between GAW-PFR and AERONET-Cimel is of the order of 10^{-3} for 380 nm and 440 nm channels, while, for 500 nm channel, it is even lower, of the order of 10^{-4}. So, differences in NO_2 absorption are negligible in the 1-minute AOD non-traceability of our study. However, NO_2 absorption might have some impact on AOD in highly polluted regions, such as in large industrial cities, where column NO_2 values are much larger than the climatological ones.

Taking into account the corrections for Rayleigh scattering and for the absorptions by O_3 and NO_2, we have calculated the combined effect of all of them on the non-traceability of the 1-minute AOD values. The highest impact occurs in the 380 nm channel, in which 25 % of the AOD data outside the *U*95 limits (~2% of the total compared data) are due to significant differences in pressure, and in O_3 and NO_2 absorption. The 1-minute AOD data outside the *U*95 limits by these corrections is negligible in the 870 nm channel.

- Impact of dust forward scattering in AOD retrieval uncertainty for different instrument FOVs

Since GAW-PFR has almost double the FOV (~2.5°) compared to the AERONET-Cimel (~1.3°), and direct solar irradiance measurements are biased by the amount of aureole radiation that is assumed to be direct solar radiation, it is reasonable to expect that GAW-PFR is more affected by the circumsolar irradiance than AERONET-Cimel radiometer when AOD is relatively high. Modelling the dust forward scattering we have shown that a non-negligible percentage of the non-traceable 1-minute AOD data for AOD > 0.1, ranging from ~0.3 % at 870 nm to ~1.9 % at 380 nm is caused by the different FOV. Due to this effect, the GAW-PFR provides AOD values which are ~3% lower at 380 nm, and ~2% lower at 500 nm, compared with AERONET-Cimel. However, AOD underestimation could only have some relevance in dusty regions if radiometers with relatively large FOV are used. A comparison of the AE provided by GAW-PFR and AERONET-Cimel has been performed using in both cases AOD data obtained from the four nearby common channels with a total of 70716 data-pairs. This is a very strict AE calculation since it is necessary that AOD be accurately measured by the four channels simultaneously. AE differences > 0.2 increase exponentially under very pristine conditions (AOD ≤ 0.03 and AE ≥ 1), reaching AE differences of up to 1.6. However, for these conditions the atmospheric aerosol load is practically zero and so, its characterization with AE does not have any importance in practice. Under non-pristine conditions or those with a high mineral dust content (associated AOD > 0.03 and AE < 1), the AE differences remain < 0.1.

Summarizing, we have presented for the first time a long-term (2005-2015) 1-minute AOD comparison among different types of radiometers belonging to different aerosol global networks. This comparison is a very demanding test of both GAW-PFR and AERONET-Cimel validated AOD datasets since aerosol scenarios correspond to extreme conditions: either very low aerosol loading, a “pristine” scenario that reveals small uncertainties in the calibration and in the cloud screening, or large dust load, which leads to a significant increase in the forward scattering aerosol with AOD, resulting in a slightly higher AOD underestimation by the GAW-PFR. From this comprehensive comparison, we can conclude that both AOD datasets are representative of the same AOD population, which is a remarkable fact for the global aerosol community. It should be noted that AOD traceability at 380 nm (92.7 %) does not reach 95 % of the

common data, the percentage recommended by WMO U95 criterion, so more efforts should be made to improve AOD in the UV range. In this study we have also investigated the data that are outside of the WMO U95 limits in order to understand their causes and to be eventually able to correct the small inconsistencies detected in instrumental and methodological aspects in the future.

Our results suggest that WMO/CIMO traceability limits could be redefined as a function of wavelength, and the recommended radiometer FOV range should be reconsidered. The widely deployed AERONET-Cimel and GAW-PFR datasets play a crucial role in understanding long-term AOD changes and detecting trends, so it would be desirable for both networks to be linked to the same GAW-WMO related reference.

Competing interests. The authors declare that they have no conflict of interest.

Acknowledgements. The authors thank Luc Blarel and Philippe Goloub (LOA, CNRS-University of Lille, France) for supervising the periodic calibrations of the Cimel Reference instruments. This study has been performed in the frame of the WMO CIMO Izaña Testbed for Aerosols and Water Vapour Remote Sensing Instruments. The work was supported by the project "The Global Atmosphere Watch Precision Filter Radiometer (GAW-PFR) Network for Aerosol Optical Depth long term measurements" funded by the Federal Office of Meteorology and Climatology MeteoSwiss International Affairs Division, Swiss GCOS Office. Part of the AERONET-Cimel radiometers have been calibrated at Izaña Observatory by AERONET- EUROPE Calibration Service, financed by the European Community specific programs for Integrating Activities: Research Infrastructure Action under the Seventh Framework Programme (FP7/2007-2013), ACTRIS grant agreement No. 262254, and Horizon 2020 Research and Innovation Program, ACTRIS-2 grant agreement No. 654109. This research has received funding from the European Union's Horizon 2020 Research and Innovation Programme under grant agreement No. 654109 (ACTRIS-2).The funding by MINECO (CTM2015-66742-R) and Junta de Castilla y León (VA100P17) is also gratefully acknowledged. We thank the staff of the Izaña Observatory for their effort and dedication in maintaining the instruments. We acknowledge the constructive comments of the anonymous referees. Our colleague Celia Milford has improved the English language of the paper. In memory of Prof Klaus Fröhlich, former director of PMOD-WRC, who initiated the AOD measurements programme at the Izaña Observatory in 1984 within the WMO Background Atmospheric Pollution Monitoring Network (BAPMoN).

References

Amiridis, V., Marinou, E., ***Tsekeri***, A., Wandinger, U., Schwarz, A., Giannakaki, E., Mamouri, R., Kokkalis, P., Binietoglou, I., Solomos, S., Herekakis, T., Kazadzis, S., Gerasopoulos, E., Proestakis, E., Kottas, M., Balis, D., Papayannis, A., Kontoes, C., Kourtidis, K., Papagiannopoulos, N., Mona, L., Pappalardo, G., Le Rille, O., and Ansmann, A.: LIVAS: a 3-D multi-wavelength aerosol/cloud

database based on CALIPSO and EARLINET, Atmos. Chem. Phys., 15, 7127-7153, https://doi.org/10.5194/acp-15-7127-2015, 2015.

Angstrom, A.: On the atmospheric transmission of sun radiation and on dust in the air, Geografiska Annaler, 11, 156–166, 1929. Balkanski, Y., Schulz, M., Marticorena, B., Bergametti, G.,Guelle, W., Dulac, F., Moulin, C.,and Lambert, C.E.: Importance of the source term and of the size distribution to model the mineral dust cycle, in The Impact of Desert Dust Across the Mediterranean, edited by S. Guerzoni and R. Chester, pp. 69–76, Kluwer Academic Pub., Boston, MA. 2, 9, 2, 1996.

Barker, H. W.: Solar radiative transfer through clouds possessing isotropic variable extinction coefficient, Quart. J. Roy. Meteor. Soc., 118, 1145-1162, doi: 10.1002/qj.49711850807, 1992.

Barker, H. W.: Estimating cloud field albedo using one-dimensional series of optical depth, J. Atmos. Sci., 53, 2826-2837, doi: 10.1175/1520-0469(1996)053<2826:ECFAUO>2.0.CO;2}, 1996.

Barreto, A., Cuevas, E., Pallé, P., Romero, P. M., Guirado, C., Wehrli, C. J., and Almansa, F.: Recovering long-term aerosol optical depth series (1976-2012) from an astronomical potassium-based resonance scattering spectrometer, Atmospheric Measurement Techniques, 7, 5 4103–4116, https://doi.org/10.5194/amt-7-4103-2014, 2014.

Barreto, A., Cuevas, E., Granados-Muñoz, M.-J., Alados-Arboledas, L., Romero, P. M., Gröbner, J., Kouremeti, N., Almansa, A. F., Stone, T., Toledano, C., Román, R., Sorokin, M., Holben, B., Canini, M., and Yela, M.: The new sun-sky-lunar Cimel CE318-T multiband photometer a comprehensive performance evaluation, Atmospheric Measurement Techniques, 9, 631–654, https://doi.org/10.5194/amt-9-63110 2016, https://www.atmos-meas-tech.net/9/631/2016/, 2016.

Basart, S., Pérez, C., Cuevas, E., Baldasano, J. M., and Gobbi, G. P.: Aerosol characterization in Northern Africa, Northeastern Atlantic, Mediterranean Basin and Middle East from direct-sun AERONET observations, Atmospheric Chemistry and Physics, 9, 8265–8282, https://doi.org/10.5194/acp-9-8265-2009, https://www.atmos-chem-phys.net/9/8265/2009/, 2009.

Basart, S., Pérez, C., Nickovic, S., Cuevas, E., and Baldasano, J.: Development and evaluation of the BSC-DREAM8b dust regional model over Northern Africa, the Mediterranean and the Middle East, Tellus B: Chemical and Physical Meteorology, 64, 18539, https://doi.org/10.3402/tellusb.v64i0.18539, 2012.

Benedetti, A., Reid, J. S., Knippertz, P., Marsham, J. H., Di Giuseppe, F., Rémy, S., Basart, S., Boucher, O., Brooks, I. M., Menut, L., Mona, L., Laj, P., Pappalardo, G., Wiedensohler, A., Baklanov, A., Brooks, M., Colarco, P. R., Cuevas, E., da Silva, A., Escribano, J., Flemming, J., Huneeus, N., Jorba, O., Kazadzis, S., Kinne, S., Popp, T., Quinn, P. K., Sekiyama, T. T., Tanaka, T., and Terradellas, E.: Status and future of numerical atmospheric aerosol prediction with a focus on data requirements, Atmospheric Chemistry and Physics, 18, 10615–10643, https://doi.org/10.5194/acp-18-10615-2018, https://www.atmos-chem-phys.net/18/10615/2018/, 2018.

Berjón, A., Barreto, A., Hernández, Y., Yela, M., Toledano, C., and Cuevas, E.: A 10-year characterization of the Saharan Air Layer lidar ratio in the subtropical North Atlantic, Atmos. Chem. Phys. Discuss., https://doi.org/10.5194/acp-2018-1315, in review, 2019.

Blanc, P., Espinar, B., Geuder, N., Gueymard, C., R., M., Pitz-Paal, R., Reinhardt, B., Renné, D., M., S., Wald, L., and Wilbert, S.: Direct normal irradiance related definitions and applications: The circumsolar issue, Solar Energy, 110, 561 – 577, https://doi.org/https://doi.org/10.1016/j.solener.2014.10.001, 2014.

Bodhaine, B. A., Wood, N. B., Dutton, E. G., and Slusser, J. R.: On Rayleigh optical depth calculations, Journal of Atmospheric and Oceanic Technology, 16, 1854–1861, 1999.

Böhm-Vitense, E.: Introduction to stellar astrophysics, volume 2: stellar atmospheres, Cambridge University Press, 260 pp., 1989.

Bokoye, A. I., Royer, A., O'Neill, N. T., Cliche, P., Fedosejevs, G., Teillet, P. M., and McArthur, L. J. B.: Characterization of atmospheric aerosols across Canada from a ground-based sunphotometer network:

AEROCAN, Atmosphere-Ocean, 39, 429–456, https://doi.org/10.1080/07055900.2001.9649687, 2001.

Cachorro, V., Toledano, C., Sorribas, M., Berjón, A., De Frutos, A., and Laulainen, N.: An “in situ” calibration-correction procedure (KCICLO) based on AOD diurnal cycle: Comparative results between AERONET and reprocessed (KCICLO method) AOD-alpha data series at El Arenosillo, Spain, Journal of Geophysical Research: Atmospheres, 113, https://doi.org/https://doi.org/10.1029/2007JD009001, 2008.

Cachorro, V. E., Romero, P. M., Toledano, C., Cuevas, E., and de Frutos, A. M.: The fictitious diurnal cycle of aerosol optical depth: A new approach for “in situ” calibration and correction of AOD data series, Geophysical Research Letters, 31, https://doi.org/10.1029/2004GL019651, 2004.

Campanelli, M., Nakajima, T., and Olivieri, B., 2004: Determination of the solar calibration constant for a sun - sky radiometer: proposal of an in situ procedure. Appl. Opt., 43(1), 651-659. Carlund, T., Kouremeti, N., Kazadzis, S., and Gröbner, J.: Aerosol optical depth determination in the UV using a four-channel precision filter radiometer, Atmos. Meas. Tech., 10, 905-923, https://doi.org/10.5194/amt-10-905-2017, 2017.

Carrillo, J., Guerra, J. C., and Cuevas, E.and Barrancos, J.: Characterization of the Marine Boundary Layer and the Trade-Wind Inversion over the Sub-tropical North Atlantic, Boundary-Layer Meteorology, 158, 311–330, https://doi.org/10.1007/s10546-015-0081-1, https://doi.org/10.1007/s10546-015-0081-1, 2016.

Chance, K. and Kurucz, R.: An improved high-resolution solar reference spectrum for earth’s atmosphere measurements in the ultraviolet, visible, and near infrared, Journal of quantitative spectroscopy and radiative transfer, 111, 1289–1295, https://doi.org/https://doi.org/10.1016/j.jqsrt.2010.01.036, http://www.sciencedirect.com/science/article/pii/S0022407310000610, 2010.

Che, H., Zhang, X.-Y., Xia, X., Goloub, P., Holben, B., Zhao, H., Wang, Y., Zhang, X.-C., Wang, H., Blarel, L., Damiri, B., Zhang, R., Deng, X., Ma, Y., Wang, T., Geng, F., Qi, B., Zhu, J., Yu, J., Chen, Q., and Shi, G.: Ground-based aerosol climatology of China: aerosol optical depths from the China Aerosol Remote Sensing Network (CARSNET) 2002–2013, Atmos. Chem. Phys., 15, 7619–7652, https://doi.org/10.5194/acp15-7619-2015, 2015.

Chedin, A., Capelle, V., and Scott, N.: Detection of IASI dust AOD trends over Sahara: How many years of data required?, Atmospheric Research, 212, 120–129, https://doi.org/https://doi.org/10.1016/j.atmosres.2018.05.004, http://www.sciencedirect.com/science/article/pii/ S0169809517310566, 2018.

Chubarova, N. Y., Poliukhov, A. A., and Gorlova, I. D.: Long-term variability of aerosol optical thickness in Eastern Europe over 2001– 2014 according to the measurements at the Moscow MSU MO AERONET site with additional cloud and NO_2 correction, Atmospheric Measurement Techniques, 9, 313–334, https://doi.org/10.5194/amt-9-313-2016, https://www.atmos-meas-tech.net/9/313/2016/, 2016.

Cuevas, E., González, Y., Rodríguez, S., Guerra, J. C., Gómez-Peláez, A. J., Alonso-Pérez, S., Bustos, J., and Milford, C.: Assessment of atmospheric processes driving ozone variations in the subtropical North Atlantic free troposphere, Atmospheric Chemistry and Physics, 13, 1973–1998, https://doi.org/10.5194/acp-13-1973-2013, https://www.atmos-chem-phys.net/13/1973/2013/, 2013.

Cuevas, E., Camino, C., Benedetti, A., Basart, S., Terradellas, E., Baldasano, J. M., Morcrette, J. J., Marticorena, B., Goloub, P., Mortier, A., Berjón, A., Hernández, Y., Gil-Ojeda, M., and Schulz, M.: The MACC-II 2007-2008 reanalysis: atmospheric dust evaluation and characterization over northern Africa and the Middle East, Atmospheric Chemistry and Physics, 15, 3991–4024, https://doi.org/10.5194/acp-153991-2015, https://www.atmos-chem-phys.net/15/3991/2015/, 2015.

Cuevas, E., Gómez-Peláez, A., Rodríguez, S., Terradellas, E., Basart, S., García, R., García, O., and Alonso-Pérez, S.: The pulsating nature of large-scale Saharan dust transport as a result of interplays between mid-latitude Rossby waves and the North African Dipole Intensity, Atmospheric Environment, 167, 586–602, https://doi.org/https://doi.org/10.1016/j.atmosenv.2017.08.059, http://www.sciencedirect.com/ 20 science/article/pii/S1352231017305757, 2017a.

Cuevas, E., Milford, C., Bustos, J. J., del Campo-Hernández, García, O., D., G. R., Gómez-Peláez, Guirado-Fuentes, C., Marrero, C., Prats, N., Ramos, R., Redondas, A., Reyes, E., Rodríguez, S., Romero-Campos, P., Scheneider, M., Belmonte, J., Yela, M., Almansa, F., Barreto, A., López-Solano, C., Basart, S., Terradellas, E., Afonso, S., Bayo, C., Berjón, A., Bethencourt, J., Carreño, V., Castro, N. J., Cruz, A. M., Damas, M., De Ory-Ajamil, F., García, M. I., Gómez-Trueba, V., González, Y., Hernández, C., Hernández, Y., Hernández-Cruz, B., Jover, M., León, S., López-Fernández, R., López-Solano, J., Rodríguez, E., Rodríguez-Franco, J., Rodríguez-Valido, M., Sálamo, C., Sanromá, E., Santana, D., Santo-Tomás, F., Sepúlveda, E., Sierra, M., and Sosa, E.: Izaña Atmospheric Research Center Activity Report 2015-2016, State Meteorological Agency (AEMET), 2017b.

Denjean, C., Cassola, F., Mazzino, A., Triquet, S., Chevaillier, S., Grand, N., Bourrianne, T., Momboisse, G., Sellegri, K., Schwarzenbock, A., Freney, E., Mallet, M., and Formenti, P.: Size distribution and optical properties of mineral dust aerosols transported in the western Mediterranean, Atmos. Chem. Phys., 16, 1081-1104, https://doi.org/10.5194/acp-16-1081-2016, 2016.

Driemel, A., Augustine, J., Behrens, K., Colle, S., Cox, C., Cuevas-Agulló, E., Denn, F. M., Duprat, T., Fukuda, M., Grobe, H., Haeffelin, M., Hodges, G., Hyett, N., Ijima, O., Kallis, A., Knap, W., Kustov, V., Long, C. N., Longenecker, D., Lupi, A., Maturilli, M., Mimouni, M., Ntsangwane, L., Ogihara, H., Olano, X., Olefs, M., Omori, M., Passamani, L., Pereira, E. B., Schmithüsen, H., Schumacher, S., Sieger, R., Tamlyn, J., Vogt, R., Vuilleumier, L., Xia, X., Ohmura, A., and König-Langlo, G.: Baseline Surface Radiation Network (BSRN): structure and data description (1992–2017), Earth System Science Data, 10, 1491–1501, https://doi.org/10.5194/essd-10-1491-2018, https: //www.earth-syst-sci-data.net/10/1491/2018/, 2018.

Dubovik, O., Holben, B., Eck, T. F., Smirnov, A., Kaufman, Y. J., King, M. D., Tanré, D., and Slutsker, I.: Variability of absorption and optical properties of key aerosol types observed in worldwide locations, Journal of the atmospheric sciences, 59, 590–608, https://doi.org/https://doi.org/10.1175/1520-0469(2002)059<0590:VOAAOP>2.0.CO;2, 2002.

Eck, T., Holben, B., Reid, J., Dubovik, O., Smirnov, A., O'neill, N., Slutsker, I., and Kinne, S.: Wavelength dependence of the optical depth of biomass burning, urban, and desert dust aerosols, Journal of Geophysical Research: Atmospheres, 104, 31333–31349, https://doi.org/10.1029/1999JD900923, 1999.

Eissa, Y., Blanc, P., Wald, L., and Ghedira, H.: Can AERONET data be used to accurately model the monochromatic beam and circumsolar irradiances under cloud-free conditions in desert environment?, Atmospheric Measurement Techniques, 8, 5099–5112, https://doi.org/DOI = 10.5194/amt-8-5099-2015, 2015.

Eissa, Y., Blanc, P., Ghedira, H., Oumbe, A., and Wald, L.: A fast and simple model to estimate the contribution of the circumsolar irradiance to measured broadband beam irradiance under cloud-free conditions in desert environment, Solar Energy, 163, 497–509, https://doi.org/https://doi.org/10.1016/j.solener.2018.02.015, 2018.

Eskes, H. J. and Boersma, K. F.: Averaging kernels for DOAS total-column satellite retrievals, Atmospheric Chemistry and Physics, 3, 1285–1291, https://doi.org/10.5194/acp-3-1285-2003, https://www.atmos-chem-phys.net/3/1285/2003/, 2003.

Freidenreich, S. M., and Ramaswamy, V.: A new multiple-band solar radiative parameterization for general circulation models, J. Geophys. Res., 104, 31389-31409, doi: 10.1029/1999JD900456, 1999.

García, R. D., Cuevas, E., García, O. E., Cachorro, V. E., Pallé, P., Bustos, J. J., Romero-Campos, P. M., and de Frutos, A. M.: Reconstruction of global solar radiation time series from 1933 to 2013 at the Izaña Atmospheric Observatory, Atmospheric Measurement Techniques, 7, 3139–3150, https://doi.org/10.5194/amt-7-3139-2014, https://www.atmos-meas-tech.net/7/3139/2014/, 2014.

García, R. D., Barreto, A., Cuevas, E., Gröbner, J., García, O. E., Gómez-Peláez, A., Romero-Campos, P. M., Redondas, A., Cachorro, V. E., and Ramos, R.: Comparison of observed and modeled cloud-free longwave downward radiation (2010–2016) at the high mountain BSRN Izaña station, Geoscientific Model Development, 11, 2139–2152, https://doi.org/10.5194/gmd-11-2139-2018, https://www.geosci-model-dev.net/11/2139/2018/, 2018.

García, R. D., Cuevas, E., Ramos, R., Cachorro, V. E., Redondas, A., and Moreno-Ruiz, J. A.: Description of the Baseline Surface Radiation Network (BSRN) station at the Izaña Observatory (2009–2017): measurements and quality control/assurance procedures, Geosci. Instrum. Method. Data Syst., 8, 77-96, https://doi.org/10.5194/gi-8-77-2019, 2019.

Giles, D. M., Sinyuk, A., Sorokin, M. G., Schafer, J. S., Smirnov, A., Slutsker, I., Eck, T. F., Holben, B. N., Lewis, J. R., Campbell, J. R., Welton, E. J., Korkin, S. V., and Lyapustin, A. I.: Advancements in the Aerosol Robotic Network (AERONET) Version 3 database – automated near-real-time quality control algorithm with improved cloud screening for Sun photometer aerosol optical depth (AOD) measurements, Atmos. Meas. Tech., 12, 169-209, https://doi.org/10.5194/amt-12-169-2019, 2019.

Goloub, P., Li, Z., Dubovik, O., Blarel, L., Podvin, T., Jankowiak, I., Lecoq, R., Deroo, C., Chatenet, B., Morel, J., Cuevas, E., and Ramos, R.: PHOTONS/AERONET sunphotometer network overview: description, activities, results, in: Fourteenth International Symposium on Atmospheric and Ocean Optics/Atmospheric Physics, vol. 6936, p. 69360V, International Society for Optics and Photonics, 2007.

Grassl, H.: Calculated Circumsolar Radiation as a Function of Aerosol Type, Field of View, Wavelength, and Optical Depth, Applied Optics, Vol. 10, No. 11, 2543, 1971.

Gueymard, C.: SMARTS2: a simple model of the atmospheric radiative transfer of sunshine: algorithms and performance assessment, Florida Solar Energy Center Cocoa, FL, 1995.

Guirado, C., Cuevas, E., Cachorro, V. E., Toledano, C., Alonso-Pérez, S., Bustos, J. J., Basart, S., Romero, P. M., Camino, C., Mimouni, M., Zeudmi, L., Goloub, P., Baldasano, J. M., and de Frutos, A. M.: Aerosol characterization at the Saharan AERONET site Tamanrasset,Atmospheric Chemistry and Physics, 14, 11753–11773, https://doi.org/10.5194/acp-14-11753-2014, https://www.atmos-chem-phys.net/ 14/11753/2014/, 2014.

Holben, B., Eck, T., Slutsker, I., Tanré, D., Buis, J., Setzer, A., Vermote, E., Reagan, J., and Kaufman, Y.: Multi-band automatic sun and sky scanning radiometer system for measurement of aerosols, pp. 75–83, CNES, Proceedings of 6th International Symposium on Physical Measurements and Signatures in Remote Sensing, 1994.

Holben, B., Eck, T., Slutsker, I., Tanré, D., Buis, J., Setzer, A., Vermote, E., Reagan, J., Kaufman, Y., Nakajima, T., Lavenu, F., Jankowiak, I., and Smirnov, A.: AERONET—A Federated Instrument Network and Data Archive for Aerosol Characterization, Remote Sensing of Environment, 66, 1 – 16, https://doi.org/https://doi.org/10.1016/S0034-4257(98)00031-5, 1998. Holben, B., Tanre, D., Smirnov, A., Eck, T., Slutsker, I., Abuhassan, N., Newcomb, W., Schafer, J., Chatenet, B., Lavenu, F., et al.: An emerging ground-based aerosol climatology: Aerosol optical depth from AERONET, Journal of Geophysical Research: Atmospheres, 106, 12067–12097, https://doi.org/https://doi.org/10.1029/2001JD900014, 2001.

Huijnen, V. and Eskes, H.: Skill scores and evaluation methodology for the MACC II project, MACC-II Deliverable D_85, 2, http://www. gmes-atmosphere.eu/documents/maccii/deliverables/val/MACCII_VAL_DEL_D_85.2_ScoringReport01_20120222.pdf, 2012.

Huneeus, N., Basart, S., Fiedler, S., Morcrette, J.-J., Benedetti, A., Mulcahy, J., Terradellas, E., Pérez García-Pando, C., Pejanovic, G., Nickovic, S., Arsenovic, P., Schulz, M., Cuevas, E., Baldasano, J. M., Pey, J., Remy, S., and Cvetkovic, B.: Forecasting the northern African dust outbreak towards Europe in April 2011: a model intercomparison, Atmospheric Chemistry and Physics, 16, 4967–4986, 15 https://doi.org/10.5194/acp-16-4967-2016, https://www.atmos-chem-phys.net/16/4967/2016/, 2016.

IPCC: The Physical Science Basis. Intergovernmental Panel on Climate Change, https://doi.org/doi:10.1017/CBO9781107415324, 2013. Jarosyawski, J., Krzyscin, J.W., Puchalski, S., Sobolewski, P.: On the optical thickness in the UV range: analysis of the ground-based data taken at Belsk, Poland. Journal of Geophysical Research 108 (D23), doi: 10.1029/ 2003JD003571, 2003.

Kahn, R. A. and Gaitley, B. J.: An analysis of global aerosol type as retrieved by MISR, Journal of Geophysical Research: Atmospheres, 120, 4248–4281, https://doi.org/10.1002/2015JD023322, https://agupubs.onlinelibrary.wiley.com/doi/abs/10.1002/2015JD023322, 2015.

Kalnay, E., Kanamitsu, M., Kistler, R., Collins, W., Deaven, D., Gandin, L., Iredell, M., Saha, S., White, G., Woollen, J., et al.: The 20 NCEP/NCAR 40-year reanalysis project, Bulletin of the American meteorological Society, 77, 437–472, 1996.

Kasten, F.: A new table and approximation formula for the relative optical air mass, Archiv für Meteorologie, Geophysik und Bioklimatologie, Serie B, 14, 206–223, https://doi.org/https://doi.org/10.1007/BF02248840, 1966.

Kasten, F. and Young,A. T.: Revised optical air mass tables and approximation formula, Appl. Opt., 28, 4735–4738, https://doi.org/10.1364/AO.28.004735, 1989.

Kazadzis, S., Veselovskii, I., Amiridis, V., Gröbner, J., Suvorina, A., Nyeki, S., Gerasopoulos, E., Kouremeti, N., Taylor, M., Tsekeri, A., and Wehrli, C.: Aerosol microphysical retrievals from precision filter radiometer direct solar radiation measurements and comparison with AERONET, Atmospheric Measurement Techniques, 7, 2013–2025, https://doi.org/10.5194/amt-7-2013-2014, https: //www.atmos-meas-tech.net/7/2013/2014/, 2014.

Kazadzis, S., Kouremeti, N., Diémoz, H., Gröbner, J., Forgan, B. W., Campanelli, M., Estellés, V., Lantz, K., Michalsky, J., Carlund, T., Cuevas, E., Toledano, C., Becker, R., Nyeki, S., Kosmopoulos, P. G., Tatsiankou, V., Vuilleumier, L., Denn, F. M., Ohkawara, N., Ijima, O., Goloub, P., Raptis, P. I., Milner, M., Behrens, K., Barreto, A., Martucci, G., Hall, E., Wendell, J., Fabbri, B. E., and Wehrli, C.: Results from the Fourth WMO Filter Radiometer Comparison for aerosol optical depth measurements, Atmospheric Chemistry and Physics, 18, 3185–3201, https://doi.org/10.5194/acp-18-3185-2018, 2018a.

Kazadzis, S., Kouremeti, N., Nyeki, S., Gröbner, J., and Wehrli, C.: The World Optical Depth Research and Calibration Center (WORCC) quality assurance and quality control of GAW-PFR AOD measurements, Geoscientific Instrumentation, Methods and Data Systems, 7, 39–53, https://doi.org/10.5194/gi-739-2018, https://www.geosci-instrum-method-data-syst.net/7/39/2018/, 2018b.

Kentarchos, A., Roelofs, G.J., Lelieveld, J., and Cuevas, E.: On the origin of elevated surface ozone concentrations at Izaña Observatory during the last days of March 1996: a model study, Geophys. Res. Lett., Vol. 27, 22, 3,699-3,702, 2000.

Kim, S.-W., Jefferson, A., Soon-Chang, Y., Dutton, E., Ogren, J., Valero, F., Kim, J., and Holben, B.: Comparisons of aerosol optical depth and surface shortwave irradiance and their effect on the aerosol surface radiative forcing estimation, Journal of Geophysical Research: Atmospheres, 110, https://doi.org/10.1029/2004JD004989, 2005.

Kim, S.-W., Yoon, S.-C., Kim, J., and Kim, S.-Y.: Seasonal and monthly variations of columnar aerosol optical properties over east Asia determined from multi-year MODIS, LIDAR, and AERONET Sun/sky radiometer measurements, Atmospheric Environment, 41, 1634– 1651, https://doi.org/https://doi.org/10.1016/j.atmosenv.2006.10.044, 2007.

Kim, S.-W., Yoon, S.-C., Dutton, E., Kim, J., and Wehrli, C.and Holben, B.: Global surface-based sun photometer network for long-term observations of column aerosol optical properties: intercomparison of aerosol optical depth, Aerosol Science and Technology, 42, 1–9, https://doi.org/https://doi.org/10.1080/02786820701699743, 2008.

Klingmüller, K., Pozzer, A., Metzger, S., Stenchikov, G. L., and Lelieveld, J.: Aerosol optical depth trend over the Middle East, Atmospheric Chemistry and Physics, 16, 5063–5073, https://doi.org/10.5194/acp-16-5063-2016, 2016.

Komhyr, W.: Dobson spectrophotometer systematic total ozone measurement error, Geophysical Research Letters, 7, 161–163, 1980.

Komhyr, W. D., Grass, R. D., and Leonard, R. K.: Dobson spectrophotometer 83: A standard for total ozone measurements, 1962–1987, Journal of Geophysical Research: Atmospheres, 94, 9847–9861, https://doi.org/10.1029/JD094iD07p09847, 1989. Mahowald, N., M., Albani, S. Kok, J. F., Engelstaeder, S., Scanza, R., Ward, D. S., Flanner, M. G.: The size distribution of desert dust aerosols and its impact on the Earth system, Aeolian Research, 15, 53-71, 2014.

McArthur, L. J. B., Halliwell, D. H., Niebergall, O. J., O'Neill, N. T., Slusser, J. R., and Wehrli, C.: Field comparison of network Sun photometers, Journal of Geophysical Research: Atmospheres, 108, https://doi.org/10.1029/2002JD002964, 2003.

McPeters, R., Frith, S., and Labow, G.: OMI total column ozone: extending the long-term data record, Atmospheric Measurement Techniques, 8, 4845–4850, https://doi.org/https://doi.org/10.5194/amt-8-4845-2015, 2015.

Mitchell, R. and Forgan, B.: Aerosol measurement in the Australian outback: Intercomparison of sun photometers, Journal of Atmospheric 20 and Oceanic Technology, 20, 54–66, https://doi.org/https://doi.org/10.1175/1520-0426(2003)020<0054:AMITAO>2.0.CO;2, 2003.

Mitchell, R. M., Forgan, B. W., and Campbell, S. K.: The Climatology of Australian Aerosol, Atmos. Chem. Phys., 17, 5131-5154, https://doi.org/10.5194/acp-17-5131-2017, 2017.

Nakajima, T., Yoon, S. C., Ramanathan, V., Shi, G. Y., Takemura, T., Higurashi, A., Takamura, T., Aoki, K., Sohn, B. J., Kim, S. W., Tsuruta, H., Sugimoto, N., Shimizu, A., Tanimoto, H., Sawa, Y., Lin, N. H., Lee, C. T., Goto, D., and Schutgens, N.: Overview of the Atmospheric Brown Cloud East Asian Regional Experiment 2005 and a study of the aerosol direct radiative forcing in east Asia, J. Geophys. Res., 112, D24S91, doi:10.1029/2007JD009009, 2007.

Nyeki, S., Halios, C., Baum, W., Eleftheriadis, K., Flentje, H., Gröbner, J., Vuilleumier, L., and Wehrli, C.: Ground-based aerosol optical depth trends at three high-altitude sites in Switzerland and southern Germany from 1995 to 2010, Journal of Geophysical Research: Atmospheres, 117, https://doi.org/https://doi.org/10.1029/2012JD017493, 2012.

Nyeki, S., Gröbner, J., and Wehrli, C.: Ground-based aerosol optical depth inter-comparison campaigns at European EUSAAR super-sites, 25 vol. 1531, pp. 584–587, https://doi.org/10.1063/1.4804837, 2013.

Nyeki, S., Wehrli, C., Gröbner, J., Kouremeti, N., Wacker, S., Labuschagne, C., Mbatha, N., and Brunke, E.-G.: The GAW-PFR aerosol optical depth network: The 2008–2013 time series at Cape Point Station, South Africa, Journal of Geophysical Research: Atmospheres, 120, 5070–5084, 2015. Räisänen, P., Isaac, G. A., Barker, H. W. and Gultepe, I.: Solar radiative transfer for stratiform clouds with horizontal variations in liquid-water path and droplet effective radius, Quart. J. Roy. Meteor. Soc., 129, 2135-2149, doi: 10.1256/qj.02.149, 2003.

Rodríguez, S., González, Y., Cuevas, E., Ramos, R., Romero, P. M., Abreu-Afonso, J., and Redondas, A.: Atmospheric nanoparticle observations in the low free troposphere during upward orographic flows at IzaÃña Mountain Observatory, Atmospheric Chemistry and Physics, 9, 6319–6335, https://doi.org/10.5194/acp-9-6319-2009, 2009.

Rodríguez, S., Alastuey, A., Alonso-Pérez, S., Querol, X., Cuevas, E., Abreu-Afonso, J., Viana, M., Pérez, N., Pandolfi, M., and de la Rosa, J.: Transport of desert dust mixed with North African industrial pollutants in the subtropical Saharan Air Layer, Atmospheric Chemistry and Physics, 11, 6663–6685, https://doi.org/10.5194/acp-11-6663-2011, 2011.

Rodríguez, S., Cuevas, E., Prospero, J. M., Alastuey, A., Querol, X., López-Solano, J., García, M. I., and Alonso-Pérez, S.: Modulation of Saharan dust export by the North African dipole, Atmospheric Chemistry and Physics, 15, 7471–7486, https://doi.org/10.5194/acp-157471-2015, 2015.

Rodriguez-Franco, J. J., and Cuevas, E.: Characteristics of the subtropical tropopause region based on long-term highly-resolved sonde records over Tenerife, J. Geophys. Res. Atmos., 118, doi:10.1002/jgrd.50839, 2013.

Romero, P. M. and Cuevas, E.: Variación diurna del espesor óptico de aerosoles:¿ ficción o realidad?, 3 Asamblea Hispano Portuguesa de Geofísica y Geodesia. Valencia, 2002.

Romero-Campos, P., Cuevas, A., Kazadzis, S., Kouremeti, N., García, R., and Guirado-Fuentes, C.: Análisis de la trazabilidad en los valores del AOD obtenidos a partir de las medidas de las redes AERONET-CIMEL y GAW-PFR durante el período 2005-2015 en el Observatorio Atmosférico de Izaña, 2017.

Russell, P. B., Livingston, J. M., Dubovik, O., Ramirez, S. A., Wang, J., Redemann, J., Schmid, B., Box, M., and Holben, B. N.: Sunlight transmission through desert dust and marine aerosols: Diffuse light corrections to Sun photometry and pyrheliometry, J. Geophys. Res., 109, D08207, 10.1029/2003JD004292, 2004.

Sakerin, S. M., Kabanov, D. M., Panchenko, M. V., Pol'kin, V. V., Holben, B. N., Smirnov, A. V., Beresnev, S. A., Gorda, S. Y., Kornienko, G. I., Nikolashkin, S. V., Poddubnyi, V. A., and Tashchilin, M. A.: Monitoring of atmospheric aerosol in the Asian part of Russia in 2004 within the framework of AEROSIBNET program, Atmos. Oceanic Optics, 18, 871–878, 2005.

Sayer, A. M., Hsu, N. C., Bettenhausen, C., Jeong, M., Holben, B. N., and Zhang, J.: Global and regional evaluation of over-land spectral aerosol optical depth retrievals from SeaWiFS, Atmospheric Measurement Techniques, 5, 1761–1778, https://doi.org/10.5194/amt-51761-2012, 2012.

Sayer, A. M., Hsu, N. C., Bettenhausen, C., and Jeong, M.: Validation and uncertainty estimates for MODIS Collection 6 "Deep Blue" aerosol 10 data, Journal of Geophysical Research: Atmospheres, 118, 7864–7872, https://doi.org/10.1002/jgrd.50600, https://agupubs.onlinelibrary.wiley.com/doi/abs/10.1002/jgrd.50600, 2013.

Schmid, B. and Wehrli, C.: Comparison of Sun photometer calibration by use of the Langley technique and the standard lamp, Appl. Opt., 34, 4500–4512, https://doi.org/10.1364/AO.34.004500, http://ao.osa.org/abstract.cfm?URI=ao-34-21-4500, 1995.

Schmid, B., Michalsky, J., Halthore, R., Beauharnois, M., Harrison, L., Livingston, J., Russell, P., Holben, B., Eck, T., and Smirnov, A.: Comparison of aerosol optical depth from four solar radiometers during the fall 1997 ARM intensive observation period, Geophysical Research Letters, 26, 2725–2728, https://doi.org/10.1029/1999GL900513, https://agupubs.onlinelibrary.wiley.com/doi/abs/10.1029/1999GL900513, 1999.

Sinyuk, A., Holben, B.N., Smirnov, A., Eck, T.F., Slutsker, I., Schafer, J.S., Giles, D.M., and Sorokin, M.: Assessment of error in aerosol optical depth measured by AERONET due to aerosol forward scattering, Geophys. Res. Lett., 39, 23806, doi:10.1029/2012GL053894, 2012.

Smirnov, A., Holben, B., Eck, T., Dubovik, O., and Slutsker, I.: Cloud-screening and quality control algorithms for the AERONET database, Remote sensing of environment, 73, 337–349, https://doi.org/https://doi.org/10.1016/S0034-4257(00)00109-7, http://www.sciencedirect. 20 com/science/article/pii/S0034425700001097, 2000.

Takamura, T., and Nakajima, T.: Overview of SKYNET and its activities, Opt. Pura Apl., 37, 3303-3308, 2004.

Thomason, L.W., Herman, B. M., Schotland, R.M., and Reagan, J.A.: Extraterrestrial solar flux measurement limitations due to a Beer's law assumption and uncertainty in local time, Appl. Opt., 21, 1191–1195, https://doi.org/10.1364/AO.21.001191, 1982.

Todd, M. C., Washington, R., Martins, J. V., Dubovik, O., Lizcano, G., M'bainayel, S., and Engelstaedter, S.: Mineral dust emission from the Bodélé Depression, northern Chad, during BoDEx 2005, Journal of Geophysical Research: Atmospheres, 112, https://doi.org/https://doi.org/10.1029/2006JD007170, 2007.

Toledano, C., Cachorro, V. E., Berjón, A., de Frutos, A. M., Sorribas, M., de la Morena, B. A., and Goloub, P.: Aerosol optical depth and Ångström exponent climatology at El Arenosillo AERONET site (Huelva, Spain), Quarterly Journal of the Royal Meteorological Society, 133, 795–807, https://doi.org/10.1002/qj.54, https://rmets.onlinelibrary.wiley.com/doi/abs/10.1002/qj.54, 2007.

Toledano, C., Cachorro, V. E., Berjon, A., de Frutos, A. M., Fuertes, D., Gonzalez, R., Torres, B., Rodrigo, R., Bennouna, Y., Martin, L., and Guirado, C.: RIMA-AERONET network: long-term monitoring of aerosol properties, Opt. Pura Apl., 44, 629–633, 2011.

Toledano, C., Cachorro, V., Gausa, M., Stebel, K., Aaltonen, V., Berjón, A., de Galisteo, J. P. O., de Frutos, A. M., Bennouna, Y., Blindheim, S., Myhre, C. L., Zibordi, G., Wehrli, C., Kratzer, S., Hakansson, B., Carlund, T., de Leeuw, G., Herber, A., and Torres, B.: Overview of Sun Photometer Measurements of Aerosol Properties in Scandinavia and Svalbard, Atmospheric Environment, 52, 18–28, 30 https://doi.org/10.1016/j.atmosenv.2011.10.022, 2012.

Toledano, C., González, R., Fuertes, D., Cuevas, E., Eck, T. F., Kazadzis, S., Kouremeti, N., Gröbner, J., Goloub, P., Blarel, L., Román, R., Barreto, A., Berjón, A., Holben, B. N., and Cachorro, V. E.: Assessment of Sun photometer Langley calibration at the high-elevation sites Mauna Loa and Izaña, Atmospheric Chemistry and Physics, 18, 14555–14567, https://doi.org/10.5194/acp-18-14555-2018, 2018.

Torres, B., Toledano, C., Berjón, A., Fuertes, D., Molina, V., Gonzalez, R., Canini, M., Cachorro, V. E., Goloub, P., Podvin, T., Blarel, L., Dubovik, O., Bennouna, Y., and de Frutos, A. M.: Measurements on pointing error and field of view of Cimel-318 Sun photometers in the scope of AERONET, Atmospheric Measurement Techniques, 6, 2207–2220, https://doi.org/10.5194/amt-6-2207-2013, 2013.

Wagner, F. and Silva, A. M.: Some considerations about Angström exponent distributions, Atmospheric Chemistry and Physics, 8, 481–489, https://doi.org/10.5194/acp-8-481-2008, 2008.

Wang, J., Xia, X., Wang, P., and Christopher, S.: Diurnal variability of dust aerosol optical thickness and Ångströ¨m exponent over dust source regions in China, Geophysical Research Letters, 31, https://doi.org/10.1029/2004GL019580, 2004.

Weinzierl, B., Sauer, D., Esselborn, M., Petzold, A., Veira, A., Rose, M., Mund, S., Wirth, M., Ansmann, A., Tesche, M., Gross, S., and Freudenthaler, V.: Microphysical and optical proper-ties of dust and tropical biomass burning aerosol layers in the Cape Verde region-an overview of the airborne in situ and lidar measurements during SAMUM-2, Tellus B, 63, 589–618, doi:10.1111/j.1600-0889.2011.00566.x, 2011.

Wehrli, C.: Calibrations of filter radiometers for determination of atmospheric optical depth, Metrologia, 37, 419, http://stacks.iop.org/ 0026-1394/37/i=5/a=16, 2000. Wehrli, C.: GAWPFR: A network of aerosol optical depth observations with precision filter radiometers, Global Atmosphere Watch 2005.

Wehrli, C.: Precision Filter Radiometer Documentation, Version 4.0, 38 pp., Davos Dorf, 2008a.Wehrli, C.: Remote sensing of aerosol optical depth in a global surface network, Ph.D. thesis, ETH Zurich, https://www.research-collection.ethz.ch/bitstream/handle/20.500.11850/150574/eth-30693-02.pdf, 2008b.

Wilbert, S.: Determination of circumsolar radiation and its effect on concentrating solar power, Ph.D. thesis, Hochschulbibliothek der Rheinisch-Westfälischen Technischen Hochschule Aachen, https://d-nb.info/1059537710/34, 2014.

WMO: Recent Progress in Sunphotometry. Determination of the aerosol optical depth, Environmental Pollution Monitoring and Research Programme, Nº 43, 21 pp, November, https://library.wmo.int/pmb_ged/wmo-td_143.pdf, 1986.

WMO: Aerosol measurement procedures, guidelines and recommendations, GAW Report No. 153, WMO TD No. 1178, https://library.wmo. int/pmb_ged/wmo-td_1178.pdf, 2003.

WMO: WMO/GAW Experts Workshop on a Global Surface-Based Network for Long Term Observations of Column Aerosol Optical Properties,GAW Report No. 162, WMO TD No. 1287, https://library.wmo.int/pmb_ged/wmo-td_1287.pdf, 2005.

WMO: Abridged final report with resolutions and recommendations, GAW Report WMO TD No. 1019, WMO-CIMO Fourteenth session Geneva 7–14 December 2006, 2007. WMO: WMO/GAW Aerosol Measurement Procedures, Guidelines and Recommendations, 2nd Edition, WMO No 1177, GAW Report No. 227, 93 pp, https://library.wmo.int/doc_num.php?explnum_id=3073, 2016.

Young, A. T.: Revised depolarization corrections for atmospheric extinction, Appl. Opt., 19, 3427–3428,https://doi.org/10.1364/AO.19.003427, 1980.

Supplement of

Aerosol Optical Depth comparison between GAW-PFR and AERONET-Cimel radiometers from long term (2005-2015) 1-minute synchronous measurements

Emilio Cuevas[1], Pedro Miguel Romero-Campos[1], Natalia Kouremeti[2], Stelios Kazadzis[2], Petri Räisänen[3], Rosa Delia García[4,1], Africa Barreto[5,1,4], Carmen Guirado-Fuentes[4,1], Ramón Ramos[1], Carlos Toledano[4], Fernando Almansa[5,1,4], and Julian Gröbner[2]

[1]Izaña Atmospheric Research Center (IARC), State Meteorological Agency (AEMET), Spain

[2]Physikalisch-Meteorologisches Observatorium Davos, World Radiation Center (PMOD/WRC), Davos, Switzerland

[3]Finnish Meteorological Institute, Helsinki, Finland

[4]Atmospheric Optics Group, Valladolid University, Valladolid, Spain

[5]Cimel Electronique, Paris, France

Correspondence: Emilio Cuevas (ecuevasa@aemet.es)

Supplement S1. One-minute AOD data differences between AERONET-Cimel (V3) and GAW-PFR.

One-minute AOD data differences between AERONET-Cimel (V3) and GAW-PFR for (a) 380 nm (75303 data-pairs), (b) 440 nm (76290 data-pairs), (c) 500 nm (75335 data-pairs) and (d) 870 nm (76307 data-pairs) for the period 2005-2015. Black dots correspond to the *U*95 limits. A small number of outliers are out of the ±0.06 AOD differences range. Black arrows indicate a change of Reference AERONET-Cimel radiometer and red arrows indicate a change of the GAW-PFR instrument.

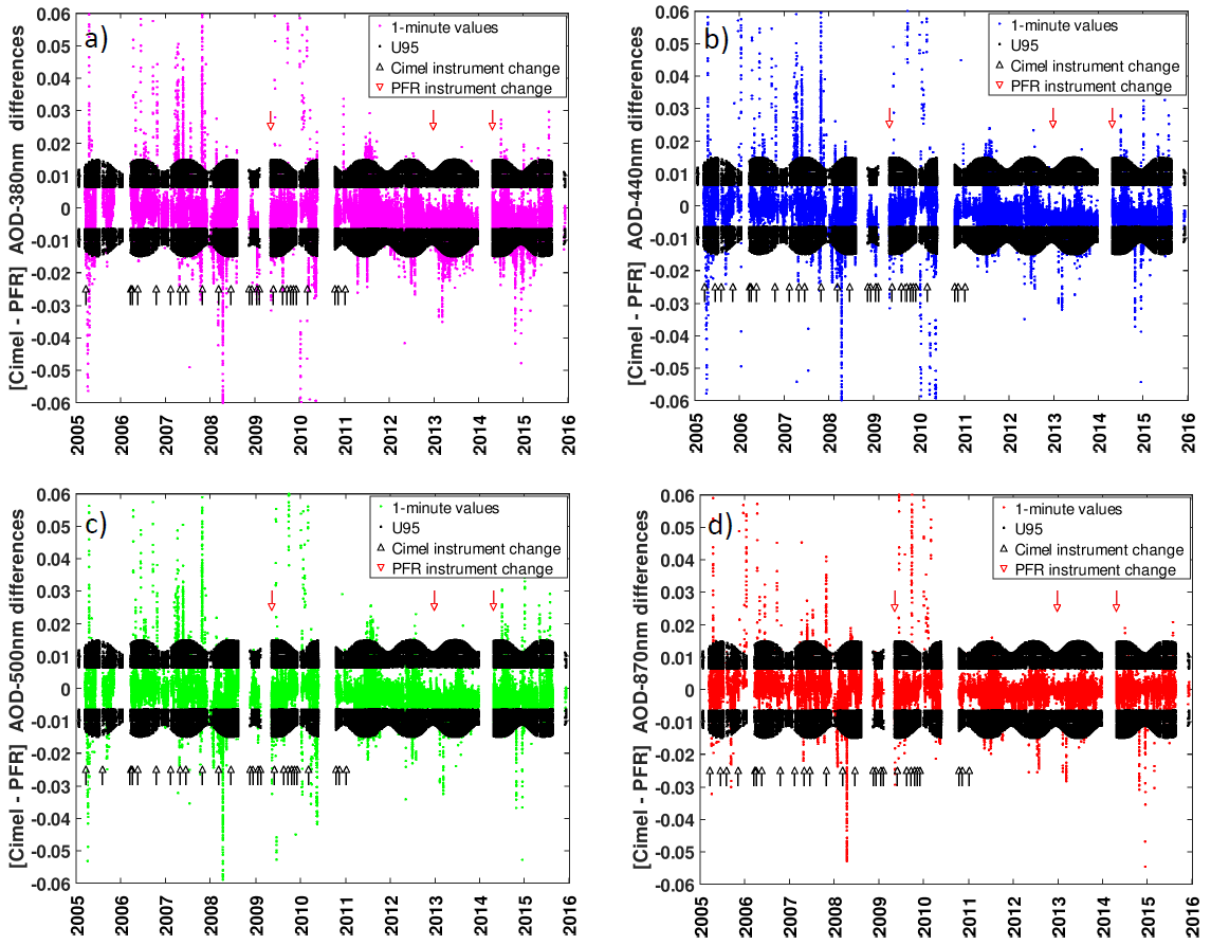

Supplement S2. Percentage of [Cimel (V3)-PFR] 1-minute AOD differences meeting the WMO criteria for the four compared channels.

Percentage of AERONET-Cimel 1-minute AOD data (V3) meeting the WMO criteria for the four compared channels, and different AOD and AE scenarios for the period 2005-2015, number of data pairs are shown in brackets. The last row corresponds to the total percentages for the sub-period 2010-2015. AOD and AE traceability > 95% are marked in bold.This Table is equivalent to Table 4 of the manuscript for AERONET V2.

% of data within WMO limits	380 nm	440 nm	500 nm	870 nm
AOD≤0.05	93.6 (60264)	**96.3 (62836)**	**97.1 (62545)**	**98.4 (64213)**
0.05<AOD≤0.10	91.0 (5138)	92.0 (5217)	92.6 (5222)	94.7 (5372)
AOD>0.10	77.1 (4085)	84.1 (4537)	81.6 (4326)	93.3 (5034)
AE≤0.25	78.7 (2472)	82.3 (2588)	79.0 (2483)	92.9 (6530)
0.25<AE≤0.6	90.2 (5941)	94.3 (6321)	94.9 (6255)	**97.4 (6530)**
AE>0.6	94.1 (56952)	**96.5 (59181)**	**97.1 (58793)**	**98.7 (60514)**
Total 2005-2015	92.3 (69487)	**95.2 (72590)**	**95.7 (72093)**	**97.8 (74619)**
Total 2010-2015	92.8 (42463)	**96.8 (44328)**	**96.8 (44329)**	**98.8 (44329)**

Supplement S3. AOD variability 1 minute interval.

Standard deviation values of 20117 AOD triplets measured with the Cimel#244 in 2013 for 380 and 500nm.

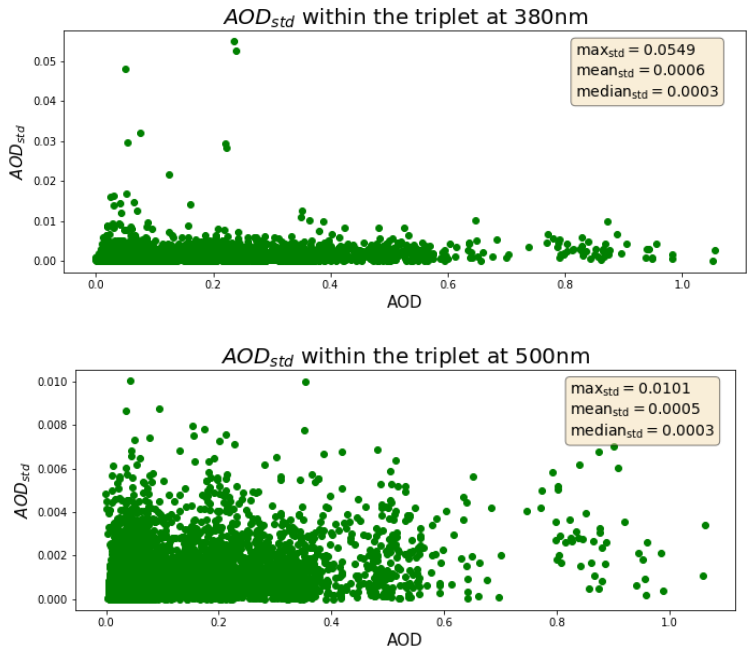

The percentage of data with 1-minute AOD variability for the four GAW-PFR channels are shown in the next figure.

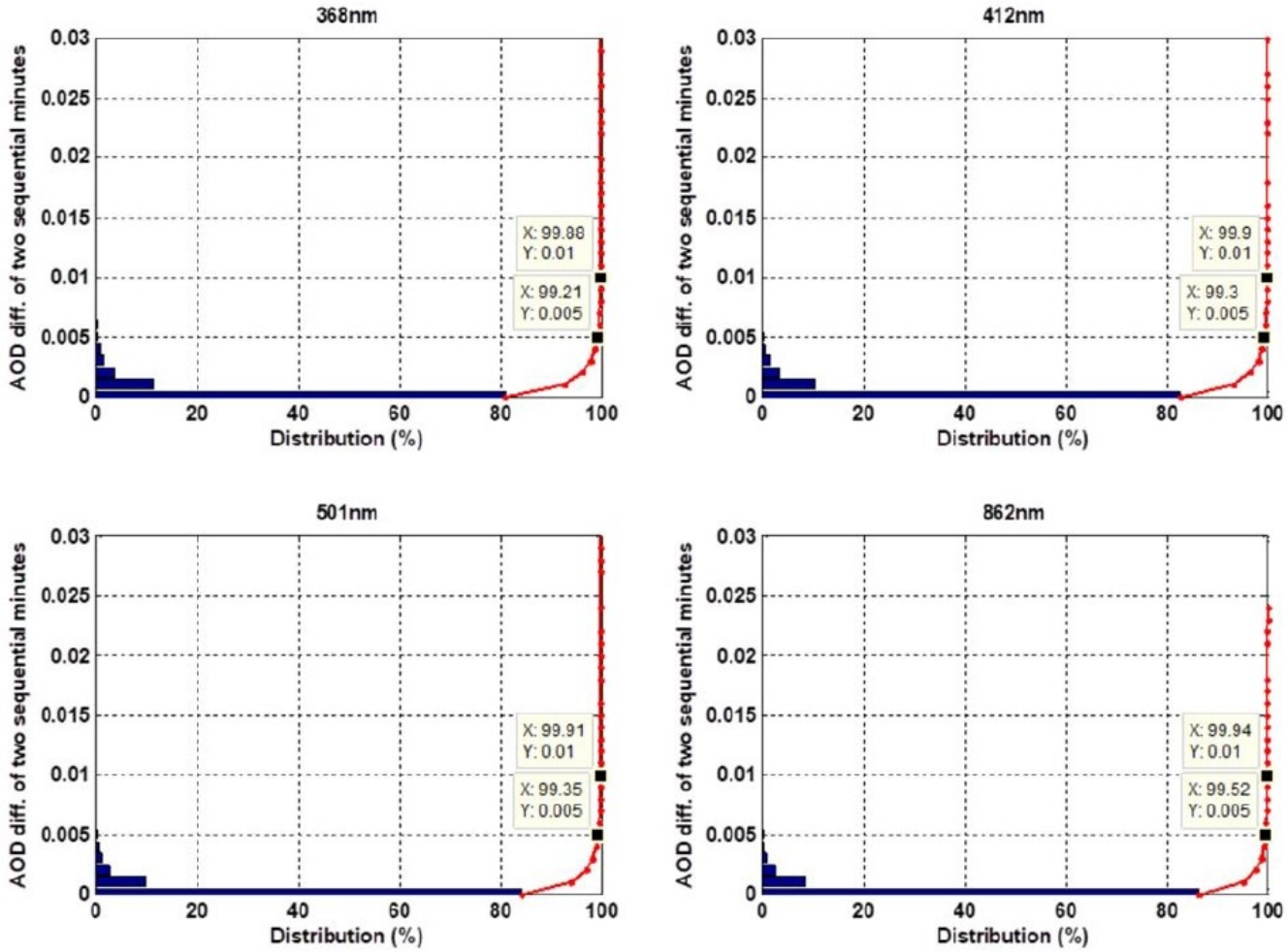

Supplement S4. One-minute AOD differences between AERONET-Cimel (V2 and V3) GAW-and PFR versus optical air mass (m).

One-minute AOD differences between AERONET-Cimel (V2 and V3) and GAW-PFR versus optical air mass (m) under pristine conditions ($AOD_{500nm} \leq 0.03$) in the period 2005-2015 for (a) 380 nm, (b) 440 nm, (c) 500 nm and (d) and 870 nm.

V2

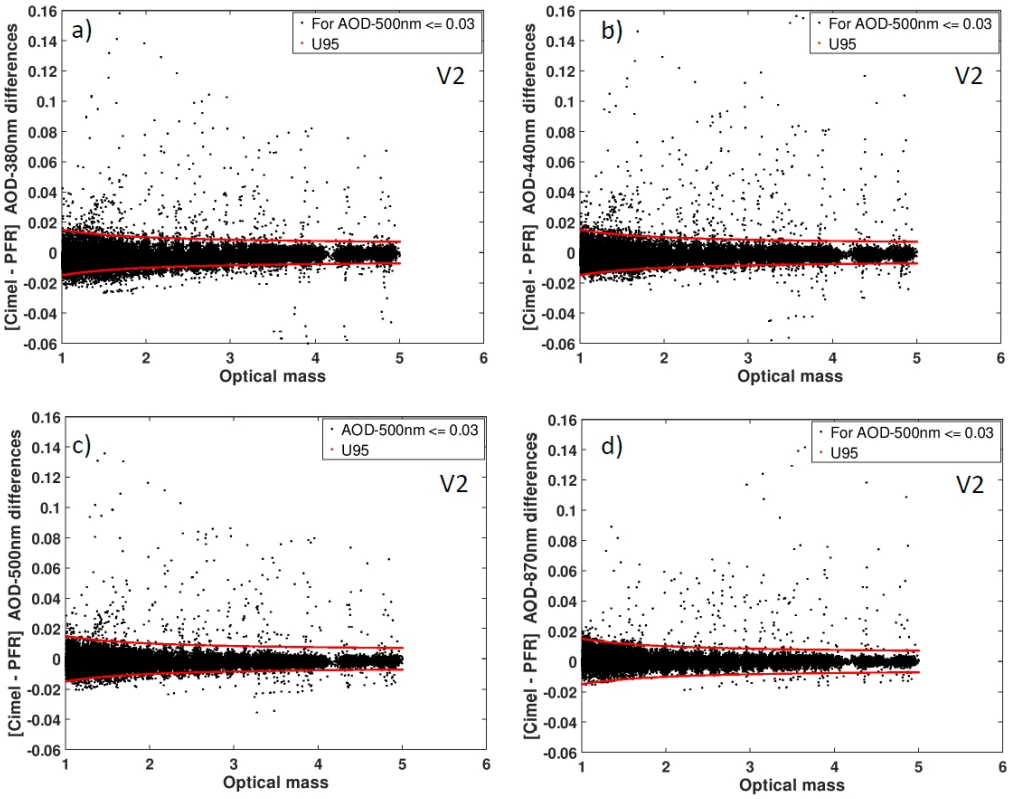

V3

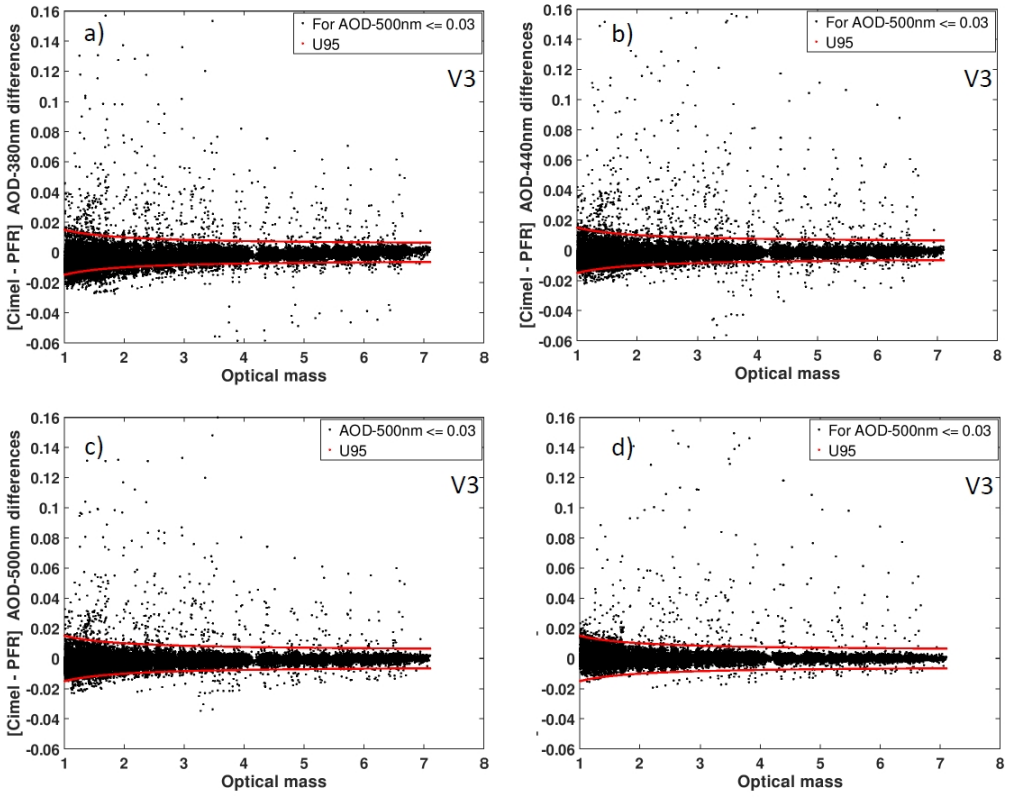

Supplement S5. Percentage of [Cimel (V3)-PFR] 1-minute AOD differences meeting the WMO criteria for each wavelength and for different optical air mass.

Percentage of 1-minute AOD data (V3) meeting the WMO criteria for each wavelength for different optical air mass intervals under pristine conditions ($AOD_{500nm} \leq 0.03$) in the period 2005-2015. This Table is equivalent to Table 7 in the manuscript for AERONET V2.

Percentage of AOD differences within the U95 limits AOD500*nm*≤ 0.03	Total (%)	1 ≤ m < 2 (%)	2 ≤ m < 3 (%)	3 ≤ m < 4 (%)	4 ≤ m < 5 (%)	5 ≤ m < 6 (%)
380 nm	94.9	92.9	95.5	96.7	96.6	96.6
440 nm	97.5	97.2	97.3	98.0	97.6	97.7
500 nm	98.3	98.2	98.2	98.5	98.2	98.3
870 nm	99.0	99.1	99.1	99.1	98.6	98.7

Supplement S6. AOD diurnal range corresponding to AOD outliers under pristine conditions.

AOD diurnal range variation (maximum value minus minimum value of AOD in one day) corresponding to AOD outliers (non-traceable AOD) under pristine conditions ($AOD_{Cimel\text{-}500nm} \leq 0.03$) in the period 2005-2015 for AERONET V2 and V3 and for 440 nm, 500 nm and 870 nm: a) 440 nm V2; b) 440 nm V3; c) 500 nm V2; d) 500 nm V3; e) 870 nm V2; and f) 870 nm V3.

This Figure is equivalent to Figure 3 of the manuscript for 380 nm.

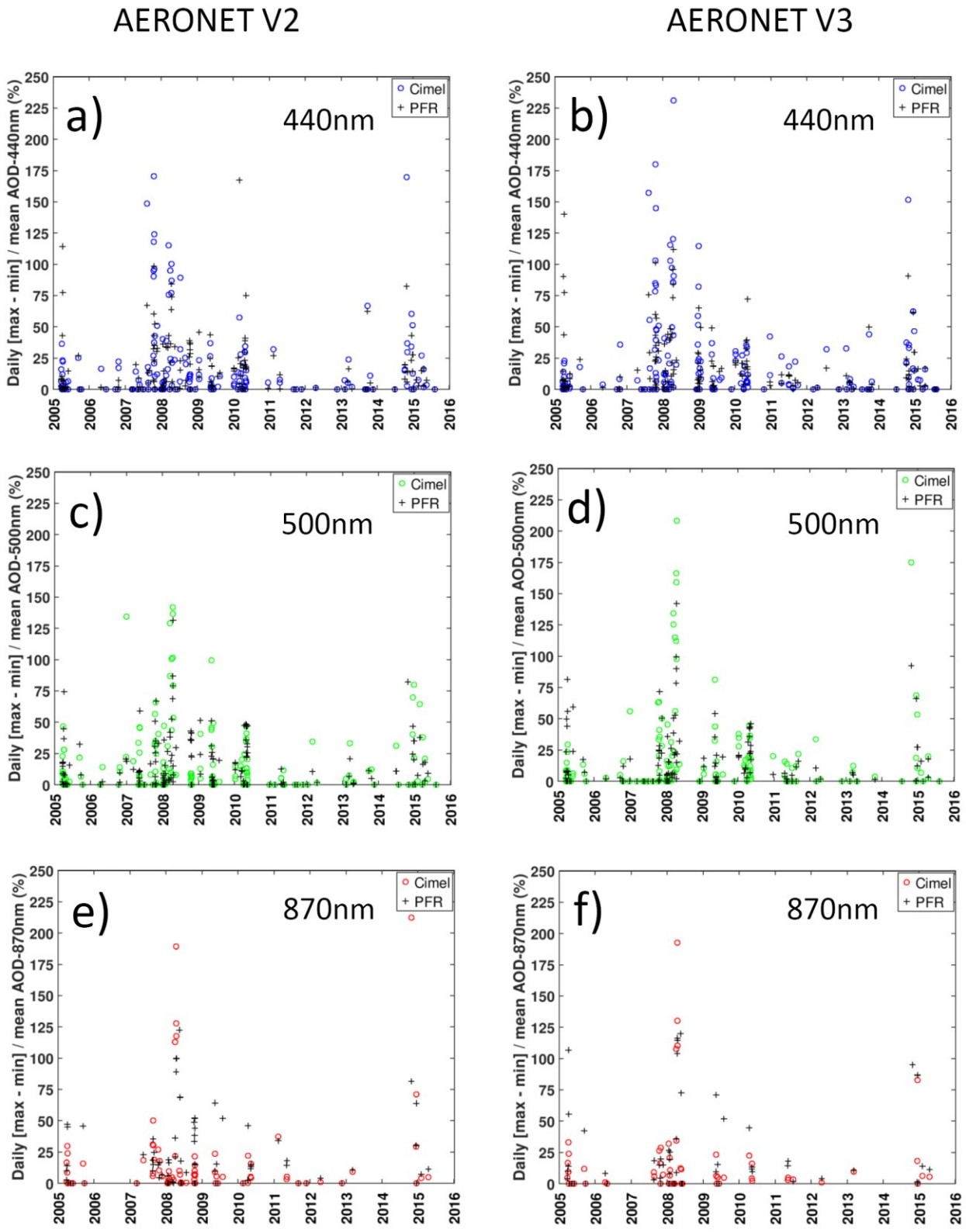

Supplement S7. Percentage of AOD_{380nm} outliers of GAW-PFR and AERONET Cimel (V3).

Percentage of cases with AOD_{380nm} outliers of both GAW-PFR and AERONET Cimel (V3) under pristine conditions (Cimel $AOD_{500nm} \leq 0.03$). In these cases the diurnal AOD range was higher than 25% of the daily mean AOD value for which a certain cause has been determined: calibration inaccuracies, cloud screening algorithm failures, mixture of the two previous causes, poor sun pointing, or unknown causes.

	PFR 51 cases	Cimel 81 cases
Calibration inaccuracies	7.8%	44.4%
Cloud screening failures	29.4%	21.0%
Calibration+ cloud screening errors	9.8%	11.1%
Sun misalignments	17.6%	0%
Unknown	35.3%	33.5%

Supplement S8. Examples of fictitious AOD diurnal variation in both GAW-PFR and AERONET-Cimel.

Examples of fictitious AOD diurnal variation in both GAW-PFR and AERONET-Cimel V3 due to small calibration inaccuracies in the UV channel (368 nm for GAW- PFR and 380 nm for AERONET-Cimel). The date is indicated in the x-axis. In all these cases a clear fictitious AOD diurnal cycle is observed in AERONET-Cimel V3, normally less than 0.01. In cases d), e), and f) an anomalous diurnal cycle is also observed, but in the opposite direction (convex curve), in the case of the GAW-PFR. These cases reflect a non-perfect calibration in the UV channel and are a cause of non-traceability.

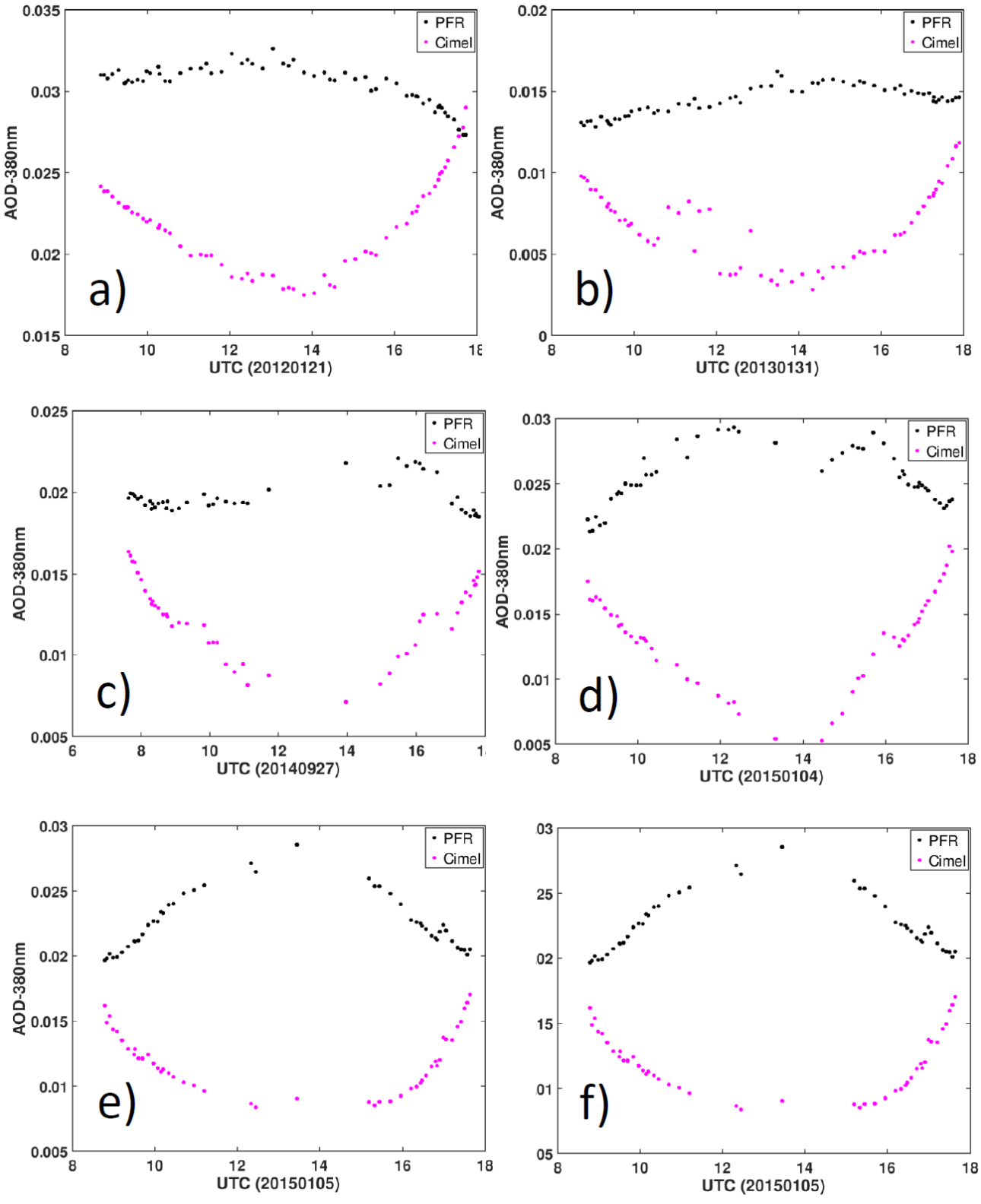

Supplement S9. Examples of AOD diurnal variation of all chanels from AERONET-Cimel Level 2 V3.

The screenshots of AERONET V3 level 2 show that the fictitious diurnal cycle is accentuated, or only clearly observed, in the 340 and 380nm channels.

Screenshots from http://aeronet.gsfc.nasa.gov (last access: 1 february 2019). Izana AERONET station Level 2 Version 3.

28-03-2005

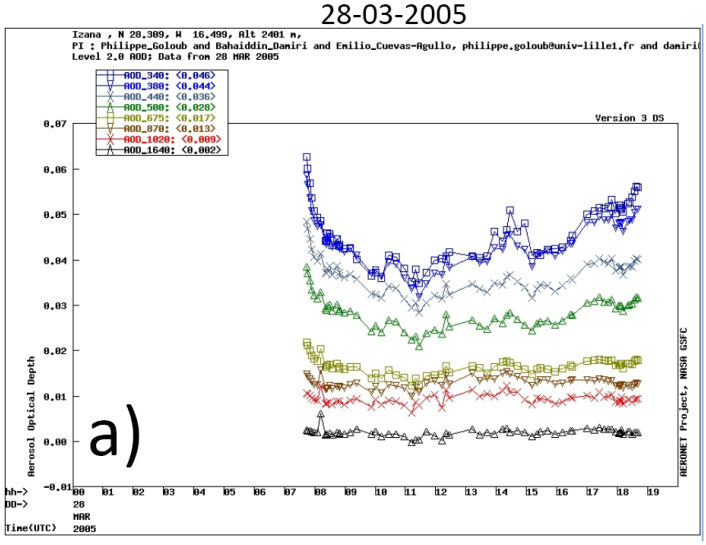

8-10-2007

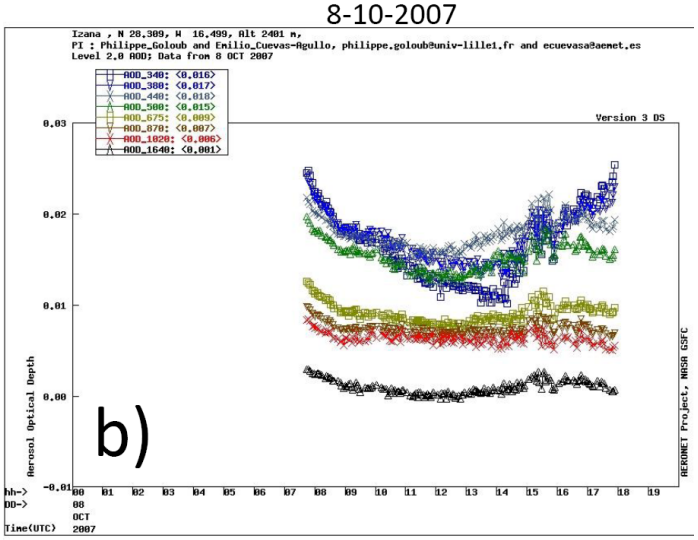

27-03-2015

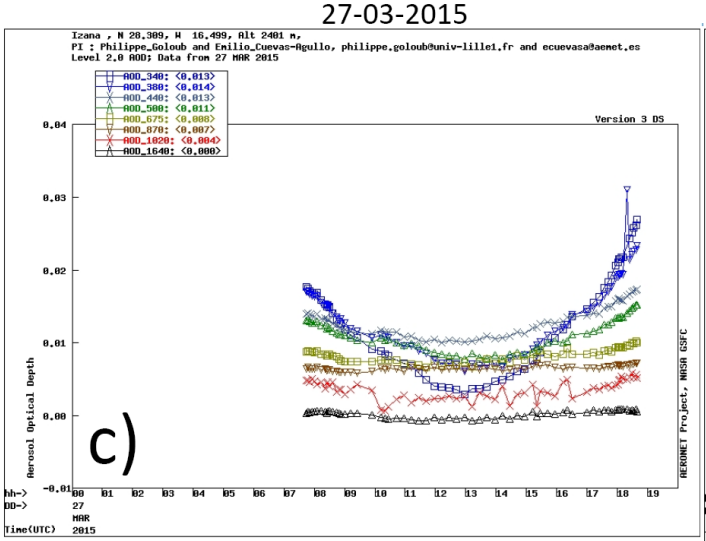

14-04-2015

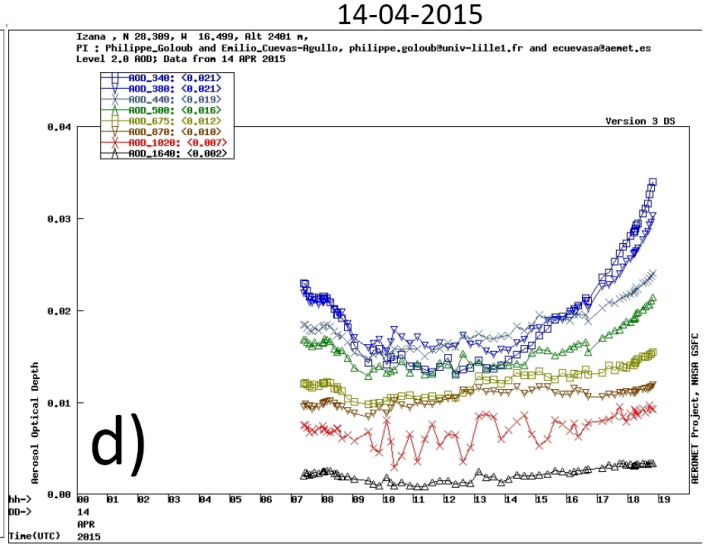

Supplement S10. Case analysis of altostratus above the Saharan Air Layer top.

In this section of the supplement some case analyses are shown analysed in order to highlight the complexity of properly filtering some types of clouds during moderate dust intrusions.

Case analysis S10.1 (18 July 2012): The range corrected backscattering signal vertical cross section of the Micropulse lidar (MPL) (a) shows the presence of altostratus just above the top of the Saharan Ar Layer (SAL), around 6 km height. The total-sky camera images show the presence of middle clouds and dust at 09UTC (b), 11UTC (c) and 16UTC (d). The AERONET V2 AOD records are filtered correctly at those three hours (e), but the AOD values "recovered" by AERONET V3 at those times are very high unreal AOD values, greater than 1.

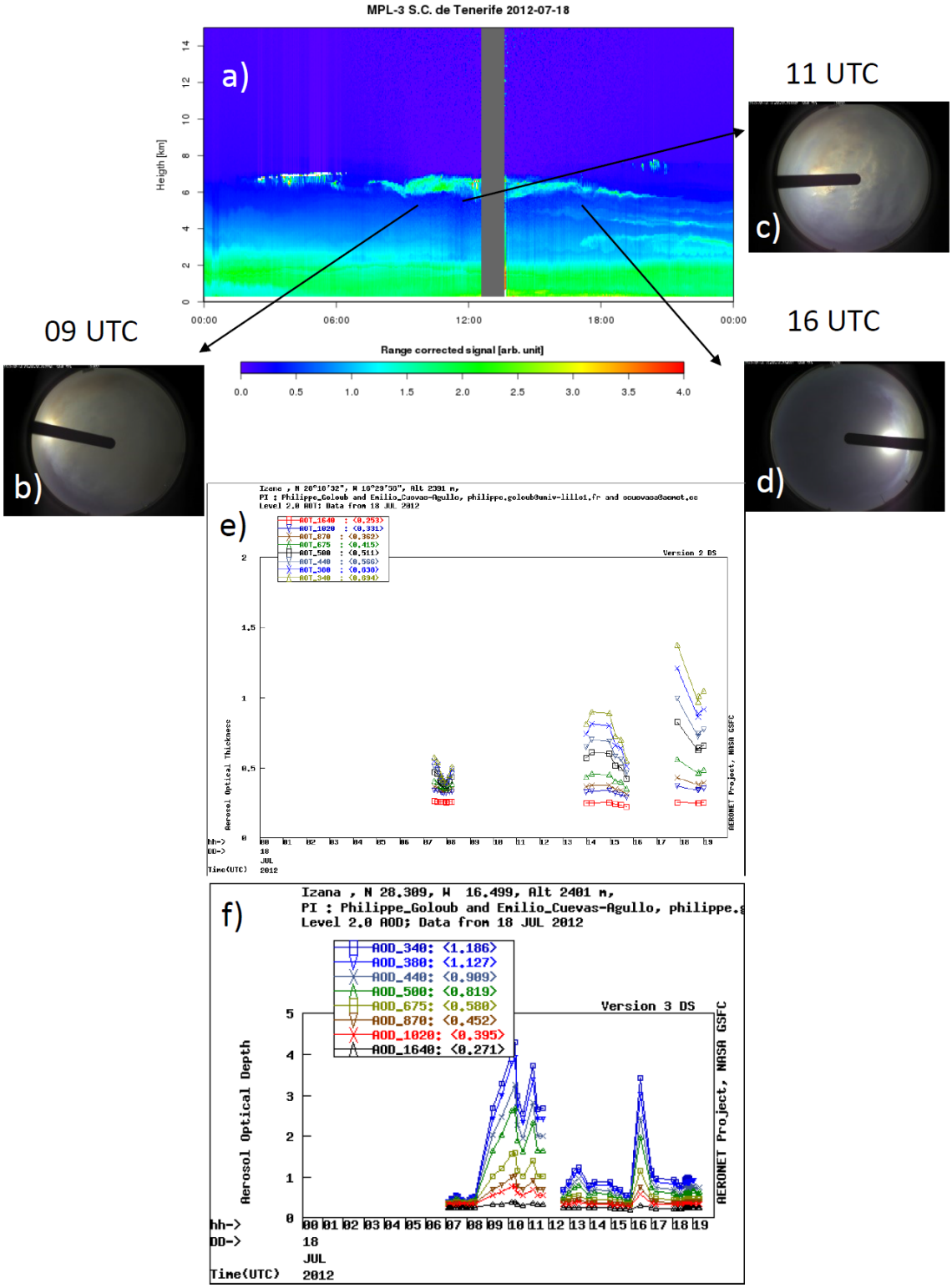

Case analysis S10.2 (8 March 2015): The range corrected backscattering signal vertical cross section of the Micropulse lidar (MPL) (a) shows the presence of thick altostratus just above the top of the Saharan Ar Layer (SAL) that increase altitude throughout the day from 5 to 8 km height to gradually disappear after 15:30 UTC. The total-sky camera image shows the presence of middle clouds and dust at 15:00 UTC (b). Both GAW-PFR and AERONET-V3 have successfully filtered contaminated data by altostratus until 15:00 UTC but do not do so after that time and until they disappear. During that time the clouds are between 7 and 8 km height and give a weaker signal. AOD contaminated by clouds (AOD500nm = 0.35) is substantially higher than at the end of the day (AOD500nm = 0.35) (c) when the SAL shows a greater thickness.

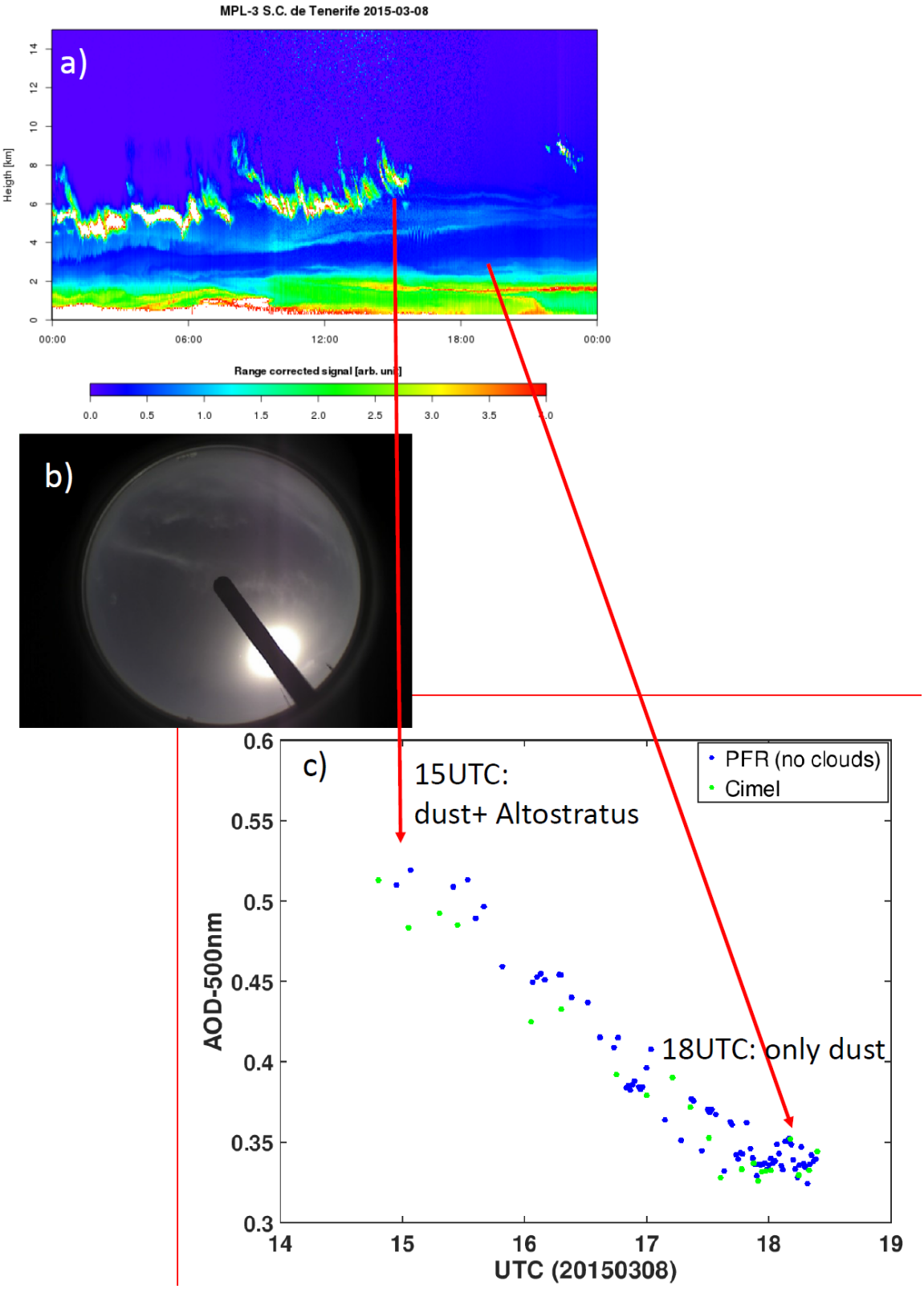

S11. Case analysis of cirrus clouds.

A second type of clouds that cause problems in AOD retrieval are the cirrus clouds, usually being present at Izaña between January and April, associated with the presence of the subtropical jet that is normally found in the vicinity of the Canary Islands at this time of year (Rodríguez-Franco and Cuevas, 2013). A constant cloud optical thickness (COT) corresponding to a cloud of a certain horizontal extension would cause the successive measurements within a minute to correspond to the same cloud stage, and therefore it would not be discernible from the extinction caused by aerosols. In the case of very thin cirrus clouds, AOD could increase up to 0.03 (Chew et al., 2011; Giannakaki et al., 2007) with small fluctuations, that cloud-screening algorithms could interpret as the presence of an aerosol layer. Huang et al. (2012) evaluated the impact on AERONET level 2.0 AOD retrievals from cirrus contamination highlighting the difficulties to remove completely their signature, mainly from those subvisual thin cirrus. According to Kinne et al. (1997), optical depth estimates from cirrus derived with sunphotometers have to include forward-scattering effects. Their results show that for cirrus, and instruments with 2.0° and 2.4° FOV, the correction factors vary between 1.6 and 2.5 depending on the crystal size. Taking into account that the FOV of the GAW-PFR is 2.5°, while that of the AERONET-Cimel is 1.3°, such cases will affect the comparison results.

Three case analyses on cirrus clouds are shown below.

Case analysis S11.1 (September 23, 2015): The range corrected backscattering signal vertical cross section of the Micropulse lidar (MPL) (a) shows scattered cirrus clouds throughout the day (a), and one in particular around 17:45UTC that affects the Cimel AOD measurements. Unfortunately, we do not have measurements for the PFR at this time. The all-sky camera confirms the presence of cirrus clouds at that time (d). The AERONET V2 snapshot registers the impact of the cirrus (b), punctually increasing the AOD values by two. AERONET V3 (c) does not filter these values.

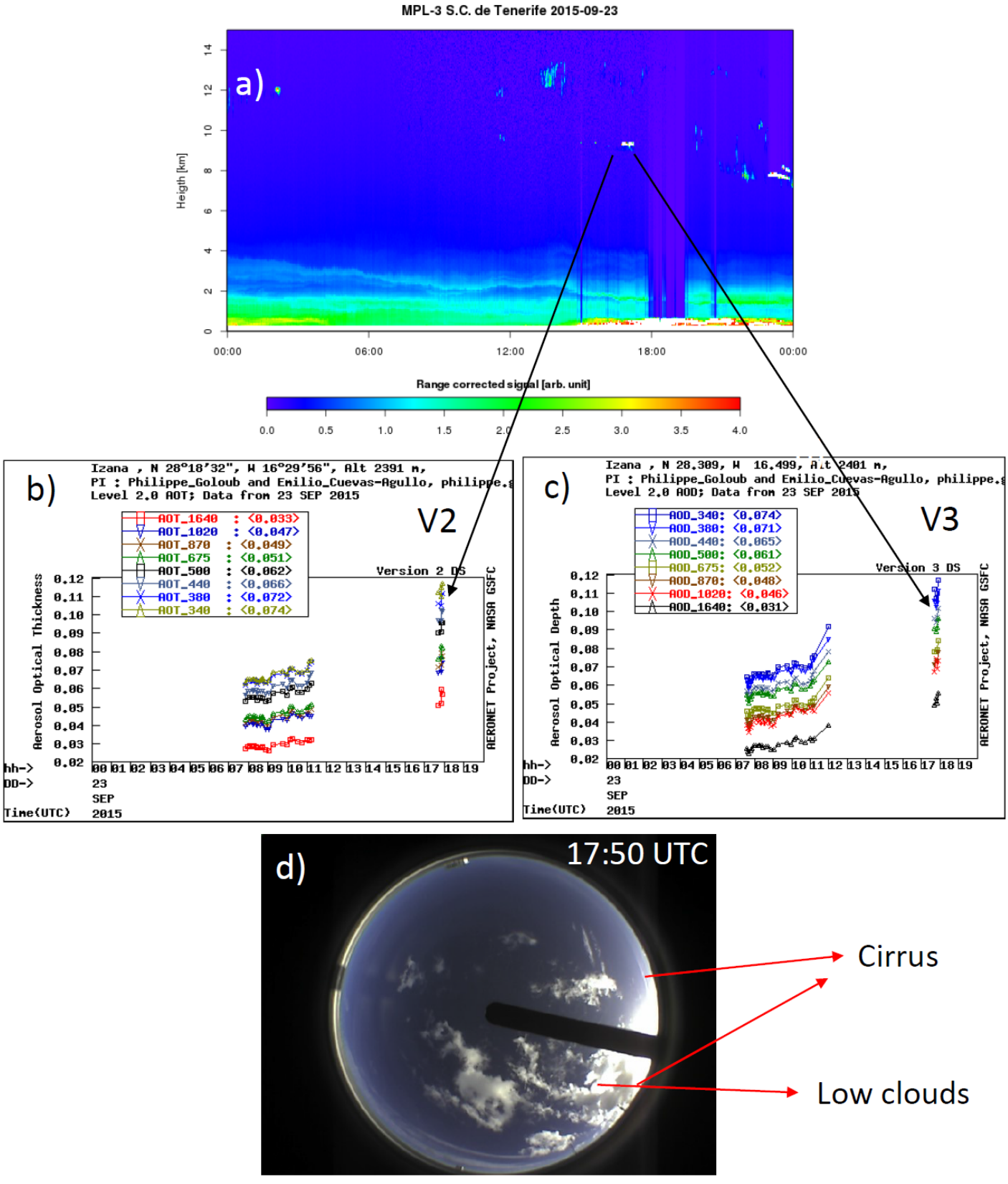

Case analysis S11.2 (February 12, 2015): The range corrected backscattering signal vertical cross section of the Micropulse lidar (MPL) (a) shows the presence of cirrus clouds at around 11 km height between 17:30 and 19:00UTC (a), this is confirmed by the all-sky camera image (b). These cirrus clouds affected the AERONET V2 AOD, increasing the AOD values between 2 and 5 times, depending on the channel (c). AERONET V3 cloud screening correctly filtered these anomalous AOD values (d).

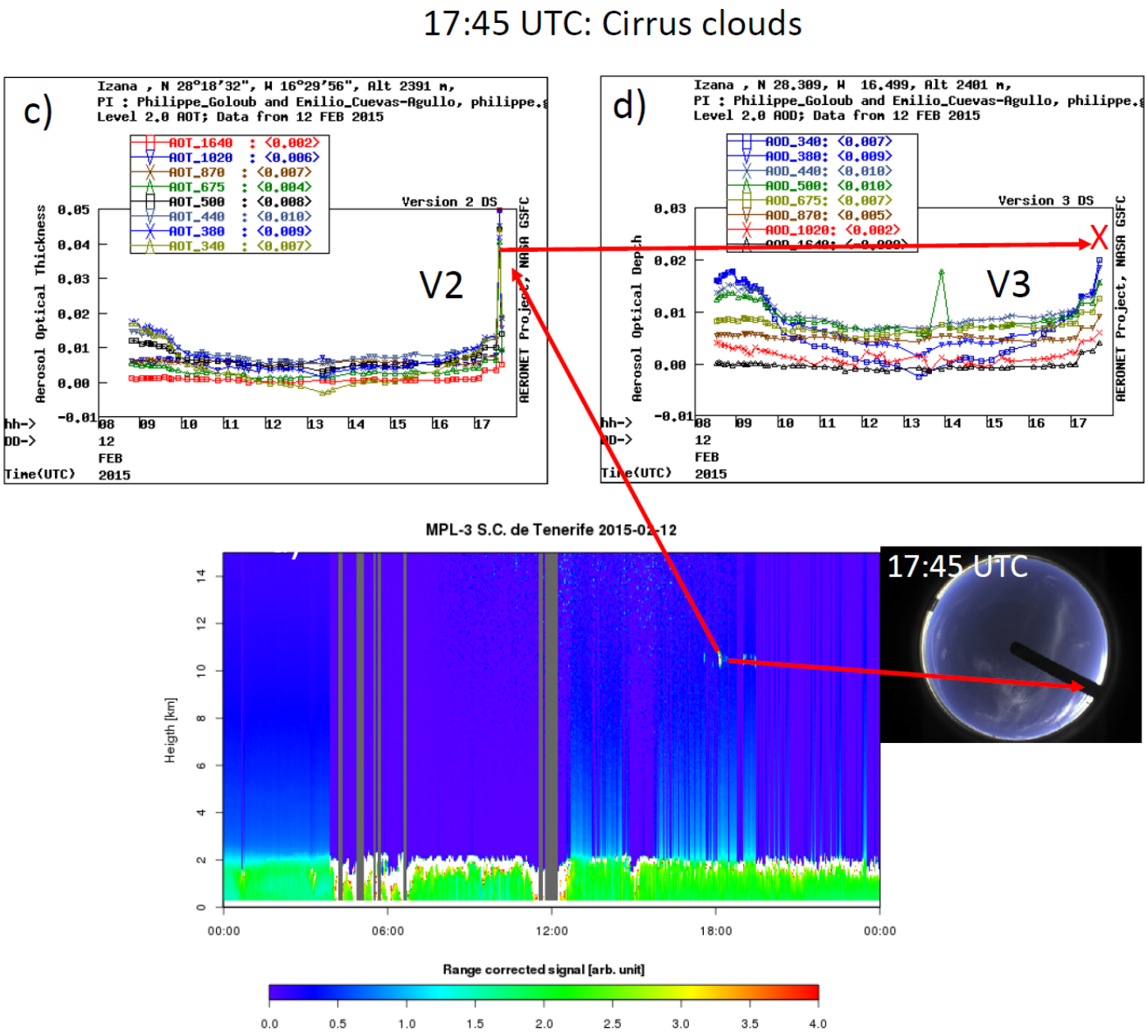

Case analysis S11.3 (March 27, 2010): The cirrus cloud observed by the all-sky camera around 18:30UTC affected both GAW-PFR and AERONET V3, giving AOD values about 8 times higher than those observed early in the morning. The erroneous AOD values of the GAW-PFR are slightly lower than those of AERONET V3. The cause could be a greater forward-scattering effect of the cirrus cloud on the GAW-PFR due to its higher FOV (compared with that of the Cimel).

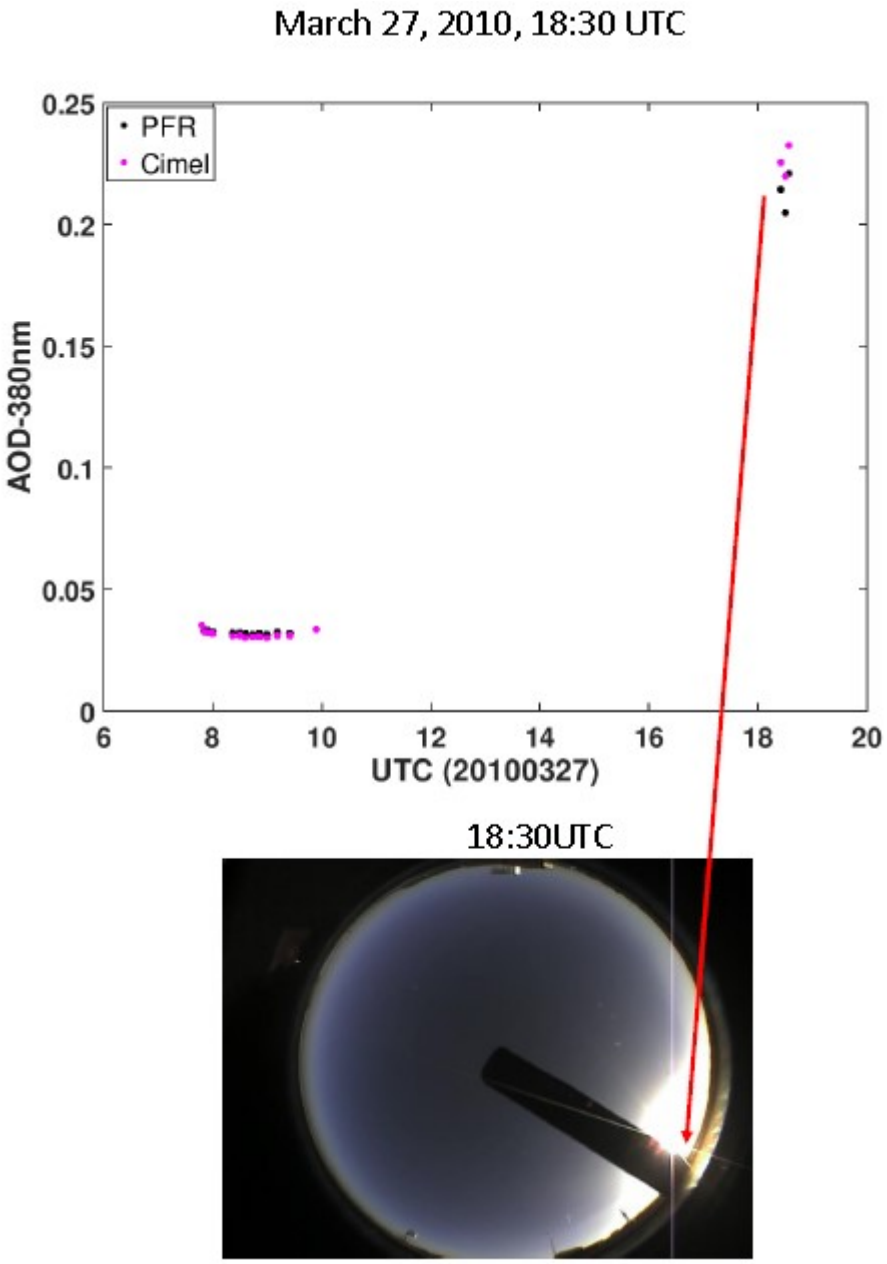

Supplement S12. Impact of low stratocumulus on AOD retrieval.

Another cloud scenario that can affect AOD traceability is the presence of low clouds (stratocumulus) that sometimes exceed the observatory height level because the temperature inversion is around 2400 m height. Sometimes the fog can affect the radiometers as shown in the following case analysis in which the GAW-PFR cloud screening algorithm fails giving a few erroneous 1-minute AOD data around 09:00UTC.

Case analysis February 12, 2015: The range corrected backscattering signal vertical cross section of the Micropulse lidar (MPL) (a) shows the presence low stratocumulus very close to the Izaña level in the early morning as confirmed by the all-sky camera (b) and the webcam (c) images. In the all-sky camera it is possible to appreciate the presence of ice due to recent freezing fog. These clouds exceed the level of the observatory in some moments, slightly hiding the sun with mist. The result in this case are very high AOD values from GAW-PFR (one order of magnitude) (d) due to a failure of its cloud screening algortithm. The rest of the day the agreement between GAW-PFR and AERONET-Cimel AOD (V3) measurements was very good.

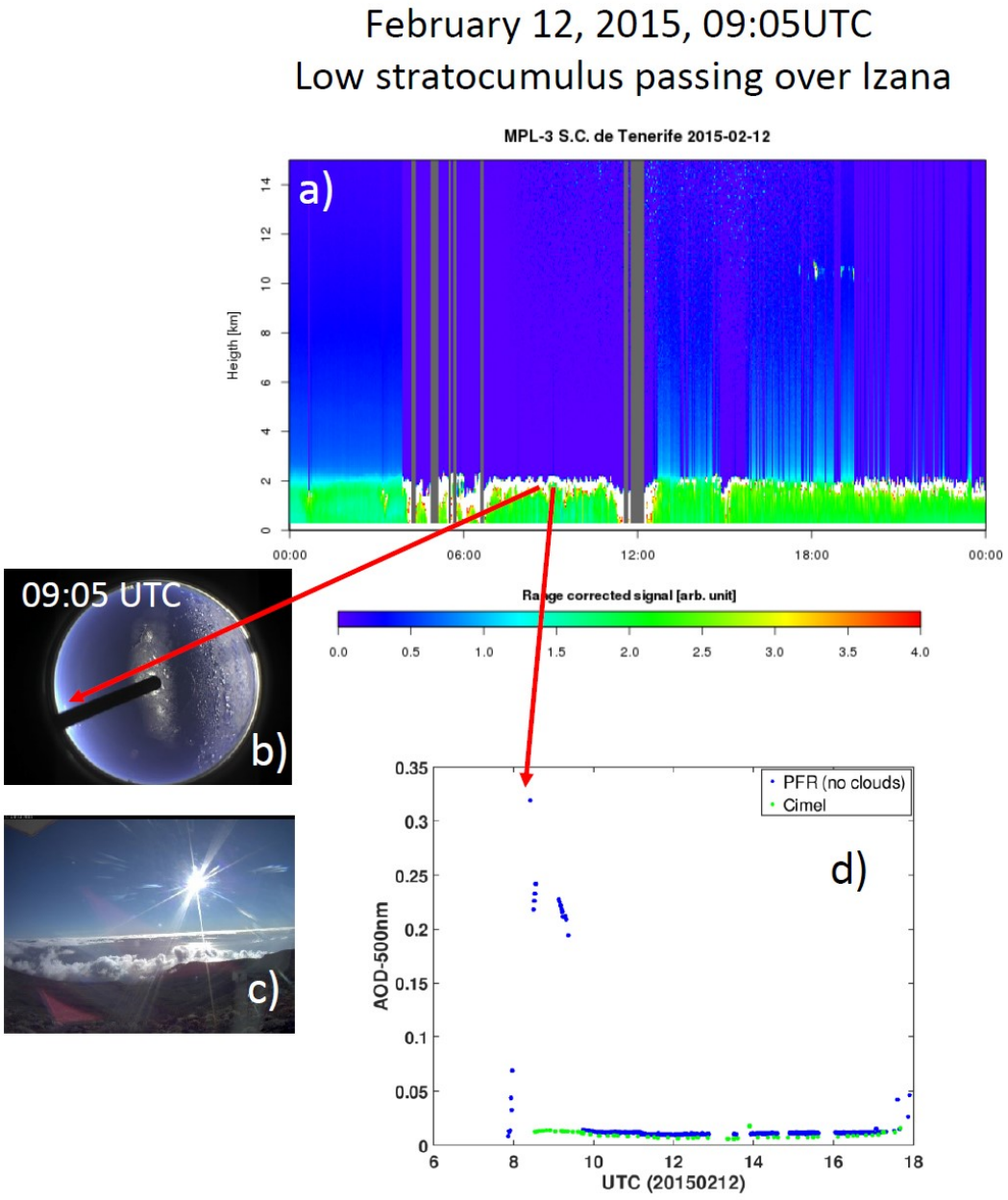

Supplement S13. Actual AOD differences between AERONET-Cimel V3 and GAW-PFR vs PFR AOD

Actual AOD differences between AERONET-Cimel V3 and GAW-PFR vs PFR AOD at (a) 380 nm (b) and 500 nm for the period 2005-2015. The fitting line has been calculated with AOD data > 0.1 and Cimel-PFR AOD difference > 0. Number of data used in the plots are indicated in the legend. The percentage of non-traceable AOD data with these conditions is ~22% for 380nm, and ~13% for 500nm. Note that some traceable (black) points show larger AOD differences than non-traceable (red) points because of air mass dependence of the WMO traceability criterion.

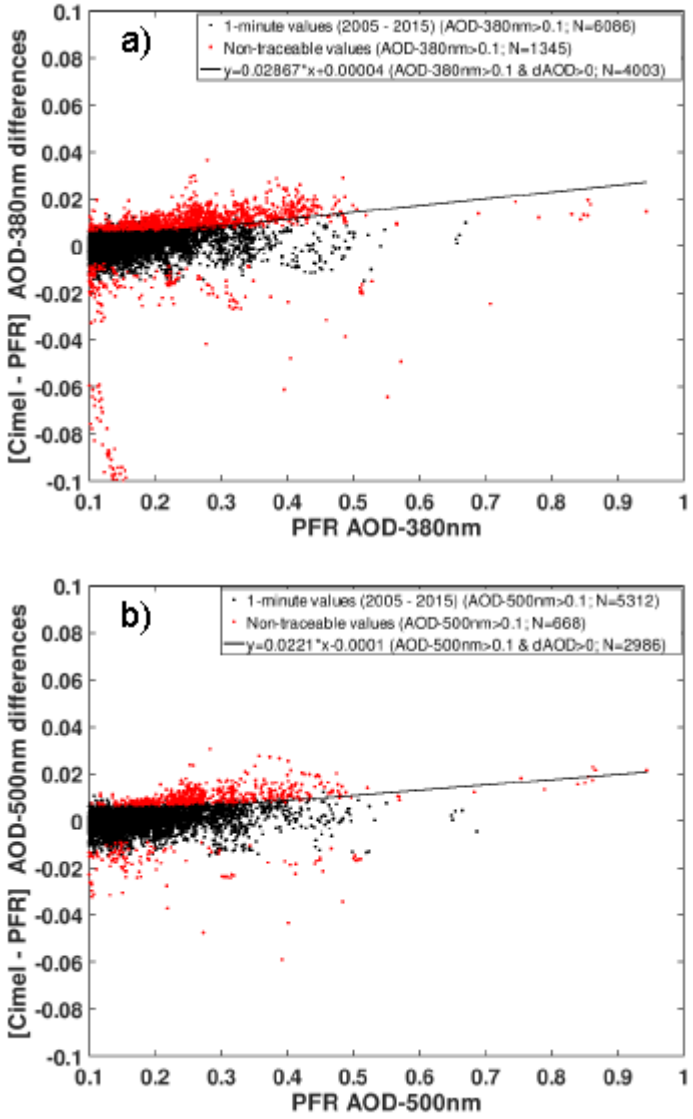

Supplement S14. Percentage of AERONET V3 AOD data outside the U95 limits for high AOD conditions

Percentage of AERONET V3 AOD data outside the U95 limits at 380 nm, 440 nm, 500 nm and 870 nm channels and for three AOD_{500nm} thresholds with respect to all data and with respect to all data for each AOD interval (in brackets).

	Percentage of AOD data outside the $U95$ limits (%)		
	$AOD_{500nm} > 0.1$	$AOD_{500nm} > 0.2$	$AOD_{500nm} > 0.3$
380 nm	1.6 (22.9)	1.1 (42.0)	0.4 (54.4)
440 nm	1.1 (15.9)	0.9 (32.5)	0.4 (49.0)
500 nm	1.3 (18.4)	1.0 (37.6)	0.5 (55.7)
870 nm	0.5 (6.7)	0.4 (13.4)	0.2 (19.0)

Comparing versions V2 and V3, we can see that, except for the 380 nm channel, in V3 the non-AOD traceability increases with respect to that found in V2.

Supplement S15. Simulations of scattered to direct radiation simulations.

Scattered to direct radiation simulations made with a forward Monte Carlo model (Barker 1992, Barker 1996, Räisänen et al. 2003) for FOVs of 2.5° and 1.2° for seven values of effective radius (r_e=0.2, 0.5, 1.0, 1.5, 2.0, 2.5, and 3.0 μm), for five AOD values (AOD= 0.1, 0.2, 0.3, 0.4, and 0.5), and for five solar zenith angles (θ = 20°, 30°, 45°, 60° and 80°).

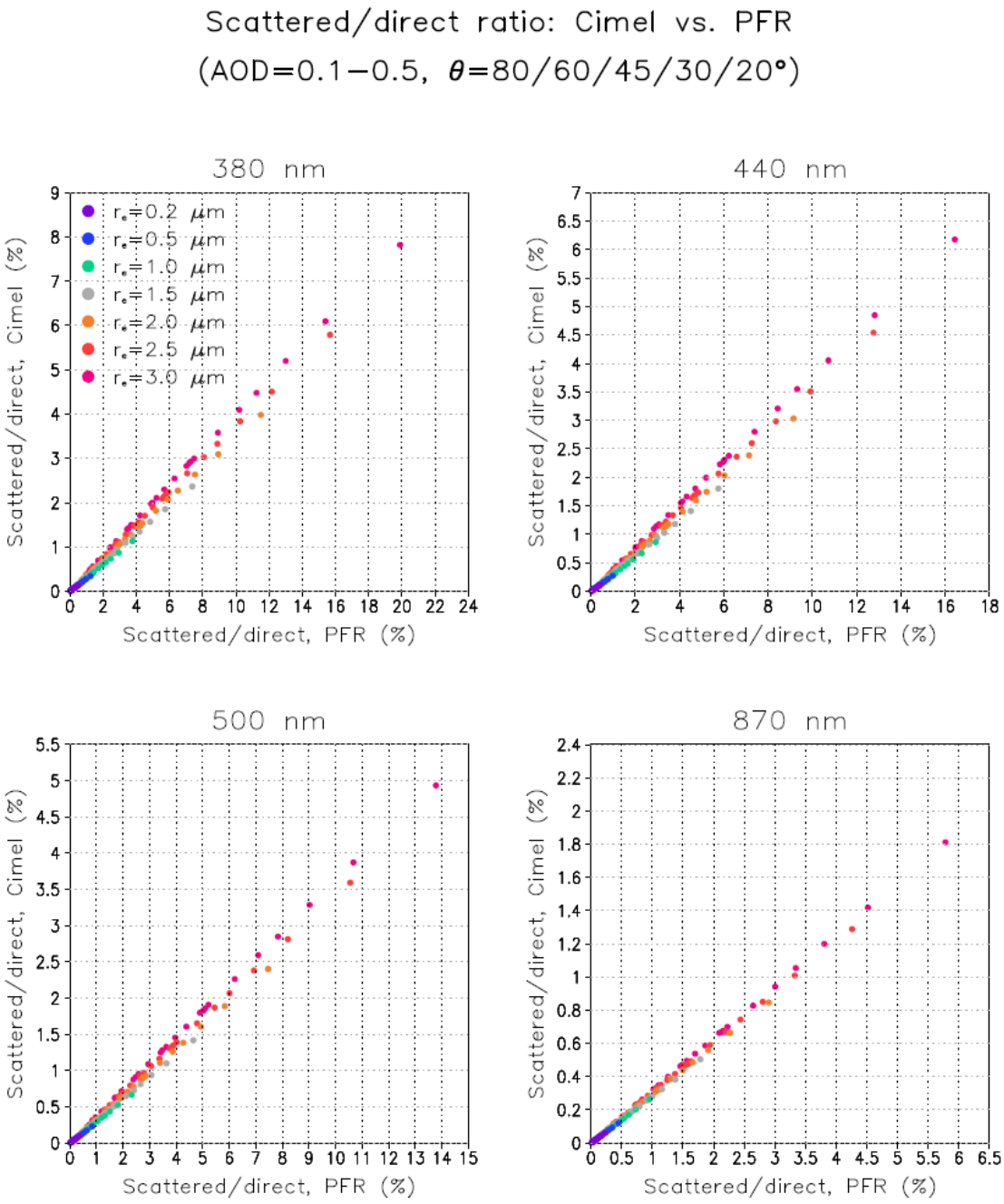

Supplement S16. Relative error in AOD for PFR and Cimel.

Relative error in AOD for PFR (x-axis) and Cimel (y-axis) for seven values of effective radius (r_e=0.2, 0.5, 1.0, 1.5, 2.0, 2.5 and 3.0 μm), for five AOD values (AOD= 0.1, 0.2, 0.3, 0.4, and 0.5), and for five solar zenith angles (θ = 20°, 30°, 45°, 60° and 80°).

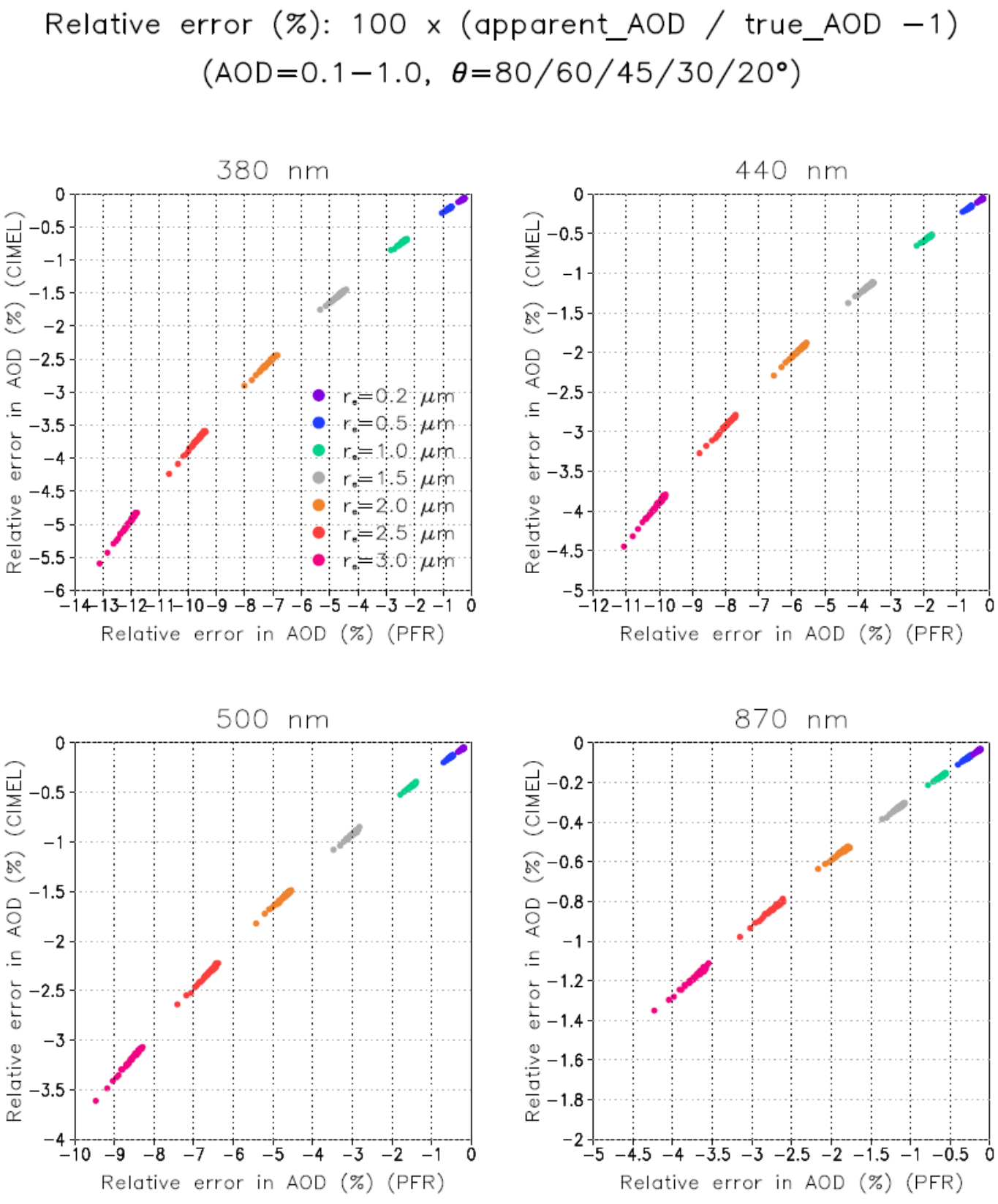

Supplement S17. Actual AOD differences between AERONET-Cimel V3 and GAW-PFR vs PFR AOD after AOD_{PFR} correction.

The same as the Figure of Supplement S13 (AERONET V3) after the PFR AOD data were "corrected" by adding + 3.3% at 380nm and + 2.2.% at 500 nm to the 1-minute AOD PFR data > 0.1.

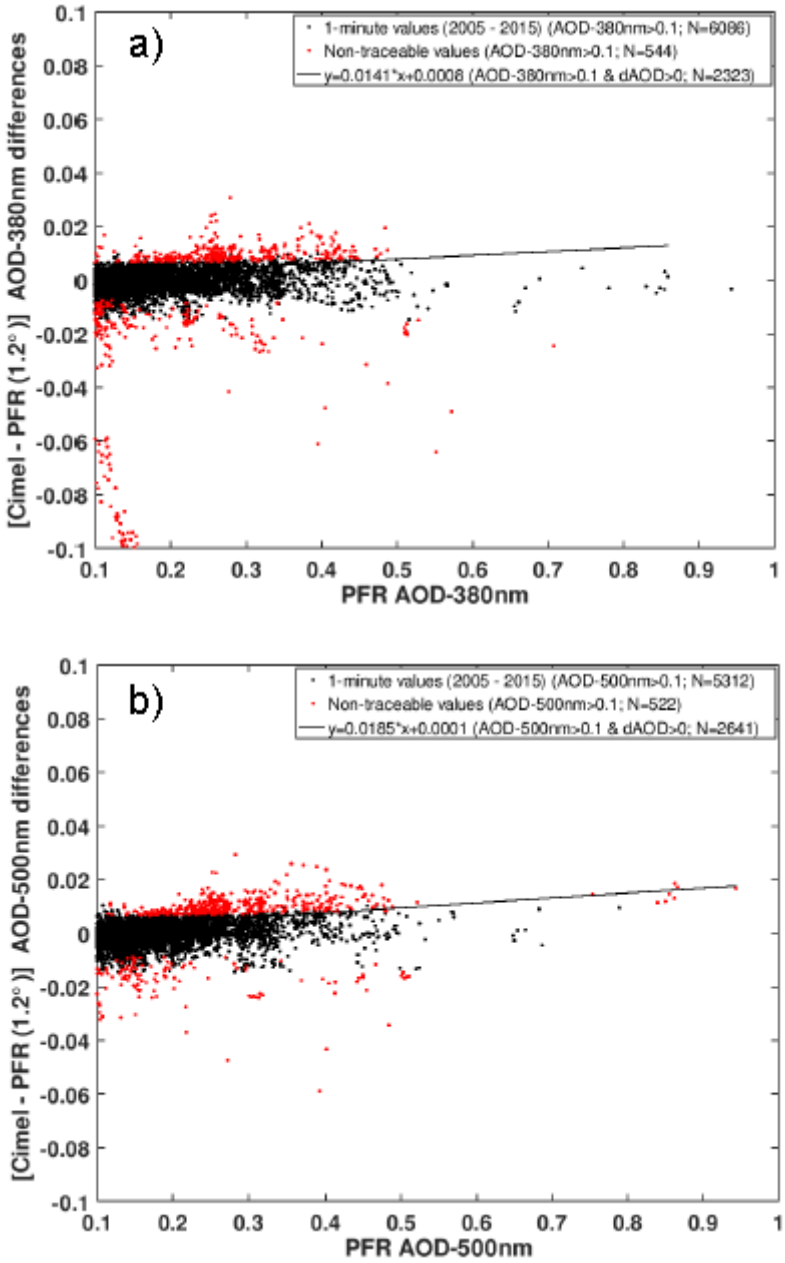

Supplement S18. Ångström exponent comparison

Percentage of cases in which GAW PFR and AERONET V2 (a) and V3 (b) coincide in each AE scenario (period 2005-2015).

a)

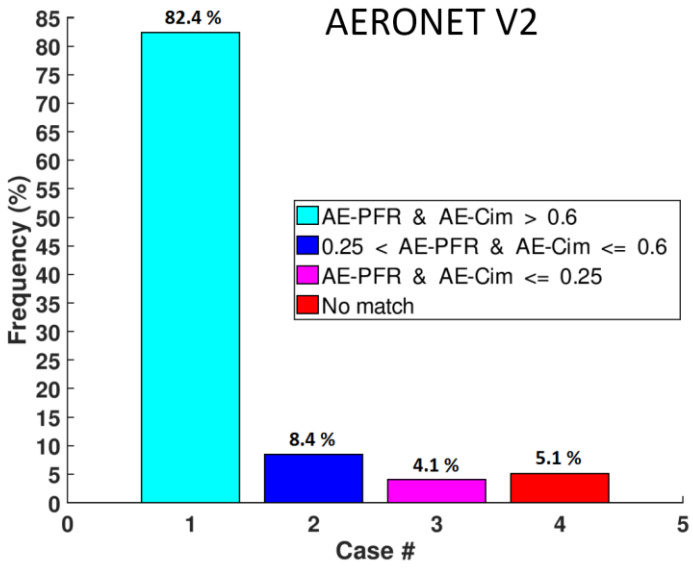

b)

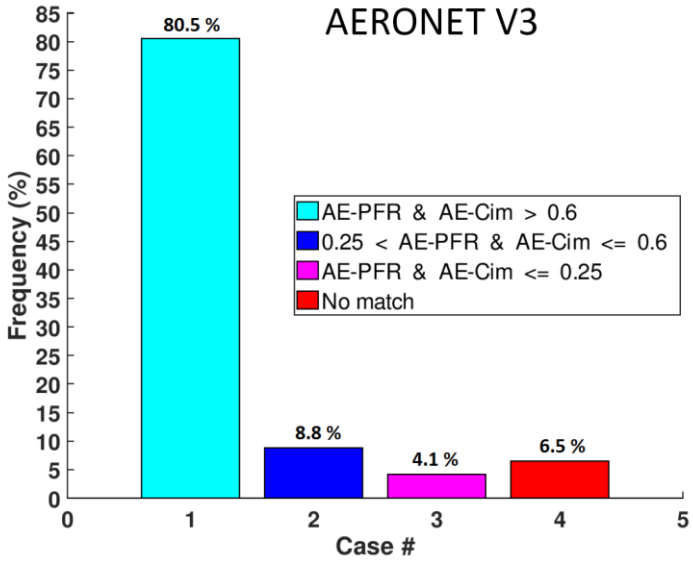

References

Chew, B. N., Campbell, J.R., Reid, J.S., Giles, D.M., Welton, E.J., Salinas, S.V., and Liew, S.C.: Tropical cirrus cloud contamination in sun photometer data, Atmos. Environ., 45, 6724-6731. 10.1016/j.atmosenv.2011.08.017, 2011.

Giannakaki, E., Balis, D. S., Amiridis, V., and Kazadzis, S.: Optical and geometrical characteristics of cirrus clouds over a Southern European lidar station, Atmos. Chem. Phys., 7, 5519-5530, https://doi.org/10.5194/acp-7-5519-2007, 2007.

Huang, J., Hsu, N.C., Tsay, S.-C., Holben, B.N., Welton, E.J., Smirnov, A., Jeong, M.-J., Hansell, R.A., Berkoff, T.A., Liu, Z., Liu, G.-R., Campbell, J.R., Liew, S.C., and Barnes, J.E.: Evaluations of cirrus contamination and screening in ground aerosol observations using collocated lidar systems, J. Geophys. Res., 117, D15204, doi:10.1029/2012JD017757, 2012.

Kinne, S., Akerman, T. P., Shiobara, M., Uchiyama, A., Heymsfield, A. J., Miloshevich, L., Wendell, J., Eloranta, E., Purgold, C., and Bergstrom, R. W.: Cirrus cloud radiative and microphysical properties from ground observations and in situ measurements during FIRE 1991 and their application to exhibit problems in cirrus solar radiative transfer modeling, J. Atmos. Sci., 54, 2320–2344, https://doi.org/10.1175/1520-0469(1997)054<2320:CCRAMP>2.0.CO;2, 1997.

Rodriguez-Franco, J. J., and Cuevas, E.: Characteristics of the subtropical tropopause region based on long-term highly-resolved sonde records over Tenerife, J. Geophys. Res. Atmos., 118, doi:10.1002/jgrd.50839, 2013.

5

Aerosol Optical Depth comparison between GAW-PFR and AERONET-Cimel radiometers from long-term (2005-2015) 1-minute synchronous measurements

Emilio Cuevas[1], Pedro Miguel Romero-Campos[1], Natalia Kouremeti[2], Stelios Kazadzis[2], Petri Räisänen[3], Rosa Delia García[4,1], Africa Barreto[5,1,4], Carmen Guirado-Fuentes[4,1], Ramón Ramos[1], Carlos Toledano[4], Fernando Almansa[5,1,4], and, Julian Gröbner[2]

[1]Izaña Atmospheric Research Center (IARC), State Meteorological Agency (AEMET), Spain

[2]Physikalisch-Meteorologisches Observatorium Davos, World Radiation Center (PMOD/WRC), Davos, Switzerland

[3]Finnish Meteorological Institute, Helsinki, Finland

[43]Air Liquide España, Delegación Canarias, Candelaria, 38509, Spain

[4]Atmospheric Optics Group, Valladolid University, Valladolid, Spain

[5]Cimel Electronique, Paris, France

Correspondence: Emilio Cuevas
(ecuevasa@aemet.es)

Abstract.

A comprehensive comparison of more than 70000 synchronous 1-minute aerosol optical depth (AOD) data from three Global Atmosphere Watch-Precision Filter Radiometers (GAW-PFR), traceable to the World AOD reference, and 15 Aerosol Robotic Network-Cimel (AERONET-Cimel, Versions V2 and V3) radiometers, calibrated individually with the Langley plot technique, was performed for the four common or near nearby wavelengths (380 nm, 440 nm, 500 nm and 870 nm) in the period 2005-2015. The goal of this study is to assess whether, despite the marked technical differences between both networks (AERONET, GAW-PFR) and the number of instruments used, their long-term AOD data are comparable and consistent. AOD traceability established by the World Meteorological Organization (WMO) consists in determining the percentage of synchronous data within specific limits. If, at least, 95 % of the AOD differences of an instrument compared to the WMO standards lie within these limits, both data populations are considered equivalent. The percentage of data meeting the WMO traceability requirements (95% of the AOD differences of an instrument compared to the WMO standards lie within specific limits) is >traceable data is 92.7 % at (380 nm), > 95 %.7 % at (440 nm and), 95.8 % (500 nm), and 98.0 % at (870 nm), with being the results being quite similar for both AERONET V2 and V3. When small misalignments in GAW-PFR sun-pointing were fixed (period 2010-2015), the percentage of traceable data increased. For the data outside these limits ttThe contribution of calibration related aspects to comparison outside the 95 % traceability limits is insignificant in all channels, except in 380 nm. The simultaneous failure of both cloud screening algorithms might occur only under the presence of cirrus, or altostratus clouds on the top of a dust-laden Saharan air layer.and ddifferences in the calculation of the optical depth contribution due to Rayleigh scattering, and O_3 and NO_2 absorption have a negligible impact. For AOD > 0.1, a small but non-negligible percentage (~ 1.9 %) of the AOD data outside the 95 % traceabilityWMO limits at 380 nm can be partly assigned to the impact of dust aerosol forward scattering on the AOD calculation due to the different field of view of the instruments. Due to this effect the GAW-PFR provides AOD values which are ~3% lower at 380 nm, and ~2% lower at 500 nm, compared with AERONET-Cimel. The comparison of the Angström exponent (AE) shows that under non-pristine conditions (AOD > 0.03 and AE < 1) the AE differences remain < 0.1. This long-term comparison shows an excellent traceability of AERONET-Cimel AOD with the World RC AOD reference at 440 nm, 500 nm and 870 nm channels and a fairly good agreement at 380 nm. . The excellent traceability in this study has been obtained using well calibrated Master instruments.

5

1. 1 Introduction

In recent decades there has been a growing interest in the role played by atmospheric aerosols in the radiation budget and the Earth's hydrological cycle, mainly through their physical and optical properties (IPCC, 2013). The most comprehensive and important parameter that accounts for the optical activity of aerosols in the atmospheric column is the aerosol optical depth (AOD) (WMO, 2003, 2005). This is also a key parameter used in atmospheric column aerosol modelling (e.g. Basart et al.,2012; Benedetti et al., 2018; Cuevas et al., 2015; Huneeus et al., 2016) and in satellite observations (e.g. Sayer et al., 2012, 2013; Kahn and Gaitley, 2015; Amiridis et al., 2015). The second aerosol optical parameter in importance is the Angström exponent (AE) (Angstrom, 1929) that accounts for the spectral dependency of the AOD. Since the Angström exponent (AE) is inversely related to the average size of the aerosol particles, it is a qualitative indicator of the atmospheric aerosol particle size and therefore a useful parameter to assess the aerosol type (WMO, 2003).

At present, two global ground-based radiometer networks provide aerosol optical properties of the atmospheric column using centralized data processing procedures based on their respective standard criteria and also centralized protocols for calibration and quality control, linking all network instruments. These are AERONET-Cimel (AErosol RObotic NETwork - Cimel Elec-tronique radiometer; http://aeronet.gsfc.nasa.gov; last access: 01 September 2018) and GAW-PFR (Global Atmospheric Watch – Precision Filter Radiometer; http://www.pmodwrc.ch/worcc/; last access: 05 September 2018) and AERONET-Cimel (AErosol RObotic NETwork - Cimel Electronique radiometer; http://aeronet.gsfc.nasa.gov; last access: 01 September 2018) networks. AERONET is, in fact, a federation of ground-based remote sensing aerosol networks established by NASA (The National Aeronautics and Space Administration) and PHOTONS (PHOtométrie pour le Traitement Opérationnel de Normalisation Satellitaire; University of Lille- Service d'Observation de l'INSU, France; Goloub et al., 2007), being complemented by other sub-networks, such as, AEROCAN (Canadian sunphotometry networkAERONET Canada; Bokoye et al., 2001), AeroSibnet (Siberian system for Aerosol monitoringRussia; Sakerin et al., 2005), AeroSpan (Aerosol characterisation via Sun photometry: Australia Network; Mitchell et al., 2017), CARSNET (China Aerosol Remote Sensing NETwork; Che et al., 2015), and RIMA (The Iberian network for aerosol measurementsRed Ibérica de Medida fotométrica de Aerosoles; Spain and Portugal; Toledano et al., 2011).

There are other radiometer networks that in recent years have incorporated centralized protocols for data evaluation and databases, and performed regular intercomparisons with GAW-PFR and AERONET-Cimel. It must be mentionedThese include, for example, SKYNET (SKYradiometer NETwork), and its seven associated sub-networks, that uses the Prede-POM sky radiometer to investigate aerosol-cloud-solar radiation interactions (e.g. Campanelli et al., 2004; Nakajima et al., 2007; Takamura et al., 2004).

The World Optical Depth Research Calibration Center (WORCC) was established in 1996 at the Physikalisch Meteorologisches Observatorium Davos / World Radiation Center (PMOD / WRC ~~(https://www.pmodwrc.ch/; last access: 25 June 2018~~). The GAW-PFR network (Wehrli, 2005) was initiated within PMOD/WRC for global and long-term atmospheric aerosol monitoring and accurate detection of trends. Aerosol data series measured at 12 core sites away from local and regional pollution sources, representative of atmospheric background conditions in different climates and environments of the planet, in addition to another 20 associated stations are included in this global network (Kazadzis et al., 2018a). For this reason, GAW-PFR uses the ~~Precision Filter Radiometer (~~PFR~~)~~, an accurate and reliable instrument regarding its absolute response stability over time that was designed for long-term AOD measurements (Wehrli, 2008a). The GAW-PFR was specifically designed by WORCC for this goal following the technical specifications defined by WMO (2003; 2016). In 2006, the Commission for Instruments and Methods of Observation (CIMO) of WMO (WMO, 2007) recommended that the WORCC at the PMOD/WRC should be designated as the primary WMO Reference Centre for AOD measurements (WMO, 2005).

The AERONET-Cimel network (Holben et al., 1998) was, in principal, designed to validate satellite products and to characterize the spatial-temporal distribution of atmospheric aerosols based on their optical properties. It is the largest surface-based ~~aerosol~~ global aerosol network with more than 84~~25~~ sites with measurement series longer than 10 years and more than 242~~150~~ sites having data sets > 5 years ~~(https://aeronet.gsfc.nasa.gov; last accessed 8/1/2019)~~. Cimel radiometer data, part of AERONET, are processed centrally and freely delivered in near real time by the NASA Goddard Space Flight Center.

Both networks, although designed to meet different objectives, are now global benchmarks for the study and characterization of aerosol optical properties worldwide, and for the evaluation of aerosol observations on board satellites and simulations with models. Multiple studies have proliferated in recent years to obtain aerosol climatology and to determine AOD trends in different parts of the world (e.g. Nyeki et al., 2012; Klingmüller et al., 2016; Chedin et al., 2018).

However, these networks use radiometers with significant technical differences. Moreover, calibration methodologies, AOD calculation algorithms and data evaluation methods are also relatively different ~~among~~between the two networks. Consequently~~So~~, ~~it is essential to assess to what extent AOD and Angström exponent (AE) from these networks are equivalent with each other. In addition, it is crucial to know the differences towards common homogenization activities among different instruments/networks measuring AOD.~~the objective of this study is to assess whether, despite the marked differences between both networks, including the different day-to-day maintenance and operation procedures of the respective instruments during the study period, the long-term AOD provided by the two networks is comparable and consistent.

The WMO has defined the GAW-PFR Triad (three Master PFR instruments) as the world-wide reference for AOD measurements (WMO, 2005). Based on this concept, an instrument provides traceable measurements of AOD to this WMO reference, when this instrument can demonstrate an unbroken chain of calibrations between itself and the GAW-PFR Triad with AOD measurements within specified limits of

the GAW-PFR reference. This can either be achieved by a direct comparison to the GAW-PFR Triad (Kazadzis et al., 2018a), or by using a portable transf-er standard radiometer as ~~it is~~ presented in this study.

Several comparisons between AERONET-Cimel, GAW-PFR and other radiometers have been carried out in different places (Barreto et al., 2016; Kazadzis et al., 2014, 2018b~~a~~; Kim et al., 2008; McArthur et al., 2003; Mitchell and Forgan, 2003; Nyeki et al., 2015; Schmid et al., 1999; Toledano et al., 2012). However, these comparisons have been performed during field intercomparison campaigns or during relatively short periods of time, so they are not representative of a large variety of atmospheric conditions. In addition, the type of instrument maintenance and the number and qualifications of staff serving them during campaigns is generally of a higher quality compared to that of the instrument daily operation in unattended mode. ~~–~~This might cause an improvement of the instrument performance during intensive campaigns ~~to be significantly better than that during~~ compared to the operational mode.

The growing interest in the analysis of long-term AOD and AE data series for ~~-~~climatological purposes requires an assessment of their quality assurance and long-term intercomparability. This is the first study to ~~analyze~~analyse the long-term traceability of AERONET-Cimel with respect to GAW-PFR, and therefore to assess the validity of the long AOD and AE AERONET-Cimel data series for climatological and climate change studies under specific quality control requirements.

GAW-PFR has a comprehensive calibration system (Kazadzis et al., 2018a; Schmid and Wehrli, 1995) that is transferred by a worldwide suite of reference instruments. ~~However,~~ AERONET-Cimel does not have a CIMO-WMO linked reference and, as described by Holben et al. (1998), Eck et al. (1999), and Toledano et al. (2018), is based on:

~~-~~ Maintaining ~~Master~~Reference AERONET radiometers based on the Langley calibration technique at Izaña, Spain and Mauna Loa, USA.

~~-~~ Calibration of all other instruments based on raw voltage ratios comparisons with ~~Master~~Reference instruments at dedicated sites (Carpentras-France, Washington DC-USA, Valladolid-Spain).

~~This is the first study to analyze the long-term traceability of AERONET-Cimel with respect to GAW-PFR, and therefore to assess the validity of the long AOD and AE AERONET-Cimel data series for climatological and climate change studies under specific quality control requirements.~~

There are few places in the world where synchronous observations of these two networks are available for long time periods ~~in which a great variety of atmospheric turbidity conditions take place~~ and variable AOD conditions. The Izaña Observatory (IZO; Tenerife, ~~the~~ Canary Islands) is one of them. The GAW-PFR measurements started at Izaña Observatory in 2001 (Wehrli, 2005) while AERONET-Cimel started in 2003 (Goloub et al., 2007). Since 2005, synchronous measurements (1-minute values), that have been evaluated following the calibration procedures of each of the networks, are available.

In addition, the Izaña Observatory is one of the two places in the world (the other is Mauna Loa - Hawaii, USA) where ~~absolute~~ sun-calibrations are performed using the Langley plot technique for both AERONET-Cimel and GAW-PFR reference instruments (Toledano et al., 2018) because of ~~thanks to~~ stable (and very low) AOD conditions during many days per year. ~~Therefore~~Consequently, the instruments

compared at the Izaña Observatory have been calibrated under the same environmental conditions, and therefore AOD differences can be directly linked with calibration principles, AOD post-processing and other instrumental differences. In this work, we analyzeanalyse and evaluate the comparison of 11 years (2005-2015) of 1-minute synchronous observations of AOD with AERONET-Cimel and GAW-PFR in four common or near wavelengths, assessing the results and explaining the possible causes of these differences. Some preliminary technical details on the traceability between GAW-PFR and AERONET-Cimel were reported in a technical report by Romero-Campos et al. (2017).

In Section 2 the facility in which this long-term comparison has been carried out is described. The technical characteristics of the AERONET-Cimel and GAW-PFR instruments are provided shown in Section 3, with special emphasis on the technical and methodological differences of both networks. Section 4 describes the methodology followed in this intercomparison based on the concept of WMO-GAW traceability. Results are given in Section 5. A summary and conclusions are provided in Section 6.

2. Site Description.

Izaña Observatory (IZO; 28.3◦ N, 16.5◦ W; 2373 m a.s.l.) is located in Tenerife (Canary Islands, Spain) and is managed by the Izaña Atmospheric Research Center (IARC) which), which is part of the State Meteorological Agency of Spain (AEMET). It is a suitable place for long-term studies of aerosol optical properties under quite contrasting atmospheric and meteorological conditions. This is because IZO is located in the free troposphere (FT) above the temperature inversion caused by the trade wind regime in lower levels and general subsidence associated withto the branch of the decay of Hadley's cell aloft (Carrillo et al., 2016). This meteorological feature favours, during most of the year, the presence of pristine skies and clean air representative of atmospheric background conditions (Cuevas et al., 2013; Rodríguez et al., 2009). On the other hand, its proximity to the African continent makes it a privileged site for observing and characterizing the Saharan Air Layer (SAL) that normally presents a high burden of desert mineral dust, especially during the summer months (Basart et al., 2009; Rodríguez et al., 2011; Cuevas et al., 2015). At this time of the year, the Saharan Air Layer (SAL) impacts the subtropical free troposphere over the North Atlantic with large interannual (Rodríguez et al., 2015) and sharp intraseasonal (Cuevas et al., 2017a) variability. The contrasting atmospheric conditions that occur at IZO allow the comparison of the two networks, which can be performed under a wide range of AOD values;- mMostly for pristine conditions (AOD ≤ 0.03) but also for relatively high turbidity (AOD > 0.6) linked with dust aerosol related intrusions. In addition, the location offers the possibility of observing rapid changes in AOD, going from pristine conditions to dusty skies, and vice versa, in a matter of a few hours, especially in the summer period. The periodical presence of a dust laden SAL allows us to evaluate the impact that the dust forward scattering into the field of view has on AOD retrieval. All Tthis defines IZO as an excellentgood atmospheric aerosol

natural laboratory to compare the performance of different radiometers measuring AOD. One of the first international AOD intercomparison campaigns was carried out at IZO in April 1984 (WMO, 1986) promoted and coordinated by PMOD / WRC.

The privileged conditions of pristine skies that characterize IZO during many days a year have allowed this observatory to become a calibration site for the GAW-PFR and AERONET-Cimel networks since 2001 and 2003, respectively, where the extraterrestrial constants are determined with direct sun observations using the Langley plot technique (Toledano et al., 2018). Note that the extraterrestrial constant (calibration constant) is the signal the instrument would read outside the atmosphere at a normalized earth-sun distance. In addition, since July 2014, IZO has also been designated by the WMO as a CIMO (WMO, 2014) testbed for aerosols and water vapour remote sensing instruments. IZO is a station of the Baseline Surface Radiation Network (BSRN) (Driemel et al., 2018; García et al., 2019~~98~~)). Details of ~~the~~ IZO facilities, measurement programmes and main research activities~~ults~~ can be found in Cuevas et al. (2017b).

3. GAW-PFR and AERONET-Cimel radiometers

The two types of radiometers intercompared in this study are Cimel CE318-N (Holben et al., 1998), hereinafter referred to as Cimel, the standard instrument of AERONET until the recent appearance of CE318-T (Barreto et al., 2016), and the ~~Precision Filter Radiometer~~PFR (Wehrli, 2005) standard instrument of the GAW-PFR network. The main features of these two radiometers are described in Table 1. The Cimel (Holben et al., 1994, 1998) is a radiometer equipped with a 2-axis robot that performs two types of basic radiation measurements: direct solar irradiance and sky (radiance) observations, thanks to an automatic pointing robot that executes the observation sequences that have been scheduled. The robot performs automatic pointing to the sun by stepping azimuth and zenith motors using ephemeris based on time, latitude and longitude. Additionally~~fter that~~, a four-quadrant detector is used to improve the sun tracking before each scheduled measurement sequence. This sensor guides the robot to the point where the intensity of the signal ~~on both Silicon and InGaAs~~ channel~~s~~ is maximum. Diffuse-sky measurements are also performed by Cimel to infer aerosol optical and microphysical properties. Two different routines are executed: almucantar (varying the azimuth angle keeping constant the zenith angle) and principal plane (varying the zenith angle keeping constant the azimuth angle). The ability of Cimel to perform both direct and diffuse-sky measurements makes it necessary ~~the~~to use ~~of~~ a ~~dedicated~~specific robot rather than a simple sun tracker. The field of view angle (FOV) of the instrument is 1.29° (~1.3° from now on) (Torres et al., 2013)~~.~~. The wavelengths in which the measurements are sequentially made by a single detector depend on the interference filters that each version of the radiometer has installed in the filter wheel, which is located inside the sensor head and which is moved by a stepper motor.

The Cimel versions used in this study have at least eight interference filters centred at 340 nm, 380 nm, 440 nm, 500 nm, 675 nm, 870 nm, 940 nm, and 1020 nm and 10 nm full width at half maximum (FWHM) bandwidth, except for 340 nm and 380 nm which have 2 nm and 4 nm FWHM, respectively. Solar irradiance is measured with a Silicon detector in these channels. The possible deterioration of the interference filters is reduced since they are only sun-exposed during three consecutive 1-second direct-sun measurements per channel, ~~being scheduled~~ this cycle being scheduled every ~15 minutes. The rest of the time the Cimel is taking sky radiance measurements, or at rest position, looking downwards.

The PFR (Wehrli, 2000, 2005, 2008a, b) is designed for continuous and automated operation under a broad range of weather conditions. It accurately measures direct solar radiation transmitted in four independent narrow wavelength ~~-~~channels centred at 368 nm, 412 nm, 500 nm and 862 nm, with 5 nm FWHM bandwidth. The FOV of the instrument is 2.5° and the slope angle is 0.7°. Dielectric interference filters manufactured by the ion-assisted-deposition technique are used to assure significantly larger stability in comparison to the one manufactured by classic soft-coatings. The PFR was designed for long-term stable measurements, therefore the instrument is hermetically sealed with an internal atmosphere slightly pressurized (2000 hPa) with dry nitrogen, and is stabilized in temperature with a Peltier-type thermostatic system maintaining the temperature of the detector head at 20° C ± 0.5° C. ~~-~~T~~So, t~~his system ~~-~~makes corrections of the sensitivity for temperature unnecessary, and also prevents accelerated ageing of filters, ensuring the high stability of the PFR. ~~The PFR has been selected by the WMO as the reference instrument for long-term AOD observations.~~ The PFR is mounted on a sun tracker, pointing always at the sun without any active optimization of the sun-pointing.~~position,~~ The detectors are only exposed for ~~a~~ short time periods, since an automated shutter opens every minute for 10s for sun measurements, minimizing degradation related to~~with~~ the filters exposure.~~.~~

The expected uncertainty of AOD in the four channels of the PFR radiometer is from 0.004 (862 nm) up to 0.01 (368 nm) (Wehrli, 2000). For the Cimel radiometer, the expected uncertainty of level 2-AOD product is ~~found~~ between 0.002 and 0.005, ~~larger for shorter wavelengths~~ for ~~Masters~~reference instruments, larger for shorter wavelengths, and between 0.01 and 0.02~~,~~ for field instruments, larger in the UV, ~~for field instruments,~~ under conditions of clear skies (Eck et al., 1999; Barreto et al., 2016). It should be taken into account that, in general, in the ultraviolet range the AOD uncertainty is higher and depends on the optical mass (Carlund et al., 2017).

In relation to the calibration of both networks, GAW and AERONET, they use measurements at high mountain stations with very stable and low AOD over a day in which consecutive measurements can be performed over a wide range of optical air mass (approximately between 2 and 5) in the shortest possible time, in order to calibrate ~~Masters~~Reference instruments using the Langley plot technique. In case of AERONET-Cimel ~~T~~these calibrations are subsequently transferred to the field instruments of the network in other sites through regular intercomparison campaigns. ~~, in the case of the AERONET-Cimel and to the reference PFR triad maintained at PMOD/WRC for the GAW-PFRs.~~ In case of the GAW-PFR, the calibration system is more complex in order to ~~-~~ensure~~ing~~ traceability with the WORCC world reference. The maintenance of the AOD standard by the ~~WMO~~ WORCC Calibration Central laboratory is described

in Kazadzis et al. (2018). It consists of a triad ~~(three)~~ of instruments that measure continuously, and three additional portable transfer standard radiometers located at Mauna Loa (one instrument) and Izaña (two instruments) observatories. Every six months, one of the portable transfer standard radiometers visits the reference triad based at PMOD/WRC (Davos) and compares the calibration constants defined by the 6-month Langley calibrations in the two high mountain stations (Table 1 of Kazadzis et al. ~~(~~2018)~~)~~ with the one defined by the triad. The comparison is based on the signals (voltages) and not o~~i~~n AOD values. The differences between the Izaña GAW-PFR radiometers and the reference triad have been always lower than 0.5%, being within the uncertainty of the Langley method plus the small possible instrument degradations that can be detected in a 6-12 month period. Such degradations are quite small and are accounted for in the calibration analysis since extraterrestrial constants are linearly interpolated between two triad visits or every 6-month periods. Additionally, the Izaña GAW-PFR "field" radiometers are calibrated on a routine basis using the Langley-plot technique for double checking quality assurance. Therefore, these radiometers cannot be considered as simple "field" instruments, but as regularly calibrated radiometers with assured traceability with the WORCC triad reference.

IZO is one of the two sites of ~~absolute~~ Langley-plot calibration of both networks, which represents an advantage when comparing the two instruments, eliminating, to a large extent, errors caused by the calibration transfer. However, there are differences between the calibration methodologies used by both networks. AERONET obtains the calibration by means of the average of a few extraterrestrial ~~V_o~~ constants (V_o), obtained from Langleys, performed in a relatively short time (the time needed to collect data ~~necessary to perform~~ from at least 10 ~~good~~ morning Langley plots ~~3-4 months~~). However, ~~GAW~~ PFR related Langleys are calculated ~~obtains the calibration~~ by ~~means of the~~ temporal lineal fit to a larger number of extra-terrestrial constants V_0 obtained from Langley plots performed during 6 months (Wehrli, 2000; Kazadzis et al., 2018a). Details on requirements for performing Langley calibrations of reference instruments by GAW-PFR and AERONET, and their uncertainties, are ~~analyzed~~analysed in detail by Toledano et al. (2018).

4. ~~-~~Data and methodology used in this study~~:~~

The AOD at each wavelength is obtained from the Beer-Bouguer-Lambert law (Thomason et al. 1982; WMO, 2003) for radiometers collecting spectral direct sun measurements.

$$I(\lambda) = I_0(\lambda)\exp(-\tau m) \quad (1)$$

where $I(\lambda)$ is the direct sun signal at ground level at wavelength λ, $I_0(\lambda)$ is the extraterrestrial signal of the instrument corrected by the Earth-Sun distance, and m is the optical air mass in the measurement path (Kasten and Young, 1989). A detailed description of how AOD is obtained and the determination of extraterrestrial constants by GAW-PFR and AERONET-Cimel are provided by Holben et al. (1994, 1998; 2001), Toledano et al. (2018), and Wehrli (2000; 2008b).

5

4.1. GAW-PFR and AERONET-Cimel data.

GAW-PFR provides AOD values every 1 minute as an average of 10 sequential measurements of total duration less than 1 second (~20 ms for each channel), then dark current is measured, going to the sleep mode until the next minute. . while AERONET-Cimel takes a sequence of three separate measurements (1-second per filter) in one minute interval (each one every 30 seconds). This sequence of measurements is called "triplet" and it is performed every ~15 minutes for air masses lower than 2, and with higher frequency for lower solar elevations. SoTherefore, AERONET-Cimel provides AOD values for each triplet, at least, every ~15 minutes. Note that AERONET-Cimel performs AOD measurements interspersed with sky radiance measurements, whose duration varies throughout the day, and therefore the AOD measurements are not necessarily provided at full minutes. WFor all this, we consider the synchronous 1-minute data as synchronous when GAW-PFR and AERONET-Cimel AOD data were obtained with a difference of ~30 s.

GAW-PFR and AERONET-Cimel instruments use the same time reference. The synchronization between PC and GAW-PFR data-logger was performed every 12 hours since 2005, andbeing improved to 6 hours after 2013 using NTP servers via Internet. From 2005 to 2012 the time of the AERONET-Cimel Masterreferences instruments was checked manually once per day using a handheld GPS. From 2012 onwards, the time was adjusted automatically 3three times per day using the ASTWIN Cimel software. In turn, the PC time is adjusted through the AEMET internal time server every 15 minutes.

The AOD comparison has been performed using 1-minute synchronous data from the four closest channels of both instruments in the period 2005-2015 (more than 70000 data-pairs in each channel). Thus, in the case of GAW-PFR, the four available channels of 368 nm, 412 nm, 500 nm and 862 nm were analyzedanalysed, while in the case of AERONET-Cimel, only the 380 nm, 440 nm, 500 nm and 870 nm channels were considered (Table 1). For the 500 nm channel, the differences between nominal wavelengths of the two both networks differ by a maximum of 1.8 nm. However, the nominal wavelengths in the rest of the compared channels present higher differences. Therefore, the AOD values of the original GAW-PFR 368 nm, 412 nm and 862 nm channels have been interpolated or extrapolated to the corresponding AERONET-Cimel channels (380 nm, 440 nm and 870 nm) using the Angström power law, and the GAW-PFR AE calculated from the four PFR AOD measurements.

Synchronous AE data provided by both instruments have also been compared (see section 5.5). GAW-PFR determines AE using all four PFR wavelengths (Nyeki et al., 2015), while AERONET-Cimel uses different pairs of wavelength rangess (340-440 nm, 380-500 nm, 440-675 nm,

440-870 nm, 500-870 nm) (Eck et al., 1999)~~Holben et al., 1998)~~. As a consequence, we have calculated a new AE for the Cimel radiometer using the four channels equivalent to those of the PFR.

In this study we have used the two versions of the AERONET database. Version 2 (V2; https://aeronet.gsfc.nasa.gov/new_web/Documents/AERONETcriteria_final1.pdf; last access: 2 February 2019) has been used so far in many scientific publications in high impact journals, and Version 3 (V3) has been released just recently (Giles et al., 2019). In section 5.1., a ~~preliminary and concise~~ comparison of V2 and V3 is presented. A total of three GAW-PFR and 15 AERONET-Cimel instruments have participated in this intercomparison study covering the period 2005-2015. Their corresponding reference numbers are shown in Table 2.

Table 1. Main features of the GAW-PFR (PFR (Wehrli, 2000, 2005, 2008a, b) and AERONET-Cimel (Holben et al., 1994, 1998; Torres et al., 2013) ~~-~~radiometers used in this study.

	GAW-PFR	AERONET-Cimel
Type of instrument	Standard version ~~Field instrument~~	Standard version ~~Master~~Reference instrument
Type of observation	Automatic continuous direct sun irradiance	Automatic sun-sky tracking
Available standard channels	368, 412, 500, 862 nm	340, 380, 440, 500, 675, 870, 1020~~,1640~~ nm
FWHM	5 nm	2 nm (340 nm), 4 nm (380 nm), 10 nm(VIS-NIR)~~, 25nm(1640nm)~~
AOD uncertainty	± 0.01	± 0.005 (~~Master~~Reference instruments)
FOV (FWHM)	2.5° (1.2° plateau, 0.7° slope angle)	~~1.2~~1.3° (slope angle unknown)
Sun tracker	~~No specific~~Any ~~Sun tracker~~sun tracker with a resolution of at least 0.08°	~~Sun tracker~~ Robot specifically designed by Cimel and controlled in conjunction with the radiometer
Temperature control	Temperature controlled 20°C ± 0.5°C	Temperature correction is applied in V2. Corrections from filter-specific temperature characterization in V3 (Giles et al., 2019)
Power	Grid	Solar panels/grid

Data transmission	Local PC /FTP ~~FTP~~	Local PC / FTP Satellite transmission ~~Satellite transmission~~
Calibration	Comparison with reference triad. Additional ~~I~~in situ long-term Langleys ~~plots/traceability with reference triad~~	At least 10 good morning ~~2-3 months~~ Langleys plots

~~A total of three GAW-PFR and 15 AERONET-Cimel instruments have participated in this intercomparison study covering the period 2005-2015. Their corresponding reference numbers are shown in Table 2.~~

4.2. Cloud filtering~~:~~

The data matching in our comparison analysis was performed with synchronous 1-minute AOD values of both networks labelled with quality control (QC) flags that guarantee proven quality data not affected by the presence of clouds. ~~In the case of the GAW-PFR network (Wehrli, 2008a) the flags take the value 0 (cloudless conditions, no wavelength crossings and sun pointing within certain limits, more details in Kazadzis et al. (2018a)) for all those selected records.~~ In the case of the AERONET-Cimel network, the selected AOD data are Level 2 data from both V2 and V3 AERONET databases, which have been cloud filtered by the Smirnov algorithm (Smirnov et al., 2000), based on the triplet method, with a second-order temporal derivative constraint (McArthur et al., 2003), and visually screened in V2. The cloud screening in AERONET V3 has been completely automated, and notably improved, especially by refining the triplet variability and cirrus cloud detection and removal (Giles et al., 2019). GAW-PFR cloud screening algorithms also use the Smirnov triplet measurement, and the second-order derivative check, but add a test for optically thick clouds with $AOD_{500nm} > 2$ (Kazadzis et al., 2018b). In the case of the GAW-PFR network (Wehrli, 2008a) the flags take the value 0 (cloudless conditions, no wavelength crossings and sun pointing within certain limits, more details in Kazadzis et al. (2018a)) for all those selected records.

~~Level 2 AERONET AOD data corresponds to version 2 of the algorithm which has been, until recently, the most updated version available in AERONET. Recently, version 3 has just been~~

~~10 introduced (Giles et al., 2018). Since a huge amount of published results are based on AERONET V2, a detailed comparison assessment between AERONET V2 and V3 must be presented before comparing AERONET V3 AOD with GAW-PFR.~~

Table 2. GAW-PFR and AERONET-Cimel instrument numbers used in this study in the period 2005-2015. Data from Reference Cimel #398 was not upgraded to Level 2 in V3 during the period 12 July 2008 - 15 September 2008.

Instruments used in this study	Period 2005-2009	Period 2010-2015
GAW-PFR	2 instruments: #6,#25	2 instruments: #6,#21
AERONET-Cimel	13 instruments: #25,#44,#45,#79,#117,#140 #244,#245,#380,#382,#383,#398,#421	5 instruments: #244, #347, #380 #421, #548

~~GAW-PFR provides AOD values every 1 minute as an average of 10 sequential measurements of total duration less than 1 second, while AERONET-Cimel provides AOD values every 15 minutes (from 3 measurements separated by 30 seconds). We consider synchronous 1-minute data when GAW-PFR and AERONET-Cimel AOD data were obtained with a difference of ~ 30 s.~~

~~5~~

4.3. WMO traceability criteria~~.~~

The criterion~~um~~ for traceability used in this study follows the recommendation of the WMO (WMO, 2005) which states that 95% of the AOD measurements fall within the specified acceptance limits, taking the ~~GAW~~ PFR as a reference:

$$U_{95} = \pm(0.005 + 0.010/m) \quad (2)$$

where m is the optical air mass. Note that the U95 range is larger for smaller optical mass.

The acceptance limits proposed by WMO take into account, on the one hand, the uncertainty inherent in the calculations of the AOD, and on the other hand, the uncertainty associated with the calibration of the instrument. The latter, for the case of instruments with finite field of view direct transmissions, such as the PFR and the Cimel, is dominated by the influence of the top-of-the-atmosphere signal determined by Langley plot measurements~~d~~, divided by the optical air mass.

The first term of Eq. 2 (0.005) represents the maximum ~~desirable~~ tolerance for the uncertainty due to the atmospheric parameters used for the AOD calculation (additional atmospheric trace gas corrections, and Rayleigh scattering). The second term describes the calibration related relative uncertainties~~ which scale therefore with the inverse of air mass~~. The WMO recommends an upper limit for the calibration uncertainty of 1%.

~~A first simple approach to calculate the circumsolar radiation of each radiometer taking into account their respective FOVs, AOD, total O_3 and pressure values, has been performed with the SMARTS (Simple Model of the Atmospheric Radiative Transfer of Sunshine) model version 2.9.5 (Gueymard, 1995). This spectral model, that covers the UVA, UVB, Visible and Near-Infrared bands, can be used to simulate the spectral irradiance that would be measured by a spectroradiometer (Gueymard, 2001). This model, which has been used and compared with LibRadtran for determining circumsolar radiation (Eissa et al., 2015) is used in~~

this study to estimate, in a first approximation, the differences in AOD caused by the different FOV of PFR and Cimel radiometers.

4.4. Modelling the impact of near-forward scattering on the AOD measured by the PFR and Cimel radiometers

In order to study the impact of near-forward scattering on the irradiance measured by the PFR and CimelIMEL instruments, a forward Monte Carlo model (Barker 1992, Barker 1996, Räisänen et al. 2003) was employed. For the present work, the model was updated to account for the finite width of the solar disk. The starting point of each photon was selected randomly within the solar disk, assuming a disk half-width of 0.267° and the impact of limb darkening on the intensity distribution was included following Böhm-Vitense (1989). Some diagnostics were also added to keep track of the distribution of downwelling photons at the surface with respect to the angular distance from the centre of the sun. Gaseous absorption was accounted for following Freidenreich and Ramaswamy (1999), while the Rayleigh scattering optical depth was computed using Bodhaine et al. (1999) below..

5. Results.

5.1. CPreliminary comparison of long-term AERONET V2 and V3 data basesdatasets at Izaña site.

Since V3 has been released recently (Giles et al., 2019), we present a comparison between V2 and V3 for the Cimel channels 380 nm, 440 nm, 500 nm and 870 nm for the period 2005-2015.

The results indicate that for the Izaña site the agreement and consistency between the two AERONET versions is very high for the four channels (R^2>0.999) in full agreement with the results of the V2-V3 comparison reported by Giles et al. (2019). So, we can advanceIt follows that the results of the comparison between GAW-PFR and the two versions of AERONET are very similar as shown throughout this work. A detailed description ofn AERONET V3 and its improvements with respect to V2 is given in Giles et al. (2019). A detailed description of the improvements introduced in V3 are given in Giles et al. (2019). As such Logically, these improvements depend on aerosol type, are not homogeneous in terms of theirfor the different types of aerosols and their nature and variable impact at a global level. A according to the changes introduced in V3, for thea high mountain site such as Izaña characterized by low background AOD values or, alternatively, by the presence of dust presence of dust (, but with no pollution or biomass burning aerosols), the expected AOD differences between V2 and V3 are expected to be minimum as it is confirmed in this studyhas been shown. (Figure 1).

the

However, it should be noted ~~the important fact~~ that ~~the~~ AERONET V3 does not restrict the calculation of AOD to optical masses less than 5.0 (Giles et al., 2019), as V2 does. This results in an increase in the number of solar measurements occurring in the early morning and the late evening. Consequently~~So~~, the GAW-PFR comparisons with AERONET V3 ~~could be performed with~~consisted of ~ 5000 more data pairs~~oints~~ than ~~in~~ the GAW-PFR comparison with V2 (see Supplement S.1.1.).

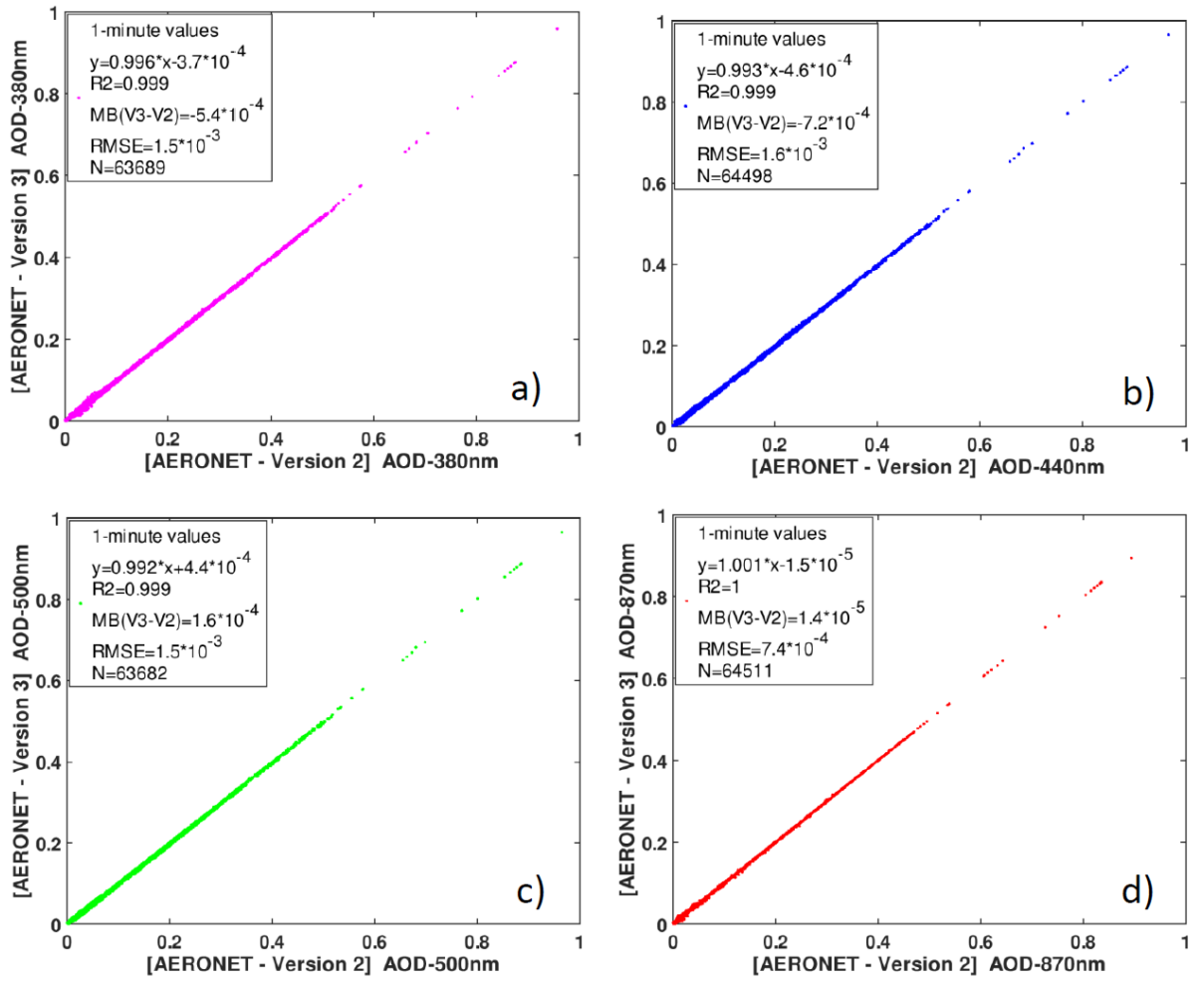

Figure 1. AERONET Version 3~~2~~ (V3~~2~~) vs Version 2~~3~~ (V2~~3~~) AOD 1-minute data scatterplot at ~~Izana~~Izaña Observatory ~~site~~ for the period 2005-2015: a) 380 nm; b) 440 nm; c) 500 nm and d) 870 nm. The corresponding equations of the linear fits, the coefficients of determination (R2), Mean Bias (MB), Root Mean Square Error (RMSE) and the number of data pairs (N) used are included in each legend.

5.2.- AERONET-Cimel AOD comparison with GAW-PFR data~~traceability~~.

The comparison with GAW-PFR AOD ~~analysis~~ shows that the AOD from AERONET-Cimel radiometers meet the WMO traceability criteria (“traceable AOD data” from now on) at~~in~~ 440 nm, 500 nm and 870 nm ~~all four common wavelength~~ channels. The lowest agreement is found in the UV channel (380 nm) with 92.7 % of the ~~minute average~~ data, and ~~5~~ the highest in the infrared channel (870 nm) with 98.0 % for V2 (Figure 2~~1~~; Table 3~~4~~). Almost identical results are obtained for V3 (Supplement S1 and S2).

However, in the first half of the comparison period (2005-2009~~10~~) there were~~as a~~ some ~~number of~~ mechanical problems in the solar tracker where the GAW-PFR was mounted on, which caused sporadic~~frequent~~ problems of sun pointing. This finding was confirmed with data from the four–quadrant silicon detector (Wehrli, 2008a) that showed diurnal variation of the PFR sensors position up to 0.3°~~°, and relatively poor long term stability~~. From 2010 onwards, the PFR was mounted on an upgraded solar tracker of higher performance and precision. This reduced problems in sun pointing, that were the main cause of ~~the~~ most of the AOD discrepancies between PFR and Cimel, and therefore not attributable to the instruments themselves.

In addition, since 2010, Cimel #244 has been in continuous operation for most of the time at the Izaña Observatory~~AERONET station~~, greatly simplifying calibration procedures and the corresponding data evaluation, and minimizing errors of calibration uncertainties introduced by the use of a high number of radiometers in the intercomparison. During the 2010-2015 period, the fraction of traceable AOD measurements of the total between the AERONET-Cimel radiometer and the GAW-PFR improves to 93.46 % in the 380 nm channel, and this percentage rises to 99.07 % for the 870 nm channel. ~~We must clarify that this improvement is mostly due to the upgraded solar tracker used with the PFR since 2010.~~

Despite the technical differences between both radiometers, described above, and the different calibration protocols, cloud screening ~~algorithms~~ and data processing ~~procedures~~algorithms, the data series of both instruments, can be considered as equivalent, except for 380 nm, according to the WMO traceability criteria defined previously (Eq. 2). This explains the excellent agreement in the long-term AOD climatology shown for GAW-PFR and AERONET-Cimel in Toledano et al. (2018).

~~In order to confirm the appropriateness of performing the AOD comparison in common channels by interpolating those of the GAW-PFR to those of AERONET-Cimel, w~~We have compared the percentages of AERONET-Cimel AOD V2 data meeting the WMO criteria for the four interpolated GAW-PFR channels with those of AERONET V3~~using the original GAW-PFR channels~~ (Table 3).

~~For shorter wavelengths, the percentage of data within the WMO limits decreases when the original GAW-PFR channels are used as a reference (not shown here), mainly, and as expected, in the 412 nm channel as this differs considerably from the nominal value of the corresponding AERONET-Cimel channel (440 nm). For 500 nm and 870/862 nm there are no significant differences. Hereinafter, in this study the interpolated GAW-PFR channels are used.~~

A more detailed statistical evaluation for different scenarios of aerosol loading (three -ranges of AOD) and aerosol size (three ranges of AE) for each compared channel has been performed (see Table 4). We

observe~~can see~~ that the poorest agreement is obtained at the shorter wavelength channels (440 nm, and especially 380 nm).

Kazadzis et al. (2018b) also found a decrease in the percentage of AOD meeting the WMO criteria for 368 nm and 412 nm spectral bands during the Fourth WMO Filter Radiometer Comparison for aerosol optical depth measurements. As these authors pointed out, the shorter the wavelength, the poorer the agreement because of several reasons: AOD in the UV suffers from out-~~–~~of-band or at least different blocking of the filters, small differences in central wavelength or FWHM have a larger impact, the Rayleigh correction is more critical, and NO_2 absorptions are treated differently. Regarding the effect of the aerosol load and particle size on the AOD differences, our results confirm the decrease of agreement between the two instruments for very large particles coincident with almost pure dust (AE $\leq$ 0.3), and high turbidity conditions (AOD > 0.1). However, it should be noted that the percentage of data pairs in these situations is relatively low (e.g., 6% for AOD > 0.1, and 3.2% for AE > 0.25 at 380nm) with respect to the total data (Table 4). A similar result was reported by Kim et al. (2008), who attributed these discrepancies to the possible spatial and temporal variability of aerosols under larger optical depths in addition to the effect of the different FOV of both radiometers. In our case, and according to previous studies on AOD climatology at IZO (Barreto et al., 2014), the presence of high mineral dust burden when the station is within the SAL, does not necessarily imply lower atmospheric stability conditions resulting in daily AOD means with greater standard deviation. For these reasons, we assumed that the different FOV of these instruments is ~~can be one of~~ the main cause~~s~~ of part of the AOD 1-minute differences outside the U95 limits, under high AOD conditions. This issue is specifically addressed in Section 5.3~~4~~.

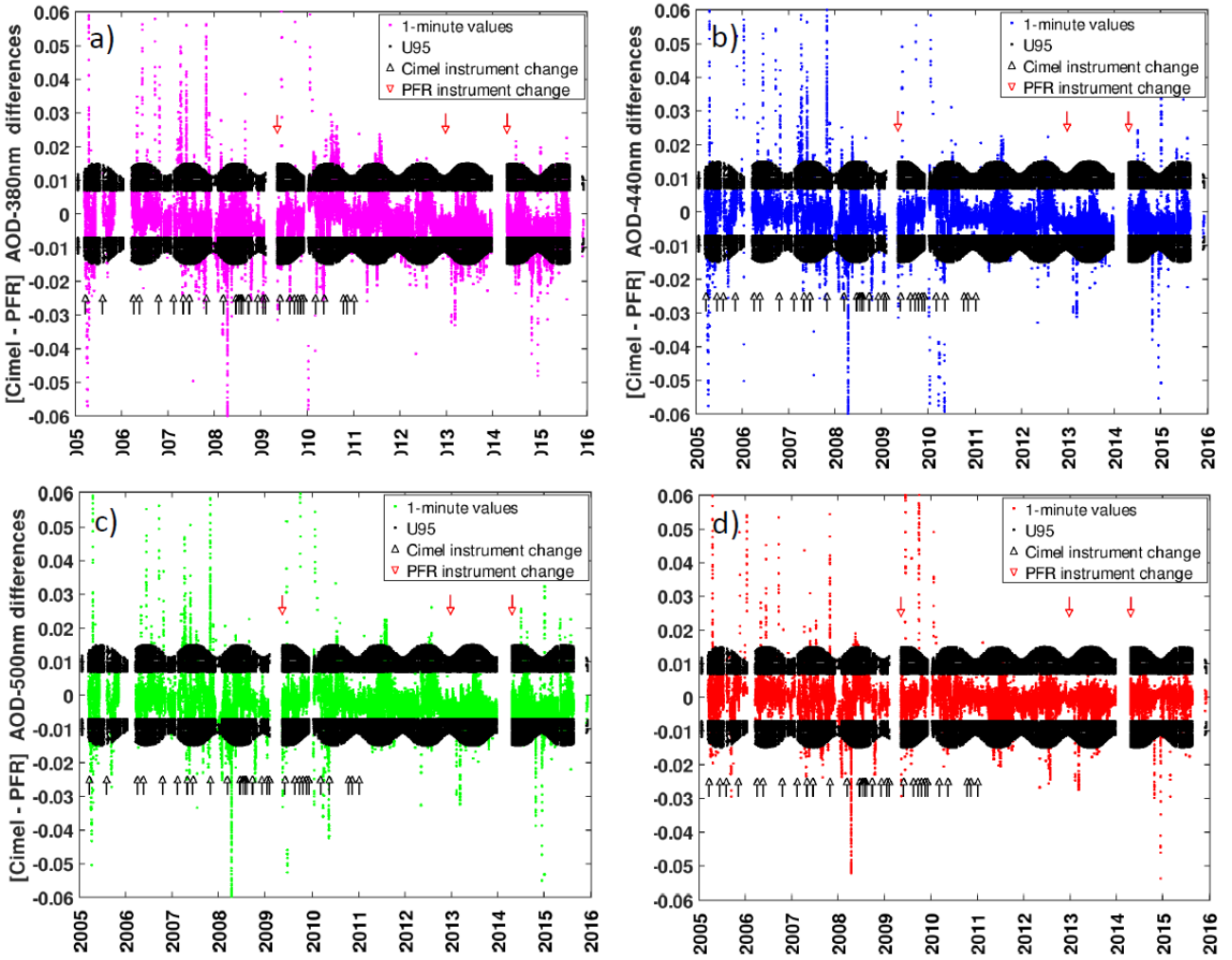

Figure 2~~1~~. One~~1~~-minute AOD data differences between AERONET-Cimel (V2) and GAW-PFR for (a) 380 nm (70838 data-pairs), (b) 440 nm (71645 data-pairs), (c) 500 nm (70833 data-pairs) and (d) 870 nm (71660 data-pairs) for the period 2005-2015. Black dots correspond to the U95 limits. A small number of ~~Some~~ outliers are out of the ~~~~±0.06 AOD differences range. Black arrows ~~pointing up~~ indicate a change of Reference AERONET-Cimel radiometer and red arrows indicate a change of the GAW-PFR instrument.

Table 3. Percentage of AERONET-Cimel (V2 and V3) 1-minute AOD data meeting the WMO criteria for the four interpolated~~, and original~~ GAW-PFR channels for the period 2005-2015.

~~Interpolated GAW-PFR channel (%)~~	~~Original GAW-PFR channel (%)~~
~~380 nm (92.7)~~	~~368 nm (91.1)~~
~~440 nm (95.7)~~	~~412 nm (92.8)~~
~~500 nm (95.8)~~	~~500 nm (96.3)~~
~~870 nm (98.0)~~	~~862 nm (97.8)~~

Channel	V2 (%)	V3 (%)

380 nm	92.7	92.3
440 nm	95.7	95.2
500 nm	95.8	95.7
870 nm	98.0	97.8

Table 4. Percentage of AERONET-Cimel 1-minute AOD data (V2) meeting the WMO criteria for the four compared channels, and different AOD and AE scenarios for the period 2005-2015, . number of data pairs are shown in brackets. The lLast row corresponds to the total percentages for the sub-period 2010-2015. In bold, AOD and AE traceability is > 95% are marked in bold. Number of data pairs are in brackets.

% of data within WMO limits	380 nm	440 nm	500 nm	870 nm
AOD ≤ 0.05	94.4 (57008)	**96.8 (59130)**	**97.0 (58572)**	**98.5 (60191)**
0.05 < AOD ≤ 0.10	91.0 (4723)	93.1 (4850)	92.8 (4817)	94.2 (4908)
AOD > 0.10	75.0 (3938)	86.5 (4615)	85.1 (4466)	**95.9 (5118)**
AE ≤ 0.25	73.1 (2145)	82.3 (2417)	80.1 (2351)	**96.2 (2824)**
0.25 < AE ≤ 0.6	91.2 (5407)	**96.2 (5810)**	**96.0 (5691)**	**97.9 (5911)**
AE > 0.6	94.6 (55114)	**96.9 (57089)**	**97.0 (56504)**	**98.7 (58146)**
Total 2005-2015	92.7 (65669)	**95.7 (68595)**	**95.8 (67855)**	**98.0 (70217)**
Total 2010-2015	93.5 (41977)	**97.4 (43745)**	**97.2 (43627)**	**99.1 (44498)**

In general, the agreement obtained with the 1-minute AOD data is slightly lower than that obtained during short campaigns, such as those reported by (Kazadzis et al. (, 2014) at Athens observatory (4685 data-pairs), and Barreto et al. (2016) at Izaña ObservatoryIZO (5566 data-pairs), with agreements > 99 % for AOD_{870nm} and AOD_{500nm} in case of Barreto et al. (2016). However, our results for AOD_{500nm} (> 95 % of 70833 data-pairs) areis significantly better that that observed by Kazadzis et al. (2014) (~ 48 % of 4685 data-pairs) covering a relatively narrowshort range of AOD. The probable cause for the poor agreement found by (Kazadzis et al., 2014) was a poor calibration in the 500 nm channel in at least one of the instruments operating at Athens.

In addition, short-term campaigns usually cover a small range of AOD, normally with low AOD, and instruments are carefully and frequently supervised. On the contrary, during our intercomparison over a period of 11 years, the operation of the instruments can be described much moreconsidered as the normal operation of such a system. for a long term period of measurements, 20 than that of intensively attended instrumentation during short period intercomparison campaigns.

An additional interesting aspect of this study is that it is not a simple intercomparison exercise between two instruments but a comparison of a number of instruments that acted as reference instruments ~~s~~ for the AERONET/Europe Network.

Table 5. Basic skill-scores from the AOD intercomparison between GAW-PFR and AERONET-Cimel V2 for the period 2005-2015. The skill scores definitions are found in Huijnen and Eskes (2012).

Period	2005-2015			
Wavelengths (nm)	380	440	500	870
Mean Bias (MB)	-0.0026	-0.0018	-0.0021	-0.0001
Modified Normalized Mean Bias (MNMB)	-0.1301	-0.1046	-0.1474	0.0129
Fractional Gross Error (FGE)	0.1727	0.1546	0.1918	0.1837
Root Mean Square Error (RMSE)	0.0081	0.0070	0.0064	0.0049
Pearson's correlation coefficient (r)	0.9910	0.9925	0.9939	0.9949
Number of data-pairs	70838	71645	70833	71660

In the first period (2005-2009), a total of 13 Cimel radiometers were used, while in the second period (2010-2015), five Cimel radiometers have participated, and for much of this period, the Cimel #244 was operating as the permanent AERONET reference instrument at IZO. Once the most important causes of non-traceability in the first period, which were associated with a poor pointing of GAW-PFR due to problems in the sun-tracker, were discounted~~ruled out~~, we can conclude that there are no significant differences in the percentages of traceable data between the two ~~of both~~ periods. This means that the continuous change of ~~Master~~Reference Cimel instruments used in the 2005-2009~~10~~ period did not have a significant impact on AOD data comparison differences. This provides proof of ~~proves~~ the consistency and homogeneity of the long AERONET-Cimel AOD data series, and their comparability with the GAW-PFR AOD data series, regardless of the number of instruments used to generate these data series.

In our study, with a number of comparison data-pairs one or two orders of magnitude higher than those used in short campaigns, the results shown in Table 4 can be considered ~~excellent~~as fairly good.

In addition to the traceability scores, we have introduced some basic skill scores corresponding to the AOD intercomparison between GAW-PFR and AERONET-Cimel for the period 2005-2015 (Table 5) to be in line with previous studies that have performed short-term comparisons between these two instruments. The definitions of the used skill scores can be found in Huijnen and Eskes (2012).

The Pearson's correlation coefficient (r) values of the PFR-Cimel 1-minute AOD data-pairs~~,~~ are higher than 0.99 in all channels. Concerning Mean Bias (MB) and Root Mean Square Error (RMSE) associated with~~to~~ AOD differences, our results show quite similar skill scores to those found at Mauna Loa, USA for AOD_{500nm} (Kim et al., 2008), although the number of data pairs used at ~~Izaña Observatory~~IZO (~71000) is

much higher ~~than that of Mauna Loa (~9700)~~, and the AOD range of our study is much larger than that of the comparison performed in Mauna Loa. Kim et al. (2008) summarize results of previous short-term intensive studies (McArthur et al., 2003; Mitchell and Forgan, 2003; Kim et al., 2005; Schmid et al., 1999) carried out in stations where the radiometers were calibrated by intercomparison with ~~Master or~~ R~~r~~eference instruments. These results show MB values to be within 0.01 bias, one order of magnitude lower than in Mauna Loa and Izaña Observatories, highlighting the importance of having well calibrated instruments to carry out these type of comparisons.

For the period 2010-2015 (not shown here), ~~and~~ as expected, the RMSE and the Pearson's correlation improve slightly compared with the whole period 2005-2015.

5.~~2~~3. Non-traceability assessment

As presented in T~~the t~~able 3, data outside the WMO traceability criteria vary from 2% for 870 nm up to 7.3% for 380 nm. In this section, the different possible causes of non-traceability in AOD are evaluated and, if possible, quantitatively estimated. In order to assess the relevance and quantitative impact of these causes, and estimate errors derived from a non-perfect AOD data synchronization, we first made an analysis on the natural variability of AOD in a very short time period (1 minute) shown below.

5.3.1. Short-time AOD variability

In order to determine~~know~~ the variability of AOD within one minute, we have performed two independent analyses with AOD data from the PFR and Cimel for the ~~channels of~~ 368/380 nm and 501/500nm channels during one year (2013). On the one hand, and taking into account that GAW-PFR provides AOD every minute, we have calculated all the AOD differences for each channel in the successive minutes. So~~, with which~~ we have the variation of AOD from one minute to the next one during a whole year. On the other hand, for AERONET-Cimel, we have taken advantage of the triplets, since each triplet consists of three successive measurements made in one minute ~~time period~~. In this case, the strategy has been to calculate the standard deviation of the triplet AOD measurements during a whole year. We have verified that the AOD variability in 1 minute is independent of AOD (see Supplement S3).

Table 6. Percentage of AOD data with variability within 1 minute less than 0.01 and 0.005, respectively, using AOD data from GAW-PFR (at 368 and 501nm) and AERONET-Cimel (at 380 and 500 nm) for 2013. A total of ~32000 d~~XX d~~ata-pairs per channel have been used from GAW-PFR, and 20117 triplets (60351 individual AOD measurements) from the Cimel#244 to calculate the AOD variability.

GAW- PFR

Percentage of data with 1-minute AOD variability (%)		
	368 nm	501 nm
< 0.01	99.88	99.91
< 0.005	99.21	99.35
AERONET-Cimel Percentage of data with 1-minute AOD variability (%)		
	380 nm	500 nm
< 0.01	99.87	99.99
< 0.005	99.82	99.42

The results obtained on the AOD variability in 1-minute from PFR data are very similar and consistent to those obtained with Cimel. Less than ~ 0.8% of the AOD data show variability higher than 0.005 in all wavelength ranges. It should be noted that the possible instrumental noise is included in this variability, so that the actual natural AOD variability would be, in any case, lower than that expressed in Table 6. The percentage of data with 1-minute AOD variability for all~~the~~ four GAW-PFR channels are given in Supplement S3. These results indicate that the natural AOD variability is very low thus the non-ideal measurement synchronization cannot explain the percentages of non-traceable AOD cases shown in Tables 3 and 4.

5.3.2. Uncertainties of~~by~~ GAW-PFR channel interpolation to AERONET-Cimel channels

The interpolation of the CIMEL AODs to the PFR AOD wavelengths can be one of the sources of uncertainty in this comparison assessment. The greatest uncertainty arises in the extrapolation of the $AOD_{412\ nm}$ of the PFR to the Cimel wavelength 440 nm~~retrieve AODs at the Cimel~~~~CIMEL~~ ~~AOD_{440nm}~~.

Using the Angström formula we have calculated that for an uncertainty of ±0.5 in the ~~Angström exponent~~AE ~~and for AOD of 0.1 at 412 nm,~~ the introduced uncertainty in the AOD extrapolation from 412 nm to 440 nm is ~5% (i.e., 0.005 for AOD_{412nm}=0.1). The introduced uncertainty is reduced to ~2% for an uncertainty of ±0.3 in AE. ~~of the order of ±0.003, while for an AOD_{412nm} of 0.5 and an AE uncertainty of ±0.3, the introduced uncertainty is ±0.008.~~ For all other AOD interpolations the errors are smaller.

5.~~3~~2.~~3~~1 Calibration related errors

As described in Section 3~~mentioned~~,~~T~~ the calibration procedures of the AERONET-Cimel and GAW-PFR radiometers are different. While in the case of GAW-PFR, frequent calibrations are established throughout the year and the calibration value is linearly interpolated in time, in AERONET- Cimel a

constant calibration value is assumed in the intermediate period between two consecutive calibrations carried out on an annual basis.

The typical calibration uncertainty for a single Langley plot is 0.7-0.9 % (at the 95 % confidence level), and it is reduced to 0.4 % in the case of ~~Izaña Observatory~~IZO when averaging at least 10 Langley-derived extraterrestrial constants (~~-~~which is the normal procedure) (Toledano et al., 2018). Regarding ~~-t~~the GAW-PFR~~s~~ radiometers operated at IZO, a direct yearly comparison of the Langley based V_o's with the reference triad at PMOD/WRC showed differences lower than 1 % for all channels for the 2005-2015 period.

A not sufficiently accurate determination of the calibration constant results in a fictitious AOD diurnal evolution presenting a concave or convex characteristic curve due to the calibration error dependence on solar air mass. The largest error occurs in the central part of the day (~~or~~ lower air masses), mainly, in clean days with very low aerosol load (< 0.02 in 500 nm)~~,~~ as reported by Romero and Cuevas (2002) and Cachorro et al. (2004), and as ~~it~~ can be derived from Equation 2. According to Cachorro et al. (2004, 2008) fictitious differences of up to 0.06 between the minimum and the maximum AOD can be recorded in a day with constant AOD as a result of a non-accurate calibration or no~~n-t~~ cleaned instruments. ~~–~~However, these fictitious differences in AOD depend on the related calibration magnitude errors.

We have represented the AOD differences between GAW-PFR and AERONET-Cimel versus optical air mass for the four channels for~~under~~ pristine conditions (~~PFR~~ $AOD_{500nm} \leq 0.03$) for both V2 and V3 (See Supplement S4). It should be noted that although the few outliers are evenly distributed throughout the whole airmass range, they are not equally distributed with respect to the zero of the AOD difference, but there is a bias with positive large outliers (higher Cimel AOD), already reported by Nyeki et al. (2013), and small negative outliers for optical air mass lower than 2.

The total percentage of AOD traceable data pairs under pristine conditions ($AOD_{500nm} \leq 0.03$) is very high for all wavelengths (> 97.7~~9~~ %) falling within the *U*95 limits (~~Table 6~~Table 7), except for 380 nm. There is no dependence on 1-minute AOD differences with optical air mass for 440, 500 and 870 nm, and a slight dependence for 380 nm (~~Table 6~~Table 7) with higher ~~lower traceability~~percentage of AOD differences outside the U95 limits at lower optical air masses. For the extended range of optical mass > 5 in V3, the AOD differences do not increase with optical mass (Supplement S5). The lower traceability at 380 nm for low air masses is especially clear in V3 with ~~a modest~~ 92.9% of traceable data (See Supplement S5). ~~On the contrary, we can see that for the extended range of optical mass > 5 in V3, the AOD differences does not increase with m (Supplement S5).~~

~~The percentage of non-traceable AOD values increases for shorter wavelengths and for lower optical masses ()(Supplement S5).~~ This result is consistent with the fact that the highe~~str~~~~greatest~~ uncertainty in the determination of the calibration constants is observed in the UV range, and the lowest uncertainty in the near-infrared channel (Eck et al., 1999; Jarosyawski et al. 2003; Toledano et al., 2018). This is attributable to an imperfect calibration, or to very small changes in the filters' transmittance, that can only be ~~only~~ detectable in extreme conditions: UV range, very low optical air mass, and pristine conditions. According to Toledano et al. (2018), the greatest variance in the extraterrestrial constant in the UV channel could be due to a number of factors: 1) higher AOD variability at the shorter wavelengths; 2) filter blocking issues;

and 3) temperature effects affecting AERONET-Cimel instruments that have not been accounted for in the UV range.

Table 7. Percentage of 1-minute AOD data (V2) meeting the WMO criteria for each wavelength for different optical air mass intervals under pristine conditions ($AOD_{500nm} \leq 0.03$) in the pe-riod 2005-2015. See Supplement S5 for equivalent results with V3.

Traceability Percentage of AOD differences within the U95 limits for AOD500$nm \leq 0.03$	Total (%)	$1 \leq m \leq 2$ (%)	$2 \leq m \leq 3$ (%)	$3 \leq m \leq 4$ (%)	$4 \leq m \leq 5$ (%)
380 nm	95.8	94.5	96.0	97.4	97.2
440 nm	97.9	97.9	97.7	98.2	97.7
500 nm	98.3	98.4	98.1	98.6	98.4
870 nm	99.2	99.4	99.3	99.2	98.6

-The correct cause attribution of each outlier would require manual inspection and additional specific information on instrumental checking and -maintenance information that is not always available. -We have investigated in more in detail the origin of the outliers and whether one of the two instruments predominantly caused them.

-

Thus, we have calculated for the non-traceable AOD data the diurnal range of AOD variation (maximum value minus minimum value of AOD in one day) at 380 nm for each instrument under pristine conditions (Figure 3) using Cimel -AOD_{500nm} daily mean < 0.03 to select the pristine days. According to this approach, the instrument that shows the highest daytime AOD range is the one that is responsible for the outlier. -As the wavelength increases both the number of outliers and the magnitude thereof decreases significantly-. (Supplement S6). Then, we identified those outliers with a diurnal AOD range higher was than 25% of the mean daily AOD value -and investigated their possible causes. A total of 51 cases for GAW-PFR and 81 cases for AERONET Cimel V3 were obtained and carefully analysed one by onein detail, using as auxiliary information, such as 1-minute in-situ meteorological data, 5-minute all-sky images, 1-minute BSRN data, and satellite imagery (not shown here). We obtained the percentage of AOD outliers of GAW-PFR and AERONET Cimel (V3) for which a certain cause has been identified, such as calibration inaccuraciuncertainties, cloud screening algorithm failures, mixture of the two previous causes, poor sun pointing, or not well-defined unknown causes (electronic problems, humidity inside the lenses, filter dirtiness, obstruction of the lenses collimators, insects on the optics outside, etc.) (see Supplement S7).

From the analysis of these cases, under the conditions described above, it should be noted that ~ 44% of the cases with fictitious AOD diurnal cycles were due to small uncertainties in the calibration of AERONET-Cimel (V3), while for this same reasoncause a ~ 8% of cases were identified in GAW-PFR.

Some examples of ~~non-~~AOD non-traceability for both AERONET-Cimel and GAW-PFR in the ~380 nm channel are shown in Supplement S8. The fictitious diurnal AOD cycle is mainly visible in the UV channels as shown in the examples reported in ~~of~~ Supplement S9. ~~-~~Note~~,~~ that the fictitious diurnal AOD ~~only~~ can be more easily identified ~~only~~ under very low AOD conditions.

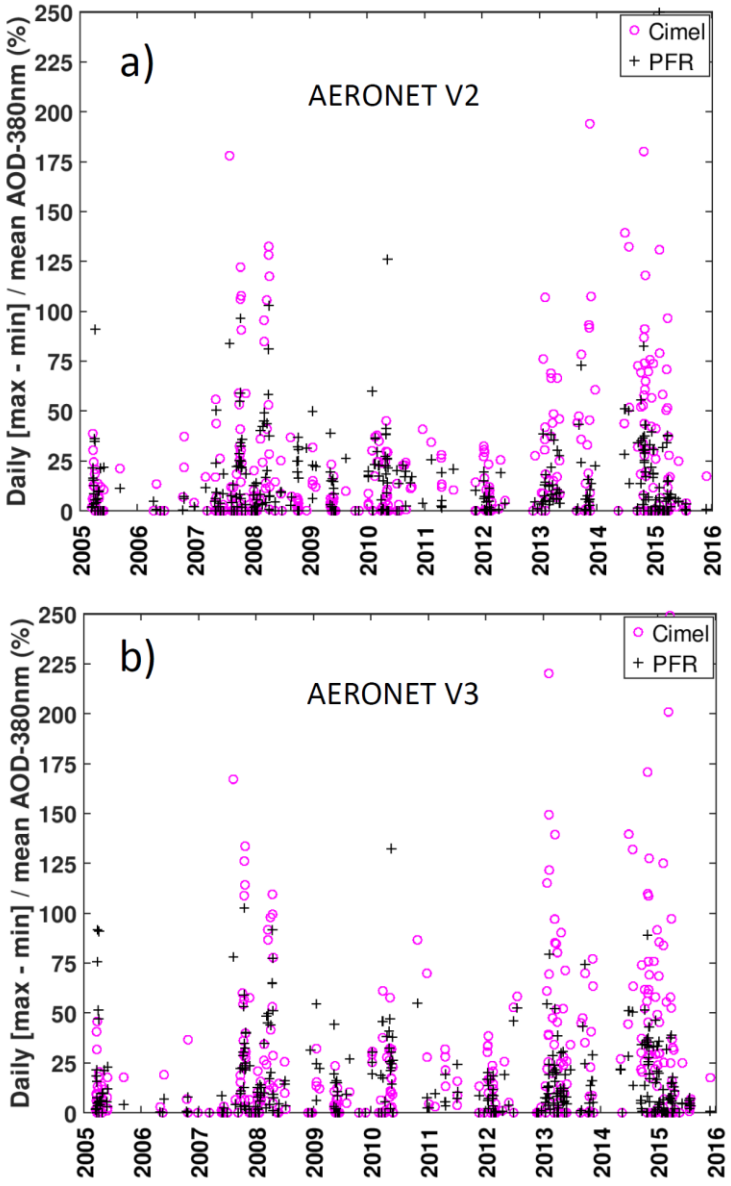

Figure 3. AOD ~~D~~diurnal range ~~of AOD$_{380nm}$~~ variation (maximum value minus minimum value of AOD in one day) at 380nm corresponding to AOD outliers (non-traceable AOD) ~~AOD data~~ under pristine conditions (AOD$_{Cimel\text{-}500nm} \leq 0.03$) in the period 2005-2015 for AERONET V2 (a) and V3 (b).

5

5.32.4.2 *Differences in cloud-screening and sun tracking.*

In this section wWe have examined the effect that the presence of clouds might have on AOD differences and the number percentage of cases outside the U95 limits. The impact of clouds on AOD differences only occurs when both GAW-PFR and AERONET-Cimel cloud screening algorithms fail to identify clouds in the direct sun path. AERONET-Cimel Version 2 data uses the so-called "triplet check" cloud-screening algorithm developed by Smirnov et al. (2000) and a second-order temporal derivative constraint (McArthur et al., 2003) to rule out AOD measurements potentially contaminated by clouds. GAW-PFR algorithms also use the Smirnov triplet measurement, and the second-order derivative check, but add a test for optically thick clouds with $AOD_{500nm} > 2$ (Kazadzis et al., 2018b). This algorithm, used by both networks with certain variants, assumes a transitory character in the presence of a cloud, which causes a sudden change of AOD. This sharp change would be detected by measuring the stability of three successive optical depth measurements, so that, when a cloud totally or partially blocks the sun, the standard deviation associated with the average of the triplets increases enormously. Note that if either one or both cloud screening algorithms (GAW-PFR and AERONET-Cimel) are flagged as cloudy, then the corresponding AOD data pair does not take part in the comparison.However, in the case of stratiform and very stable clouds or in the case of very thin clouds such as cirrus clouds, the algorithm could erroneously interpret that there are no clouds since there would be no appreciable changes in the stability of the triplets. A hint that cloud flagging failure could lead to large AOD calculated differences is coming from an analysis of AOD differences for days with different cloudy sky fractions. We do not have precise ancillary information to verify in each 1-minute data the influence that a certain cloud could cause in the non-traceability found. As a first approach forIn order to assess assessing the impact that cloud conditions might cause on AOD traceability, we have used the concept of daily fractions of clear sky (FCS) that has been applied before to solar radiation data at Izaña ObservatoryIZO (García et al., 2014). FCS represents the percentage of observed sunshine hours in a day with respect to the maximum possible sunshine hours in that day. The higher the daily FCS, the higher the clear sky percentage we have on that day.

The percentages of traceable and non-traceable AOD data versus FCS values grouped into 5five intervals are shown in Table 7Table 8. The results indicate that with a FCS lower than 20 % (almost overcast skies), and for wavelengths lower than 870 nm, data outside the U95 limits comprises, at least, 50 % of the total AOD data. It should be emphasized that the number of cases linked with FCS between 0% and 60% are less than 2% of the total cases. There, ~8% (870nm) to 24% (380nm) of the data are outside the WMO limits (maximum of 0.5% of the total data for 380nm outside the WMO limits). As the fraction of clear

sky increases, the percentage of traceable AOD data significantly exceeds the number of non-traceable AOD data. The percentage of traceable data is especially large (> 90 %) when FCS > 80 % (almost clear skies).

This is the FCS range in which a significant percentage of days with cases presenting scattered clouds areis recorded, which qualitatively confirms that V3 has introduced more efficient cloud screening than V2. However, the real impact of clouds on AOD traceability at Izaña ObservatoryIZO is very low due to its special characteristics of a high mountain station with very little cloudiness. As indicated in Table 7 (figures in brackets), the percentage of cases in which FCS < 60 % is lower than 1.33 %. Therefore, in practice, the possible impact of clouds on the non-traceability of AOD data-pairs is insignificant at the Izaña ObservatoryIZO since most of the time there are clear skies or skies with very little presence of clouds. On the other hand, and in order to interpret these results correctly, it should be emphasized that both GAW-PFR and AERONET-Cimel cloud screening algorithms provide successful identification on clear direct-sun conditions during cloudy skies (FCS < 40 %) for ,99.75 % of the cases, excluding those with very thin clouds. Future specific studies with AERONET V3 will allow to elucidate if the AOD traceability increases substantially under the presence of cirrus because its detection is one of the notable improvements of the V3 compared to V2. of AERONET V3 (Giles et al., 2018).

However, we admit that this methodology can only be used qualitatively, as it has serious limitations since sunshine recorders are not sensitive enough to detect the presence of cirrus that, to a large extent, might cause failures in cloud-screening algorithmsHowever, in the case of stratiform and very stable clouds or in the case of very thin clouds such as cirrus clouds, the algorithm could erroneously interpret that there are no clouds since there would be no appreciable changes in the stability of the triplets..

In the particular case of Izaña there are some very specific cloud scenarios in which cloud screening algorithms could fail resulting in non-AOD traceability: 1) Altostratus above the top of the SAL, at ~6 Km altitude (see Supplement S10); 2) Cirrus clouds (see Supplement S11); and 3) low clouds (stratocumulus) that sometimes exceed the observatory height level (see Supplement S11).

A more detailed analysis of more rare atmospheric conditions, such as those of strati-form and homogeneous cirrus clouds, or when altostratus are present above the Saharan Air Layer (SAL), around 6 Km altitude, and thus masked by a heavy mineral dust layer below needs further investigation. A constant cloud optical thickness (COT) corresponding to a cloud of a certain horizontal extension would cause the successive measurements within a minute to correspond to the same cloud stage, and therefore it would not be discernible from the extinction caused by aerosols. In the case of very thin cirrus clouds, the fluctuations in AOD would be very small and could be interpreted as the presence of a light layer of aerosols. Another factor that must be taken into account is that the FOV of the instruments is different. Thus, GAW-PFR (FOV = 2.5°) could detect the entry of a constant COT cloud in part of its

~~field of view in a different way than AERONET-Cimel (FOV = 1.2°). In all these cases, the cloud-screening algorithms may fail simultaneously in both GAW-PFR and AERONET-Cimel, resulting in a different AOD measurement derived by the two instruments.~~ shown ~~reported1-minute~~

As can be deduced from the analysis of these cloud cases, the impact of the different types of clouds o~~i~~n AOD retrieval is very complex and further specific investigations are required in order to understand~~,~~ the reasons behind failures in the GAW-PFR and AERONET-Cimel cloud screening algorithms.

~~These type of rare situations should be the subject of future studies through measurement campaigns using ancillary observation systems (e.g. lidar, all sky camera).~~

~~Table 7~~Table 8. Percentage of ~~traceable (T) data and percentage of~~ AOD data ~~outside~~ within the U95 limits ~~(NT)~~ for each channel and 5 daily fractions of clear sky (FCS) intervals. In brackets, relative frequency of each FCS interval for AERONET V2 and V3, respectively. In bold, the percentages of V3 that are greater than those of V2.

	~~380 nm~~		~~440 nm~~		~~500 nm~~		~~870 nm~~	
	~~T (%)~~	~~NT (%)~~	~~T (%)~~	~~NT (%)~~	~~T (%)~~	~~NT (%)~~	~~T (%)~~	~~NT (%)~~
~~0%≤FCS<20% (0.03%)~~	~~47.6~~	~~52.4~~	~~43.5~~	~~56.5~~	~~47.6~~	~~52.4~~	~~87.0~~	~~13.0~~
~~20%≤FCS<40% (0.22%)~~	~~69.3~~	~~30.7~~	~~73.3~~	~~26.7~~	~~73.6~~	~~26.4~~	~~86.3~~	~~13.7~~
~~40%≤FCS<60% (1.08%)~~	~~79.1~~	~~20.9~~	~~87.8~~	~~12.2~~	~~88.8~~	~~11.2~~	~~91.9~~	~~8.1~~
~~60%≤FCS<80% (7.10%)~~	~~88.4~~	~~11.6~~	~~93.9~~	~~6.1~~	~~93.4~~	~~6.6~~	~~97.8~~	~~2.2~~

FCS≥80% (91.6%)	93.3	6.7	96.2	3.8	96.2	3.8	98.3	1.7

	380 nm		440 nm		500 nm		870 nm	
	V2	V3	V2	V3	V2	V3	V2	V3
0%≤FCS<20% (0.03%) (0.04%)	47.6	44.4	43.5	44.4	47.6	44.4	87.0	**92.6**
20%≤FCS<40% (0.22%) (0.22%)	69.3	**76.6**	73.3	**82.2**	73.6	**80.8**	86.3	**94.1**
40%≤FCS<60% (1.08%) (1.09%)	79.1	77.5	87.8	84.8	88.8	87.2	91.9	**92.0**
60%≤FCS<80% (7.10%) (7.17%)	88.4	**89.6**	93.9	93.9	93.4	**94.4**	97.8	97.6
FCS≥80% (91.6%) (91.5%)	93.3	92.8	96.2	95.6	96.2	96.1	98.3	98.1

5.32.53. Different corrections in attenuation by Rayleigh scattering, and absorption by O_3 and NO_2 corrections.

In this sectionsection, we evaluate the possible impact on the 1-minute AOD data outside the *U*95 limits due toby the different processing ofthat each network regardingmakes in the correction by Rayleigh scattering and by the light absorption of column O_3 and NO_2.

Although GAW-PFR and AERONET-Cimel use spectral channels with weak absorption by atmospheric gases, AOD can only be determined if optical depth contributions from those gases are well estimated and subtracted from the total optical depth (τ). GAW-PFR and AERONET-Cimel separate the contributions of the molecules (Rayleigh scattering, τ_R), aerosols (τ_a; in this study referred to as AOD) and absorbing gases: , generally total column ozone (τ_{O3}) and nitrogen dioxide (τ_{NO2}) due to their different optical air masses at low solar elevation:

$$I(\lambda) = I0(\lambda)\exp-(\tau_R m_R + \tau ama\ AOD m_a + \tau_{O3} m_{O3} + \tau_{NO2} m_{NO2}) \quad (3)$$

So, AOD can be derived from:

$$AOD = \frac{1}{m_a}(ln\frac{I_0(\lambda)}{I(\lambda)} - \tau_R m_R - \tau_{O3} m_{O3} - \tau_{NO2} m_{NO2}) \quad (4)$$

5.3.54.1 Rayleigh scattering

The Rayleigh scattering contribution to total optical depth would be:

$$\tau_R = \delta_R \frac{m_R}{m_a} \quad (5)$$

where, m_R is writtencalculated, according to Kasten and Young (1989), as:

$$m_R = \frac{1}{sin\theta + 0.50572(\theta + 6.07995)^{(-1.6364)}} \quad (6)$$

and m_a, according to Kasten (1966), has the following expression:

$$m_a = \frac{1}{sin\theta + 0.0548(\theta + 2.65)^{(-1.452)}} \quad (7)$$

where θ is the sun elevation, and δ_R can be expressed as (Bodhaine et al., 1999):

$$\delta_R(\lambda) = 0.00864\lambda^{-(3.916+0.074\lambda+\frac{0.050}{\lambda})}\frac{P}{P_o} \quad (8)$$

where P_o = 1013.25 hPa, λ is the wavelength in microns (μ) and P is the pressure in hPa at the measurement site. The depolarization factor recommended by (Young, 1980) is already included in Eq. 8.

From Eq. 8, we can derive the differences in τ_R contribution ($4\tau_R$):

$$\triangle\tau_R = (0.00864\lambda^{-(3.916+0.074\lambda+\frac{0.050}{\lambda})}\frac{1}{1013.25}\frac{m_R}{m_a})(P_{PFR} - P_{Cimel}) \quad (9)$$

Accordingly~~So~~, the main Δ~~4~~τ_R from GAW-PFR and AERONET-Cimel ~~might basically~~ can arise from the different way the two instruments ~~measure~~ obtain the atmospheric pressure (P_{PFR} and P_{Cimel}, respectively).

While AERONET-Cimel ~~determines~~ obtains the site station pressure from the National Centers for Environmental Prediction (NCEP) and the National Center for Atmospheric Research (NCAR) reanalysis at standard levels, GAW-PFR has a solid-state pressure transducer in the control box to read barometric pressure simultaneously with each PFR measurement. As Giles et al. (2018) have stated, the expected error in the station pressure P_{Cimel} is generally < 2 hPa provided the elevation of the station is well-known and the weather conditions are stable. In order to assess this possible difference, we have compared the 1-minute synchronous pressure data of both instruments, and the corresponding 1-minute Δ~~4~~τ_R from Eq. 9. Note that, in practice, this comparison is performed~~made~~ at ~~6 hour~~6-hour intervals since the NCEP/NCAR reanalysis data are available routinely with this ~~at six hourly~~ temporal resolution (Kalnay et al., 1996). The results are depicted in Figure 4.

The results indicate that most of the 1-minute pressure differences are within ± 5 hPa (Figure 4a), resulting in 1-minute Δ~~4~~τ_R data within ± 0.001. However, when pressure differences are significantly higher, such as those registered at the end of 2014 (> 30 hPa) (Figure 4a), Δ~~4~~τ_R increases ~~to~~ significantly ~~values~~ (~ 0.01) (Figure 4b). However, it should be noted that only 99 AOD data pairs have been registered for which the pressure difference between PFR and Cimel is greater than 20 hPa at 870nm and 440nm, and one AOD data pair at 500nm and 380nm channels.

Taking into account that the accuracy of the new barometers built into new radiometers is ~~about~~ ~3 hPa only dramatic barometer malfunctioning could cause $\Delta\tau_R$ > 0.01. As stated by Kazadzis et al. (2018b), the use of erroneous pressure values can lead to wavelength-dependent AOD errors and to large errors in

AE. However, these flagrant barometer malfunctions are quickly detected and easily corrected if there are other pressure measurements at the station, as is the case in Izañaour case.

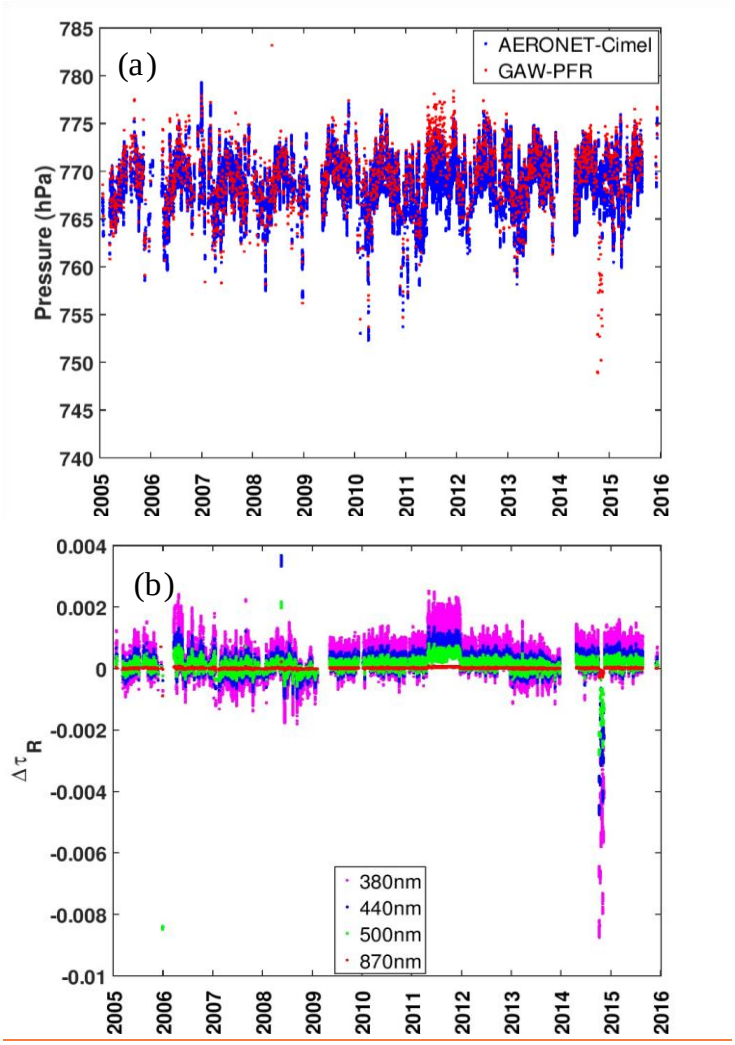

Figure 4. (a) 1-minute pressure data (hPa) from GAW-PFR and 6-hour pressure data at Izaña Observatory altitude from the National Centers for Environmental Prediction (NCEP) and the National Center for Atmospheric Research (NCAR) reanalysis for the case of AERONET-Cimel, and (b) corresponding 1-minute $\Delta\tau_R$ caused by pressure differences in the period 2005-2015.

5.3.54.2 Differences in O_3 absorption

The O_3 related optical depth is determined with the following expression:

$$\tau_{O3}(\lambda) = \sigma_{O3}(\lambda)\frac{O_3}{1000}\frac{m_{O3}}{m_a} \quad (10)$$

Where O_3 is expressed in Dobson units (DU), and the absorption coefficients ($\sigma_{O3}(\lambda)$) take the following values (Gueymard, 1995): 0.0026 cm^{-1} (440 nm), 0.03150 cm^{-1} (500 nm), and 0.00133 cm^{-1} (870 nm). The ozone absorption is maximum in the 500 nm channel and practically zero in the 380 nm channel. GAW-PFR uses the following expression for m_{O3} the following expression (Komhyr, 1980):

$$m_{O3} = \frac{R+h}{\sqrt{(R+h)^2 - (R+r)^2(cos\theta)^2}} \quad (11)$$

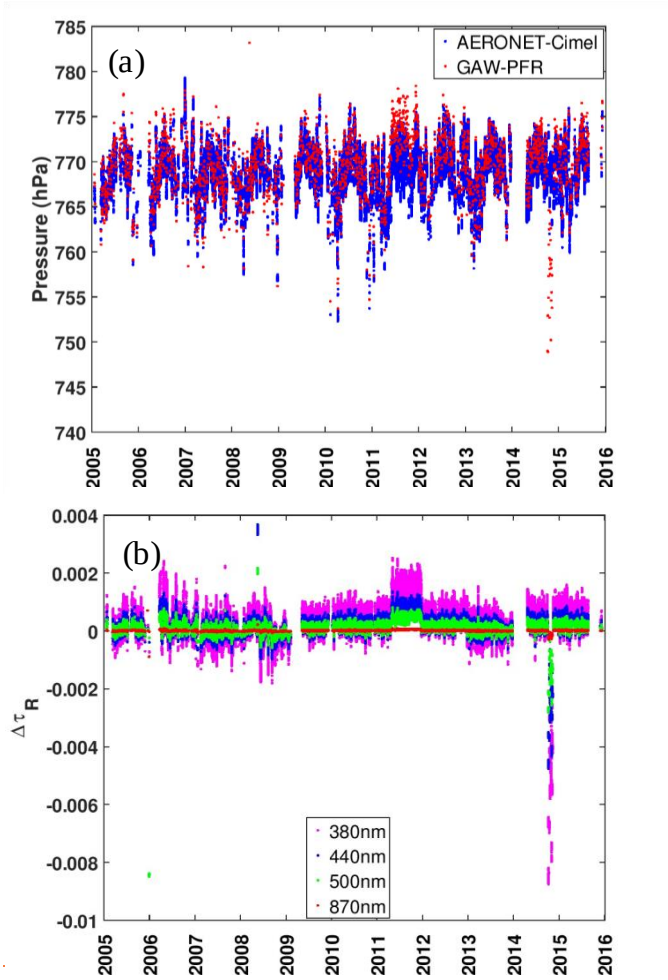

Figure 4. (a) 1-minute pressure data (hPa) from AERONET-Cimel and GAW-PFR and 6-hour pressure data at Izaña level from the National Centers for Environmental Prediction (NCEP) and the National Center for Atmospheric Research (NCAR) reanalysis for the case of AERONET-Cimel, and (b) corresponding 1-minute Δτ$_R$ caused pressure differences in the period 2005-2015.

where R = 6370 km is the mean radius of the Earth, r = 2.370 km is the altitude of the station, h = 22 km is the estimated height of the ozone layer, and θ is the solar elevation. However, AERONET-Cimel uses an updated expression (Komhyr et al., 1989) in which h is not fixed and takes a value ~~in~~ as a function of the latitude, and the absorption coefficients are obtained for each particular filter using the spectral response provided by the manufacturer. For most of the period covered in this study, measured total ozone values from IZO~~the GAW Izaña station~~ (Brewer spectrometer) were used to calculate τ_{O3} (Wehrli, 2008a). If no Brewer data is available, data are retrieved from the Total Ozone Mapping Spectrometer (TOMS) or more recently ~~satellite sensor was used. Nowadays, GAW-PFR uses ozone data from AURA satellite overpass observations with~~ from the Ozone Monitoring Instrument (OMI) (McPeters et al., 2015) for daily operations (Kazadzis et al., 2018b). In the case of Izaña, if the OMI overpass fails, GAW-PFR uses the Brewer O_3

climatology. Concerning AERONET-Cimel Version 2, a NASA TOMS 1° x 1.25° resolution O_3 climatology is used. From Eq. 10, the differences in O_3 optical depth $\Delta\tau_{O3}$ can be derived:

$$\Delta\tau_{O3} = \sigma_{O3}(\lambda)\frac{1}{1000}\frac{m_{O3}(O_{3PFR} - O_{3Cimel})}{m_a} \quad (12)$$

The largest influence of total ozone data uncertainty in τ_{O3} occurs, by far, at 500 nm (Figure 5). According to Wehrli (2008b) and Kazadzis et al. (2018b), total ozone needs to be determined to ± 30 DU or 10 % of typical values, to ensure an uncertainty of ± 0.001 in τ_{O3} at 500 nm. In the case of the GAW-PFR / AERONET-Cimel comparison, and due to the very different method in which both networks obtained O_3 values for their corresponding corrections, the ozone differences found on some days (1761 out of 71965 days; 2.4 %) are very large (> 40 DU), exceeding a difference in the ozone optical depth of 0.001. Even so, the potential contribution toof AOD differences outside the *U*95 limits between the two networks is negligible. Total O_3 over the Izaña ObservatoryIZO is quite stable, showingshows a relatively small amplitude throughout the year, but both surface ozone concentrations and column ozone amount could sharply increase under the influence of cut-off lows injecting air from the high-mid troposphere into the lower subtropical troposphere, which is not uncommon in spring and the first half of summer (Cuevas et al., 2015; Kentarchos et al., 2000). In addition through exchange processes in the Upper Troposphere Lower Stratosphere (UTLS) due to the presence of the subtropical jet (mainly from February to April) (Rodríguez-Franco and Cuevas, 2013). However, if we wanted to repeat this traceability study of 1-minute AOD data in mid or high latitude stations where sharp O_3 variations (several tens of DU) could be registered in a few hours, the correction of 1-minute AOD measurements by τ_{O3} might be a challenging issue.

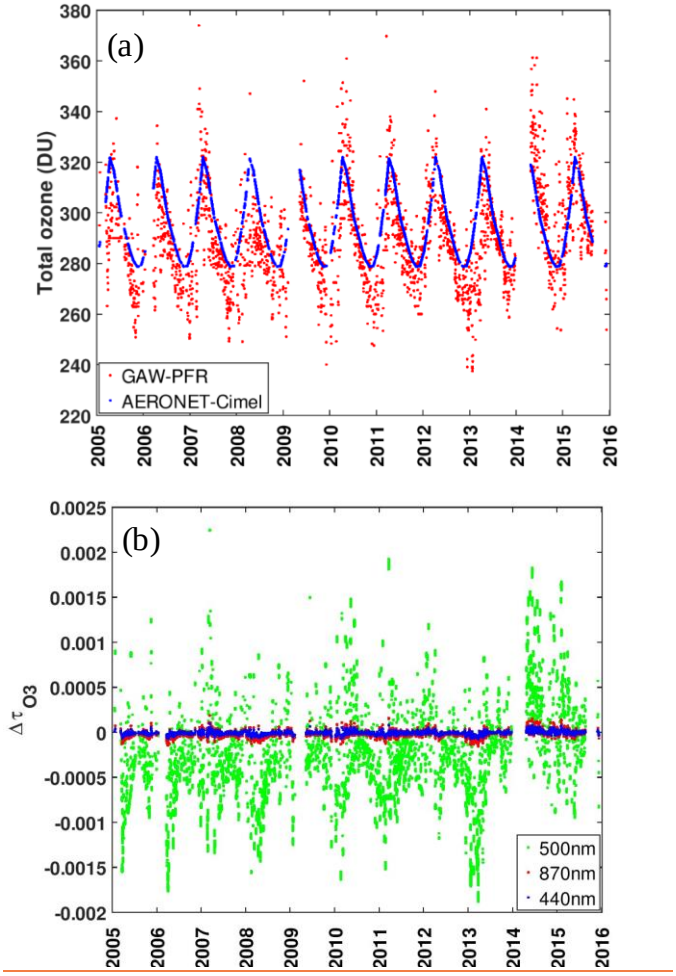

Figure 5. (a) Total O_3 used by GAW-PFR (measured Brewer O_3 values from IZO, OMI O_3 overpass or Brewer O_3 climatology) and AERONET-Cimel (TOMS O_3 climatology), and (b) $\Delta\tau_{O3}(\lambda)$ caused by differences in daily total O_3 between the two instruments in the period 2005-2015.

5.3.5~~4~~.3 Differences in NO_2 absorption

AERONET-Cimel applies a correction by absorption of NO_2, but GAW-PFR does not include this correction. AERONET-~~-~~Cimel obtains daily total NO_2 data from a 0.25° ~~°~~x 0.2° ~~°~~ resolution NO_2 monthly climatology obtained from the ESA Scanning Imaging Absorption SpectroMeter for Atmospheric CHartographY (SCIAMACHY) (Eskes and Boersma, 2003). In order to assess the contribution to~~in~~ AERONET-Cimel 1-minute AOD data non-traceability by NO_2 absorption ~~what~~ we have~~really~~ to estimate ~~is~~ the NO_2 optical depth ($\tau_{NO2}(\lambda)$) of AERONET-Cimel since GAW-PFR does not perform this correction. Analogously to $\Delta\tau_{O3}$, the differences in nitrogen dioxide optical depth Δ~~4~~τNO_2 can be obtained from:

$$\triangle\tau_{NO2} = \sigma_{NO2}(\lambda)\frac{1}{1000}\frac{m_{NO2}}{m_a}(-NO_{2Cimel}) \quad (13)$$

Where m_a is given by Eq. 7, NO_{2Cimel} (DU) is the daily total NO_2 used by AERONET-Cimel, $\sigma_{NO2}(\lambda)$ is the NO_2 absorption ~~coefficient with values that depend on wavelength~~ (Gueymard, 1995) ~~and are~~ weighted by the specific filter response: 15.6 cm^{-1} (380 nm), 12.3 cm^{-1} (440 nm), and 4.62 cm^{-1} (500 nm). Finally~~,~~ ~~and~~ m_{NO2} has the following expression (Gueymard, 1995):

$$m_{NO2} = \frac{1}{sin\theta + 602.30(90-\theta)^{0.5}(27.96+\theta)^{-3.4536}} \quad (14)$$

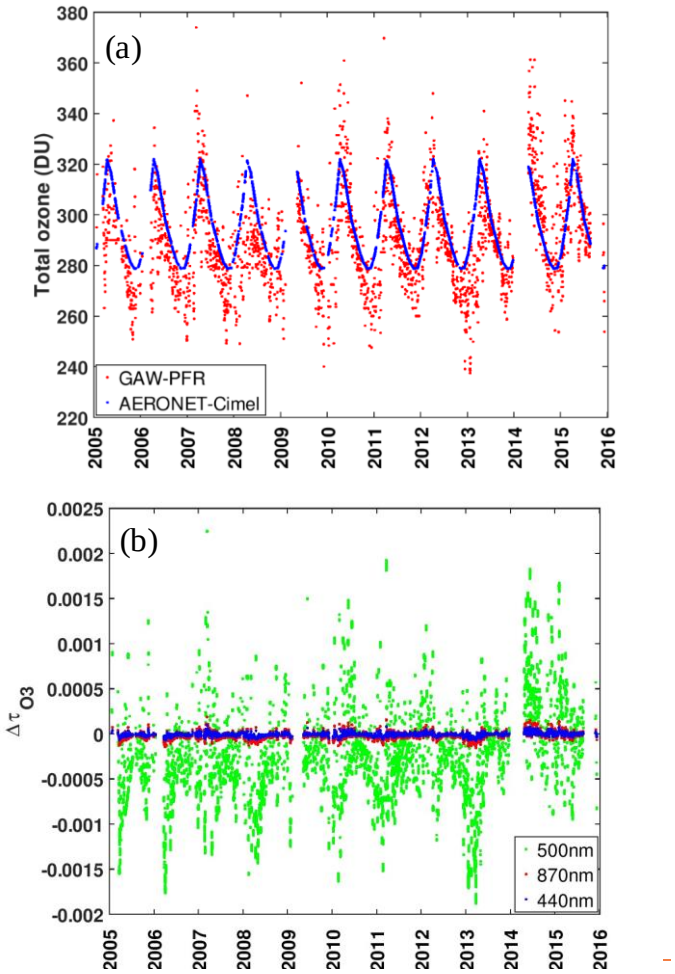

~~*Figure 5. (a) Total O_3 used by GAW-PFR (OMI O_3 overpass or Brewer O_3 climatology) and AERONET-Cimel (TOMS O_3 climatology), and (b) $\Delta\tau_{O3}(\lambda)$ caused by differences in daily total O_3 between the two instruments in the period 2005-2015.*~~

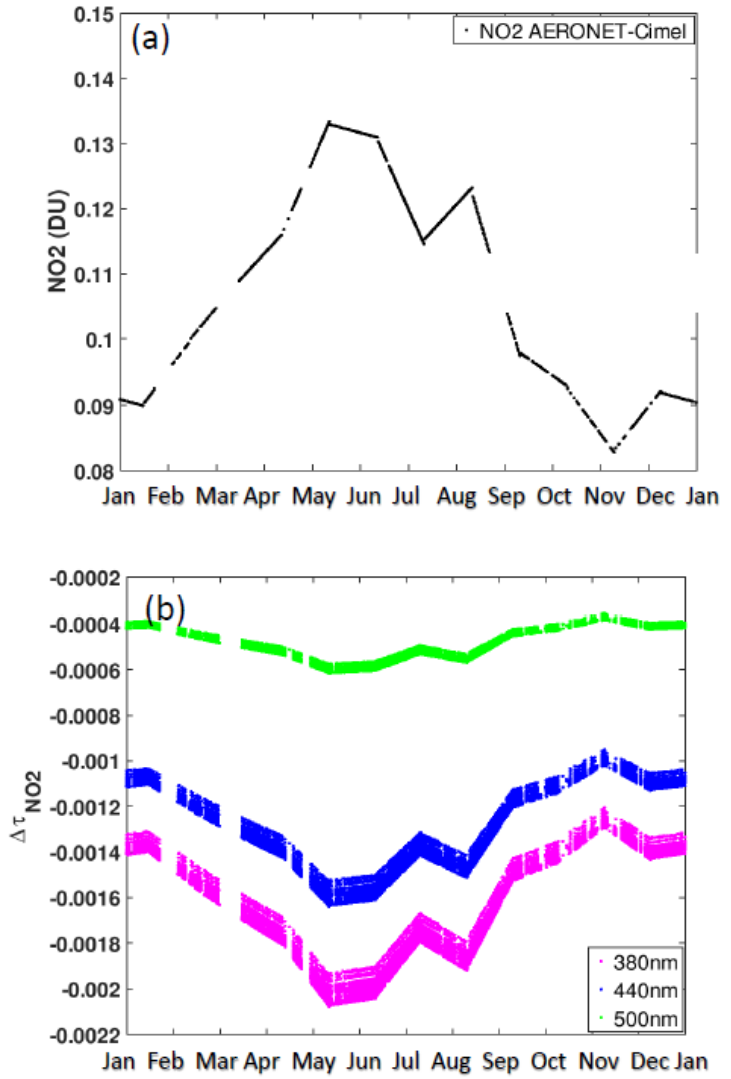

Figure 6. (a) ~~NO_2 annual course from a~~ NO_2 monthly climatology obtained from the ESA SCanning Imaging Absorption SpectroMeter for Atmospheric CHartographY (SCIAMACHY), used by AERONET-Cimel at ~~Izaña Observatory~~IZO, and (b) Δ4~~τσ~~$_{NO2}$ (λ) caused by differences in daily total NO_2 between GAW-PFR and AERONET-Cimel in the period 2005-2015. Note that GAW-PFR does not take into account the correction for the NO_2 absorption.

~~Table 8~~Table 9. *Percentage (%) of additional traceable AERONET-Cimel AOD 1-minute data (V2 and V3) ~~and AOD data outside the U95 limits that become traceable~~ after correcting by pressure, and total column O_3 and NO_2 for the period 2005-2015.~~.~~*

Channel	Increment (%) of traceable data after P, O_3 and NO_2 corrections
380 nm	1.3
440 nm	0.2
500 nm	0.3
870 nm	~ 0.0

Channel	Increment (%) of traceable AOD data after P, O_3 and NO_2 corrections	
	V2	V3
380 nm	1.3	1.7
440 nm	0.2	0.3
500 nm	0.3	0.1
870	~0.0	~0.1

In Figure 6a the total NO_2 used by AERONET-Cimel to evaluate $\tau_{NO2}(\lambda)$ is depicted. Figure 6b shows the $\Delta\tau_{NO2}(\lambda)$ caused by differences in daily total NO_2 between GAW-PFR and AERONET-Cimel. $\Delta\tau_{NO2}$ is of the order of 10^{-3} for 380 and 440 nm channels, while, for 500 nm channel, it is of the order of 10^{-4}. As for O_3, the absorption due to total NO_2 is negligible in the 1-minute AOD non-traceability in our study. However, it should must be noted taken into account that an impact on AOD calculation is expected when replicating similar analysis in if this type of traceability analysis is replicated in highly NO_2 polluted regions where the NO_2 absorption might have somean impact on AOD calculation is expected. Such cases include, such as in large industrial cities from East Asia and Central and Eastern Europe , in which tropospheric NO_2 adds to the natural stratospheric NO_2 resulting in column values much larger than the climatological ones (e.g., Chubarova et al., 2016).

Taking into account the corrections for Rayleigh scattering and for the absorptions by O_3 and NO_2, we have calculated the additional traceable AOD of datacombin that lie within the U95 AOD limits ed effect of all of them on percentage the non-traceability of the 1-minute AOD values (Figure 6; Table 8Table 9). This percentage is maximum at 380 nm with 1.3% (V2) and 1.7% (V3) of the whole dataset. At most (in the 380 nm channel), 25 % (1.3 % of total common measurements) of data outside the *U*95 limits are due to significant differences in pressure, and in O_3 and NO_2 absorption. Most of the AOD data outside the *U*95 limits that becomes traceable data after corrections are applied, had errors in the pressure measurement and therefore in the Rayleigh scattering correction. The 870 nm channel is only affected by the Rayleigh correction component and therefore the increment of traceable data after the mentioned corrections is

minimalmum.The 1minute AOD data outside the *U*95 limits by these corrections is negligible in the 870 nm channel.

5.4.3 *GAW PFR and AERONET-Cimel comparison under high AOD conditions: the impact of dust forward scattering role of the for on different FOVs.*

When we represent the AOD differences between AERONET-Cimel and GAW-PFR versus AOD (GAW-PFR) for AOD > 0.1, we observe a positive slope that increases when the AOD fitted data are > 0.05 (dusty non-pristine conditions), we noteing that AERONET-Cimel shows slightly higher AOD values than GAW-PFR, being higher than +0.01 for AOD > 0.15 (Figure 7). , and more clearly at 500 nm. The AOD data outside the *U*95 limits (in red) increases notably from AOD > 0.1.

In fact, the percentage of data outside the U95 limitsnon-traceable AOD data increases as AOD increases (Table 9Table 10), so that for dust--related aerosol conditions (AOD_{500nm} > 0.3) the percentage of AOD data outside the *U*95 limits is > 50 % for 380 nm and 440 nm (all channels except for 870 nm (Table 9Table 10, percentages in brackets). Similar results are found when using AERONET V3 (see Supplement S13). The increase in the percentage of AOD data outside the *U*95 limits is especially significant at the 380 nm channel. Taking into account the number of data compared with the total cases, Tthese results show a small but non-negligible percentage of AOD differences outside the *U*95 limits for AOD > 0.1, ranging from ~0.3 % at 870 nm to ~ 1.9 % at 380 nm. This especially affects the shorter wavelengths (Table 9Table 10).

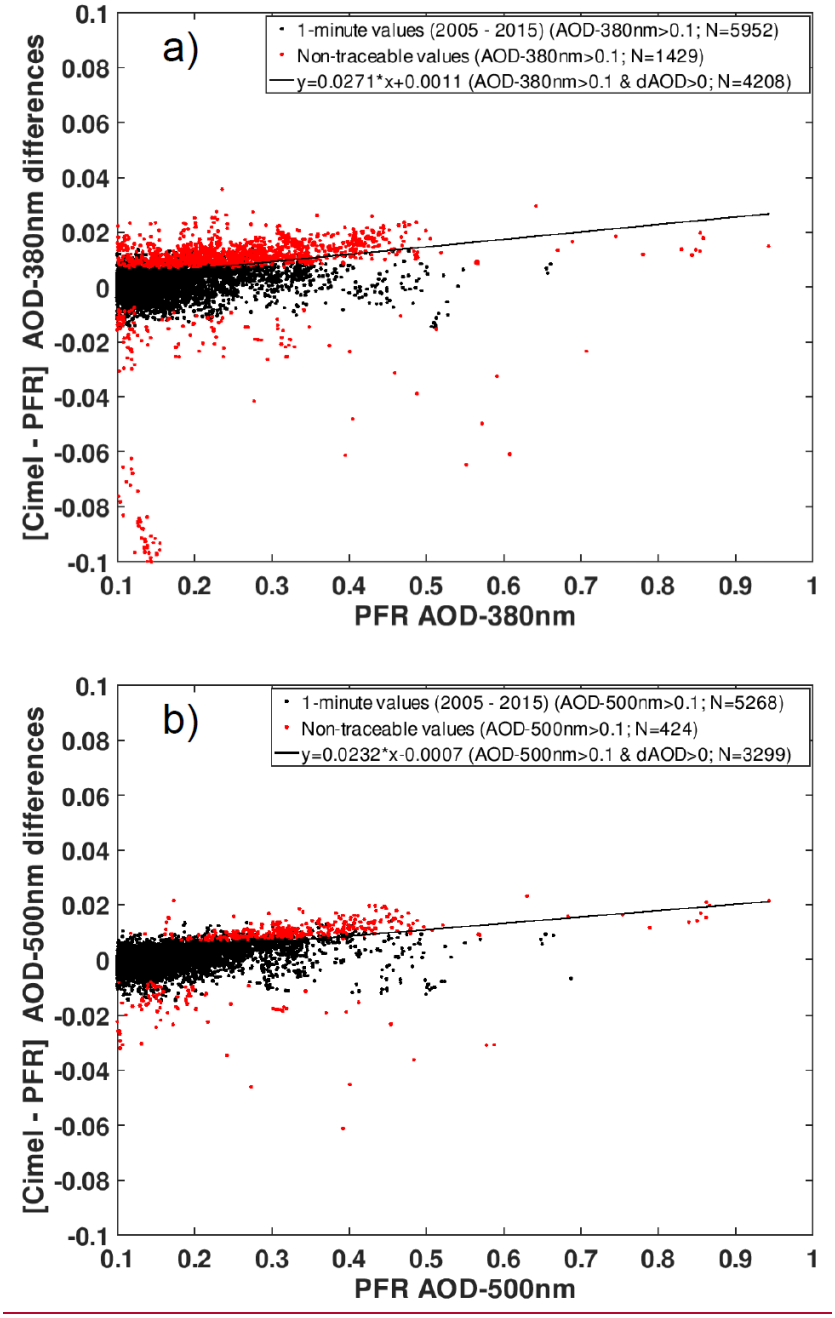

Figure 7. Actual AOD differences between AERONET-Cimel V2 and GAW-PFR vs ~~PFR~~ AOD$_{PFR}$ at (a) 380 nm (b) and 500 nm for the period 2005~~10~~-2015. The fitting line has been calculated with those data points with AOD ~~data~~ > 0.1 and ~~whose~~ Cimel-PFR AOD difference > 0. The n~~N~~umber of data used in the plots are indicated in the legend. The percentage of non-traceable AOD data with these conditions is ~24% for 380 nm, and ~8% for 500 nm. Note that some traceable (black) points show larger AOD differences than non-traceable (red) points because of the air mass dependence of the WMO traceability criterion.

~~Table 9~~*Table 10. Percentage of AERONET V2 AOD data outside the U95 limits at 380, 440, 500 and 870 nm channels and for three AOD_{500nm} thresholds respect to all data and respect to all data for each AOD interval (in brackets).*

	Percentage of AOD data outside the *U*95 limits (%)		
	AOD_{500nm}>0.1	AOD_{500nm}>0.2	AOD_{500nm}>0.3
380 nm	1.9 (25.0)	1.2 (47.2)	0.5 (59.8)
440 nm	1.0 (13.5)	0.8 (32.0)	0.5 (57.6)
500 nm	0.6~~1.1~~ (8.0~~14.9~~)	0.5~~9~~ (18.7~~35.1)~~	0.3~~5~~ (39.3~~60.8~~)
870 nm	0.3 (4.1)	0.2 (6.4)	0.1 (14.0)

~~Forward~~ A~~a~~erosol forward scattering within the FOV of various instruments and calculated AOD was investigated some decades ago by Grassl (1971) who determined that at AOD=1 the circumsolar radiation increases by >10% the incoming radiation. Russell et al (2004), using dust and marine aerosols data, quantified the effect of diffuse light for common sun photometer FOV. They reported that the correction to AOD is negligible (<1% of AOD) for sun photometers with narrow FOV (< 2°), which is greater~~higher~~ than ~~the one of~~ the Cimel FOV and slightly ~~lower~~smaller than the PFR FOV ~~of the PFR~~ (2.5°). Sinyuk et al. (2012) assessed the impact of the forward scattering aerosol on the uncertainty of the AERONET AOD, concluding that only dust aerosol ~~dust~~ with high AOD and low solar elevation could cause a significant bias in AOD (> 0.01). ~~Torres et al. (2013) investigated the uncertainty of the FOV in the AERONET-Cimel measurements indicating that direct solar irradiance measurements are biased by the amount of aureole radiation that is assumed to be direct solar radiation. The solar aureole, also known as the circumsolar region, is the bright region surrounding the solar disc, which becomes especially visible when there is a burden of moderate-high aerosols in the atmosphere.~~

GAW-PFR has double the FOV (2.5~~°~~; Wehrli (2000)) compared to the AERONET-Cimel (~~1.2~~1.3° ± 4.8~~10~~ %; Torres et al., ~~(~~2013~~)~~), so it is reasonable to expect that it is more affected by the circumsolar radiation than the AERONET-Cimel radiometer.

Taking advantage of the fact that Saharan dust intrusions regularly affect IZO, we provide a detailed analysis on the impact ~~-~~that dust forward scattering causes o~~i~~n the AOD retrieval of the two radiometers with different FOV, ~~-~~explaining the AOD differences ~~-~~under ~~-~~moderate~~-~~to~~-~~high dust load (AOD > 0.1) conditions. ~~To do this~~For this purpose we have used a forward Monte Carlo model (see section 4.4) with which we perform simulations that include accurate dust aerosol near-forward scattering effects.

Dust aerosol single-scattering properties were computed using Mie theory, assuming a refractive index of 1.47+0.0025i at the wavelengths 380 nm, 440 nm and 500 nm and 1.46+0.012i at 870 nm, based on AERONET measurements at IZOzañnaa. Seven values of aAerosol effective radiius (r_e) in the range 0.2 to 3.0 μm were considered, and a lognormal size distribution with a geometric standard deviation of 2 was assumed. A mid-latitude summer atmospheric profile starting from the Izañna altitude (2.4 km a.s.l.) was assumed, withbeing the aerosol layer located at 5-6 km a.s.l. (typical of summertime). A spectrally uniform surface albedo of 0.11 was employed. Computations were performed for nine AOD values (AOD= 0, 0.1, 0.2, 0.3, 0.4, 0.5, 0.6, 0.8, and 1.0) and for fiveour solar elevation angles (θ=80°, 60°, 45°, 340° and 20°). Ten million photons were used for each case and wavelength . The Monte Carlo model assumes a plane-parallel atmosphere, so the air mass factor is m=1/sinθ. Ten million photons were used for each case and wavelength.

Supplement S15 shows the ratio of scattered to direct radiation for cases with AOD up to 0.5. We have performed scattered to direct radiation simulations for FOVs of 2.5° and 1.2° for six values of effective radius (r_e=0.2, 0.5, 1.0, 1.5, 2.0 and 3.0 μm), for five AOD values (AOD= 0.1, 0.2, 0.3, 0.4, and 0.5), and for five solar zenith angles (θ = 10°, 30°, 45°, 60°, and 70°) (see Supplement S15). The ratio increases with increasing r_e, as the aerosol forward-scattering peak grows stronger. In the case of Saharan dust intrusions at IZOzañna Observatory, the median r_e median determined from both AERONET data inversion and the in-situ aerodynamic particle sizer (APS) analyzer is ~1.5 μm. This value agrees with the dust size distribution found during SAMUM-2 during long-range transport regime (Weinzierl et al., 2011). For this particle size, the ratio of scattered to direct radiation is ~3 times larger for FOV of 2.5° than FOV of 1.3°.

The error in the retrieved AOD due to scattered radiation within the instrument FOV was evaluated by comparing the apparent AODs, defined as:

$$AOD_{app,PFR} = -\frac{1}{m} ln \frac{F_{PFR}}{F_{PFR}(AOD=0)} \quad (15)$$

$$AOD_{app,Cimel} = -\frac{1}{m} ln \frac{F_{Cimel}}{F_{Cimel}(AOD=0)} \quad (16)$$

with the true AOD

$$AOD_{true} = -\frac{1}{m} ln \frac{F_{dir}}{F_{dir}(AOD=0)}. \quad (17)$$

HWhere, F_{dir} is the irradiance due to direct (i.e., non-scattered) radiation, and F_{PFR} (F_{Cimel}) is the total irradiance that would be measured by the PFR (Cimel) radiometer, considering the instrument FOV and the FOV angular function. The relative error in AOD depends strongly on the particle size but it is fairly constant for each r_e value considered (see Supplement S16). For r_e ~1.5 μm, the relative error in AOD at

380 nm (500 nm) is ~1.6% (1.0%) for Cimel, and ~5% (~3%) for PFR. These errors are in good agreement with those estimated by Russell at al. (2004), and slightly higher than the relative AOD error of 0.7% due to coarse dust ~~coarse~~ aerosol forward scattering reported by Eck et al. (1999).

The Monte-Carlo-simulated relative differences in retrieved AOD (in %) that would result from the scattered radiation within the FOV of the PFR~~RF~~ and Cimel instruments, and the difference in retrieved AOD between P~~R~~FR and Cimel~~IMEL~~ as a function of the AOD retrieved with P~~F~~FR~~R~~, for 380 nm and 500 nm, are shown in Figure 8. ~~These simulations were performed with Monte Carlo radiative transfer for seven values of aerosol effective radius between 0.2 and 3.0 µm, at (c) 380 nm and (d) 500 nm.~~ The main results of th~~e~~ise simulations are: 1) the higher FOV of the PFR, compared to that of the Cimel, results in lower AOD values for the PFR ~~when AOD > 0.1~~; 2) the fractional AOD difference related to the different FOVs of P~~R~~FR and Cimel~~IMEL~~ is fairly constant for any aerosol effective radius, but increases with increasing the effective radius; and 3) this fact might explain at least some of the systematic differences seen in Fig. 7. ~~-~~Note that, as ~~for AOD> 0.1,~~ lower AOD values derived from the PFR are expected based on its larger FOV, the linear fit~~sting~~ in Fig.~~figure~~ 7 have~~s~~ been calculated for those data points with ~~values in which~~ the Cimel~~IMEL~~-PFR AOD differences> 0. In this way, we discard those pairs of AOD data whose difference is not only due to the different FOV between both instruments, obtaining in this way a better approximation to quantify this effect.

The slopes of the fitting lines of the Cimel-PFR AOD differences vs. PFR AOD for AOD> 0.1 (dusty conditions) are~~,~~ 2.7% for 380 nm and 2.3% for 500 nm (Figure 7), which are quite consistent with the percentage differences of AOD between Cimel and PFR for an effective radius of 1.5 µm (Figures 8a and 8b). These percentages correspond to absolute AOD differences of 0.016 at 380 nm, and 0.011 at 500 nm for AOD=0.5 (Figures 8c and 8d), that are of sufficient magnitude to cause an appreciable number of 1-minute AOD data outside the U95 limits, as indicated in Table 10.

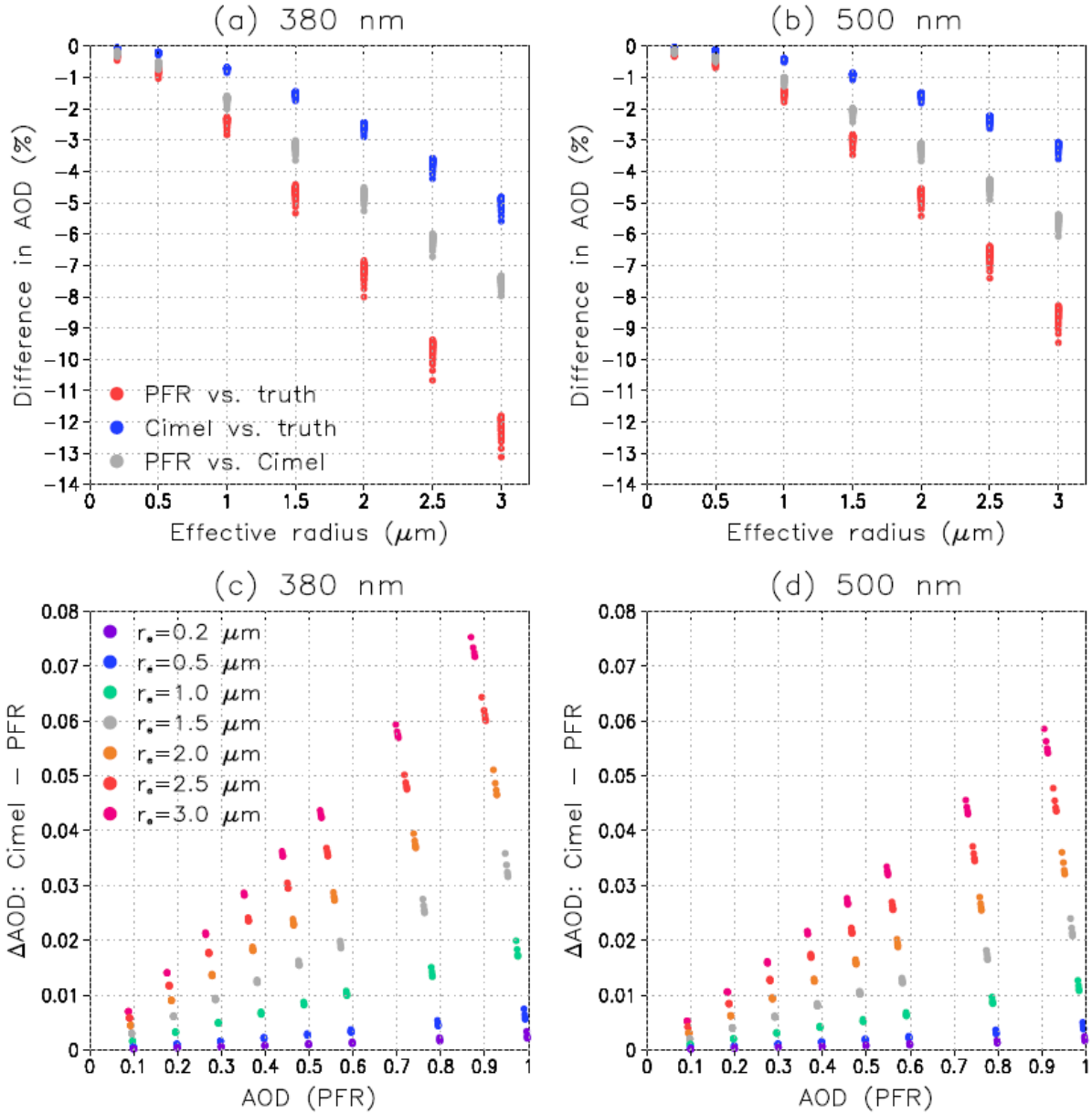

Figure 8. Panels a) and b): the simulated relative differences in retrieved AOD (in %) that would result from the scattered radiation within the FOV of the P~~R~~FR and Cimel instruments. The red (blue) dots show the differences between the AOD that would be retrieved using P~~R~~FR (Cimel) and the actual AOD, and the grey dots the difference between P~~R~~FR and Cimel, at wavelengths (a) 380 nm and (b) 500 nm. Panels c) and d): the difference in retrieved AOD between P~~R~~FR and Cimel~~IMEL~~, plotted as a function of the AOD retrieved with PFR, for seven values of aerosol effective radius between 0.2 and 3.0 μm, at (c) 380 nm and (d) 500 nm.

If we apply the corresponding corrections to the 1-minute AOD PFR data > 0.1 assuming an effective radius of 1.5μm, + 3.3% at 380nm and + 2.2.% at 500 nm, it turns out that the slopes of the fitting lines of the Cimel~~IMEL~~-PFR AOD differences vs. PFR AOD ~~they~~ become practically zero (Figure 9). Moreover, the number of AOD data outside the U95 limits is reduced by approximately 53% for 380 nm and by 13% for 500 nm. It must be taken into account that the percentage of AOD data for AOD> 0.1 outside the U95 limits, before the corrections, is only 8% at 500 nm, while at 380 nm it is a significant value (24%).

5

This~~e~~ AOD "correction" reduces the Cimel-PFR AOD differences substantially but does not eliminate them completely~~is fairly good but it is not complet~~, ~~e~~ mainly for two reasons. The first one ~~it~~ is the inherent limitation of data correction using the percentage difference in AOD obtained by model simulation for a fixed effective radius.

We have assumed an effective radius of 1.5 μm but, in reality, the radius of dust particles varies. A reasonable range of dust particle radius~~size~~ is between 0.1 and 3 μm (Balkanski et al., 1996; Denjean et al., 2016; Mahowald et al., 2014). So, depending on the distance from the dust source to ~~Izaña Observatory~~IZO and the size of the emitted dust, the effective radius could vary slightly between dust episodes. As can be seen in Figures 8a and 8b, the percentage differences in AOD between Cimel and PFR for a 1-2~~[1,2 μum]~~ effective radius interval, the PFR-Cimel AOD relative difference at 380 nm (500 nm) might change between ~~(around)~~ ~-1.8% (-1.1%) to -4.9% (3.3%).

The second reason is a possible cloud contamination in AOD retrieval when altostratus are present above the SAL, as discussed in Section 5.3.4.

A similar analysis has been carried out for AERONET V3 (see Supplement S17), where we observe that the corrections obtained are not as good as those obtained for V2. This may be due to the very high AOD data retention in V3 which could include more cases in which altostratus clouds and dust are present. The effect of FOV on AOD retrieval should be taken into account for those radiometers with a relatively high FOV (>3°) measuring in regions with relatively high AOD (> 0.2) for most of the year, as is the case in many sites of Northern Africa, the Middle East and East Asia (Basart et al., 2009; Cuevas et al., 2015; Eck et al., 1999; Kim et al., 2007). This effect leads to AOD underestimation, and the variable number of high AOD episodes in each season of the year might affect the AOD long-term trends. AOD measurements under these conditions would be especially affected for optical air mass < 3.

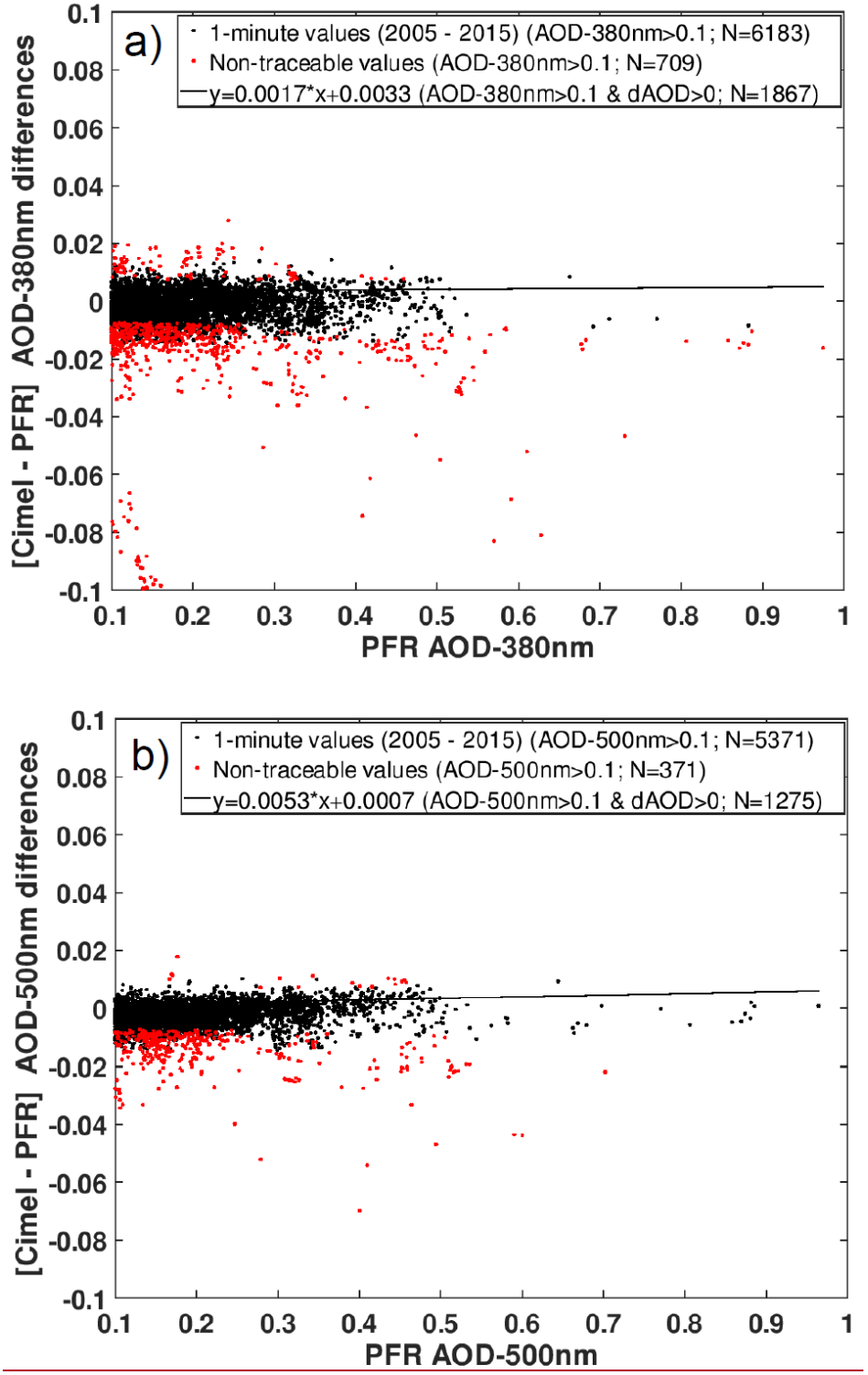

Figure 9. The same as Figure 7 after "correcting" the PFR AOD data by adding + 3.3% at 380nm and + 2.2.% at 500 nm to the 1-minute PFR AOD data > 0.1.

~~Furthermore, it should be taken into account that, as discussed in section 5.2.2., under relatively high AOD conditions, the presence of altostratus above SAL is not infrequent, and they could also cause non-traceability in AOD when the cloud screening algorithms~~

fail. Note that a graphic equivalent to Figure 9 is shown in Supplement S17 but for AERONET V3, observing that the corrections obtained are not as good as those obtained for V2. This may be due to the very high AOD data retention in V3 which could include more cases in which altostratus clouds and dust are present. Therefore, the FOV study should be done once the dust events with presence of clouds over the SAL have been ruled out.

The effect of FOV on AOD retrieval should be taken into account for those radiometers with a relatively high FOV (>3°) measuring in regions with relatively high AOD (> 0.2) for most of the year (Basart et al., 2009; Cuevas et al., 2015; Eck et al., 1999; Kim et al., 2007), as is the case in many places sites of Northern Africa, the Middle East and East Asia (Basart et al., 2009; Cuevas et al., 2015; Eck et al., 1999; Kim et al., 2007). This effect could leads to AOD underestimation, and the variable number of high AOD episodes in each season of the year might affect the AOD long-term trends. AOD measurements under these conditions would be especially affected for optical air mass < 3.

5.5.4 *Angström exponent comparison*

We have performed a compari comparison of the AE provided by GAW-PFR and AERONET-Cimel using in both cases the AOD data obtained from the four common channels (380 nm, 440 nm, 500 nm and 870 nm) with a total of 70716 data-pairs. The PFR-AOD values have been ordered from lowest to highest by grouping them in intervals of 500 values for which the averages (and corresponding standard deviations) of the PFR-Cimel AE differences have been calculated (to produce Figure 10a). In a similar way we proceeded with the PFR-AE values (Figure 10b).

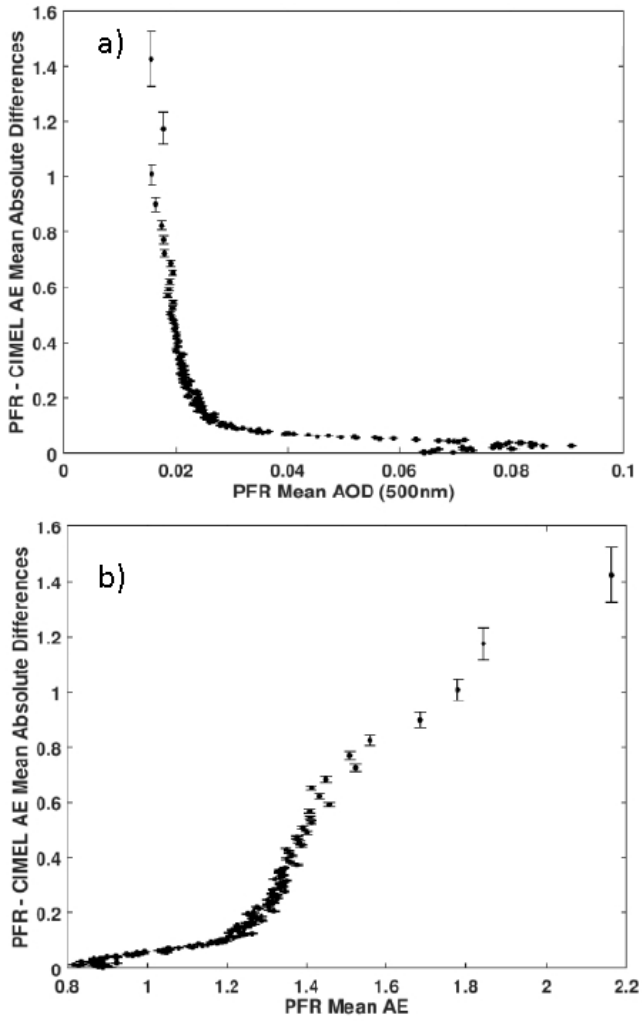

Figure 10. (a) PFR-Cimel AE mean absolute differences (and corresponding standard deviations) vs PFR mean AOD_{500nm} in 500 data intervals (b) and vs PFR mean AE in 500 data intervals. AE has been computed for both PFR and Cimel using the four common channels (380, 440, 500 and 870nm).

AE differences > 0.2 increase exponentially for AOD < 0.02, reaching AE differences of up to 1.6 under pristine conditions (Figure 109a). For very low AOD the provided instruments uncertainty is the source of the sharp increase in AE, and at the same time AE becomes very sensitive to slight AOD changes. However, for AOD < 0.02 the atmospheric aerosol load is practically zero and so, its characterization with AE have in practice relatively minor importance~~, in practice~~.

In addition, the AE differences remain ≤~~below~~ 0.1 when AE_{PFR} values are ≤~~below~~ 1 (Figure 109b), which shows that these differences are small in most of the possible atmospheric scenarios. For 1 < AE_{PFR} < 1.2 the AE differences increase slightly to values ≤~~below~~ 0.2, and for AE_{PFR} > 1.2 (very fine particles or pristine conditions) the AE differences increase sharply to reach values of ~~around~~ 1.2. In our case, the non-pristine conditions, or those with a high content of mineral dust, have associated AOD > 0.03 and AE < 1, where the AE differences remain ≤~~below~~ 0.1. In case of pristine conditions AOD ≤ 0.03 and AE ≥ 1 the AE differences can reach a maximum of 1.6.

Wagner and Silva (2008) estimated the usual maximum AE error by error propagation using a pair of spectral channels in which AOD is measured. Their results show that for clean optical conditions (AOD_{440nm}= 0.06) the maximum AE error is 1.17, and for hazy conditions (AOD_{440nm}=0.17) the error is 0.17, assuming an underlying AE of 1.5. These values decrease~~rop down~~ to 0.73 and 0.11, respectively, if AE=0. The AE differences found between GAW-PFR and AERONET-Cimel lie within the estimated errors reported by Wagner and Silva (2008).

~~Table 10~~*Table 11*. *Uncertainty in AE determination for three typical atmospheric situations.*

	Uncertainty in AE
Normal pristine conditions AOD_{500nm}= 0.03 and AE = 1.4	≥ 1
Hazy conditions AOD_{500nm}= 0.14 and AE = 1.15	≥ 0.2
Strong dust intrusion AOD_{500nm}= 0.3 and AE = 0.3	~ 0

In any case, as in our study the AE has been determined from AOD measured in the four common channels of GAW-PFR and AERONET-Cimel, we ~~have made an~~ estimated ~~of~~ the uncertainty in the calculation of the AE for three typical aerosol scenarios ~~that are typically recorded~~ at Izaña. F~~f~~ollowing ~~the~~ the methodology shown by Wagner and Silva (2008), ~~methodology but including the AOD uncertainty related with each of the two instruments and for different conditions. T~~the AE uncertainty~~s~~e estimations have been calculated using AOD measurements at four wavelengths and AOD uncertainty error propagation ~~following the Wagner and Silva (2008) methodology but including the AOD uncertainty related with each of the two instruments and for different conditions. The uncertainty estimations are shown in Table 10~~(Table 11). The AE derived from more than 2 wavelengths is less affected by AOD ~~inaccuracies~~ uncertainties than AE calculated with pairs of wavelengths, since the latter are calculated from the ratio of AOD at two channels (Cachorro et al., 2008).

The AE differences of our study (Figure 10~~9~~) are within the AE uncertainty estimated for each type of atmospheric condition (pristine, hazy and heavily dust loaded).

However, although AE is a quantitative parameter, it is only used in a qualitative way to estimate the range of sizes (fine, medium, coarse) of the predominant aerosol in the inevitable mixture of aerosols that we observe. With this parameter, and together with the information that is available in the measurement

site about the most frequent types of aerosols and their concentration, we can estimate the type of aerosols that are being measured.

There are many publications with different thresholds of AE and AOD in order to classify different types of aerosols (e.g. Basart et al., 2009; Cuevas et al., 2015; Dubovik et al., 2002; Guirado et al., 2014; Holben et al., 2001; Kim et al., 2007; Todd et al., 2007; Toledano et al., 2007; Wang et al., 2004). However, there is no consensus on these thresholds since at each site there are different mixtures of aerosols, and each type of aerosol shows specific frequencies of appearance and different concentrations.

~~Taking into account all of the above, an~~An alternative way of analyzing the degree of agreement in AE between GAW-PFR and AERONET-Cimel is to verify to what extent both networks provide the same information regarding the type of aerosol they observe in a certain site.

Considering the AE criteria established by Cuevas et al. (2015) and Berjón et al. (2019), ~~As an example, and according to the studies referenced above,~~ we have ~~established~~ identified the following ~~three~~ four main ~~classes~~ categories according to ~~of aerosol scenarios present in most of the situations at the Izaña Observatory based on~~ the AE_{PFR} and AE_{Cimel} values~~AE value~~:

1. AE_{PFR} & AE_{Cimel} > 0.6~~7~~: Pristine conditions.
2. 0.25~~3~~ < AE_{PFR} & AE_{Cimel} ≤ 0.6~~7~~: Hazy, ~~being~~ mineral dust being the main aerosol component.
3. ~~3.~~ AE_{PFR} & AE_{Cimel} ≤ 0.25~~3~~: Pure dust.

AE_{PFR} and AE_{Cimel} do not fit any of the previous categories.

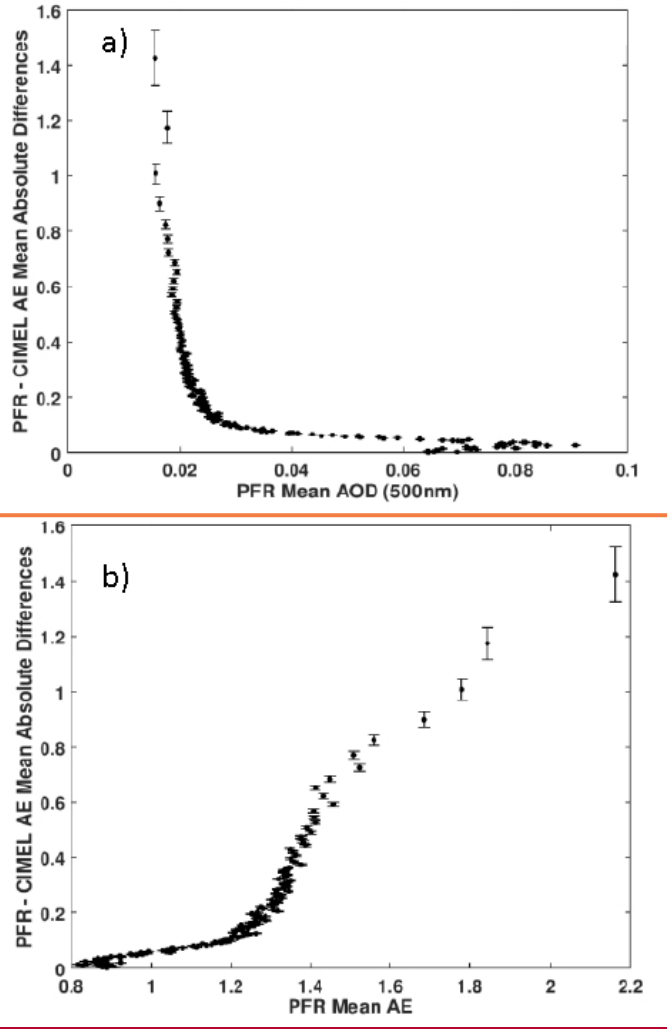

5

Figure 109. (a) PFR-Cimel AE mean absolute differences (and corresponding standard deviations) vs PFR mean AOD_{500nm} in 500 data intervals (b) and vs PFR mean AE in 500 data intervals. AE has been computed for both PFR and Cimel using the four common channels (380, 440, 500 and 870nm).

4.

In 94.93.8 % of the casescases, GAW-PFR and AERONET-Cimel V2 match the AE intervals of each aerosol scenario. Similar results (93.4%) were obtained when comparing with AERONET V3. Most of the agreement (>80 79 %) occurs in the predominant scenario of pristine conditions despite the AE uncertainty under pristine conditions being ≥ 1. See Supplement S18 for more details. Notice that given the special characteristics of the Izaña Observatory, and according to Cuevas et al. (2015) and Berjón et al. (2019), AE is a self-sufficient parameter to define different types of aerosol scenarios without the need to combine its information with AOD.

6. Summary and Conclusions

In this study, a long-term comparison of synchronous 1-minute AOD data from GAW-PFR and AERONET-Cimel was carried out in four wavelengths (380, 440, 500 and 870 nm) for an 11 year period (2005-2015).

While GAW-PFR is the WMO--defined global AOD reference globally, being directly linked to WMO / CIMO, and was specifically designed to detect long-term AOD trends, AERONET-Cimel is the densest AOD measurement network globally, and the network most frequently used for aerosol characterization and for model and satellite observation evaluation. However, these networks use radiometers that have important technical differences, and very different calibration and evaluation methodologies, and their calibration systems are completely independent of one another.

AnMoreover, the AERONET-Cimel 11-year AOD data series at Izaña ObservatoryIZO was obtained using a large number of radiometers. A total of 13 Rreference instruments were used (Masters) in the period 2005-2009, which means that every 4 and a half months, approximately, an instrument was replaced by another one to be calibrated. Their calibrations were performed during their respective measurement time periods at Izaña ObservatoryIZO. Therefore, these calibrations were not in any way linked with those of the instruments that preceded or replaced them, nor with GAW-PFR reference. This fact introduced some concern These facts led us to investigateabout the homogeneity of the AERONET-Cimel AOD data series and their intercomparability with the much more homogeneous AOD data series from GAW-PFR (3 instruments in 11 years).

The objective of this study is to assess whether, despite the marked differences between both networks, and the different day to day maintenance and operation procedures of the respective instruments during the study period, it is possible to consider that the information provided in the long term by the two networks

~~is comparable and consistent.~~ The traceability concept for AOD suggested by WMO consists in determining whether the AOD difference of the AERONET CIMELs vs the GAW PFRs lie within the U95~~specific~~ limits.

We have used uncertainty limits for AOD traceability established by WMO (2005) for these~~is~~ type of instruments with finite FOV. The acceptable traceability is when 95 % of the absolute AOD differences lie within these limits, in which case both data populations are considered equivalent. It should be clarified that "traceability" is not used in a strict metrological sense.

This study has addressed the comparison of the GAW-PFR dataset ~~base~~ with the two versions of AERONET (V2 and V3) in the period 2005-2015. An excellent agreement between V2 and V3 for the four ~~analyzed~~analysed channels ($R^2 > 0.999$) has been obtained.

More than 70000 synchronous GAW-PFR (PFR) and AERONET-Cimel (Cimel) 1-~~-~~minute data-pairs in each channel in the period 2005-2015 were analysed. An excellent traceability of AOD from the AERONET-Cimel (V2 and V3) is found for 440 nm, 500 nm and 870 nm, and fairly good results for 380 nm~~in the four channels~~. The lowest percentage of traceable AOD data is registered in 380 nm with 92.7 % of the 1-minute data within the WMO limits, and the highest in 870 nm with 98.0 % of the data. ~~The percentage of traceable data-pairs~~

The different possible causes of non-traceability in AOD ~~Trying to identify the reasons of the AOD data outside the WMO limits we have~~were investigated as follows:

- Absolute AOD measurements synchronization.

  Analyzing 1-minute AOD variability we concluded that its impact on the AOD differences is negligible as only ~0.8% of the AOD data has a variability larger than 0.005 in all spectral ranges.

- ~~-~~Sun tracking misalignments.

~~The 1-minute AOD differences Mean Bias of this study is 0.001, an order of magnitude lower than those obtained from previous short-term PFR-Cimel comparison campaigns, in which the Cimel instruments were calibrated by transferring the calibration coefficients by comparison with co-located Master instruments. This indicates the importance of good calibration and maintenance of the Cimel instruments to obtain AOD data very similar to that of GAW-PFR.~~

~~In this study, since the AERONET-Cimel radiometers were calibrated using the Langley plot technique at the Izaña Observatory, and the calibrations of the GAW-PFRs are directly traceable to the WMO-GAW reference, being double-checked by Langley plot calibrations at Izaña, we have the best possible calibrations in the instruments used by both networks.~~

~~The results confirm that the AOD data outside the *U*95 limits due to calibration related errors is quite small and not observable for 440, 500 and 870 nm since AOD non-traceability is < 2.1 % for pristine conditions ($AOD_{500nm} \leq 0.03$) in these channels. In addition, no dependence of the 1-minute AOD differences with the air optical mass is observed. However, for 380 nm the percentage of non-traceable values increases up to~~

5

~~5.5 % for 1 ≤ m < 2, being the most likely cause an insufficient 10 accurate calibration of AERONET-Cimel in this channel.~~

~~Small misalignments in the sun-pointing~~Sun tracking misalignments ~~It~~ constitute~~s~~ a serious problem and a major cause of non-traceability of AOD data-pairs as demonstrated by the AOD data outside the U95 limits from the period 2005-200910~~10~~ as a consequence of episodic problems with the sun-tracker of the GAW-PFR radiometer. For the 2010-2015 period the percentage of traceable data-pairs improves to 93.5% (380 nm), 97.4% (440 nm), 97.2% (500 nm) and 99.1% (870 nm). However, most of these cases could be identified and excluded from the analysis.

- Cloud screening failure by both network algorithms.

~~Regarding AOD non-traceability due to the different cloud-screening algorithms of both networks, it must be said that both algorithms are very similar. GAW-PFR uses the same cloud screening as AERONET-Cimel but incorporates some additional controls. The only reason for AOD non-traceability comes from the simultaneous failure of both cloud screening algorithms because if one or both of them detect clouds, the data will not be part of the comparison.~~ According to our observations, the simultaneous failure of both cloud screening algorithms might occur only under the presence of large and stable cirrus, or altostratus (~ 6000 m a.s.l.) on the top of a heavily dust loaded Saharan air layer, hiding very wide and stable clouds. In these ~~cases~~cases, the radiometers interpret these clouds as aerosol layers~~s~~ and might provide values very different ~~values of what is~~from the real AOD~~really cloud optical depth~~. F~~This effect, f~~or the comparison at IZO, however, this effect is negligible ~~as such cases represent only a small number of comparison data.~~since GAW-PFR and AERONET-Cimel cloud screening algorithms provide successful cloud identification on clear direct-sun conditions during cloudy skies (FCS < 40 %) for 99.75 % of the cases.

- Pressure measurements related errors.

~~According to our analysis, only dramatic barometer malfunctioning of one of the instruments could cause significant differences in the Rayleigh scattering contribution to total optical depth, and hence AOD non-traceability.~~ Since the accuracy of the new barometers built into new radiometers is about 3 hPa, and only errors in atmospheric pressure > 30 hPa might produce an impact on Rayleigh scattering, the AOD non-traceability due to errors in Rayleigh scattering is negligible. ~~The impact of barometer malfunctioning is well detected because it leads to wavelength-dependent AOD errors and to large errors in Ångström exponent.~~

- Total column ozone input uncertainty.

The largest influence of total ozone data uncertainty o~~i~~n ozone absorption occurs mainly at 500 nm. Total ozone needs to be determined to ±30 DU or 10 % of typical values, to ensure an uncertainty of ±0.001 ozone absorption at 500 nm. In the case of the GAW-PFR / AERONET-Cimel comparison, despite the very different methods in which both networks obtained O_3 values for their corresponding corrections, large ozone differences were found (> 40 DU) only on 2.4 % of the days ~~(1761 out of 71965 data)~~, resulting in a

difference in the ozone optical depth slightly above ~0.001. ~~Even so, t~~The potential contribution to non-traceable AOD values between the two networks is negligible. However, in mid or high latitude stations where fast O_3 variations of several tens of DU might be registered, the correction of 1-minute AOD measurements by ozone absorption might be an issue to be considered.

- Total column NO_2 input uncertainty.

The differences in NO_2 absorption caused by differences in daily total NO_2 between GAW-PFR and AERONET-Cimel is of the order of 10^{-3} for 380 nm and 440 nm channels, while, for 500 nm channel, it is even lower, of the order of 10^{-4}. So, differences in NO_2 absorption are negligible in the 1-minute AOD non-traceability of our study. However, NO_2 absorption might have some impact o~~i~~n AOD in highly polluted regions, such as in large industrial cities, where column NO_2 values are much larger than the climatological ones.

Taking into account the corrections for Rayleigh scattering and for the absorptions by O_3 and NO_2, we have calculated the combined effect of all of them on the non-traceability of the 1-minute AOD values. The highest impact occurs in the 380 nm channel, in which 25 % of the AOD data outside the *U*95 limits (~2% of the total compared data) are due to significant differences in pressure, and in O_3 and NO_2 absorption. ~~Most of the AOD data outside the *U*95 limits that becomes traceable data after corrections are applied had errors in the pressure measurement and therefore in the Rayleigh scattering correction.~~ The 1-minute AOD data outside the *U*95 limits by these corrections is negligible in the 870 nm channel. ~~This suggests that, probably, CIMO traceability limits shouted redefined as a function of wavelength.~~

~~We have to note that the excellent results of this 11 year comparison and the small differences found under the strict *U*95 criterion cannot be linked with the relatively low AODs that can be found at IZO. This is because absolute calibration errors contribute to the AOD calculation in an absolute way so larger than 1 % calibration errors for a given period of time can lead to even negative AOD calculations for IZO site.~~

- Impact of dust forward scattering in AOD retrieval uncertainty for different instrument FOVs

~~The AOD differences between AERONET-Cimel and GAW-PFR versus AOD (GAW-PFR) show a positive slope that increases when the AOD fitted data are > 0.05. Therefore, as AOD increases the AOD differences increase, noting that AERONET-Cimel shows AOD values higher than GAW-PFR.~~ Since GAW-PFR has almost double the FOV (~2.5°) compared to the AERONET-Cimel (~~1.2~~1.3°), and direct solar irradiance measurements are biased by the amount of aureole radiation that is assumed to be direct solar radiation, it is reasonable to expect that GAW-PFR is more affected by the circumsolar irradiance than AERONET-Cimel radiometer when AOD is relatively high. ~~However, we have to bear in mind that WMO defines the PFR FOV as the recommended one for sun radiometers.~~ Modelling the dust forward scattering we have shown ~~We have explained part of the non-traceabilities found for relatively high AOD values, by analysing the relationship between the differences in circumsolar radiation measured by both instruments with the differences observed in AOD. We have observed a clear relationship between the Cimel-PFR AOD differences and the PFR-Cimel circumsolar radiation differences, with the slope of the fitted line greater for shorter wavelengths (380 nm). These results show~~ that a non-negligible percentage of

the non-traceable 1-minute AOD data for AOD > 0.1, ranging from ~0.3 % at 870 nm to ~1.9 % at 380 nm is, might be caused by the different FOV. This systematic error especially affects the shorter wavelengths. . Due to this effect, the GAW-PFR provides AOD values which are ~3% lower at 380 nm, and ~2% lower at 500 nm, compared with AERONET-Cimel. However, AOD underestimation This error couldan only have only some relevance be especially important in dusty regions if radiometers with relatively large FOV are used.

A comparison of the AE provided by GAW-PFR and AERONET-Cimel has been performed using in both cases AOD data obtained from the four nearby common channels with a total of 70716 data-pairs. This is a very strict AE calculation since it is necessary that AOD be accurately measured by the four channels simultaneously. AE differences > 0.2 increase exponentially under very pristine conditions (AOD ≤ 0.03 and AE ≥ 1), reaching AE differences of up to 1.6. However, for these conditions the atmospheric aerosol load is practically zero and so, its characterization with AE does not have any importance in practice. Under non-pristine conditions or those with a high mineral dust content (associated AOD > 0.03 and AE < 1), the AE differences remain <below 0.1.

Summarizing, we have presented for the first time a long- -term (2005-2015) 1-minute AOD comparison among different types of radiometers belonging to different aerosol global networks. This comparison is a very demanding test of both GAW-PFR and AERONET-Cimel validated AOD datasets bases since aerosol scenarios correspond to extreme conditions: either very low aerosol loading, a "pristine" scenario that reveals small uncertainties in the calibration and in the cloud screening, or large dust load, which leads to a significant increase in the forward scattering aerosol with AOD, resulting in a slightly higher AOD underestimation by the GAW-PFR. From this comprehensive comparisoncomparison, analysis of the 1-minute AOD and AE data provided by the GAW-PFR and AERONET-Cimel instruments operating at the Izaña Observatory in the 2005-2015 period, we can conclude that the biases in the statistics are very small (< 0.003 in all channels) and therefore both AOD datasets bases are representative of the same AOD population, which it is a remarkable fact for the global aerosol community. It should be noted that AOD traceability at 380 nm (92.7 %) does not reach 95 % of the common data, the percentage recommended by WMO U95 criterion, so more efforts should be made to improve AOD in the UV range. In this study we have also focused much of our attention on investigated the data that are outside of the WMO U95 limits (<5% of the data at 440, 500 and 870 nm and <8% at 380nm) in order to understandknow the weak points of both GAW-PFR and AERONET-Cimel their causes and to be eventually able to correct the small inconsistencies detected in instrumental and methodological aspects in the future.

Our results suggest that, probably, WMO/CIMO traceability limits could be redefined as a function of wavelength, and the recommended radiometer FOV range of radiometers FOVs should be reconsidered.

The widely deployed AERONET-Cimel and GAW-PFR datasets play a crucial role in understanding AOD long-term AOD changes and detecting trends, so it would be desirable for both networks to be linked to the same GAW-WMO related reference. In this sense, these results will be used in future studies, not only to evaluate long-term AOD trends at Izaña Observatory based on two independent instruments, but

~~also to provide additional insight on long-term AOD trend analysis, and its significance and validity, based on single instruments and their calibration and AOD processing procedure and uncertainty budget. Finally, special attention should be paid to the AERONET-Cimel AOD data series used in trend detection in combination with the used data set homogeneity and their periodic calibration transfer from Master instruments.~~

Competing interests. The authors declare that they have no conflict of interest.

Acknowledgements. The authors thank Luc Blarel and Philippe Goloub (LOA, CNRS-University of Lille, France) for supervising the periodic calibrations of the Cimel ~~Masters~~Reference instruments. This study has been performed in the frame of the WMO CIMO Izaña Testbed for Aerosols and Water Vapour Remote Sensing Instruments. The work was supported by the project "The Global Atmosphere Watch Precision Filter Radiometer (GAW-PFR) Network for Aerosol Optical Depth long term measurements" funded by the Federal Office of Meteorology and Climatology MeteoSwiss International Affairs Division, Swiss GCOS Office. Part of the AERONET-Cimel radiometers have been calibrated at Izaña Observatory by AERONET- EUROPE Calibration Service, financed by the European Community specific programs for Integrating Activities: Research Infrastructure Action under the Seventh Framework Programme (FP7/2007-2013), ACTRIS grant agreement No. 262254, and Horizon 2020 Research and Innovation Program, ACTRIS-2 grant agreement No. 654109. This research has received funding from the European Union's Horizon 2020 Research and Innovation Programme under grant agreement No. 654109 (ACTRIS-2).The funding by MINECO (CTM2015-66742-R) and Junta de Castilla y León (VA100P17) is also gratefully acknowledged. We thank the staff of the Izaña O~~o~~bservatory for their effort and dedication in maintaining the instruments. We acknowledge the constructive comments of the anonymous referees. Our colleague Celia Milford has improved the English language of the paper. In memory of Prof Klaus Fröhlich, former director of PMOD-WRC, who initiated the AOD measurements programme at the Izaña Observatory in 1984 within the WMO Background Atmospheric Pollution Monitoring Network (BAPMoN).

~~References~~References

Amiridis, V., Marinou, E., ***Tsekeri***, A., Wandinger, U., Schwarz, A., Giannakaki, E., Mamouri, R., Kokkalis, P., Binietoglou, I., Solomos, S., Herekakis, T., Kazadzis, S., Gerasopoulos, E., Proestakis, E., Kottas, M., Balis, D., Papayannis, A., Kontoes, C., Kourtidis, K., Papagiannopoulos, N., Mona, L., Pappalardo, G., Le Rille, O., and Ansmann, A.: LIVAS: a 3-D multi-wavelength aerosol/cloud database based on CALIPSO and EARLINET, Atmos. Chem. Phys., 15, 7127-7153, https://doi.org/10.5194/acp-15-7127-2015, 2015.

Angstrom, A.: On the atmospheric transmission of sun radiation and on dust in the air, Geografiska Annaler, 11, 156–166, 1929.

Balkanski, Y., Schulz, M., Marticorena, B., Bergametti, G.,Guelle, W., Dulac, F., Moulin, C.,and Lambert, C.E.: Importance of the source term and of the size distribution to model the mineral dust cycle, in The Impact of Desert Dust Across the Mediterranean, edited by S. Guerzoni and R. Chester, pp. 69–76, Kluwer Academic Pub., Boston, MA. 2, 9, 2, 1996.

Barker, H. W.: Solar radiative transfer through clouds possessing isotropic variable extinction coefficient, Quart. J. Roy. Meteor. Soc., 118, 1145-1162, doi: 10.1002/qj.49711850807, 1992.

Barker, H. W.: Estimating cloud field albedo using one-dimensional series of optical depth, J. Atmos. Sci., 53, 2826-2837, doi: 10.1175/1520-0469(1996)053<2826:ECFAUO>2.0.CO;2}, 1996.

Barreto, A., Cuevas, E., Pallé, P., Romero, P. M., Guirado, C., Wehrli, C. J., and Almansa, F.: Recovering long-term aerosol optical depth series (1976-2012) from an astronomical potassium-based resonance scattering spectrometer, Atmospheric Measurement Techniques, 7, 5 4103–4116, https://doi.org/10.5194/amt-7-4103-2014, 2014.

Barreto, A., Cuevas, E., Granados-Muñoz, M.-J., Alados-Arboledas, L., Romero, P. M., Gröbner, J., Kouremeti, N., Almansa, A. F., Stone, T., Toledano, C., Román, R., Sorokin, M., Holben, B., Canini, M., and Yela, M.: The new sun-sky-lunar Cimel CE318-T multiband photometer a comprehensive performance evaluation, Atmospheric Measurement Techniques, 9, 631–654, https://doi.org/10.5194/amt-9-63110 2016, https://www.atmos-meas-tech.net/9/631/2016/, 2016.

Basart, S., Pérez, C., Cuevas, E., Baldasano, J. M., and Gobbi, G. P.: Aerosol characterization in Northern Africa, Northeastern Atlantic, Mediterranean Basin and Middle East from direct-sun AERONET observations, Atmospheric Chemistry and Physics, 9, 8265–8282, https://doi.org/10.5194/acp-9-8265-2009, https://www.atmos-chem-phys.net/9/8265/2009/, 2009.

Basart, S., Pérez, C., Nickovic, S., Cuevas, E., and Baldasano, J.: Development and evaluation of the BSC-DREAM8b dust regional model over Northern Africa, the Mediterranean and the Middle East, Tellus B: Chemical and Physical Meteorology, 64, 18539, https://doi.org/10.3402/tellusb.v64i0.18539, 2012.

Benedetti, A., Reid, J. S., Knippertz, P., Marsham, J. H., Di Giuseppe, F., Rémy, S., Basart, S., Boucher, O., Brooks, I. M., Menut, L., Mona, L., Laj, P., Pappalardo, G., Wiedensohler, A., Baklanov, A., Brooks, M., Colarco, P. R., Cuevas, E., da Silva, A., Escribano, J., Flemming,

J., Huneeus, N., Jorba, O., Kazadzis, S., Kinne, S., Popp, T., Quinn, P. K., Sekiyama, T. T., Tanaka, T., and Terradellas, E.: Status and future of numerical atmospheric aerosol prediction with a focus on data

requirements, Atmospheric Chemistry and Physics, 18, 10615–10643, https://doi.org/10.5194/acp-18-10615-2018, https://www.atmos-chem-phys.net/18/10615/2018/, 2018.

Berjón, A., Barreto, A., Hernández, Y., Yela, M., Toledano, C., and Cuevas, E.: A 10-year characterization of the Saharan Air Layer lidar ratio in the subtropical North Atlantic, Atmos. Chem. Phys. Discuss., https://doi.org/10.5194/acp-2018-1315, in review, 2019.

Blanc, P., Espinar, B., Geuder, N., Gueymard, C., R., M., Pitz-Paal, R., Reinhardt, B., Renné, D., M., S., Wald, L., and Wilbert, S.: Direct normal irradiance related definitions and applications: The circumsolar issue, Solar Energy, 110, 561 – 577, https://doi.org/https://doi.org/10.1016/j.solener.2014.10.001, 2014.

Bodhaine, B. A., Wood, N. B., Dutton, E. G., and Slusser, J. R.: On Rayleigh optical depth calculations, Journal of Atmospheric and Oceanic Technology, 16, 1854–1861, 1999.

Böhm-Vitense, E.: Introduction to stellar astrophysics, volume 2: stellar atmospheres, Cambridge University Press, 260 pp., 1989.

Bokoye, A. I., Royer, A., O'Neill, N. T., Cliche, P., Fedosejevs, G., Teillet, P. M., and McArthur, L. J. B.: Characterization of atmospheric aerosols across Canada from a ground-based sunphotometer network: AEROCAN, Atmosphere-Ocean, 39, 429–456, https://doi.org/10.1080/07055900.2001.9649687, 2001.

Cachorro, V., Toledano, C., Sorribas, M., Berjón, A., De Frutos, A., and Laulainen, N.: An "in situ" calibration-correction procedure (KCICLO) based on AOD diurnal cycle: Comparative results between AERONET and reprocessed (KCICLO method) AOD-alpha data series at El Arenosillo, Spain, Journal of Geophysical Research: Atmospheres, 113, https://doi.org/https://doi.org/10.1029/2007JD009001, 2008.

Cachorro, V. E., Romero, P. M., Toledano, C., Cuevas, E., and de Frutos, A. M.: The fictitious diurnal cycle of aerosol optical depth: A new approach for "in situ" calibration and correction of AOD data series, Geophysical Research Letters, 31, https://doi.org/10.1029/2004GL019651, 2004.

Campanelli, M., Nakajima, T., and Olivieri, B., 2004: Determination of the solar calibration constant for a sun - sky radiometer: proposal of an in situ procedure. Appl. Opt., 43(1), 651-659.

Carlund, T., Kouremeti, N., Kazadzis, S., and Gröbner, J.: Aerosol optical depth determination in the UV using a four-channel precision filter radiometer, Atmos. Meas. Tech., 10, 905-923, https://doi.org/10.5194/amt-10-905-2017, 2017.

Carrillo, J., Guerra, J. C., and Cuevas, E.and Barrancos, J.: Characterization of the Marine Boundary Layer and the Trade-Wind Inversion over the Sub-tropical North Atlantic, Boundary-Layer Meteorology, 158, 311–330, https://doi.org/10.1007/s10546-015-0081-1, https://doi.org/10.1007/s10546-015-0081-1, 2016.

Chance, K. and Kurucz, R.: An improved high-resolution solar reference spectrum for earth's atmosphere measurements in the ultraviolet, visible, and near infrared, Journal of quantitative spectroscopy and radiative transfer, 111, 1289–1295, https://doi.org/https://doi.org/10.1016/j.jqsrt.2010.01.036, http://www.sciencedirect.com/science/article/pii/S0022407310000610, 2010.

Che, H., Zhang, X.-Y., Xia, X., Goloub, P., Holben, B., Zhao, H., Wang, Y., Zhang, X.-C., Wang, H., Blarel, L., Damiri, B., Zhang, R., Deng, X., Ma, Y., Wang, T., Geng, F., Qi, B., Zhu, J., Yu, J., Chen, Q., and Shi, G.: Ground-based aerosol climatology of China: aerosol optical depths from the China Aerosol Remote Sensing Network (CARSNET) 2002–2013, Atmos. Chem. Phys., 15, 7619–7652, https://doi.org/10.5194/acp15-7619-2015, 2015.

Chedin, A., Capelle, V., and Scott, N.: Detection of IASI dust AOD trends over Sahara: How many years of data required?, Atmospheric Research, 212, 120–129, https://doi.org/https://doi.org/10.1016/j.atmosres.2018.05.004, http://www.sciencedirect.com/science/article/pii/ S0169809517310566, 2018.

Chubarova, N. Y., Poliukhov, A. A., and Gorlova, I. D.: Long-term variability of aerosol optical thickness in Eastern Europe over 2001– 2014 according to the measurements at the Moscow MSU MO AERONET site with additional cloud and NO_2 correction, Atmospheric Measurement Techniques, 9, 313–334, https://doi.org/10.5194/amt-9-313-2016, https://www.atmos-meas-tech.net/9/313/2016/, 2016.

Cuevas, E., González, Y., Rodríguez, S., Guerra, J. C., Gómez-Peláez, A. J., Alonso-Pérez, S., Bustos, J., and Milford, C.: Assessment of atmospheric processes driving ozone variations in the subtropical North Atlantic free troposphere, Atmospheric Chemistry and Physics, 13, 1973–1998, https://doi.org/10.5194/acp-13-1973-2013, https://www.atmos-chem-phys.net/13/1973/2013/, 2013.

Cuevas, E., Camino, C., Benedetti, A., Basart, S., Terradellas, E., Baldasano, J. M., Morcrette, J. J., Marticorena, B., Goloub, P., Mortier, A., Berjón, A., Hernández, Y., Gil-Ojeda, M., and Schulz, M.: The MACC-II 2007-2008 reanalysis: atmospheric dust evaluation and characterization over northern Africa and the Middle East, Atmospheric Chemistry and Physics, 15, 3991–4024, https://doi.org/10.5194/acp-153991-2015, https://www.atmos-chem-phys.net/15/3991/2015/, 2015.

Cuevas, E., Gómez-Peláez, A., Rodríguez, S., Terradellas, E., Basart, S., García, R., García, O., and Alonso-Pérez, S.: The pulsating nature of large-scale Saharan dust transport as a result of interplays between mid-latitude Rossby waves and the North African Dipole Intensity, Atmospheric Environment, 167, 586–602, https://doi.org/https://doi.org/10.1016/j.atmosenv.2017.08.059, http://www.sciencedirect.com/ 20 science/article/pii/S1352231017305757, 2017a.

Cuevas, E., Milford, C., Bustos, J. J., del Campo-Hernández, García, O., D., G. R., Gómez-Peláez, Guirado-Fuentes, C., Marrero, C., Prats, N., Ramos, R., Redondas, A., Reyes, E., Rodríguez, S., Romero-Campos, P., Scheneider, M., Belmonte, J., Yela, M., Almansa, F., Barreto, A., López-Solano, C., Basart, S., Terradellas, E., Afonso, S., Bayo, C., Berjón, A., Bethencourt, J., Carreño, V., Castro, N. J.,

Cruz, A. M., Damas, M., De Ory-Ajamil, F., García, M. I., Gómez-Trueba, V., González, Y., Hernández, C., Hernández, Y., Hernández-Cruz, B., Jover, 25 M., León, S., López-Fernández, R., López-Solano, J., Rodríguez, E., Rodríguez-Franco, J., Rodríguez-Valido, M., Sálamo, C., Sanromá, E., Santana, D., Santo-Tomás, F., Sepúlveda, E., Sierra, M., and Sosa, E.: Izaña Atmospheric Research Center Activity Report 2015-2016, State Meteorological Agency (AEMET), 2017b.

Denjean, C., Cassola, F., Mazzino, A., Triquet, S., Chevaillier, S., Grand, N., Bourrianne, T., Momboisse, G., Sellegri, K., Schwarzenbock, A., Freney, E., Mallet, M., and Formenti, P.: Size distribution and optical properties of mineral dust aerosols transported in the western Mediterranean, Atmos. Chem. Phys., 16, 1081-1104, https://doi.org/10.5194/acp-16-1081-2016, 2016.

Driemel, A., Augustine, J., Behrens, K., Colle, S., Cox, C., Cuevas-Agulló, E., Denn, F. M., Duprat, T., Fukuda, M., Grobe, H., Haeffelin, M., Hodges, G., Hyett, N., Ijima, O., Kallis, A., Knap, W., Kustov, V., Long, C. N., Longenecker, D., Lupi, A., Maturilli, M., Mimouni, M.,

Ntsangwane, L., Ogihara, H., Olano, X., Olefs, M., Omori, M., Passamani, L., Pereira, E. B., Schmithüsen, H., Schumacher, S., Sieger, R., Tamlyn, J., Vogt, R., Vuilleumier, L., Xia, X., Ohmura, A., and König-Langlo, G.: Baseline Surface Radiation Network (BSRN): structure and data description (1992–2017), Earth System Science Data, 10, 1491–1501, https://doi.org/10.5194/essd-10-1491-2018, https://www.earth-syst-sci-data.net/10/1491/2018/, 2018.

Dubovik, O., Holben, B., Eck, T. F., Smirnov, A., Kaufman, Y. J., King, M. D., Tanré, D., and Slutsker, I.: Variability of absorption and optical properties of key aerosol types observed in worldwide locations, Journal of the atmospheric sciences, 59, 590–608, https://doi.org/https://doi.org/10.1175/1520-0469(2002)059<0590:VOAAOP>2.0.CO;2, 2002.

Eck, T., Holben, B., Reid, J., Dubovik, O., Smirnov, A., O'neill, N., Slutsker, I., and Kinne, S.: Wavelength dependence of the optical depth of biomass burning, urban, and desert dust aerosols, Journal of Geophysical Research: Atmospheres, 104, 31333–31349, https://doi.org/10.1029/1999JD900923, 1999.

Eissa, Y., Blanc, P., Wald, L., and Ghedira, H.: Can AERONET data be used to accurately model the monochromatic beam and circumsolar irradiances under cloud-free conditions in desert environment?, Atmospheric Measurement Techniques, 8, 5099–5112, https://doi.org/DOI = 10.5194/amt-8-5099-2015, 2015.

Eissa, Y., Blanc, P., Ghedira, H., Oumbe, A., and Wald, L.: A fast and simple model to estimate the contribution of the circumsolar irradiance to measured broadband beam irradiance under cloud-free conditions in desert environment, Solar Energy, 163, 497–509,

https://doi.org/https://doi.org/10.1016/j.solener.2018.02.015, 2018.

Eskes, H. J. and Boersma, K. F.: Averaging kernels for DOAS total-column satellite retrievals, Atmospheric Chemistry and Physics, 3, 1285–1291, https://doi.org/10.5194/acp-3-1285-2003, -https://www.atmos-chem-phys.net/3/1285/2003/, 2003.

Freidenreich, S. M., and Ramaswamy, V.: A new multiple-band solar radiative parameterization for general circulation models, J. Geophys. Res., 104, 31389-31409, doi: 10.1029/1999JD900456, 1999.

García, R. D., Cuevas, E., García, O. E., Cachorro, V. E., Pallé, P., Bustos, J. J., Romero-Campos, P. M., and de Frutos, A. M.: Reconstruction of global solar radiation time series from 1933 to 2013 at the Izaña Atmospheric Observatory, Atmospheric Measurement Techniques, 7, 3139–3150, https://doi.org/10.5194/amt-7-3139-2014, https://www.atmos-meas-tech.net/7/3139/2014/, 2014.

García, R. D., Barreto, A., Cuevas, E., Gröbner, J., García, O. E., Gómez-Peláez, A., Romero-Campos, P. M., Redondas, A., Cachorro, V. E., and Ramos, R.: Comparison of observed and modeled cloud-free longwave downward radiation (2010–2016) at the high mountain BSRN Izaña station, Geoscientific Model Development, 11, 2139–2152, https://doi.org/10.5194/gmd-11-2139-2018, https://www.geosci-model-dev.net/11/2139/2018/, 2018.

García, R. D., Cuevas, E., Ramos, R., Cachorro, V. E., Redondas, A., and Moreno-Ruiz, J. A.: Description of the Baseline Surface Radiation Network (BSRN) station at the Izaña Observatory (2009–2017): measurements and quality control/assurance procedures, Geosci. Instrum. Method. Data Syst., 8, 77-96, https://doi.org/10.5194/gi-8-77-2019, 2019.

~~Ge, J., Su, J., Fu, Q., Ackerman, T., and Huang, J.: Dust aerosol forward scattering effects on ground-based aerosol optical depth retrievals, Journal of Quantitative Spectroscopy and Radiative Transfer, 112, 310–319, https://doi.org/https://doi.org/10.1016/j.jqsrt.2010.07.006, 2011.~~

~~Giles, D. M., Sinyuk, A., Sorokin, M. S., Schafer, J. S., Smirnov, A., Slutsker, I., Eck, T. F., Holben, B. N., Lewis, J., Campbell, J., Welton, E. J., Korkin, S., and Lyapustin, A.: Advancements in the Aerosol Robotic Network (AERONET) Version 3 Database –~~

~~Automated Near-Real-Time Quality Control Algorithm with Improved Cloud Screening for Sun Photometer Aerosol Optical Depth 25 (AOD) Measurements, Atmospheric Measurement Techniques Discussions, 2018, 1–78, https://doi.org/10.5194/amt-2018-272, https: //www.atmos-meas-tech-discuss.net/amt-2018-272/, 2018.~~

Giles, D. M., Sinyuk, A., Sorokin, M. G., Schafer, J. S., Smirnov, A., Slutsker, I., Eck, T. F., Holben, B. N., Lewis, J. R., Campbell, J. R., Welton, E. J., Korkin, S. V., and Lyapustin, A. I.: Advancements in the Aerosol Robotic Network (AERONET) Version 3 database – automated near-real-time quality control algorithm with improved cloud screening for Sun photometer aerosol optical depth (AOD) measurements, Atmos. Meas. Tech., 12, 169-209, https://doi.org/10.5194/amt-12-169-2019, 2019.

Goloub, P., Li, Z., Dubovik, O., Blarel, L., Podvin, T., Jankowiak, I., Lecoq, R., Deroo, C., Chatenet, B., Morel, J., Cuevas, E., and Ramos, R.: PHOTONS/AERONET sunphotometer network overview:

description, activities, results, in: Fourteenth International Symposium on Atmospheric and Ocean Optics/Atmospheric Physics, vol. 6936, p. 69360V, International Society for Optics and Photonics, 2007.

Grassl, H.: Calculated Circumsolar Radiation as a Function of Aerosol Type, Field of View, Wavelength, and Optical Depth, Applied Optics, Vol. 10, No. 11, 2543, 1971.

Gueymard, C.: SMARTS2: a simple model of the atmospheric radiative transfer of sunshine: algorithms and performance assessment, Florida Solar Energy Center Cocoa, FL, 1995.

Guirado, C., Cuevas, E., Cachorro, V. E., Toledano, C., Alonso-Pérez, S., Bustos, J. J., Basart, S., Romero, P. M., Camino, C., Mimouni, M., Zeudmi, L., Goloub, P., Baldasano, J. M., and de Frutos, A. M.: Aerosol characterization at the Saharan AERONET site Tamanrasset,

Atmospheric Chemistry and Physics, 14, 11753–11773, https://doi.org/10.5194/acp-14-11753-2014, https://www.atmos-chem-phys.net/ 14/11753/2014/, 2014.

Holben, B., Eck, T., Slutsker, I., Tanré, D., Buis, J., Setzer, A., Vermote, E., Reagan, J., and Kaufman, Y.: Multi-band automatic sun and sky scanning radiometer system for measurement of aerosols, pp. 75–83, CNES, Proceedings of 6th International Symposium on Physical Measurements and Signatures in Remote Sensing, 1994.

Holben, B., Eck, T., Slutsker, I., Tanré, D., Buis, J., Setzer, A., Vermote, E., Reagan, J., Kaufman, Y., Nakajima, T., Lavenu, F., Jankowiak, I., and Smirnov, A.: AERONET—A Federated Instrument Network and Data Archive for Aerosol Characterization, Remote Sensing of Environment, 66, 1 – 16, https://doi.org/https://doi.org/10.1016/S0034-4257(98)00031-5, 1998.

Holben, B., Tanre, D., Smirnov, A., Eck, T., Slutsker, I., Abuhassan, N., Newcomb, W., Schafer, J., Chatenet, B., Lavenu, F., et al.: An emerging ground-based aerosol climatology: Aerosol optical depth from AERONET, Journal of Geophysical Research: Atmospheres, 106, 12067–12097, https://doi.org/https://doi.org/10.1029/2001JD900014, 2001.

Huijnen, V. and Eskes, H.: Skill scores and evaluation methodology for the MACC II project, MACC-II Deliverable D_85, 2, http://www. gmes-atmosphere.eu/documents/maccii/deliverables/val/MACCII_VAL_DEL_D_85.2_ScoringReport01_20120222.pdf, 2012.

Huneeus, N., Basart, S., Fiedler, S., Morcrette, J.-J., Benedetti, A., Mulcahy, J., Terradellas, E., Pérez García-Pando, C., Pejanovic, G., Nickovic, S., Arsenovic, P., Schulz, M., Cuevas, E., Baldasano, J. M., Pey, J., Remy, S., and Cvetkovic, B.: Forecasting the northern African dust outbreak towards Europe in April 2011: a model intercomparison, Atmospheric Chemistry and Physics, 16, 4967–4986, https://doi.org/10.5194/acp-16-4967-2016, https://www.atmos-chem-phys.net/16/4967/2016/, 2016.

IPCC: The Physical Science Basis. Intergovernmental Panel on Climate Change, https://doi.org/doi:10.1017/CBO9781107415324, 2013.

Jarosyawski, J., Krzyscin, J.W., Puchalski, S., Sobolewski, P.: On the optical thickness in the UV range: analysis of the ground-based data taken at Belsk, Poland. Journal of Geophysical Research 108 (D23), doi: 10.1029/ 2003JD003571, 2003.

Kahn, R. A. and Gaitley, B. J.: An analysis of global aerosol type as retrieved by MISR, Journal of Geophysical Research: Atmospheres, 120, 4248–4281, https://doi.org/10.1002/2015JD023322, https://agupubs.onlinelibrary.wiley.com/doi/abs/10.1002/2015JD023322, 2015.

Kalnay, E., Kanamitsu, M., Kistler, R., Collins, W., Deaven, D., Gandin, L., Iredell, M., Saha, S., White, G., Woollen, J., et al.: The 20 NCEP/NCAR 40-year reanalysis project, Bulletin of the American meteorological Society, 77, 437–472, 1996.

Kasten, F.: A new table and approximation formula for the relative optical air mass, Archiv für Meteorologie, Geophysik und Bioklimatologie, Serie B, 14, 206–223, https://doi.org/https://doi.org/10.1007/BF02248840, 1966.

Kasten, F. and Young,A. T.: Revised optical air mass tables and approximation formula, Appl. Opt., 28, 4735–4738, https://doi.org/10.1364/AO.28.004735, 1989.

Kazadzis, S., Veselovskii, I., Amiridis, V., Gröbner, J., Suvorina, A., Nyeki, S., Gerasopoulos, E., Kouremeti, N., Taylor, M., Tsekeri, A., and Wehrli, C.: Aerosol microphysical retrievals from precision filter radiometer direct solar radiation measurements and comparison with AERONET, Atmospheric Measurement Techniques, 7, 2013–2025, https://doi.org/10.5194/amt-7-2013-2014, https: //www.atmos-meas-tech.net/7/2013/2014/, 2014.

Kazadzis, S., Kouremeti, N., Diémoz, H., Gröbner, J., Forgan, B. W., Campanelli, M., Estellés, V., Lantz, K., Michalsky, J., Carlund, T., Cuevas, E., Toledano, C., Becker, R., Nyeki, S., Kosmopoulos, P. G., Tatsiankou, V., Vuilleumier, L., Denn, F. M., Ohkawara, N., Ijima, O., Goloub, P., Raptis, P. I., Milner, M., Behrens, K., Barreto, A., Martucci, G., Hall, E., Wendell, J., Fabbri, B. E., and Wehrli, C.: Results from the Fourth WMO Filter Radiometer Comparison for aerosol optical depth measurements, Atmospheric Chemistry and Physics, 18, 3185–3201, https://doi.org/10.5194/acp-18-3185-2018, 2018a.

Kazadzis, S., Kouremeti, N., Nyeki, S., Gröbner, J., and Wehrli, C.: The World Optical Depth Research and Calibration Center (WORCC) quality assurance and quality control of GAW-PFR AOD measurements, Geoscientific Instrumentation, Methods and Data Systems, 7, 39–53,

https://doi.org/10.5194/gi-739-2018, https://www.geosci-instrum-method-data-syst.net/7/39/2018/, 2018b.

Kentarchos, A., Roelofs, G.J., Lelieveld, J., and Cuevas, E.: On the origin of elevated surface ozone concentrations at Izaña Observatory during the last days of March 1996: a model study, Geophys. Res. Lett., Vol. 27, 22, 3,699-3,702, 2000.

Kim, S.-W., Jefferson, A., Soon-Chang, Y., Dutton, E., Ogren, J., Valero, F., Kim, J., and Holben, B.: Comparisons of aerosol optical depth and surface shortwave irradiance and their effect on the aerosol surface radiative forcing estimation, Journal of Geophysical Research: Atmospheres, 110, https://doi.org/10.1029/2004JD004989, 2005.

Kim, S.-W., Yoon, S.-C., Kim, J., and Kim, S.-Y.: Seasonal and monthly variations of columnar aerosol optical properties over east Asia determined from multi-year MODIS, LIDAR, and AERONET Sun/sky radiometer measurements, Atmospheric Environment, 41, 1634– 1651, https://doi.org/https://doi.org/10.1016/j.atmosenv.2006.10.044, 2007.

Kim, S.-W., Yoon, S.-C., Dutton, E., Kim, J., and Wehrli, C.and Holben, B.: Global surface-based sun photometer network for long-term observations of column aerosol optical properties: intercomparison of aerosol optical depth, Aerosol Science and Technology, 42, 1–9, https://doi.org/https://doi.org/10.1080/02786820701699743, 2008.

Klingmüller, K., Pozzer, A., Metzger, S., Stenchikov, G. L., and Lelieveld, J.: Aerosol optical depth trend over the Middle East, Atmospheric Chemistry and Physics, 16, 5063–5073, https://doi.org/10.5194/acp-16-5063-2016, 2016.

Komhyr, W.: Dobson spectrophotometer systematic total ozone measurement error, Geophysical Research Letters, 7, 161–163, 1980.

Komhyr, W. D., Grass, R. D., and Leonard, R. K.: Dobson spectrophotometer 83: A standard for total ozone measurements, 1962–1987, Journal of Geophysical Research: Atmospheres, 94, 9847–9861, https://doi.org/10.1029/JD094iD07p09847, 1989.

Mahowald, N., M., Albani, S. Kok, J. F., Engelstaeder, S., Scanza, R., Ward, D. S., Flanner, M. G.: -The size distribution of desert dust aerosols and its impact on the Earth system, Aeolian Research, 15, 53-71, 2014.

McArthur, L. J. B., Halliwell, D. H., Niebergall, O. J., O'Neill, N. T., Slusser, J. R., and Wehrli, C.: Field comparison of network Sun photometers, Journal of Geophysical Research: Atmospheres, 108, https://doi.org/10.1029/2002JD002964, 2003.

McPeters, R., Frith, S., and Labow, G.: OMI total column ozone: extending the long-term data record, Atmospheric Measurement Techniques, 8, 4845–4850, https://doi.org/https://doi.org/10.5194/amt-8-4845-2015, 2015.

Mitchell, R. and Forgan, B.: Aerosol measurement in the Australian outback: Intercomparison of sun photometers, Journal of Atmospheric 20 and Oceanic Technology, 20, 54–66, https://doi.org/https://doi.org/10.1175/1520-0426(2003)020<0054:AMITAO>2.0.CO;2, 2003.

Mitchell, R. M., Forgan, B. W., and Campbell, S. K.: The Climatology of Australian Aerosol, Atmos. Chem. Phys., 17, 5131-5154, https://doi.org/10.5194/acp-17-5131-2017, 2017.

Nakajima, T., Yoon, S. C., Ramanathan, V., Shi, G. Y., Takemura, T., Higurashi, A., Takamura, T., Aoki, K., Sohn, B. J., Kim, S. W., Tsuruta, H., Sugimoto, N., Shimizu, A., Tanimoto, H., Sawa, Y., Lin, N. H., Lee, C. T., Goto, D., and Schutgens, N.: Overview of the Atmospheric Brown Cloud East Asian Regional Experiment 2005 and a study of the aerosol direct radiative forcing in east Asia, J. Geophys. Res., 112, D24S91, doi:10.1029/2007JD009009, 2007.

Nyeki, S., Halios, C., Baum, W., Eleftheriadis, K., Flentje, H., Gröbner, J., Vuilleumier, L., and Wehrli, C.: Ground-based aerosol optical depth trends at three high-altitude sites in Switzerland and southern Germany from 1995 to 2010, Journal of Geophysical Research: Atmospheres, 117, https://doi.org/https://doi.org/10.1029/2012JD017493, 2012.

Nyeki, S., Gröbner, J., and Wehrli, C.: Ground-based aerosol optical depth inter-comparison campaigns at European EUSAAR super-sites, 25 vol. 1531, pp. 584–587, https://doi.org/10.1063/1.4804837, 2013.

Nyeki, S., Wehrli, C., Gröbner, J., Kouremeti, N., Wacker, S., Labuschagne, C., Mbatha, N., and Brunke, E.-G.: The GAW-PFR aerosol optical depth network: The 2008–2013 time series at Cape Point Station, South Africa, Journal of Geophysical Research: Atmospheres, 120, 5070–5084, 2015.

Räisänen, P., Isaac, G. A., Barker, H. W. and Gultepe, I.: Solar radiative transfer for stratiform clouds with horizontal variations in liquid-water path and droplet effective radius, Quart. J. Roy. Meteor. Soc., 129, 2135-2149, doi: 10.1256/qj.02.149, 2003.

Rodríguez, S., González, Y., Cuevas, E., Ramos, R., Romero, P. M., Abreu-Afonso, J., and Redondas, A.: Atmospheric nanoparticle observations in the low free troposphere during upward orographic flows at IzaÃñ±a Mountain Observatory, Atmospheric Chemistry and Physics, 9, 6319–6335, https://doi.org/10.5194/acp-9-6319-2009, 2009.

Rodríguez, S., Alastuey, A., Alonso-Pérez, S., Querol, X., Cuevas, E., Abreu-Afonso, J., Viana, M., Pérez, N., Pandolfi, M., and de la Rosa, J.: Transport of desert dust mixed with North African industrial pollutants in the subtropical Saharan Air Layer, Atmospheric Chemistry and Physics, 11, 6663–6685, https://doi.org/10.5194/acp-11-6663-2011, 2011.

Rodríguez, S., Cuevas, E., Prospero, J. M., Alastuey, A., Querol, X., López-Solano, J., García, M. I., and Alonso-Pérez, S.: Modulation of Saharan dust export by the North African dipole, Atmospheric Chemistry and Physics, 15, 7471–7486, https://doi.org/10.5194/acp-157471-2015, 2015.

Rodriguez-Franco, J. J., and Cuevas, E.: Characteristics of the subtropical tropopause region based on long-term highly-resolved sonde records over Tenerife, J. Geophys. Res. Atmos., 118, doi:10.1002/jgrd.50839, 2013.

Romero, P. M. and Cuevas, E.: Variación diurna del espesor óptico de aerosoles:¿ ficción o realidad?, 3 Asamblea Hispano Portuguesa de Geofísica y Geodesia. Valencia, 2002.

Romero-Campos, P., Cuevas, A., Kazadzis, S., Kouremeti, N., García, R., and Guirado-Fuentes, C.: Análisis de la trazabilidad en los valores del AOD obtenidos a partir de las medidas de las redes AERONET-CIMEL y GAW-PFR durante el período 2005-2015 en el Observatorio Atmosférico de Izaña, 2017.

Russell, P. B., Livingston, J. M., Dubovik, O., Ramirez, S. A., Wang, J., Redemann, J., Schmid, B., Box, M., and Holben, B. N.: Sunlight transmission through desert dust and marine aerosols: Diffuse light corrections to Sun photometry and pyrheliometry, J. Geophys. Res., 109, D08207, 10.1029/2003JD004292, 2004.

Sakerin, S. M., Kabanov, D. M., Panchenko, M. V., Pol'kin, V. V., Holben, B. N., Smirnov, A. V., Beresnev, S. A., Gorda, S. Y., Kornienko, G. I., Nikolashkin, S. V., Poddubnyi, V. A., and Tashchilin, M. A.: Monitoring of atmospheric aerosol in the Asian part of Russia in 2004 within the framework of AEROSIBNET program, Atmos. Oceanic Optics, 18, 871–878, 2005.

Sayer, A. M., Hsu, N. C., Bettenhausen, C., Jeong, M., Holben, B. N., and Zhang, J.: Global and regional evaluation of over-land spectral aerosol optical depth retrievals from SeaWiFS, Atmospheric Measurement Techniques, 5, 1761–1778, https://doi.org/10.5194/amt-51761-2012, 2012.

Sayer, A. M., Hsu, N. C., Bettenhausen, C., and Jeong, M.: Validation and uncertainty estimates for MODIS Collection 6 "Deep Blue" aerosol 10 data, Journal of Geophysical Research: Atmospheres, 118, 7864–7872, https://doi.org/10.1002/jgrd.50600, https://agupubs.onlinelibrary.wiley.com/doi/abs/10.1002/jgrd.50600, 2013.

Schmid, B. and Wehrli, C.: Comparison of Sun photometer calibration by use of the Langley technique and the standard lamp, Appl. Opt., 34, 4500–4512, https://doi.org/10.1364/AO.34.004500, http://ao.osa.org/abstract.cfm?URI=ao-34-21-4500, 1995.

Schmid, B., Michalsky, J., Halthore, R., Beauharnois, M., Harrison, L., Livingston, J., Russell, P., Holben, B., Eck, T., and Smirnov, A.: Comparison of aerosol optical depth from four solar radiometers during the fall 1997 ARM intensive observation period, Geophysical Research Letters, 26, 2725–2728, https://doi.org/10.1029/1999GL900513, https://agupubs.onlinelibrary.wiley.com/doi/abs/10.1029/1999GL900513, 1999.

Sinyuk, A., Holben, B.N., Smirnov, A., Eck, T.F., Slutsker, I., Schafer, J.S., Giles, D.M., and –Sorokin, M.: Assessment of error in aerosol optical depth measured by AERONET due to aerosol forward scattering, Geophys. Res. Lett., 39, 23806, doi:10.1029/2012GL053894, 2012.

Smirnov, A., Holben, B., Eck, T., Dubovik, O., and Slutsker, I.: Cloud-screening and quality control algorithms for the AERONET database, Remote sensing of environment, 73, 337–349, https://doi.org/https://doi.org/10.1016/S0034-4257(00)00109-7, http://www.sciencedirect. 20 com/science/article/pii/S0034425700001097, 2000.

Takamura, T., and Nakajima, T.: Overview of SKYNET and its activities, Opt. Pura Apl., 37, 3303-3308, 2004.

Thomason, L.W., Herman, B. M., Schotland, R.M., and Reagan, J.A.: Extraterrestrial solar flux measurement limitations due to a Beer's law assumption and uncertainty in local time, Appl. Opt., 21, 1191–1195, https://doi.org/10.1364/AO.21.001191, 1982.

~~Thuillier, G., Hersé, M., Labs, D., Foujols, T., Peetermans, W., Gillotay, D., Simon, P.C., Mandel, H.: The Solar Spectral Irradiance from 200 to 2400 nm as Measured by the SOLSPEC Spectrometer from the Atlas and Eureca Missions, Solar Physics, 214, 1, 1-22, https://doi.org/10.1023/A:1024048429145, 2003.~~

Todd, M. C., Washington, R., Martins, J. V., Dubovik, O., Lizcano, G., M'bainayel, S., and Engelstaedter, S.: Mineral dust emission from the Bodélé Depression, northern Chad, during BoDEx 2005, Journal of Geophysical Research: Atmospheres, 112,

https://doi.org/https://doi.org/10.1029/2006JD007170, 2007.

Toledano, C., Cachorro, V. E., Berjón, A., de Frutos, A. M., Sorribas, M., de la Morena, B. A., and Goloub, P.: Aerosol optical depth and Ångström exponent climatology at El Arenosillo AERONET site (Huelva, Spain), Quarterly Journal of the Royal Meteorological Society, 133, 795–807, https://doi.org/10.1002/qj.54, https://rmets.onlinelibrary.wiley.com/doi/abs/10.1002/qj.54, 2007.

Toledano, C., Cachorro, V. E., Berjon, A., de Frutos, A. M., Fuertes, D., Gonzalez, R., Torres, B., Rodrigo, R., Bennouna, Y., Martin, L., and Guirado, C.: RIMA-AERONET network: long-term monitoring of aerosol properties, Opt. Pura Apl., 44, 629–633, 2011.

Toledano, C., Cachorro, V., Gausa, M., Stebel, K., Aaltonen, V., Berjón, A., de Galisteo, J. P. O., de Frutos, A. M., Bennouna, Y., Blindheim, S., Myhre, C. L., Zibordi, G., Wehrli, C., Kratzer, S., Hakansson, B., Carlund, T., de Leeuw, G., Herber, A., and Torres, B.: Overview of Sun Photometer Measurements of Aerosol Properties in Scandinavia and Svalbard, Atmospheric Environment, 52, 18–28, 30 https://doi.org/10.1016/j.atmosenv.2011.10.022, 2012.

Toledano, C., González, R., Fuertes, D., Cuevas, E., Eck, T. F., Kazadzis, S., Kouremeti, N., Gröbner, J., Goloub, P., Blarel, L., Román, R., Barreto, A., Berjón, A., Holben, B. N., and Cachorro, V. E.: Assessment of Sun photometer Langley calibration at the high-elevation sites Mauna Loa and Izaña,

Atmospheric Chemistry and Physics, 18, 14555–14567, https://doi.org/10.5194/acp-18-14555-2018, 2018.

Torres, B., Toledano, C., Berjón, A., Fuertes, D., Molina, V., Gonzalez, R., Canini, M., Cachorro, V. E., Goloub, P., Podvin, T., Blarel, L., Dubovik, O., Bennouna, Y., and de Frutos, A. M.: Measurements on pointing error and field of view of Cimel-318 Sun photometers in the scope of AERONET, Atmospheric Measurement Techniques, 6, 2207–2220, https://doi.org/10.5194/amt-6-2207-2013, 2013.

Wagner, F. and Silva, A. M.: Some considerations about Angström exponent distributions, Atmospheric Chemistry and Physics, 8, 481–489, https://doi.org/10.5194/acp-8-481-2008, 2008.

Wang, J., Xia, X., Wang, P., and Christopher, S.: Diurnal variability of dust aerosol optical thickness and Ångströ¨m exponent over dust source regions in China, Geophysical Research Letters, 31, https://doi.org/10.1029/2004GL019580, https://agupubs.onlinelibrary.wiley.com/doi/abs/10.1029/2004GL019580, 2004.

Weinzierl, B., Sauer, D., Esselborn, M., Petzold, A., Veira, A., Rose, M., Mund, S., Wirth, M., Ansmann, A., Tesche, M., Gross, S., and Freudenthaler, V.: Microphysical and optical proper-ties of dust and tropical biomass burning aerosol layers in the Cape Verde region-an overview of the airborne in situ and lidar measurements during SAMUM-2, Tellus B, 63, 589–618, doi:10.1111/j.1600-0889.2011.00566.x, 2011.

Wehrli, C.: Calibrations of filter radiometers for determination of atmospheric optical depth, Metrologia, 37, 419, http://stacks.iop.org/ 0026-1394/37/i=5/a=16, 2000.

Wehrli, C.: GAWPFR: A network of aerosol optical depth observations with precision filter radiometers, Global Atmosphere WatchLOBAL ATMOSPHERE WATCH, p. 36, 2005.

Wehrli, C.: Precision Filter Radiometer Documentation, Version 4.0, 38 pp., Davos Dorf, 2008a.

Wehrli, C.: Remote sensing of aerosol optical depth in a global surface network, Ph.D. thesis, ETH Zurich, https://www.research-collection.ethz.ch/bitstream/handle/20.500.11850/150574/eth-30693-02.pdf, 2008b.

Wilbert, S.: Determination of circumsolar radiation and its effect on concentrating solar power, Ph.D. thesis, Hochschulbibliothek der Rheinisch-Westfälischen Technischen Hochschule Aachen, https://d-nb.info/1059537710/34, 2014.

WMO: Recent Progress in Sunphotometry. Determination of the aerosol optical depth, Environmental Pollution Monitoring and Research Programme, Nº 43, 21 pp, November, https://library.wmo.int/pmb_ged/wmo-td_143.pdf, 1986.

WMO: Aerosol measurement procedures, guidelines and recommendations, GAW Report No. 153, WMO TD No. 1178, https://library.wmo. int/pmb_ged/wmo-td_1178.pdf, 2003.

WMO: WMO/GAW Experts Workshop on a Global Surface-Based Network for Long Term Observations of Column Aerosol Optical Properties,GAW Report No. 162, WMO TD No. 1287, https://library.wmo.int/pmb_ged/wmo-td_1287.pdf, 2005.

WMO: Abridged final report with resolutions and recommendations, GAW Report WMO TD No. 1019, WMO-CIMO Fourteenth session Geneva 7–14 December 2006, 2007.

WMO: WMO/GAW Aerosol Measurement Procedures, Guidelines and Recommendations, 2nd Edition, WMO No 1177, GAW Report No. 227, 93 pp, https://library.wmo.int/doc_num.php?explnum_id=3073, 2016.

Young, A. T.: Revised depolarization corrections for atmospheric extinction, Appl. Opt., 19, 3427–3428,https://doi.org/10.1364/AO.19.003427, 1980.